

**Modelling the dynamics and control of *Aedes aegypti*
populations at fine spatial scales**

Clare McCormack

Thesis submitted for the degree of Doctor of Philosophy

Department of Infectious Disease Epidemiology

Imperial College London

October 2018

Copyright Declaration

The copyright of this thesis rests with the author and is made available under a Creative Commons Attribution Non-Commercial No Derivatives licence. Researchers are free to copy, distribute or transmit the thesis on the condition that they attribute it, that they do not use it for commercial purposes and that they do not alter, transform or build upon it. For any reuse or redistribution, researchers must make clear to others the licence terms of this work.

Declaration of Originality

I declare that all work presented in this thesis is my own, completed under the supervision of Prof. Neil Ferguson and Prof. Azra Ghani. Any data used in this thesis has been generated by others, and those who have shared data have been acknowledged in the relevant sections of this thesis.

Clare McCormack

October 2018

Chapter Contributions

Chapters 2-4:

I wrote and developed all code corresponding to the model and results presented in these chapters using C++, and conducted all analyses.

Chapters 5-6:

The entomological field data presented and discussed in these chapters was generated and collected by the National Environment Agency (NEA) Singapore during Phase 1 of the Project Wolbachia study. The Phase 1 study was undertaken by the Environmental Health Institute of NEA Singapore, under the supervision of Prof. Lee Ching Ng (Principal Investigator).

As Project Wolbachia Singapore does not involve any human participants, ethical approval for the study was not required. However, prior to the study commencing, comprehensive risk assessments were conducted by both the NEA [1] and an independent consultancy (Ipsos Business Consulting) [2] to determine the safety of the release of *Wolbachia*-infected male *Aedes aegypti* into the urban environment of Singapore, and to identify potential hazards and potential secondary ecological, biological, social and economic impacts. The technology was determined to be safe, with no risk to public health and negligible ecological impacts.

NEA generously shared the data collected during the Phase 1 study with me, following the signing of a Research Collaboration Agreement between NEA Singapore and Imperial College London detailing the scope of the modelling work. I received the data as a series of Microsoft Excel files, with no subsequent cleaning of the data required. The dataset I received was comprised of:

- Weekly *Aedes aegypti* adult mosquito trapping data (wild-type females, wild-type males and *Wolbachia*-infected males)
- Weekly *Aedes aegypti* egg trapping data (viable and nonviable eggs)
- The timing, size, location and frequency of the releases of *Wolbachia*-infected male *Aedes aegypti*
- Weekly environmental data (rainfall, temperature and relative humidity)

for each study site.

I developed and wrote all code corresponding to the model and results presented in these chapters (including implementation of the particle Markov Chain Monte Carlo algorithm) using C++, and conducted all analyses. Dr. Wes Hinsley assisted me with parallel computing.

Abstract

Novel vector control measures such as the release of *Wolbachia*-infected *Aedes aegypti* offer a promising new pathway for dengue control. However, to realistically model the likely impact of these measures, improved mathematical models of *Aedes aegypti* population dynamics are needed, with the final goal being spatially explicit models of *Aedes aegypti* population dynamics, calibrated against high quality entomological data.

Here we begin to address the challenge of developing such models by (i) examining the role of spatial structure in shaping the dynamics of *Aedes aegypti* populations at fine spatial scales and (ii) using advanced inferential methods to fit a dynamical model of *Aedes aegypti* population dynamics to entomological field data, while allowing for the highly variable nature of mosquito trapping data.

We explore the effects of larval breeding habitat fragmentation on fine-scale *Aedes aegypti* population dynamics for a variety of different landscapes, examining how features of the underlying landscape and the dispersal behaviour of the mosquito affect the dynamics observed. In addition, by modelling the same population at different levels of spatial granularity, we investigate the appropriate level of spatial granularity for models to adopt to represent the fine-scale dynamics of *Aedes aegypti* populations.

We examine the results of a small-scale field trial testing the use of *Wolbachia* as a tool for *Aedes aegypti* population suppression in Singapore by calibrating a stochastic model of *Aedes aegypti* population dynamics against the detailed entomological data collected during the trial. We model both the underlying population dynamics and the trapping process, thereby accounting for variability in mosquito trapping data when estimating the impact of the trial on local *Aedes aegypti* populations.

Thus the work presented in this thesis represents an important step forward in the challenge of developing models needed to realistically assess the likely impact of novel vector control measures.

Acknowledgements

I would like to thank my primary supervisor Prof. Neil Ferguson for his help, patience, and guidance throughout my PhD. Neil has been a wonderful teacher, and I am deeply grateful for all he has taught me and for his constant support and encouragement. I would also like to thank my second supervisor Prof. Azra Ghani for her valuable advice and support throughout this project.

I thank the MRC Centre for Global Infectious Disease Analysis for funding this work and for the opportunity to attend several conferences and workshops during my studies.

The work presented in Chapters 5 and 6 would not have been possible without the National Environment Agency in Singapore, and in particular Prof. Lee Ching Ng and her team. I thank them for generously sharing their data with us, and for the many valuable, insightful discussions.

The Department of Infectious Disease Epidemiology has been a wonderful place to work and learn, and I feel very lucky to have had the opportunity to study in such a stimulating environment. In particular, I would like to thank the other members of my PhD cohort (Alastair, Joel, Lebby, Lilith and Tamsin) for their friendship and support. I thank Dr. Wes Hinsley for his advice, help and support on computing and technical issues. I also thank Dr. Natsuko Imai and Dr. Daniel Laydon for their feedback on sections of this thesis.

Last, but not least, I thank my family and close friends for their unwavering encouragement and support throughout all of my studies. In particular, I thank my parents, Mick and Catherine McCormack, and dedicate this thesis to them.

Contents

Copyright Declaration	1
Declaration of Originality	2
Chapter Contributions	3
Abstract	5
Acknowledgements	6
List of Figures	12
List of Tables	13
List of Abbreviations	14
1 Introduction	15
1.1 Dengue Burden and Natural History	15
1.2 Treatment and Control of Dengue	17
1.3 Vector Behaviour and Habitat	19
1.4 Vector Control	22
1.4.1 Traditional Methods	22
1.4.2 Novel Vector Control Methods	23
1.5 Modelling Spatial Dynamics	27
1.5.1 The Metapopulation Approach	28
1.5.2 Spatial Models of <i>Aedes aegypti</i> Population Dynamics	30
1.6 Modelling the Impact of Novel Vector Control Measures	32
1.7 Overview of Thesis	36
2 Homogeneous Landscapes	39

2.1	Introduction	39
2.2	Methods	41
2.2.1	Model Structure	41
2.2.2	Landscape Model	47
2.2.3	Model Assumptions	48
2.2.4	Parameter Values	51
2.3	Results	56
2.3.1	Impact of Fragmentation	56
2.3.2	Dispersal Dynamics	57
2.3.3	Invasion Dynamics	58
2.4	Discussion	61
3	Heterogeneous Landscapes	63
3.1	Methods	63
3.1.1	Landscape Model	63
3.2	Results	65
3.2.1	Spatial Heterogeneity and Dispersal Dynamics	65
3.2.2	Spatial Heterogeneity and Invasion Dynamics	66
3.2.3	Impact of Spatial Clustering	67
3.3	Discussion	68
4	Spatial Granularity	70
4.1	Methods	70
4.1.1	Varying Spatial Granularity	70
4.1.2	Single Patch Approximations	70
4.2	Results	72
4.2.1	Varying Spatial Granularity	72
4.2.2	Single Patch Approximations	73
4.3	Discussion	77
5	Project <i>Wolbachia</i> Singapore: Data & Model Development	82
5.1	Introduction	82
5.2	Phase 1 Field Study	84
5.2.1	Release Strategy	85

5.2.2	Data Collected	87
5.3	Model Structure	98
5.3.1	Landscape Model	104
5.4	Model Fitting	106
5.4.1	Particle MCMC	106
5.4.2	Proposing Parameter Values	113
5.4.3	Likelihood Function	114
5.5	Testing with Simulated Data	117
5.5.1	Generating the Simulated Data	117
5.5.2	Reducing Correlation	118
5.5.3	Results	119
5.6	Discussion	123
6	Project <i>Wolbachia</i> Singapore: Phase 1 Results	124
6.1	Methods	124
6.2	Results	126
6.2.1	Estimating the Basic Mosquito Reproduction Number	126
6.2.2	Sensitivity to the Basic Mosquito Reproduction Number	131
6.2.3	Mating Competitiveness	137
6.2.4	Simulating Counterfactual Release Scenarios	143
6.3	Discussion	147
6.4	Acknowledgements	153
7	Discussion	154
7.1	Summary of Key Findings	154
7.2	Implications of Research	156
7.3	Limitations and Future Work	159
7.4	Conclusions	163
A	Figure Permissions	191
B	Sample Code	193

List of Figures

1.1	Dengue Timelines	16
1.2	Predicted Global Distribution of <i>Aedes Albopictus</i>	20
1.3	<i>Aedes Aegypti</i> Control Methods	22
1.4	Cytoplasmic Incompatibility	23
1.5	Bistable Dynamics of <i>Wolbachia</i>	33
2.1	Dispersal Probabilities	46
2.2	Mean Lifetime Dispersal Distance	53
2.3	Impact of Fragmentation on an Established Mosquito Population	56
2.4	Dispersal Dynamics in Homogeneous Landscapes	57
2.5	Impact of Increasing the Dispersal Rate	58
2.6	Impact of Fragmentation on Population Invasion	59
2.7	Impact of Dispersal Behaviour on Population Invasion	59
2.8	Timing of Population Invasion	60
3.1	Example Landscapes	64
3.2	Impact of Fragmentation in Spatially Heterogeneous Landscapes	65
3.3	Spatial Heterogeneity and Dispersal	66
3.4	Invasion Dynamics in Spatially Heterogeneous Landscapes	67
3.5	Spatial Correlation and Dispersal Length	68
3.6	Spatial Correlation and Invasion Dynamics	68
4.1	Modelling Established Populations at Different Levels of Spatial Granularity	73
4.2	Modelling Invasion Dynamics at Different Levels of Spatial Granularity	73
4.3	Single Patch Approximations - Example 1	75
4.4	Single Patch Approximations - Example 2	75
4.5	Single Patch Approximations - Magnitude of Adjustment	76
5.1	Project <i>Wolbachia</i> Phase 1 - Study Sites	85

5.2	Release Sizes	86
5.3	Residential Blocks	86
5.4	Aggregated Trapping Data	88
5.5	Distribution of Adult Mosquitoes Trapped across Floors	90
5.6	Mean Number of Adult Females Trapped per Block	91
5.7	Trapping Data-Tampines	93
5.8	Trapping Data-Yishun	94
5.9	Inter-block variability-Tampines	96
5.10	Inter-block variability-Yishun	96
5.11	Schematic of Model of IIT	98
5.12	Example of Spline Function	104
5.13	Illustration of Hidden Markov Model	107
5.14	Schematic of Particle Filtering	110
5.15	Posterior Parameter Distributions	120
5.16	Correlation Structure	120
5.17	Control Site 1	121
5.18	Release Site 1	121
5.19	Control Site 2	121
5.20	Release Site 2	122
6.1	Posterior Parameter Distributions	128
6.2	Population Size & Trapping - Tampines	129
6.3	Population Size & Trapping - Yishun	129
6.4	Tampines-Control Site (fitting R_M)	129
6.5	Tampines-Release Site (fitting R_M)	130
6.6	Yishun-Control Site (fitting R_M)	130
6.7	Yishun-Release Site (fitting R_M)	130
6.8	Comparison of Log-likelihood	131
6.9	Spline Function (fixed R_M)	132
6.10	Population Size & Trapping (fixed R_M)-Tampines	135
6.11	Population Size & Trapping (fixed R_M)-Yishun	135
6.12	Tampines-Control Site ($R_M = 12$)	135
6.13	Tampines-Release Site ($R_M = 12$)	136

6.14 Yishun-Control Site ($R_M = 12$)	136
6.15 Yishun-Release Site($R_M = 12$)	136
6.16 Mating Competitiveness	137
6.17 Tampines-Control Site ($R_M = 12, \tau$ local)	141
6.18 Tampines-Release Site ($R_M = 12, \tau$ local)	141
6.19 Yishun-Control Site ($R_M = 12, \tau$ local)	141
6.20 Yishun-Release Site ($R_M = 12, \tau$ local)	142
6.21 Simulating Counterfactual Release Scenarios - Tampines	145
6.22 Simulating Counterfactual Release Scenarios - Yishun	145
6.23 Simulating Counterfactual Release Scenarios - Mating Competitiveness	146

List of Tables

1.1	<i>Aedes Aegypti</i> Breeding Habitats	21
2.1	Model Parameter Values	55
5.1	Phase 1 Summary	86
6.1	Fixed Model Parameter Values	125
6.2	Sensitivity to R_M	134
6.3	Estimating Mating Competitiveness	140

List of Abbreviations

CI	Cytoplasmic Incompatibility
CrI	Credible Interval
DENV	Dengue Virus
HEG	Homing Endonuclease Gene
IIT	Incompatible Insect Technique
MCMC	Markov Chain Monte Carlo
MRR	Mark Release Recapture
NEA	National Environment Agency
PMMH	Particle Marginal Metropolis Hastings
RIDL	Release of Insects carrying a Dominant Lethal Gene
RNA	Ribonucleic Acid
SIT	Sterile Insect Technique
WHO	World Health Organisation

Chapter 1

Introduction

1.1 Dengue Burden and Natural History

As the world's most prevalent arboviral disease, dengue poses a major challenge to public health globally. Since the virus was first isolated in Japan in 1943 [3], rapid spread across the globe has ensued with the virus now endemic in more than 100 countries across the tropics and subtropics, and approximately half of the world's population currently at risk from infection by dengue [4]. Increased trade, urbanization and globalization, combined with a lack of effective vector control, have led to the expansion of its primary (*Aedes aegypti*) and secondary (*Aedes albopictus*) vectors, and the spread of dengue has followed [5]. Recent years have seen outbreaks increasing in both severity and length [4], and localised transmission occurring for the first time in several European countries including France [6] and Croatia [7].

Dengue is a single stranded RNA virus belonging to the genus *Flavivirus*, other members of which include yellow fever, Zika and Japanese encephalitis. Four antigenically distinct but closely related serotypes of the virus exist (DENV-1, 2, 3, 4), and all four serotypes co-circulate globally. Transmission of the virus occurs via the bite of an infective female mosquito, and once transmitted, the virus incubates in the human host for between three and ten days (the intrinsic incubation period) (Figure 1.1) [8, 9]. Towards the end of this period viraemia develops, and this may be accompanied by the acute onset of fever and a range of non-specific symptoms including headache, joint pain, and vomiting [10]. Viraemia typically lasts for between two and seven days [9]. Should a naïve vector take a blood meal from an infected person during the viraemic phase, it may contract the virus. Following an incubation period of typically between four and ten days in the mosquito (the extrinsic incubation period) [11], the mosquito is then capable of transmitting

the virus for the rest of its lifetime. The transmission cycle is hence repeated.

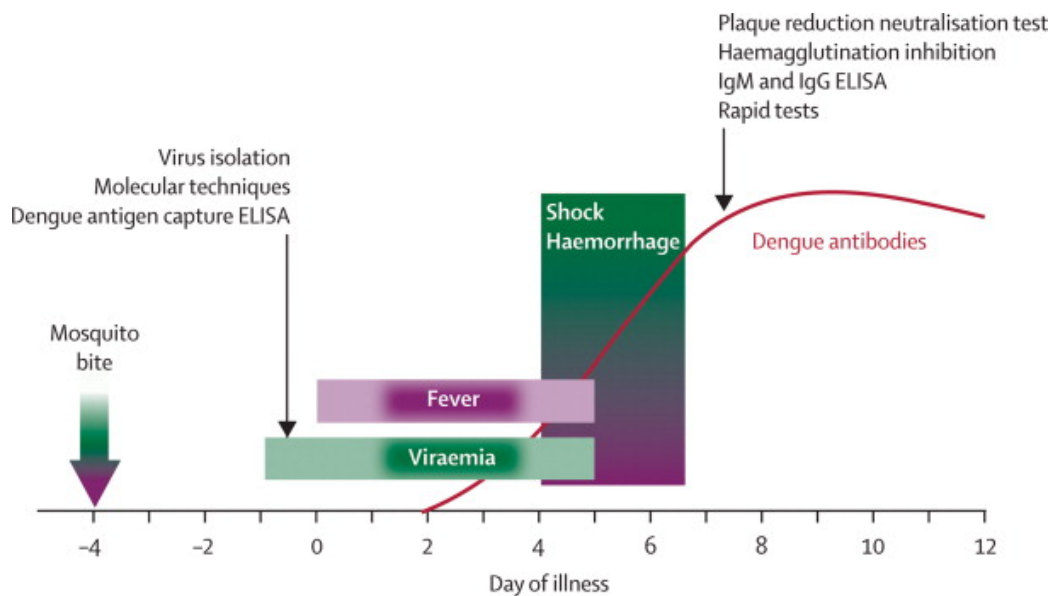


Figure 1.1: Dengue Timelines. Course of dengue infection and timings of diagnosis. Reprinted with permission from [9] (See Appendix A - Figure Permissions).

One of the most distinguishing features of dengue is its complex immunology. While recovery from primary infection by one of the four serotypes will provide lifelong immunity to that serotype, only short-term protection against the remaining serotypes is conferred [9, 10, 12]. The exact duration of cross-protection is unknown, and estimates of duration vary widely [13–16]. Early work by Sabin indicated a waning of complete protection against heterologous serotypes after two months [13], however more recent studies have estimated a duration of cross-protection of approximately two years [15], between one and three years [14], and between three and ten months [16]. Once cross-protection has waned, secondary infection with a heterologous serotype substantially increases the risk of developing severe dengue (also known as dengue haemorrhagic fever), symptoms of which include severe abdominal pain, persistent vomiting and haemorrhagic manifestations [9, 10]. This increase in risk is believed to occur as the result of an antibody-dependent enhancement mechanism, whereby antibodies produced during the primary infection crucially fail to neutralise virus particles present following infection by a heterologous serotype, thereby enhancing the severity of secondary infection [10, 17]. Recent analysis has shown that this mechanism is dependent on the level of dengue antibodies in the blood at the time of exposure to secondary infection, with an intermediate level of antibodies (pre-existing titres of $<1:40$) providing an environment in which this enhancement mechanism can occur [12, 18]. Subsequent tertiary and quaternary infections, while known to occur, are rarely reported

and often not severe [19–21]. Thus, how these infections contribute both towards transmission intensity and the burden of dengue remains poorly understood.

Indeed estimates of the global burden of dengue are both variable and uncertain. In 2013, Bhatt *et al.* estimated an annual burden of 390 million dengue infections, with 96 million apparent infections (95% credible interval (CrI) 67-136 million) [22]. This was more than three times the burden previously estimated by the World Health Organisation (WHO) of 50-100 million infections per year [4]. Using data collected through the Global Burden of Disease Study 2013, Stanaway *et al.* estimated that there were 58.4 million apparent infections in 2013 (95% CrI 23.6-121.9 million) with an associated total global cost of US\$8.9 million [23]. The global burden of dengue is particularly difficult to estimate for several reasons. First, the majority of dengue infections are asymptomatic [9, 10, 12], and thus data collected via disease surveillance systems primarily only capture clinically apparent infections. Hence they are likely to substantially underestimate the true prevalence of dengue among a given population [24]. Furthermore, should a (mild) symptomatic infection develop, symptoms are often non-specific and may be similar to those developed upon infection by other viruses such as Zika or chikungunya. Thus, in the absence of confirmed laboratory diagnosis, clinical misdiagnosis can easily occur [4]. In addition, dengue transmission intensity is highly heterogeneous, varying across time, space and between serotypes [25]. The quality of healthcare and surveillance systems also varies geographically, and thus it is difficult to achieve consistency in both reporting and diagnostic criteria used across a range of settings [26].

1.2 Treatment and Control of Dengue

Currently there is no known antiviral treatment for dengue. Therefore, treatment is limited to alleviating symptoms during the course of infection. Developing a safe and effective vaccine against dengue is particularly challenging owing to interactions between different serotypes and the risk of disease enhancement [27, 28]. Recent years however have seen considerable progress in dengue vaccine development. In December 2015, Dengvaxia[®] (CYD-TDV), a live, attenuated, tetravalent, recombinant vaccine based on the yellow fever 17D vaccine strain developed by Sanofi Pasteur Ltd., became the first dengue vaccine to be licensed for use in Mexico and is now licensed for use in 20 countries [29]. Uptake and roll-out of the vaccine has been slow however due to concerns over the long-term safety of the vaccine and its complex

efficacy profile [28].

The first glimpse into this complex efficacy profile was provided by the Phase 2b trials conducted in Thailand and Latin America, where vaccine efficacy was found to vary according to serotype, with the vaccine least efficacious against DENV2 [30]. Large-scale multi-country phase 3 trials subsequently conducted in Latin America [31] and Southeast Asia [32] found a similar result, and, furthermore, revealed that vaccine efficacy also varied by age and serostatus at the time of vaccination. Pooled analysis of the data collected across both of these trials estimated vaccine efficacy of 65.6% against confirmed dengue infection and 80.8% against hospitalization in children aged 9 or above, compared to 44.6% efficacy against confirmed infection and 56.1% against hospitalization in children under 9 [33]. Vaccine efficacy was reduced for participants seronegative at the time of vaccination (81.9% efficacy against confirmed dengue infection for seropositive individuals compared with 52.5% for seronegative individuals, among children aged 9 or above). Moreover, analysis of the long-term follow-up data revealed a greater than 7 fold increase in the risk of hospitalization for vaccinated children aged 2-5 years, and an overall increase in risk of hospitalization for vaccinated children under 9 [33]. However, the vaccine still had a protective effect against hospitalization for children in other age groups. Using mathematical modelling to translate these results into potential population level effects, Ferguson *et al.* [34] found that the overall potential impact of the vaccine would depend on the transmission setting and level of seroprevalence in the population. Namely, the vaccine would most likely have an overall beneficial effect in moderate to high transmission settings, but could increase the risk of severe dengue in low transmission settings.

Based on these analyses, in July 2016 the WHO initially recommended the vaccine for use only in countries with seroprevalence greater than 70% (and not less than 50%) and in individuals aged 9-45 [35]. However, additional analysis of the long-term safety follow-up data revealed an increased risk of hospitalization and severe dengue for seronegative individuals in all age groups [36]. Thus, in April 2018, the WHO revised this recommendation, advising instead that the vaccine should only be administered to dengue-seropositive individuals, with serostatus confirmed prior to vaccine administration [37].

Several other candidate dengue vaccines are currently in development [38], and results obtained

to date from small-scale trials have been promising. The two candidates furthest along in development are DENVax (TAK-003) [39], a two-dose tetravalent vaccine based on a DENV2 backbone developed by Takeda Pharmaceuticals Ltd., and TV-003, a single-dose tetravalent vaccine with a backbone based on three of the four dengue serotypes (DENV-1,3,4) developed by the U.S. National Institute of Health [40]. Both vaccines were well tolerated in small-scale clinical trials, and observed to elicit an antibody response against all four dengue serotypes, irrespective of baseline dengue serostatus [41–43]. Large-scale Phase 3 trials in Southeast Asia and Latin America (DENVax) [44], and in Brazil (TV-003) [45] are currently ongoing.

Given the lack of antiviral treatment and the challenges in dengue vaccine development, vector control methods thus remain at the core of current local and global dengue control strategies [4].

1.3 Vector Behaviour and Habitat

The life cycle of the mosquito is comprised of four main stages, and begins with an adult female mosquito laying eggs in a suitable breeding site following a blood meal. While some mosquito species including *Anopheles* mosquitoes lay eggs on the surface of water [46], *Aedes spp.* typically oviposit eggs above the water line [47, 48]. Then, once the oviposited eggs have been submerged in water, they hatch and develop into larvae. Following several stages of development, the larvae become pupae, which in turn develop into adult mosquitoes. The total length of this cycle (egg-larva-pupa-adult) is dependent on temperature, however for *Aedes spp.* this typically takes between 8 and 10 days in tropical areas [48]. Adult females typically oviposit every 3 days [49], and can lay eggs in a single breeding site or across multiple breeding sites, so called skip-oviposition behaviour [50, 51]. Interestingly, eggs laid by *Aedes spp.* are able to withstand desiccation, and thus can survive in a dry state for several months [52, 53]. In addition, eggs laid by *Aedes albopictus* can enter diapause in response to seasonal changes in temperature and daylight [54, 55]. This ability, combined with increased trade, is believed to be an important contributing factor to the expansion of *Aedes albopictus* to more temperate regions including North America and Europe (Figure 1.2) [56–58].

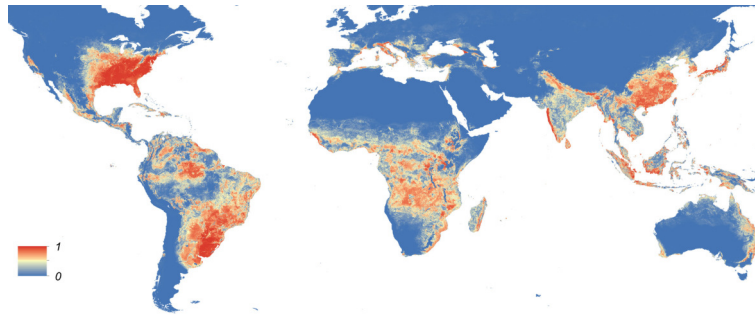


Figure 1.2: Predicted Global Distribution of *Aedes Albopictus*. The probability of occurrence of *Aedes Albopictus* globally at a spatial resolution of 5km x 5km. Reprinted with permission from [58] (See Appendix A - Figure Permissions).

While all mosquitoes experience the same life cycle, breeding habitats differ between species. *Aedes spp.* are adapted to an urban environment, and primarily breed in rain-filled man-made habitats such as household containers, buckets and discarded tyres (Table 1.1) [47, 59–61]. Thus, there can be several breeding sites per household, and breeding occurs both indoors and outdoors, in residential and non-residential areas [60]. *Aedes albopictus* also often breed in natural habitats in more densely vegetated areas and, as mentioned above, are capable of breeding in both tropical and cooler, more temperate climates [56, 57].

Container Category	Description
Cooking (N=20,396)	Pot, pan, plate, pitcher, cup, and drinking glass.
Plastic containers (N=225,666)	Bucket, bowls, basins, washtubs, and storage containers.
Large tanks (N=6,633)	Water storage tanks (cement or fiberglass), pools, some metal tanks
Medium storage (N=12,216)	55-gall drums, sinks, converted appliances (refrigerators, washing machines, small metal tanks)
Non-traditional (N=1,324)	Ditches, holes, depressions in floor, drains, puddles, plastic tarps or bags, rain gutters, PVC tubing
Tires (N=4,061)	Used car tires, usually intact, sometimes cut in half or pieces
Miscellaneous (N=3,122)	Discarded car parts, toys, boxes, ice chests, and furniture

Table 1.1: *Aedes Aegypti* Breeding Habitats. Description of the container categories most productive for *Aedes aegypti* in Iquitos, Peru, between January 1999 and August 2002. Reproduced in part with permission from [47] (See Appendix A - Figure Permissions).

The density of larvae produced by an individual breeding site varies between sites and is dependent on the type of habitat [47] and a range of environmental factors including rainfall and temperature [59]. Inherent limitations in resources at the breeding site limits the density of larvae a breeding site can support, with this limit referred to as the carrying capacity of the site. Larval populations are hence subject to regulation [59, 62–66]. It is generally assumed that larval population regulation is dominated by density-dependent competition, whereby larvae of the same species compete with one another for food and other resources [59, 62–66]. While this has the primary effect of increasing larval mortality [59, 62, 64, 66–71], a high degree of density-dependent competition may also lead to longer larval development times and a reduction in the size of adult mosquitoes emerging from the breeding site [62, 64, 70].

Dispersal allows adult mosquitoes to search beyond their immediate environment for blood meals, breeding sites, mates, resting places and nectar resources [72]. Both *Aedes aegypti* and *Aedes albopictus* are daytime feeders and, while *Aedes aegypti* primarily feed on human hosts, *Aedes albopictus* are more opportunistic feeders, taking blood meals from a range of domestic and wild animals, as well as humans [73]. The average distance travelled by the mosquito varies between species, location and environment, and is primarily estimated through mark-release-recapture (MRR) studies [74]. Owing to their largely urban habitat, *Aedes aegypti* typically disperse relatively short distances. A series of MRR experiments carried out in Thailand found a range of mean dispersal distances for *Aedes aegypti* of between 28 and 199 metres [75], while an earlier MRR study in northern Kenya found a mean dispersal distance of 44.2 metres per day and 57 metres per day, for male and female *Aedes aegypti* mosquitoes respectively [76]. Similar average dispersal distances for *Aedes aegypti* have been observed in studies conducted in northern Australia [77]. Although rare, long-range dispersal events are possible. A study of the dispersal range of *Aedes aegypti* and *Aedes albopictus* mosquitoes in Brazil found that these species could potentially travel 800 metres or more over the course of six days [78].

1.4 Vector Control

1.4.1 Traditional Methods

Traditional vector control strategies for *Aedes spp.* typically focus on source reduction, and include a variety of environmental and chemical interventions such as improving water storage

and supply facilities, the removal of potential breeding sites, larviciding, and perifacial spraying (Figure 1.3) [79, 80].

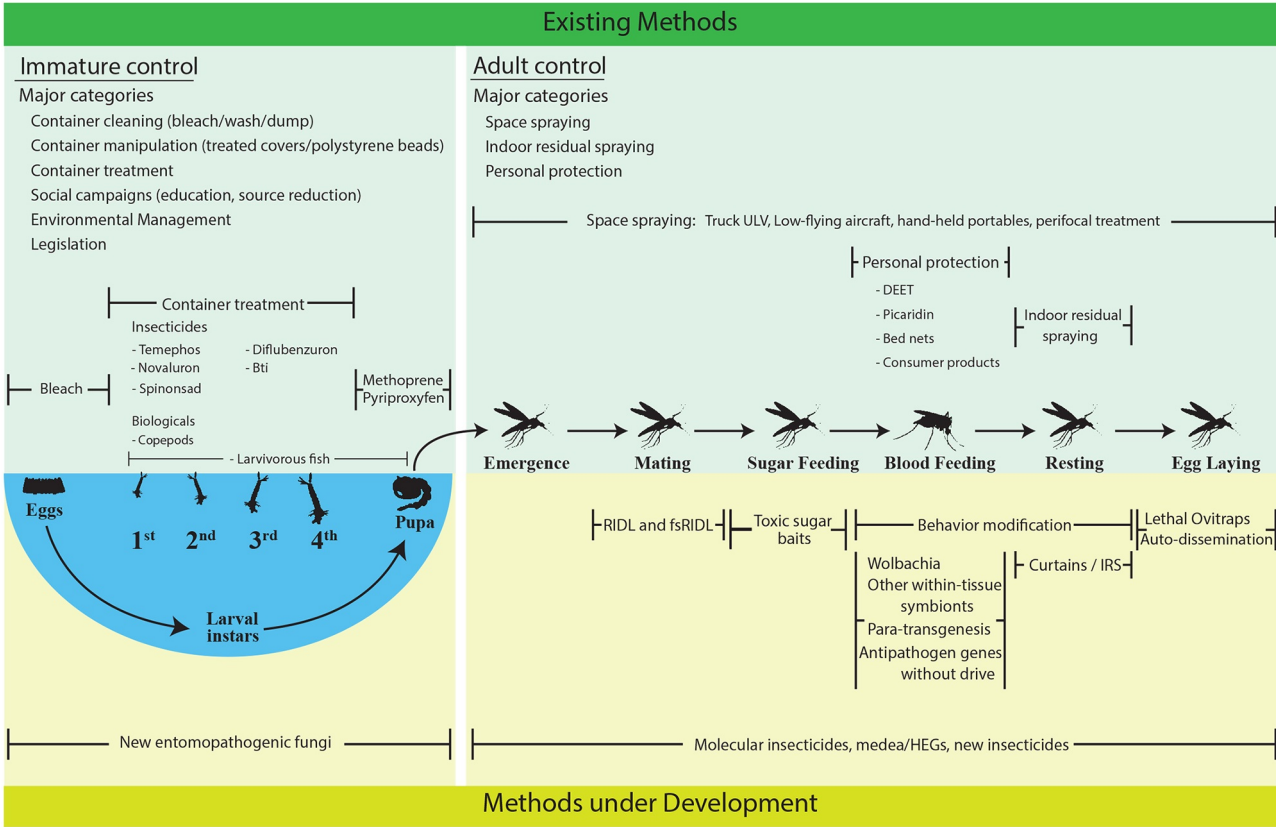


Figure 1.3: *Aedes Aegypti* Control Methods. Existing methods (upper green region) and methods under development (lower yellow region) are shown in accordance with the life-stage of the mosquito they target. Reprinted with permission from [79] (See Appendix A - Figure Permissions).

While rigorous application of these methods can lead to large reductions in vector population density as seen for example in Central and South America in the 1970s [81], Singapore in the 1970/80s [82], and Cuba in the 1980/90s [83], concerns persist over the long-term sustainability and effectiveness of these methods. These interventions are highly resource-intensive, and resistance to many commonly used insecticides, including pyrethroids and organophosphates, has emerged in many countries and is an ever growing problem [84–88]. Moreover, despite sustained vector control efforts, dengue has re-emerged in several countries following long periods of low incidence [82, 89]. Therefore, new sustainable vector control tools are urgently needed to help prevent and limit the spread of dengue [79, 80].

1.4.2 Novel Vector Control Methods

Novel vector control methods for *Aedes spp.* currently being tested include Sterile Insect Technique (SIT), Incompatible Insect Technique (IIT), Release of Insects carrying a Dominant Lethal gene (RIDL), and the release of male and female *Wolbachia*-infected *Aedes aegypti*. These approaches seek to reduce disease transmission by utilising particular aspects of the biology of the mosquito, and broadly fall into two categories; those which aim to modify the vector population such that vectors have a reduced capacity for dengue transmission (release of male and female *Wolbachia*-infected mosquitoes) and those which aim to suppress the vector population (SIT, IIT, RIDL).

Population Modification

Wolbachia is a maternally-transmitted endosymbiotic intracellular bacterium naturally present in 40%-60% of all insect species [90, 91]. Once present in a host, it manipulates the reproductive system of that host to give a reproductive advantage to *Wolbachia*-infected females relative to uninfected females, which in turn allows *Wolbachia* to spread throughout the host population. This is most commonly achieved through cytoplasmic incompatibility (CI) [90]. CI renders eggs laid following mating of an uninfected female with a *Wolbachia*-infected male non-viable (they do not hatch), whereas *Wolbachia*-infected females lay viable *Wolbachia*-infected eggs following mating with infected or uninfected males (Figure 1.4). While *Wolbachia* provides a reproductive advantage to infected hosts, it may also carry considerable fitness costs such as increased mortality and reduced fertility [90].

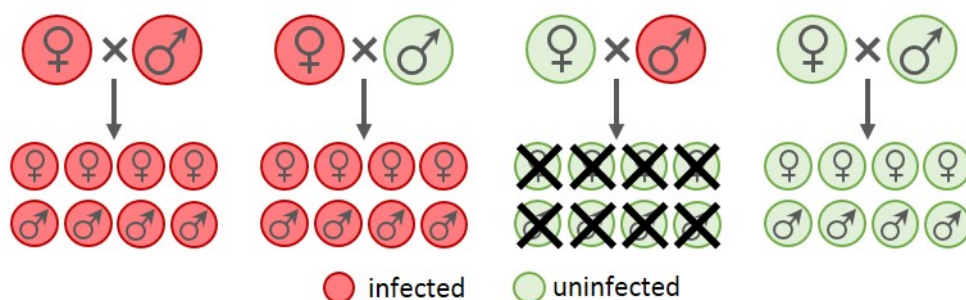


Figure 1.4: Cytoplasmic Incompatibility. Illustration of how cytoplasmic incompatibility (CI) gives *Wolbachia*-infected females a reproductive advantage. CI renders progeny of uninfected females and infected males non-viable, whereas viable progeny result from all other potential crosses. Reproduced in part from [92]. No permission required as author of study (See Appendix A - Figure Permissions).

Although naturally present in some mosquito species including *Aedes albopictus* [93] and *Culex*

pipiens [94], *Wolbachia* is not naturally present in *Aedes aegypti*. It can however be introduced into *Aedes aegypti* via transinfection, as was first illustrated by Xi *et al.* in 2005 [95]. Initially it was hypothesised that *Wolbachia* could potentially be used as a vehicle for gene-drive, with CI allowing transgenes to be introduced into *Aedes aegypti* populations. However, after infection with the highly virulent *wMelPop* *Wolbachia* strain was observed to substantially reduce the lifespan of *Drosophila melanogaster* fruit flies [96], it was proposed that *Wolbachia* could instead be used to reduce the lifespan of *Aedes aegypti*, potentially to below the extrinsic incubation period of dengue, thereby dramatically reducing transmission of the virus [97, 98].

Both *wMelPop*, and the less virulent *wMel* *Wolbachia* strain, were subsequently successfully transinfected from *Drosophila melanogaster* into *Aedes aegypti*, with associated mortality costs of approximately 50% and 10% respectively [97, 99]. The *Wolbachia*-infected *Aedes aegypti* lines created also showed almost perfect CI and maternal transmission. Moreover, unexpectedly, infection with *wMel* or *wMelPop* was shown to strongly inhibit dengue virus replication in *Aedes aegypti* [99, 100]. No evidence of dengue virus was found in the saliva of *wMelPop*-infected mosquitoes 14 days after infection with DENV2 virus, compared with 80.2% of wild-type mosquitoes [99]. While some evidence of dengue virus was found in the saliva of 4% of *wMel*-infected mosquitoes, further examination of these saliva samples suggested that this may have been caused by imperfect maternal transmission [99]. In light of these results, it is the reduced ability of *Wolbachia*-infected mosquitoes to transmit dengue, rather than the life-shortening fitness costs associated with *Wolbachia* infection, that now forms the basis of utilising *Wolbachia* for dengue control.

To test the viability of *Wolbachia*-infected *Aedes aegypti* successfully invading wild-type populations in the field, large-scale field trials were conducted in Australia and Vietnam. Field trials of *wMel* began near Cairns, Australia in January 2011 and demonstrated that successful invasion and fixation was possible, with a *Wolbachia* frequency of 90% evident five weeks after releases had ceased [101]. Analysis conducted 2-3 years after the initial releases began revealed that there was no evidence of reduced maternal transmission or CI, and that the average long-term *Wolbachia* frequency among *Aedes aegypti* was 94% [102]. Moreover, no reduction in the virus-blocking ability of *wMel*-infected *Aedes aegypti* was observed [103]. Large-scale field trials of the more virulent *wMelPop* conducted in Australia and Vietnam in

2012 and 2013 respectively revealed that, owing to high fitness costs, high initial frequencies of *wMelPop*-infected mosquitoes dropped dramatically after releases had stopped [104]. This indicated that establishment of *wMelPop*-infected *Aedes aegypti* in the field would be very challenging.

The primary aim of these trials was to establish the sustainability of this approach, and thus entomological endpoints alone were considered. However large-scale field trials (using *wMel*-infected *Aedes aegypti*) with both entomological and epidemiological endpoints are currently under way in Indonesia [105], Vietnam [106], Brazil and Columbia [107]. These trials will provide critical insight into the viability of this approach as a measure for dengue control across a range of transmission settings. Meanwhile, the first empirical epidemiological evidence of reduced dengue transmission following the establishment of *Wolbachia* in local *Aedes aegypti* populations has recently been reported. In the four years since *wMel* was successfully established in local *Aedes aegypti* populations in Townsville, northern Australia, no confirmed local dengue transmission has occurred, despite an increasing number of imported dengue cases and local transmission occurring each year since 2002 [108].

Population Suppression

The use of *Wolbachia* as a tool for dengue control is not limited to vector population modification. The CI phenotype induced by *Wolbachia* infection also allows *Wolbachia* to be used a tool for vector population suppression through the release of *Wolbachia*-infected males only (IIT). Indeed IIT was first successfully used as a vector control strategy in Myanmar in 1967 [109], during a pilot study conducted to control *Culex quinquefasciatus*, a vector of lymphatic filariasis. More recently, small scale field studies testing this approach have taken place in French Polynesia [110, 111], Kentucky [112, 113], California [114], Queensland [115, 116], and Singapore [117].

In French Polynesia, the release of *Wolbachia*-infected male *Aedes polynesiensis* (also a vector of lymphatic filariasis) over a 30 week period in 2009/10 resulted in a significant decrease in the proportion of females producing hatching egg broods (76% in the release area, compared with 93% in the control area) [111]. In 2014, *Aedes albopictus* males transinfected with the *wPip Wolbachia* strain (isolated from *Culex pipiens*) were released during a pilot study of IIT in Kentucky, resulting in a reduction in both the egg hatch rate and the mean number of adult females trapped [113]. Field studies conducted in California, Queensland and Singapore have

involved the release *Wolbachia*-infected male *Aedes aegypti*. While detailed results of the studies carried out in California and Queensland are yet to be published, initial reports have been positive. An average reduction of 68% and 80% in the occurrence of female *Aedes aegypti* in release areas compared with control areas has been reported for trials conducted California [114] and Queensland [115] respectively. The field study conducted in Singapore in 2016/2017 is the first of a series of small-scale field studies which will be undertaken to explore the use of *Wolbachia* as a tool for *Aedes aegypti* suppression in Singapore. *Wolbachia*-infected male *Aedes aegypti* were released into residential blocks in two areas of the city, and the design and results of this study will be discussed in detail in Chapters 5 and 6. To date, IIT has not been tested at a large scale.

A more traditional tool for insect population suppression is SIT which involves irradiating or chemically treating male insects so that they become sterile and therefore produce no viable offspring. Although widely used in the agricultural sector for pest control, most notably for the control of screw-worm and fruit flies [118], only a few small-scale field studies (and no large-scale studies) testing this approach in the context of mosquito population suppression have taken place [119]. Results obtained to date from small-scale studies have been mixed. A three year small-scale study conducted across multiple sites in northern Italy examining the potential impact of this technology on *Aedes albopictus* population size reported induced egg sterility ranging from 18% and 68% between sites [120, 121].

Another potential tool for *Aedes aegypti* population suppression is the release of genetically-engineered male mosquitoes which carry a dominant lethal gene (RIDL), a technology developed by Oxitec Ltd [122]. Crucially this lethal gene can be switched off by the addition of tetracycline to the diet of mosquito larvae, which in turn allows large numbers of these modified male mosquitoes to be reared. Two different transgenic *Aedes aegypti* strains have been developed to date, OX513A and OX3604C. OX513A males carry a late acting gene which causes all offspring resulting from crosses between modified males and wild-types females to die during the late stages of larval development [122]. Small-scale field trials testing this strain have been conducted in the Cayman Islands [123] and Brazil [124], resulting in 80% and 81-95% suppression respectively. Unlike OX513A which targets offspring of both sexes, OX3046C males carry a gene which targets female offspring only, rendering them flightless and thus unable

to feed and survive [125]. While initial laboratory results for this strain were promising [125], subsequent large-scale cage trials showed a mating disadvantage of approximately 60% for this strain, suggesting these males may not be suitable for large-scale releases [126].

Successful implementation of vector population suppression technologies is particularly challenging for several reasons. Irradiating, genetically engineering or chemically treating male mosquitoes may impose substantial fitness costs on the mosquito [126, 127], potentially reducing mating competitiveness and their ability to survive in the wild. For the intervention to be successful, large numbers of males need to be continuously released over a long period of time [128], and immigration of wild-type mosquitoes from surrounding areas may substantially limit the effectiveness of the intervention. Moreover, mosquito populations may quickly rebound after releases have ceased unless other effective vector control interventions are in place. Accurate sex separation of mosquitoes prior to release is also required, which can be both difficult and expensive [128]. In the case of IIT, the unintended release of *Wolbachia*-infected females risks *Wolbachia* spreading through the population, thereby modifying rather than suppressing vector populations. A combined SIT/IIT approach, which involves irradiating *Wolbachia*-infected mosquitoes, prior to release, has been suggested as a possible method of reducing this risk [127, 129, 130].

1.5 Modelling Spatial Dynamics

As mosquito population density varies geographically, so too does dengue transmission intensity, with high levels of spatial heterogeneity evident across all spatial scales, ranging from the global [22] to the individual household level [16]. While this heterogeneity stems from a variety of environmental, human and social factors including climate [131, 132], levels of urbanization [5, 133], and levels of immunity to dengue among the human population [16, 134], the primary cause of heterogeneity in transmission intensity is variation in vector density [134]. Thus, an understanding of the fine-scale dynamics (i.e. those within an area of approximately 1km² or less) of vector populations is critical to understanding the drivers of spatial heterogeneity in disease transmission and persistence at fine spatial scales, and the potential impact of vector control measures. Mathematical models provide a framework within which these dynamics can be explored, and hence play an important role in developing our understanding of the factors which shape the dynamics of mosquito populations at fine spatial scales. Therefore, there is a

large literature of models of mosquito population dynamics, particularly in relation to *Anopheles* mosquitoes, and malaria transmission and control [135]. Here, we focus on the spatial models developed to explore the fine-scale dynamics of *Aedes aegypti* populations.

1.5.1 The Metapopulation Approach

When modelling spatial dynamics, metapopulation or multi-patch models often prove a popular and flexible approach. The roots of the metapopulation concept can be traced back to the seminal work of Richard Levins in 1969, where he examined the potential effectiveness of a pest control program for “a population of populations in which local extinctions are balanced by remigration from other populations” [136]. Thus, a metapopulation is defined as a set of spatially separated local populations (‘patches’) which interact through individuals moving among these populations [137]. This concept describes a move away from considering spatially separated populations in isolation to instead considering these populations as a network of local populations (connected through movement between local populations), which together form a single larger population. This, in turn, allows the role of spatial structure in population growth and persistence to be explored. This is particularly important when population sizes are small as, in any given network of populations, a combination of demographic and environmental stochasticity may render small local populations unstable. Small local populations are therefore at continual risk of extinction. However, coupling of these local populations via dispersal may have a “rescue effect” and allow local populations to persist where otherwise extinction may occur [138, 139]. Nonetheless, this is dependent on the level of dispersal between local populations, with poorly connected small local populations at greater risk of extinction than better connected local populations of a similar size [138, 140]. This continuous cycle of extinction and recolonization means that, although persistence at the local level may be quite unstable, persistence of the population as a whole may remain stable [139]. Metapopulation models therefore often seek to describe the balance between extinction and recolonization required for a metapopulation as a whole to persist, and to determine the likely length of population persistence [141].

Several different types of metapopulation model have been developed and, since Levins first introduced the concept of a metapopulation [136], metapopulation models have increased in terms of both complexity and realism [142, 143]. Levins’ model, often termed a ‘classical metapopulation model’ [143], is a deterministic model which considers how the proportion of patches occupied

across a fragmented landscape changes over time [136]. Under this model, local populations are classified as either present or absent, all patches are assumed to be the same size and equally connected, and each local population is assumed to experience a significant risk of extinction [136]. Thus, while this model provides a useful framework for exploring changes in habitat occupancy across a landscape, the assumptions underlying the model only describe a small subset of real-world metapopulations and landscapes. Therefore, metapopulation models subsequently developed have sought to allow for more realistic characterisations of fragmented landscapes and species behaviour. For example, shortly after the Levins' model was published, Boorman and Levitt proposed the concept of a mainland-island metapopulation model [143, 144], whereby the metapopulation is comprised of one, large stable local population (the 'mainland') and several small, unstable local populations or 'islands', with persistence of these 'island' populations dependent on emigration from the mainland [143, 144]. Thus this model allows patches of in a metapopulation model to differ in size [143, 144]. Subsequent advances in metapopulation modelling resulted in the development of 'spatially-explicit' metapopulation models, which allow for distance-dependent migration between local populations [143, 145]. These models therefore describe more realistic landscapes where not all local populations are equally connected, and where interaction only occurs among neighbouring populations [143, 145]. Further extensions of this approach have led to the development of stochastic "spatially-realistic" metapopulation models which, in addition to distance-dependent migration, allow for the patch area and location to be accounted for within the modelling framework [143, 145].

Adopting a metapopulation framework allows population dynamics to be explored at different spatial scales, and therefore metapopulation models, in combination with empirical studies, have been extensively used in ecology and conservation biology to explore the population dynamics and persistence of a range of different species, across a variety of landscapes. Examples of species shown to exhibit metapopulation structure include several butterfly and bird species [146–152], round-tailed muskrats [153], the American pika [154, 155], aquatic snails [156], and populations of bull trout [157]. Evidence of the vulnerability of small local populations to extinction is common to all of these studies, with local populations experiencing a high rate of population turnover owing to recurrent extinction and recolonization at the local level.

Indeed the dynamics of the American pika population in Bodie, California is considered one of the best known examples of a real-world metapopulation, and hence is the subject of long-term empirical study which has been in place since the 1970's [143, 154, 155]. In this region, the species inhabits a network of small, connected habitats of broadly similar size, with all local populations having a significant risk of extinction [143, 154, 155]. Empirical evidence collected throughout this study has shown that, although individual patches experiencing a high rate of population turnover, patch occupancy in the northern half of the study area has remained stable during the study period [154, 155]. Conversely, patch occupancy in the southern half of the study area steadily declined over the course of the study, resulting in the eventual collapse of the population in the southern half [154, 155]. Interestingly, metapopulation modelling of this system suggests that the population decline in the southern half of the study area can largely be attributed to an imbalance between extinction and recolonization in this part of the metapopulation, rather than any substantial environmental changes [154]. Thus, this study highlights how critical maintaining a balance between extinction and recolonization is to local persistence in real-world metapopulations, and the importance of metapopulation structure to shaping the spatial dynamics of fragmented populations across a landscape.

In addition to exploring the mechanisms of species persistence, metapopulation models have also been used to explore a variety of ecological processes including, for example, predator-prey interactions [158], and the population dynamics of multiple species [159, 160] in a fragmented landscape. In addition, metapopulation models have been used in the context of infectious disease modelling to provide insight into the persistence of disease and the fine-scale dynamics of disease transmission [161, 162]. For example, metapopulation models have been used to show that the Bubonic plague can persist in small rodent populations in the absence of newly imported cases [163], and that heterogeneous biting and poor mixing between mosquitoes and human hosts may lead to slower and more variable spread of a mosquito-borne pathogen through a human population [164].

1.5.2 Spatial Models of *Aedes aegypti* Population Dynamics

Metapopulation models have also been used to explore the fine-scale dynamics of *Aedes aegypti* populations, with models varying in structure, complexity and underlying biological assumptions. One of the most detailed models which has been developed is 'Skeeter Buster', a

spatial stochastic simulation model of *Aedes aegypti* population dynamics which models juvenile populations at the individual breeding container level, and adult populations at the individual household level [165]. Each patch in the model thus represents an individual household which contains a number of different breeding sites, and adult mosquitoes can disperse from one patch to another. This model extends an earlier non-spatial deterministic life table model of *Aedes aegypti* population dynamics developed by Focks *et al.* [166] which incorporates a high level of detail on both the life cycle and environment of the mosquito, including pupal size, temperature dependent development rates, the type of breeding container and the availability of food resources. In addition to accounting for individual breeding container and household spatial structure, Skeeter Buster also allows the genetic structure of the mosquito population to be included in the model. Thus it is designed to be customized to individual locations [165], and has been shown to broadly replicate *Aedes aegypti* population dynamics observed in Iquitos, Peru and Buenos Aires, Argentina [167].

Otero *et al.* [168] also used a metapopulation approach, developing a spatial stochastic compartmental model which, while considerably simpler in structure than Skeeter Buster, still accounts for the full life cycle of the mosquito and temperature-dependent development and mortality rates. This model has also been calibrated against data from Buenos Aires [168], and recent extensions of the model have included a more detailed hatching and pupation process [169]. However the model is primarily designed to capture population dynamics at the city block level, and dispersal is limited to adjoining neighbouring patches only. Lutambi *et al.* [170] use both a continuous space and metapopulation approach to explore the effects of mosquito dispersal in an environment where human hosts and mosquito breeding sites are distributed heterogeneously across patches. The full life cycle of the mosquito is considered and, while these models were originally parameterized to represent the dynamics of *Anopheles gambiae* populations, they could also be used to explore the fine-scale dynamics of *Aedes aegypti*. However, one of the main limitations of the metapopulation model developed is that dispersal is limited to directly adjoining patches.

A small number of agent based models have also been developed to explore the fine-scale dynamics of *Aedes aegypti*. de Almeida *et al.* [171] developed a detailed multi-agent model which includes mosquitoes, humans and some animals as agents, and accounts for a variety

of environmental and human factors including the availability of human and animal blood meal sources, the availability of breeding sites, climate and vegetation. More recently, Maneerat and Daudé [172] developed an agent based model of female *Aedes aegypti* population dynamics which also accounts for a wide range of factors including features of the underlying landscape, climate, and the biting and dispersal behaviour of the mosquito.

1.6 Modelling the Impact of Novel Vector Control Measures

Part of the work presented in this section formed the basis of my contribution to:

I. Dorigatti, C. McCormack*, G. Nedjati-Gilani*, & N. M. Ferguson. Using Wolbachia for Dengue Control: Insights from Modelling. Trends in Parasitology, vol. 34, no. 2, pp.102-113, 2018 (* equal contributions)*

Mathematical modelling has played a key role in advancing our understanding of the potential impact of novel vector control measures, highlighting key factors and challenges in the application of these technologies. Models which have been developed to explore the dynamics of population suppression and modification measures include:

- deterministic delay-differential equation models which typically describe the mosquito population using a single equation but may be extended to include age structure [122, 173–176]
- spatial and non-spatial compartmental models which account for the life-cycle of the mosquito and other factors such as environmental heterogeneities and seasonal changes in mosquito abundance [177–183]
- reaction-diffusion models which describe the spatial spread of *Wolbachia* [184–186]
- population genetic models which, rather than focusing on changes in abundance, instead primarily describe the infection frequency required for *Wolbachia* to successfully invade a host population and consider the population as comprised of either discrete or overlapping generations [186–189]

Indeed, the importance of infection frequency for the use of *Wolbachia* as a tool for population modification was first illustrated by Caspari and Watson using a discrete generation population genetic model [187]. Here the authors demonstrated that, owing to the trade-off between the

fitness benefits and costs incurred by infection with the bacteria, *Wolbachia* advances through a population with bistable dynamics. Namely, once introduced into a population, *Wolbachia* frequency reaches a stable equilibrium at one of two states - one where infection frequency is zero and the other where there is a high proportion of infected individuals (Figure 1.5). For *Wolbachia* to successfully invade a population and reach this non-zero equilibrium, initial infection frequency must exceed a threshold value determined by the trade-off between the relative reduction in fecundity of *Wolbachia*-infected females and the relative reduction in the proportion of viable eggs among all eggs laid owing to incompatible matings between *Wolbachia*-infected females and wild-type males.

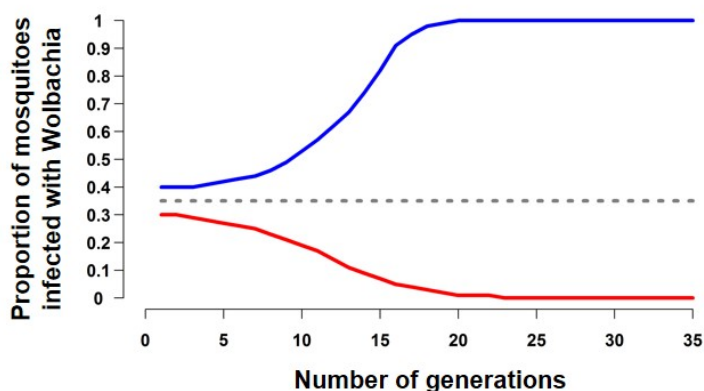


Figure 1.5: Bistable Dynamics of *Wolbachia*. CI allows *Wolbachia*-infected mosquitoes to displace wild-type mosquitoes (blue curve) if introduced into a population above a threshold frequency (dashed line) which is determined by the fitness costs of *Wolbachia*. If introduced below this threshold frequency (red curve), *Wolbachia*-infected mosquitoes are out-competed by the wild-type, despite CI. Reproduced in part from [92]. No permission required as author of study (See Appendix A - Figure Permissions).

Extensions of this model accounting for overlapping generations [190] and imperfect maternal transmission [184] provided further insight into these dynamics, showing that this critical threshold would also depend on the degree of vertical transmission of the bacteria and the age structure and growth rate of the population. Although this threshold value will vary between populations, initial analyses suggested that, for *Wolbachia* to spread throughout a population, the critical threshold frequency could not exceed 0.5 [186, 191]. However, more recent analysis has shown that the speed of spatial spread slows dramatically as the critical threshold approaches 0.5, suggesting that, in practical terms, a critical threshold frequency of 0.35 or less is necessary to initiate spatial spread of *Wolbachia* in a population [192].

Spatial spread is not a relevant factor for population suppression technologies. However, common

factors predicted to influence the effectiveness of both population suppression and population modification technologies include mosquito behaviour [175, 185, 192], the age and spatial structure of the mosquito population [177, 178, 181, 184, 190, 193, 194], density-dependent effects [122, 173, 195], the release strategy employed [174, 181, 182, 192, 193] and features of the surrounding environment [178, 179, 196, 197].

The importance of accounting for density-dependent effects when exploring the potential impact of these technologies has been recognised from an early stage, with Barclay and Mackauer using a simple logistic growth model to illustrate that accounting for density-dependent effects would be key to understanding the potential effectiveness of SIT [173]. More recently, Phuc *et al.* used mathematical modelling to investigate how density-dependent regulation of larval populations would affect the potential effectiveness of RIDL. The authors found that targeting mosquito populations during the later stages of larval development, after density-dependent regulation has occurred, would require fewer males to be released and substantially reduce the risk of inadvertently increasing population size via reduced larval competition, thereby maximising the potential of this technology [122]. The interaction between density-dependent competition and release size is also a key consideration for population modification strategies, as mathematical modelling has predicted that larger releases may be required to initiate spatial spread of *Wolbachia* in populations subject to a greater degree of competition [180, 181, 183].

Release strategy is a critical factor for all population suppression and modification technologies, as potential impact is predicted to depend strongly on the number, frequency, timing and size of releases [174, 182, 193]. For example, a modelling study by White *et al.* [174] showed that, in the context of population suppression technologies such as SIT and RIDL, smaller, more frequent releases may be more effective than larger, less frequent releases. In addition, this study suggested that, given mosquito abundance typically varies seasonally, potential impact would also depend on the timing of releases [174]. Hancock *et al.* showed a similar result in the context of population modification strategies, finding that *Wolbachia* releases performed early in the wet season to coincide with the early stages of population growth were more likely to result in successful *Wolbachia* establishment [182].

Effectiveness of novel vector control measures will also depend on the dispersal behaviour of

the mosquito. As noted earlier, dispersal of wild-type mosquitoes from surrounding areas may substantially reduce the potential impact of population suppression technologies such as SIT and IIT [128, 175, 193]. In terms of population modification, the typical dispersal range of the mosquito is predicted to affect the speed at which *Wolbachia* spreads through a population, with long range dispersal predicted to slow the speed of spatial spread [192]. The speed of spread is furthermore likely to strongly depend on the level of heterogeneity in the underlying landscape with environmental heterogeneities, such as sharp changes in mosquito population density or the quality of larval habitats, predicted to slow or even halt the spatial spread of *Wolbachia* unless migration of infected mosquitoes from neighbouring areas is sufficient to allow the critical threshold frequency to be exceeded at the local level [185, 192, 196, 197].

Although many models have been developed to explore the impact of novel vector control measures on mosquito population dynamics, to date, few models have been developed which explore the potential impact of these measures on dengue transmission. Atkinson *et al.* [198] initially explored the potential impact of RIDL on dengue transmission dynamics using a simple single serotype non-spatial compartmental model of dengue transmission, showing that this technology could have a large impact on dengue transmission, if the logistical challenges of implementing this type of intervention could be overcome. A more detailed analysis of the potential impact of RIDL was subsequently undertaken by Alphey *et al.* [176] using a two serotype model of dengue transmission and accounting for likely cost of this type of intervention. Assuming that released transgenic males were fully competitive and that the genetic construct was 100% lethal, the authors estimated that sustained releases over a long period had the potential to (cost-effectively) eliminate dengue in different settings over a very short timescale.

Several modelling studies have explored the potential impact of *Wolbachia* as a tool for vector population modification on disease transmission [92, 182, 199–202]. Simplified compartmental models of dengue transmission have been used to explore the potential impact of *Wolbachia* on transmission in non-endemic settings [200–202], primarily in the context of outbreak size. Hancock *et al.* [182] examined the impact of *Wolbachia* on transmission of a malaria-like disease, comparing male-biased and equal sex ratio releases. Here the authors found that male-biased releases could also lead to *Wolbachia* establishment, and hence to a substantial reduction in disease transmission. Hughes and Briton [199] explored the potential impact of *Wolbachia* on

dengue transmission dynamics for a variety of transmission settings, concluding that *Wolbachia* would have the largest impact in low transmission settings.

The potential impact of *Wolbachia* (as a tool for vector population modification) on transmission for different dengue serotypes has been investigated by Ferguson *et al.* [203]. Using a mathematical model which coupled data collected through experiments to assess the level of viral suppression in *wMel*-infected *Aedes aegypti* upon challenge with blood from dengue patients, with data on the dynamics of dengue infection within the human host, the authors examined the likely impact of *wMel* infection on the basic reproduction number of dengue (the average number of secondary human infections generated by a single human infection in a fully susceptible population), R_0 , for each dengue serotype. *wMel*-infection was predicted to reduce R_0 by 66% for DENV1 and 75% for DENV-2,3,4. Incorporating these estimates into a four-serotype model of dengue transmission, Dorigatti *et al.* [92] estimated that the widespread release of *wMel*-infected *Aedes aegypti* could allow dengue to be eliminated permanently in low to moderate transmission settings, and for several decades in high transmission settings, with transmission only resuming when herd immunity in the human population declines.

1.7 Overview of Thesis

Given the advances made in recent years in the development of novel vector control measures, the landscape of dengue control is evolving. These approaches offer a promising new pathway for the control of *Aedes aegypti* populations, and thus for the control of dengue across a wide range of transmission settings. Mathematical modelling has an important role to play in assessing the likely impact of these new measures, and in developing our understanding of the challenges which may be faced in successfully implementing these approaches. While models of novel vector control measures developed to date offer valuable insights into the potential impact of these approaches, improved models of fine-scale *Aedes aegypti* dynamics are needed to realistically model the likely impact of novel vector control measures, with the final goal being spatially explicit stochastic models of fine-scale *Aedes aegypti* population dynamics, calibrated against high quality entomological data. However, development of such models is challenging, as some important gaps in our knowledge remain.

First, while several very detailed mathematical models of fine-scale *Aedes aegypti* population

dynamics have been developed, such as Skeeter Buster [165], the complexity of these models hinders our ability to disentangle the different factors driving population dynamics at fine spatial scales - mosquito behaviour, spatial structure, temperature, climate, availability of resources, and genetic factors. On the other hand, simpler models often consider population dynamics at a lower level of spatial granularity [168, 170] (for example, at the city block level rather than at the individual household level, thereby often limiting dispersal to nearest neighbours only). Alternatively they have largely been developed to explore the potential impact of novel vector control measures [180–182], and therefore have not been developed with the primary aim of examining the role of spatial structure in shaping the fine-scale dynamics of *Aedes aegypti* populations. Furthermore, although larval populations of *Aedes aegypti* are often highly fragmented [47, 61], mathematical models of dengue transmission [198, 204, 205], which consider larval population dynamics, largely adopt a non-spatial approach to represent the dynamics of *Aedes aegypti* larval populations. Thus some fundamental questions about the fine-scale dynamics of *Aedes aegypti* populations remain. Namely, how important is spatial structure in shaping the dynamics of *Aedes aegypti* populations at fine spatial scales? How do vector populations persist in fragmented landscapes? What is an appropriate level of spatial granularity for models to adopt to best represent the fine-scale dynamics of *Aedes aegypti* populations?

Second, although many models assessing the likely impact of population suppression strategies have been developed, to date, none have been calibrated against the detailed entomological data collected during field studies testing these approaches. Therefore, the insight they provide into the challenges of implementing these strategies in real urban environments is limited.

In this thesis, we aim to address these gaps in our knowledge by examining the appropriate level of spatial granularity models of fine-scale *Aedes aegypti* population dynamics should adopt, and by developing a framework which allows us to calibrate stochastic models of *Aedes aegypti* population dynamics against high quality entomological data, while allowing for the highly variable nature of mosquito trapping data.

Chapters 2-4 of this thesis explore the role of spatial structure in shaping the dynamics of *Aedes aegypti* populations at fine spatial scales. In Chapter 2 we present the model of fine-scale

Aedes aegypti dynamics developed, and examine the impact of larval habitat fragmentation on *Aedes aegypti* population dynamics in spatially homogeneous landscapes. In Chapters 3 and 4 we build on the work presented in Chapter 2 by exploring how spatial heterogeneity in carrying capacity and the level of spatial granularity in our model affects the dynamics observed.

In Chapters 5 and 6 we extend the model developed in Chapter 2 to analyse the results of a small scale field trial testing the use of *Wolbachia* as a tool for *Aedes aegypti* population suppression in Singapore by calibrating a model of IIT against the detailed entomological data collected during this trial. In Chapter 5 we describe the study design, the model developed and inferential framework developed. In Chapter 6 we present our results and discuss the implications of our findings for population suppression strategies.

We conclude in Chapter 7 by discussing the key findings of this thesis, their importance in the context of modelling fine-scale *Aedes aegypti* population dynamics and novel vector control measures, and future directions of this work.

Chapter 2

Homogeneous Landscapes

In Chapters 2-4, I explore the role of spatial structure in shaping the dynamics of *Aedes aegypti* populations at fine spatial scales, with the aim of understanding what is an appropriate level of spatial granularity for models to adopt when representing the fine-scale dynamics of *Aedes aegypti* populations.

2.1 Introduction

In any given environment, the density of adult mosquitoes is largely determined by two key factors. First, the mortality rate of adult mosquitoes and, second, the rate at which new adult mosquitoes emerge from larval breeding sites. The capacity of larval breeding sites to produce new adult mosquitoes is constrained however by the availability of resources at those sites, and thus larval populations are regulated [59, 62–66]. It is generally assumed that such regulation is dominated by density-dependent intraspecific competition, whereby larvae in a single breeding site compete for food and other resources [59, 62–66].

Larval breeding sites of *Aedes aegypti* are often highly fragmented [47, 59, 60], with mixing among the population determined by the dispersal [72, 206] and oviposition behaviour [50, 207] of the mosquito. Thus, given that density-dependent competition is a non-linear process, the dynamics of larval population regulation in a fragmented landscape are likely to be complex. However, our understanding of the importance of this underlying fragmented spatial structure in shaping the fine-scale dynamics of *Aedes aegypti* populations is limited.

Mathematical models of fine-scale *Aedes aegypti* population dynamics which have been

developed to date are often highly complex in structure [165, 171, 172], incorporating a wide range of detail on environmental and biological factors. Simpler models tend to model population dynamics at lower levels of spatial granularity (e.g. city block level) [168, 170], or alternatively focus on exploring the likely impact of vector control measures, rather than role of spatial structure per se [180–182]. Furthermore, mathematical models of dengue transmission which consider larval population dynamics [198, 204, 205] tend to adopt a very simple representation of density-dependent competition. Namely, the entire larval population is treated as a well-mixed population coming from a single large breeding site, and the larval mortality rate is assumed to increase linearly with larval population size. However, as mentioned above, density-dependent competition is a non-linear process, and hence it cannot be assumed that modelling a single large well-mixed larval population will generate the same dynamics as a model which explicitly represents a network of fragmented local populations.

Ecological research has shown that habitat fragmentation can lead to increased population instability and decreased population persistence, as a combination of demographic and environmental stochasticity places small local populations at continual risk of extinction [138–140, 160, 208]. Nonetheless, coupling between fragmented local populations can offset these effects as migration from neighbouring habitats may allow extinct populations to be reseeded, thereby increasing local population persistence. Examples of species whose persistence in the face of habitat fragmentation has been enabled by metapopulation effects include several butterfly species [208–210] and the American pika [154, 155].

If similar results hold for *Aedes aegypti* populations, this could have important implications for mathematical models of *Aedes aegypti* population dynamics, which consider larval population dynamics, particularly in the context of estimating the potential impact of novel vector control measures and vector population persistence at fine spatial scales. Hence, to explore the impact of accounting for the fragmented structure of larval populations when modelling the dynamics of *Aedes aegypti* populations at fine spatial scales, we developed a stochastic metapopulation model of fine-scale *Aedes aegypti* population dynamics, and considered the effects of fragmentation on the dynamics observed by modelling the same mosquito population at different levels of spatial granularity - corresponding to different levels of fidelity in representing the true underlying spatial structure of mosquito populations. We explored how habitat fragmentation,

features of the underlying landscape and the level of spatial granularity in the model affect the dynamics observed, with the overall aim of understanding the role and importance of spatial structure in shaping the dynamics of *Aedes aegypti* populations at fine spatial scales.

This, and the following two, chapters describe the results of this work. In this chapter, I present the metapopulation model of fine-scale mosquito population dynamics developed and then begin our analysis by exploring the impact of habitat fragmentation on fine-scale mosquito population dynamics for urban landscapes with no spatial variation in larval carrying capacity across patches. At the end of this chapter and Chapter 3, a brief summary and discussion of the results contained therein is provided, and a more general discussion of the implications and importance of our results for models of *Aedes aegypti* population dynamics is provided at the end of Chapter 4.

2.2 Methods

2.2.1 Model Structure

We developed a fine scale stochastic metapopulation model of mosquito population dynamics, where patches are arranged in an $n \times n$ grid, and each individual patch (i, j) represents a local mosquito population ($1 \leq i, j \leq n$). Local populations are comprised of an egg, larval and an adult female mosquito population. Thus, when $n = 1$, the model reduces to the single patch model with homogeneous mixing. Local populations are connected through adult mosquito dispersal, where adult mosquitoes can move to and lay eggs in neighbouring patches, and the deterministic dynamics of a local mosquito population in patch (i, j) are described by the following set of equations:

$$\frac{dE_{ij}(t)}{dt} = bgO_{ij}(t) - \gamma_E E_{ij}(t) - \mu_E E_{ij}(t) \quad (2.1)$$

$$\frac{dL_{ij}(t)}{dt} = \gamma_E E_{ij}(t) - \gamma_L L_{ij}(t) - \mu_L \left(1 + \left(\frac{L_{ij}(t)}{K_{ij}(t)} \right)^\Omega \right) L_{ij}(t) \quad (2.2)$$

$$\frac{dA_{ij}(t)}{dt} = M_{ij}(t) + \gamma_L L_{ij}(t) - \mu_A A_{ij}(t) \quad (2.3)$$

$$O_{ij}(t) = g^{-1} A_{ij}(t) \quad (2.4)$$

Here $E_{ij}(t)$, $L_{ij}(t)$ and $A_{ij}(t)$ denote the egg, larval and adult population in the patch at time t respectively, $M_{ij}(t)$ denotes the net migration of adult mosquitoes into the patch at time t , $K_{ij}(t)$ denotes the larval carrying capacity of the patch at time t , Ω describes the strength of density

dependence, $O_{ij}(t)$ denotes the number of adult mosquitoes laying eggs in the patch at time t , b denotes the oviposition rate, γ_E and γ_L denote the development rate of eggs and larvae respectively, g denotes the length of the gonotrophic cycle of adult female mosquitoes, and μ_E , μ_L and μ_A denotes the egg, larval and adult mosquito mortality rate respectively.

The basic mosquito reproduction number, R_M , for our model is defined as the average number of adult females produced by a single female mosquito during her lifespan in the absence of population regulation, and is given by

$$R_M = b \frac{\gamma_E}{\gamma_E + \mu_E} \frac{\gamma_L}{\gamma_L + \mu_L} \frac{1}{\mu_A} \quad (2.5)$$

Here $\frac{b}{\mu_A}$ describes the average number of eggs laid by a female over the course of her lifetime, while the terms $\frac{\gamma_E}{\gamma_E + \mu_E}$ and $\frac{\gamma_L}{\gamma_L + \mu_L}$ account for mortality during the egg and larval stage respectively when determining the average number of females produced. Here, the value of b is assigned so that R_M remains fixed.

To approximate the continuous time dynamics described by equations 2.1-2.4 above, we implemented a discrete time stochastic version of this model as detailed below. We chose a timestep of one eighth of a day ($\delta t = 0.125$) as this was sufficiently small to avoid any timestep-dependent effects in model results. Large timesteps (e.g. $\delta t = 1$) could potentially introduce timestep-dependent effects in model results, particularly when local population sizes are small. However, we observed quantitatively similar model results for $\delta t = 0.125$, $\delta t = 0.0625$ and $\delta t = 0.03125$, hence decided $\delta t = 0.125$ was sufficiently small.

The model was implemented as follows:

Egg Population

In a time step of size $\delta t = 0.125$, we draw $O_{ij}(t)$, the number of adult mosquitoes laying eggs in patch (i, j) at time t , from a Binomial distribution

$$O_{ij}(t) \sim Bin(A_{ij}(t), g^{-1}) \quad (2.6)$$

and $N_{ij}^E(t)$ the number of eggs laid in patch (i, j) at time t , from a Poisson distribution

$$N_{ij}^E(t) \sim \text{Poisson}(bgO_{ij}(t)\delta t) \quad (2.7)$$

We then determine $N_{ij}^L(t)$ and $D_{ij}^E(t)$, the number of new larvae and deaths during the egg stage in patch (i, j) at time t respectively, using a competing hazards model as follows:

$$h_{ij}^E(t) = \gamma_E + \mu_E \quad (2.8)$$

$$p_{ij}^E(t) = 1 - e^{(-h_{ij}^E(t)\delta t)} \quad (2.9)$$

$$T_{ij}^E(t) \sim \text{Bin}(E_{ij}(t), p_{ij}^E(t)) \quad (2.10)$$

$$N_{ij}^L(t) \sim \text{Bin}\left(T_{ij}^E(t), \frac{\gamma_E}{h_{ij}^E(t)}\right) \quad (2.11)$$

$$D_{ij}^E(t) = T_{ij}^E(t) - N_{ij}^L(t) \quad (2.12)$$

where $h_{ij}^E(t)$ describes the total hazard of leaving the egg population in patch (i, j) at time t , $p_{ij}^E(t)$ describes the probability of leaving the egg population in patch (i, j) at time t , and $T_{ij}^E(t)$ denotes the total number of eggs leaving patch (i, j) at time t . The hazard describes the instantaneous rate of a particular event occurring in a small time interval $(t, t + \delta t)$ [211]. As we have a discrete-time model, we convert this rate into a probability (as described in equation 2.9 above) to enable us to model transition between compartments of our model.

The egg population in patch (i, j) at time $(t + 1)$ is given by

$$E_{ij}(t + 1) = E_{ij}(t) + N_{ij}^E(t) - N_{ij}^L(t) - D_{ij}^E(t) \quad (2.13)$$

Larval Population

A similar competing hazards model is used with respect to the larval population to determine the number of new adult mosquitoes ($N_{ij}^A(t)$) and larval deaths ($D_{ij}^L(t)$) in (i, j) at time t . Thus we have

$$h_{ij}^L(t) = \gamma_L + \mu_L \left(1 + \left(\frac{L_{ij}(t)}{K_{ij}(t)}\right)^\Omega\right) \quad (2.14)$$

$$p_{ij}^L(t) = 1 - e^{(-h_{ij}^L(t)\delta t)} \quad (2.15)$$

$$T_{ij}^L(t) \sim \text{Bin}(L_{ij}(t), h_{ij}^L(t)) \quad (2.16)$$

$$N_{ij}^A(t) \sim \text{Bin}\left(T_{ij}^L(t), \frac{\gamma^L}{h_{ij}^L(t)}\right) \quad (2.17)$$

$$D_{ij}^L(t) = T_{ij}^L(t) - N_{ij}^A(t) \quad (2.18)$$

where $h_{ij}^L(t)$ denotes the total hazard of leaving the larval population in (i, j) at time t , $p_{ij}^L(t)$ denotes the probability of leaving the larval population in (i, j) at time t , and $T_{ij}^L(t)$ denotes the total number of larvae leaving patch (i, j) at time t . The larval population in patch (i, j) at time $(t + 1)$ is therefore given by

$$L_{ij}(t + 1) = L_{ij}(t) + N_{ij}^L(t) - N_{ij}^A(t) - D_{ij}^L(t) \quad (2.19)$$

Adult Mosquito Population

We define $h_{ij}^A(t)$, the total hazard with respect to an individual adult mosquito of leaving the adult population in patch (i, j) at time t , as

$$h_{ij}^A(t) = r + \mu_A \quad (2.20)$$

where r denotes the dispersal rate of an individual adult mosquito, and μ_A denotes the adult mosquito mortality rate. We determine the number of adult mosquito deaths ($D_{ij}^A(t)$) and the total number of adult mosquitoes dispersing from patch (i, j) at time t ($F_{ij}(t)$), as follows

$$p_{ij}^A(t) = 1 - e^{(-h_{ij}^A(t)\delta t)} \quad (2.21)$$

$$T_{ij}^A(t) \sim \text{Bin}(A_{ij}(t), h_{ij}^A(t)) \quad (2.22)$$

$$D_{ij}^A(t) \sim \text{Bin}\left(T_{ij}^A(t), \frac{\mu_A}{h_{ij}^A(t)}\right) \quad (2.23)$$

$$F_{ij}(t) = T_{ij}^A(t) - D_{ij}^A(t) \quad (2.24)$$

where $p_{ij}^A(t)$ describes the probability of leaving the adult population in patch (i, j) at time t and, $T_{ij}^A(t)$ denotes the total number of adult mosquitoes leaving patch (i, j) at time t

To model the dispersal dynamics of a local adult mosquito population, we characterise the distance travelled by an adult mosquito in terms of the distance between the centroids of patches on the grid, with $d_{(ij)-(i'j')}$ denoting the distance between patches (i, j) and (i', j') . We set $d_{(ij)-(ij)} = d_0 = 0.5214$ (the average distance travelled between two random points in a unit

square) to allow for the scenario where mosquitoes disperse but remain within the same patch. While the number of mosquitoes dispersing at time t is dependent on the size of the timestep, the distance travelled by dispersing mosquitoes is not timestep-dependent.

To determine the number of mosquitoes dispersing a distance d , we use a discretised version of a continuous space negative exponential dispersal kernel of the form

$$\frac{1}{2\pi a^2} e^{(-\frac{d}{a})}, \quad a > 0 \quad (2.25)$$

where $m = 2a$ describes the mean distance travelled [212]. A negative exponential kernel was chosen to reflect that *Aedes aegypti* typically disperse short distances, and that long range dispersal events are rare [75, 76]. To aid computational efficiency we set a maximum dispersal distance D . Thus, for patches (i, j) and (i', j') , a mean dispersal length m , and dispersal distance d , we set

$$q(d_{(ij)-(i'j')}) = \begin{cases} \frac{1}{2\pi a^2} e^{(-\frac{d_{(ij)-(i'j')}}{a})} & \text{for } d \leq D \\ 0 & \text{for } d > D \end{cases} \quad (2.26)$$

Mosquitoes are assumed not to disperse outside of the modelled population. Thus to obtain $p(d_{(ij)-(i'j')})$, the probability of dispersing the distance $d_{(ij)-(i'j')}$ (Figure 2.1), we normalise the values generated by the kernel in the following way:

$$p(d_{(ij)-(i'j')}) = \begin{cases} \frac{q(d_{(ij)-(i'j')})}{S} + (1 - \frac{s_{ij}}{S}) & \text{for } d = d_0 \\ \frac{q_{ij}(d_{(ij)-(i'j')})}{S} & \text{for } d_0 < d \leq D \end{cases} \quad (2.27)$$

where

$$s_{ij} = \sum_{(i',j') | d_{(ij)-(i'j')} \leq D} q(d_{(ij)-(i'j')}) \quad (2.28)$$

$$S = \max_{(i,j)} \{s_{ij}\} \quad (2.29)$$

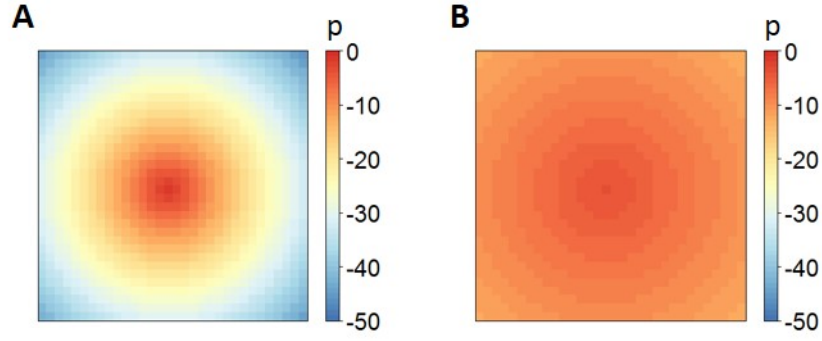


Figure 2.1: Dispersal Probabilities. The probability of dispersal from the patch at the centre of the grid to patches elsewhere on the grid when (A) the mean dispersal length is 1 and (B) the mean dispersal length is 5. Probability values are shown on a natural logarithm scale.

The hazard (with respect to an individual adult mosquito) of dispersing to a specific patch at distance d^* from (i, j) is given by

$$h_{ij}(d^*) = rp(d^*)n_{ij}(d^*) \quad (2.30)$$

where $n_{ij}(d^*)$ denotes the number of neighbours of patch (i, j) at distance d^* from (i, j) , $p(d^*)$ denotes the probability of dispersing distance d^* , and r denotes the dispersal rate. Hence we have

$$\sum_{d^*=d_0}^D h_{ij}(d^*) = r \quad (2.31)$$

Having found the total number adult mosquitoes dispersing from patch (i, j) at time t ($F_{ij}(t)$) (equation (2.24)), we determine the number of those mosquitoes dispersing to each distance d^* ($F_{ij}(t, d^*)$) using a competing hazards model as follows

$$F_{ij}(t, d^*) \sim Bin\left(F_{ij}(t) - \sum_{d=d_0}^{d^*} F_{ij}(t, d), \frac{p(d^*) \cdot n_{ij}(d^*)}{r - \sum_{d=d_0}^{d^*} p(d) \cdot n_{ij}(d)}\right) \quad (2.32)$$

Thus we have

$$\sum_{d^*=d_0}^D F_{ij}(t, d^*) = F_{ij}(t) \quad (2.33)$$

For each adult mosquito dispersing a distance d^* from (i, j) its destination patch is randomly

chosen from among its $n_{ij}(d^*)$ neighbours at this distance.

The adult population in patch (i, j) at time $(t + 1)$ is hence given by

$$A_{ij}(t + 1) = A_{ij}(t) + N_{ij}^A(t) - D_{ij}^A(t) + F'_{ij}(t) - F_{ij}(t) \quad (2.34)$$

where $F'_{ij}(t)$ denotes the number of adult mosquitoes dispersing into patch (i, j) at time t . Thus

$$M_{ij}(t) = F'_{ij}(t) - F_{ij}(t) \quad (2.35)$$

describes the net migration to (i, j) at time t .

2.2.2 Landscape Model

Spatially homogeneous landscapes are created by assuming the same carrying capacity and initial conditions for each patch. Each patch has the same initial egg, larval and adult population, and the local population is at its deterministic equilibrium at the start of each simulation. Thus, if L_{ij}^* denotes the larval population of patch (i, j) at deterministic equilibrium, E_{ij}^* and A_{ij}^* , the egg and adult population of (i, j) at deterministic equilibrium respectively, are given by

$$E_{ij}^* = \frac{b\gamma_L L_{ij}^*}{(\mu_A(\mu_E + \gamma_E))} \quad (2.36)$$

$$A_{ij}^* = \frac{\gamma_L L_{ij}^*}{\mu_A} \quad (2.37)$$

and we set \bar{K}_{ij} , which denotes the mean carrying capacity of patch (i, j) , as

$$\bar{K}_{ij} = \frac{L_{ij}^*}{\frac{\gamma_L}{\mu_L} \left(\frac{b\gamma_E}{\mu_A(\gamma_E + \mu_E)} - 1 \right) - 1} \quad \forall(i, j) \quad (2.38)$$

Larval carrying capacity is varied seasonally using a sinusoidal function of the form

$$K_{ij}(t) = \bar{K}_{ij}(1 + \Delta(\cos(2\pi(t + \phi)))) \quad (2.39)$$

where here t is in years, Δ and ϕ denote the amplitude and phase of seasonal variation in carrying capacity respectively, and \bar{K}_{ij} denotes the mean carrying capacity of patch (i, j) across the year.

We explore the population dynamics across two types of landscape. First, we consider landscapes where a stable mosquito population is already present to reflect urban environments where *Aedes aegypti* are established. Second, we consider the invasion dynamics resulting from mosquitoes being seeded into an otherwise unoccupied landscape. This reflects scenarios where *Aedes aegypti* are newly introduced or reintroduced into a landscape following, for example, temporary suppression of the vector populations resulting from vector control interventions or seasonal declines in mosquito abundance.

2.2.3 Model Assumptions

Adult Female Mosquitoes Only

We chose not to consider the adult male population, and to model adult females alone, for several reasons. While female *Aedes aegypti* lay several batches of eggs over the course of their lifetime, they typically only mate once with an adult male [48]. Thus, provided the size of the adult male population remains sufficiently large for adult females to find a mate, the dynamics of *Aedes aegypti* populations are more heavily influenced by changes in adult female density than those in adult male density. Furthermore, as only adult female *Aedes aegypti* transmit disease, the dynamics of the adult female population are of greater interest in the context of vector control, and disease transmission and control. Consequently, mathematical models of *Aedes aegypti* population dynamics (excluding those exploring the potential impact of novel vector control measures) largely consider adult female populations alone, and assume that the density of adult males is sufficient to allow females to mate successfully [168, 203–205]. Hence, in line with these studies, we adopt a similar approach here.

Functional Form of Density Dependence

For each patch (i, j) , we represent density-dependent competition during the larval stage of mosquito development by increasing larval mortality as the size of the local larval population approaches the carrying capacity of the patch. We chose to represent density-dependent competition during the larval life stage (as opposed to other life stages) in light of the results of

empirical laboratory and field studies exploring the impact of resource limitations and increased larval density at breeding sites on the dynamics of *Aedes aegypti* populations [59, 62, 64, 66–71].

One of the earliest field studies exploring density-dependent effects on mosquito populations considered *Aedes aegypti* populations in Thailand [66]. Here, the authors established that mortality during the early stages of larval development was indeed density-dependent. More recent field studies undertaken across a variety of different settings including Mexico [62, 67], Venezuela [59], and Australia [64] showed a similar negative relationship between larval population density and larval survival, owing to density-dependent intraspecific competition for resources at breeding sites. Similar results have also been observed in larval populations reared under laboratory and semi-field conditions, for both *Aedes aegypti* [68–71] and *Aedes albopictus* [213]. In addition to increasing larval mortality, empirical studies have shown that density-dependent competition during the larval life stage may also lead to slower larval development and smaller adult mosquitoes emerging from the breeding site [62, 64, 70]. Furthermore, a reduction in the size of adult mosquitoes emerging from the breeding site may in turn affect both the oviposition and mortality rate of adult females, as empirical studies have indicated that smaller adult female *Aedes aegypti* may lay fewer eggs over the course of her lifespan [214] and have a higher mortality rate [215], compared with larger females.

The effects of density-dependent competition could therefore have been represented in our model in several different ways. For example, we could have represented density-dependent competition by varying the oviposition rate (b) or the larval development rate (γ_L) with larval density (instead of, or in addition to, varying the larval mortality rate). However, we chose to represent density-dependent competition solely through changes in larval mortality, in accordance with changes in larval population density, as this is the approach most commonly used in models of mosquito population dynamics, which consider larval populations [168, 204, 205, 216, 217].

Spatial Granularity

We vary the level of fidelity we have in our model in representing the true underlying fragmented structure of *Aedes aegypti* larval populations by varying the number of patches used to represent the dynamics of the mosquito population across a given landscape, with more patches corresponding to greater fidelity. The lowest level of spatial granularity in our model corresponds to the single patch approach as here we do not account for the fragmented structure of larval

populations and consider the population as a single, well-mixed population coming from one large breeding site. Finer levels of spatial granularity allow us to account for the fragmented structure of larval populations and spatially heterogeneous mixing among populations, at different levels. In choosing the finest level of spatial granularity in our model, we consider the typical oviposition and dispersal behaviour of adult female *Aedes aegypti*.

As discussed in Chapter 1, *Aedes aegypti* primarily breed in urban domestic environments, and there can be several breeding sites per individual household [47, 48, 61]. MRR studies indicate that, owing to their domestic habitat, *Aedes aegypti* typically disperse very small distances (e.g. 20m-100m [75], 56m [77]), often only travelling to neighbouring households, with most mosquitoes released in individual households during MRR studies recaptured within the house of release [75]. Thus, mixing of *Aedes aegypti* among households is spatially heterogeneous [47, 61, 75].

Within individual households, mixing among larval populations is also dependent on the oviposition behaviour of adult females. *Aedes aegypti* often lay eggs from a single batch across multiple breeding sites (skip-oviposition) [207, 218], and thus may distribute their eggs across a household. Nonetheless, empirical field studies indicate that adult female *Aedes aegypti* actively choose oviposition sites, and thus do not distribute eggs randomly among breeding sites [207, 218]. Based on their analysis of egg laying behaviour of *Aedes aegypti* in Iquitos, Peru [207], Wong *et. al* conclude that *Aedes aegypti* breeding site selection is primarily driven by conspecific attraction, whereby members of the same species tend to breed where other members of the species are present or have recently laid eggs. The authors hypothesise that using these cues may allow female *Aedes aegypti* to identify more stable breeding sites, in terms of the availability of water and nutrients for example [207]. In addition, the physical properties of individual breeding containers may also play an important role in attracting gravid females, with empirical evidence suggesting that adult females prefer to breed in larger sites, both in terms of diameter and volume [218]. However, while larger breeding sites are likely to have greater food resources, it is unclear to what extent oviposition site selection is driven by the desire to maximise food resources for offspring. Wong *et al.* suggest that, while this is a factor, conspecific attraction and physical attributes of the breeding site play a more important role [207]. On the other hand, empirical laboratory studies have indicated that, beyond a larval density of approximately 1 larva

per millimetre of water, gravid females are less likely to be attracted to a given breeding site, even if conspecific larvae are present [219].

Given the variety of factors which contribute towards oviposition site selection within an individual household, we make the simplifying assumption that mixing within individual households is spatially homogeneous. While these processes may play a role in shaping the dynamics of populations within an individual household, our motivation for this work is not to develop a highly detailed, biologically-accurate model of *Aedes aegypti* population dynamics at the individual breeding container level. Rather, we aim to explore how allowing different levels of spatial heterogeneity in mixing among larval populations, and our choice of representation of spatial structure (if represented at all) influence our understanding of *Aedes aegypti* population dynamics at fine spatial scales. Thus, we chose the finest level of spatial granularity in our model to correspond to modelling at the individual household level as movement between patches at this level of granularity is characteristic of the typical dispersal length of *Aedes aegypti*.

Here, we consider an example urban landscape comprised of 1024 households. Thus, at the finest level of spatial granularity in our model, we have a 32x32 spatial grid. We assume each square of this 32x32 grid represents an area of approximately 20mx20m. We reduce the level of spatial granularity in our model by doubling the size of each patch. Hence, as we move from a 32x32 grid to a 16x16 grid, each patch now corresponds to a group of 4 households and an area of 40mx40m. We examine the effect of further coarsening the representation of space in our model until we represent the dynamics of the *Aedes aegypti* population across the landscape using a single patch, where the population is assumed to mix homogeneously.

2.2.4 Parameter Values

Unless otherwise stated, all parameter values used are as shown in Table 2.1, and parameter values were chosen where possible from the literature to represent the characteristics of *Aedes aegypti*.

Our choice of parameter values used to represent the typical dispersal behaviour of *Aedes aegypti* at the individual household level were guided by estimates of the mean dispersal distance derived from MRR studies. As discussed above, MRR studies indicate that *Aedes aegypti*

typically disperse very short distances [75–77]. While estimates of the mean dispersal distance vary between studies and locations, a distance of approximately 50m is typical of values the mean dispersal distance of *Aedes aegypti* estimated by MRR studies [75–77].

These estimates however largely correspond to the mean distance travelled over the course of an adult female's lifespan, rather than over the course of a single day. Hence, we sought to choose values of the daily dispersal rate and mean dispersal length (at the 32x32 grid level) to correspond to a mean lifetime dispersal distance of approximately 50m. We chose these parameter values by first using our model to explore the range of mean lifetime dispersal distances generated by combinations of the daily dispersal rate (r) and mean dispersal length (m) (keeping the adult mosquito mortality rate (μ_A) fixed).

To calculate the mean lifetime dispersal distance for a given combination of the daily dispersal rate and mean dispersal length in model run n , we first set the oviposition rate (b) to zero, and seed 1000 adult females in the same patch (i', j') at the centre of our 32x32 grid. Setting the oviposition rate to zero ensures that no new adult females enter the population. We then record the cumulative number of deaths in each patch on the grid at the end of the run, and calculate the Euclidean distance between each patch and the seeded patch. The mean lifetime dispersal distance for run n (MLD_n) is then given by

$$MLD_n = \frac{1}{1000} \sum_{(i,j)} C_{ij}(n) d_{(ij)-(i'j')} \quad (2.40)$$

where $C_{ij}(n)$ denotes the cumulative number of adult female deaths in patch (i, j) at the end of run n , and $d_{(ij)-(i'j')}$ denotes the distance between patch (i, j) and the seeded patch (i', j') . To get a final estimate of the mean lifetime dispersal distance, we take the average across 1000 model runs (seeding in the same patch in each run).

The results of this exercise are presented in Figure 2.2 below. We found that, using a negative exponential kernel, a daily dispersal rate of 0.08 and mean dispersal length of 5 patches gave a mean lifetime dispersal distance of approximately 50m. Hence we chose these values as the default parameter values in our model. However, we tested sensitivity of our modelling results to different values of these parameters to explore how the underlying population dynamics are affected by different dispersal behaviours.

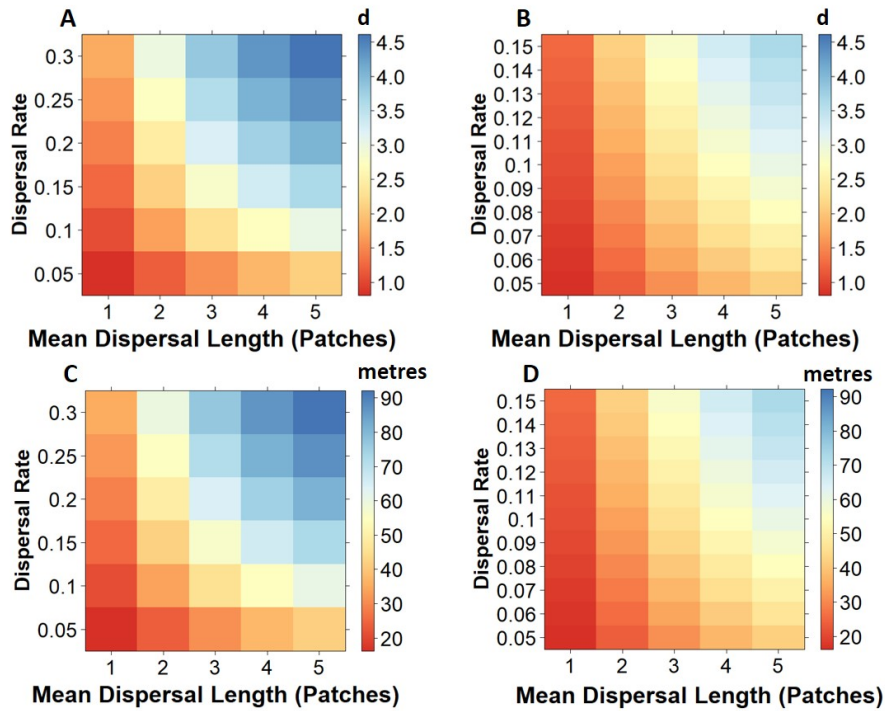


Figure 2.2: Mean Lifetime Dispersal Distance. Comparison of the estimated mean lifetime dispersal distance of adult mosquitoes for different values of the daily dispersal rate and mean dispersal length per day, for a homogeneous landscape on a 32x32 grid. This was calculated as described in equation 2.40 above. Figures A and B show estimates in terms of Euclidean distance between patches, and Figures C and D show estimates in terms of metres (assuming each patch in our 32x32 grid represents an area of approximately 20mx20m).

As the level of granularity in our model is reduced, we adjust the daily mean and maximum dispersal lengths accordingly. For example, as we move from a 32x32 grid to a 16x16 grid, we double the size of each patch. Thus the mean and maximum dispersal lengths are halved.

In line with existing models of *Aedes aegypti* population dynamics [168, 170, 198, 204, 205], we assume density-dependence during the larval stage is linear (i.e. $\Omega = 1$). In Chapter 4, we allow this parameter to vary when exploring whether the dynamics observed using the metapopulation model can be reproduced using the single patch model.

At the individual household level (32x32 grid) we chose a range of low equilibrium larval population sizes (1-10 per patch) to explore the dynamics of *Aedes aegypti* populations across different landscapes. We chose this range of values as empirical studies of *Aedes aegypti* populations at the individual household level have shown that the number of adult *Aedes aegypti* per household is often very low [61, 220, 221]. For example, empirical studies of *Aedes aegypti* population dynamics in Thailand and Puerto Rico estimated an average of 11 ± 2 and 7 ± 2 adult

mosquitoes (male and female) were captured per weekly collection per individual household in study areas in Thailand and Puerto Rico respectively [221].

We run the model for a period of 7 years to ensure an equilibrium has been reached, and to allow us to explore the effects of seasonal changes in carrying capacity on population dynamics. We consider that an equilibrium has been reached when we observe quantitatively similar dynamics over the course of several years. I coded the model in C++.

Parameter	Definition	Value	Reference
g	Length of gonotrophic cycle	3 days	[49]
R_M	Mosquito reproduction number	2.69 (based on estimate of female fecundity of 0.269/day and adult mosquito mortality rate of 0.1/day)	[190]
b	Number of eggs laid by an adult mosquito	Assigned to match R_M	-
$\frac{1}{\gamma_E}$	Mean development time of mosquito eggs	4 days	[64]
$\frac{1}{\gamma_L}$	Mean development time of mosquito larvae	15 days	[64]
μ_E	Egg mortality rate	0.01/day	[222]
μ_L	Larval mortality rate	0.025/day	[222]
μ_A	Adult mosquito mortality rate	0.1/day	[223]
m	Mean dispersal length of an adult mosquito	5 patches	[75–77]
D	Maximum dispersal length of an adult mosquito	12 patches	[75–77]
r	Dispersal rate of an adult mosquito	0.08/day	[75–77]
\bar{K}_{ij}	Mean larval carrying capacity of patch (i, j)	Variable	-
Ω	Strength of density dependence	1	-

Table 2.1: Model Parameter Values. Definition and values of parameters used in the simulation model at the 32x32 grid level. For a mean dispersal length of 5 patches, the probability of dispersal to much larger distances is negligible and hence we set a maximum dispersal length of 12 patches to aid computational efficiency.

2.3 Results

2.3.1 Impact of Fragmentation

To explore the impact of fragmentation alone, we first considered the dynamics of an established mosquito population in a homogeneous landscape with no spatial or temporal variation in carrying capacity across patches. We observed that fragmentation may lead to a reduction in both total population size and patch occupancy levels, compared with the single patch model. The magnitude of this effect depended on the carrying capacity of each patch (represented as the deterministic equilibrium larval population size in Figure 2.3). For the non-spatial single patch model, population size scaled linearly with carrying capacity as expected, while the relationship was non-linear for the metapopulation model, especially in the absence of dispersal. As expected, the largest differences occurred when the carrying capacity of individual patches in the metapopulation was low, as the probability of stochastic extinction is then highest.

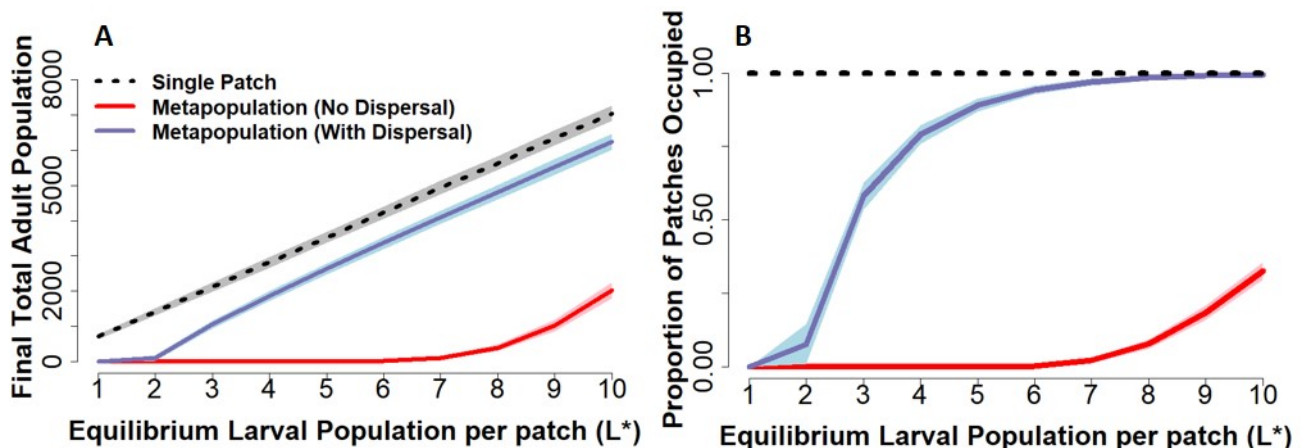


Figure 2.3: Impact of Fragmentation on an Established Mosquito Population. Mean final total population size and patch occupancy for a mosquito population modelled as a single patch and as a metapopulation on a 32x32 grid, using a dispersal rate of 0.08 per day and a mean dispersal distance of 5 patches. The initial population of each patch is at its deterministic equilibrium at the start of each simulation, and the total initial adult population in the single patch model is 32x32 times the initial adult population of each patch in the metapopulation model. The dashed black line represents the results observed under the single patch model, the solid lines show the mean value, and the shaded areas show the 95% confidence interval. Figures (A) and (B) compare the results observed for a homogeneous landscape with no temporal or spatial variation in larval carrying capacity. For each scenario, the mean is calculated across 1000 realisations of the stochastic model.

The dispersal of adult mosquitoes across the landscape counteracted these effects by enabling extinct local populations to be reseeded, thereby rescuing these populations and increasing population persistence and patch occupancy. For patches with low carrying capacity and hence an unstable local population, this recurring cycle of extinction and recolonization leads to a

continuous fluctuation in patch occupancy at the local level. However, at the global level, patch occupancy levels remained stable, indicating that a balance between extinction and recolonization across the metapopulation as a whole is maintained, thereby allowing the overall population to persist.

2.3.2 Dispersal Dynamics

The extent to which dispersal counterbalanced the effects of fragmentation was dependent both on the dispersal rate and mean dispersal length of the mosquito. Total population size and patch occupancy were highest when both the dispersal rate and mean dispersal length of the mosquito were high, as frequent and widespread movement of adult mosquitoes across the landscape enabled more rapid recolonization of patches following local extinction (Figure 2.4). Moreover, we observed that the rate of dispersal played a greater role in increasing local persistence than the mean dispersal length of the mosquito, as frequent highly local dispersal led to larger total population sizes and higher patch occupancy than less frequent dispersal over a wider distance.

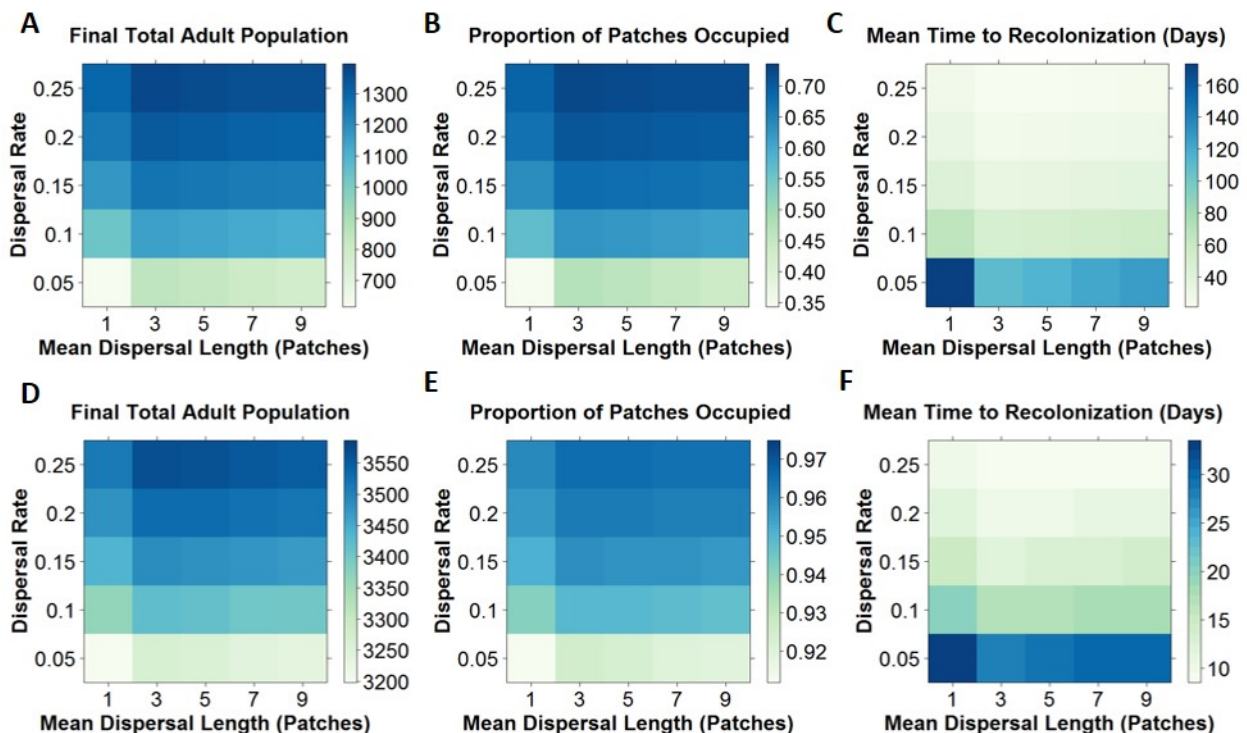


Figure 2.4: Dispersal Dynamics in Homogeneous Landscapes. Comparison of population dynamics observed for varying rates and lengths of dispersal in homogeneous landscapes on a 32x32 grid with a equilibrium larval population of 3 (A-C) or 6 (D-F) larval mosquitoes per patch. Results are compared with respect to mean final total population size (A,D), patch occupancy at equilibrium (B,E) and the mean time between extinction and recolonization of individual patches (C,F). The maximum dispersal range was set to 20 patches. For each scenario, the mean was calculated across 1000 realisations of the stochastic model.

Further stabilizing mechanisms of the metapopulation were evident from exploring the relationship between the degree of dispersal across the landscape and the variability of larval populations at the local level. Indeed, dispersal can make individual patch populations more stable than isolated patches. Examining the variance to mean ratio of the larval population in individual patches, we observed a move from over-dispersion to under-dispersion as the rate of dispersal increased (Figure 2.5). This change arises since at high rates of dispersal, the birth process in individual patches becomes decoupled from the population in the patch itself, and thus increased regulation is required at the local level to stabilize the population.

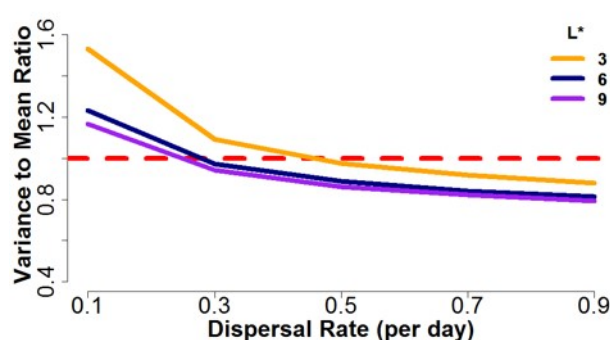


Figure 2.5: Impact of Increasing the Dispersal Rate. Variance to mean ratio of a local larval population at the final time step in a metapopulation comprised of 1024 (32x32) patches with no temporal or spatial heterogeneity in carrying capacity, and where each patch has an equilibrium larval population of 3, 6, or 9 larval mosquitoes. The dashed red line denotes the crossover point from over- to under- dispersion relative to the Poisson distribution. A negative exponential dispersal kernel with a mean dispersal distance of 5 patches was used. For each scenario, the mean and variance were calculated across 1000 realisations of the stochastic model.

2.3.3 Invasion Dynamics

Next, we examined the effects of landscape fragmentation on population invasion in an otherwise unoccupied landscape, while taking account of seasonal variation in carrying capacity. In the single patch model we observed fast population growth, with almost all model runs resulting in population persistence (Figure 2.6A). However, in a fragmented landscape, a more complex picture emerges, with fragmentation hindering both population persistence and growth, particularly when the dispersal rate is low and movement beyond the seeded patch is limited. When individual patches have a low carrying capacity, local populations are highly vulnerable to extinction from stochastic effects, which in turn reduces the likelihood of sustained invasion upon seeding and reduces the speed of population spread across the landscape (Figures 2.6A,B). Moreover, for model runs which resulted in population persistence, fragmentation also reduced the level of population growth and patch occupancy across the landscape (Figures 2.6B,C). In

addition, fragmentation increased the amount of variability in populations size during the early stages of population growth, prior to the population stabilizing, compared with the single patch model (Figure 2.6D).

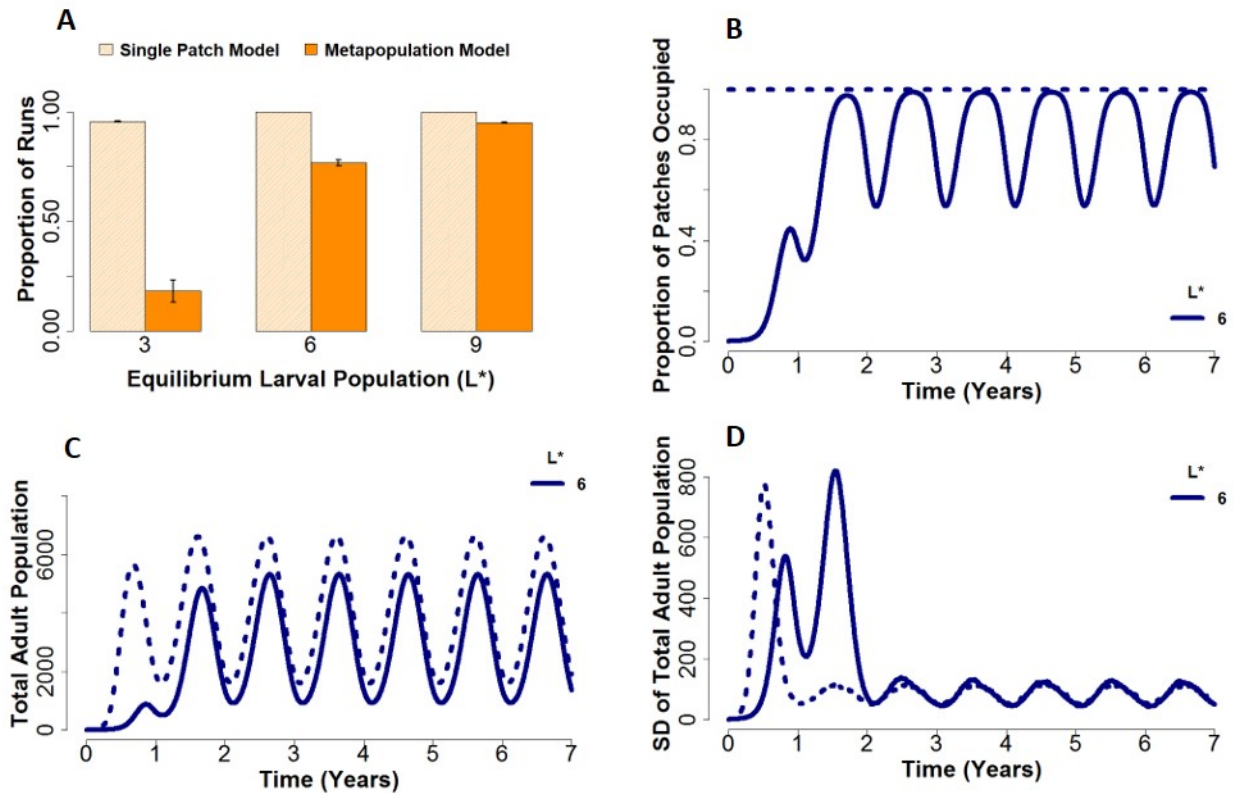


Figure 2.6: Impact of Fragmentation on Population Invasion. Population dynamics observed when a single patch in a landscape with temporal variation in carrying capacity is seeded with an adult mosquito population, and is modelled as a single patch (dashed lines) or as a metapopulation (with a dispersal rate of 0.08 per day) on a 32x32 grid (solid lines). We consider the dynamics for landscapes with a mean equilibrium larval population of 3, 6 or 9 larvae per patch (L^*), seeded with 3, 6 or 9 adult mosquitoes respectively, and where the amplitude and phase of seasonal variation in carrying capacity are 0.7 and 0.5 respectively. The results are compared with respect to the mean proportion of models runs which resulted in sustained invasion (final total adult population >1) (A), the mean proportion of patches occupied (B), mean total adult mosquito population size (C), and the standard deviation of total adult mosquito population size (D). A mean dispersal distance of 5 patches was used. For each scenario, the mean and variance were calculated across 1000 realisations of the stochastic model.

Again we found that the population dynamics observed in fragmented landscapes were heavily dependent on the dispersal behaviour of the mosquito. A high rate of movement across the landscape resulted in increased final population size (approaching that of the single patch model), increased patch occupancy and a faster speed of invasion, even when dispersal was highly local (Figures 2.7). Increasing mean dispersal length had a similar overall effect, but also resulted in smoother spatial population spread, particularly when the dispersal rate was low, as this resulted in faster local establishment in unoccupied areas of the landscape, despite seasonal fluctuations in carrying capacity (Figures 2.7E-H).

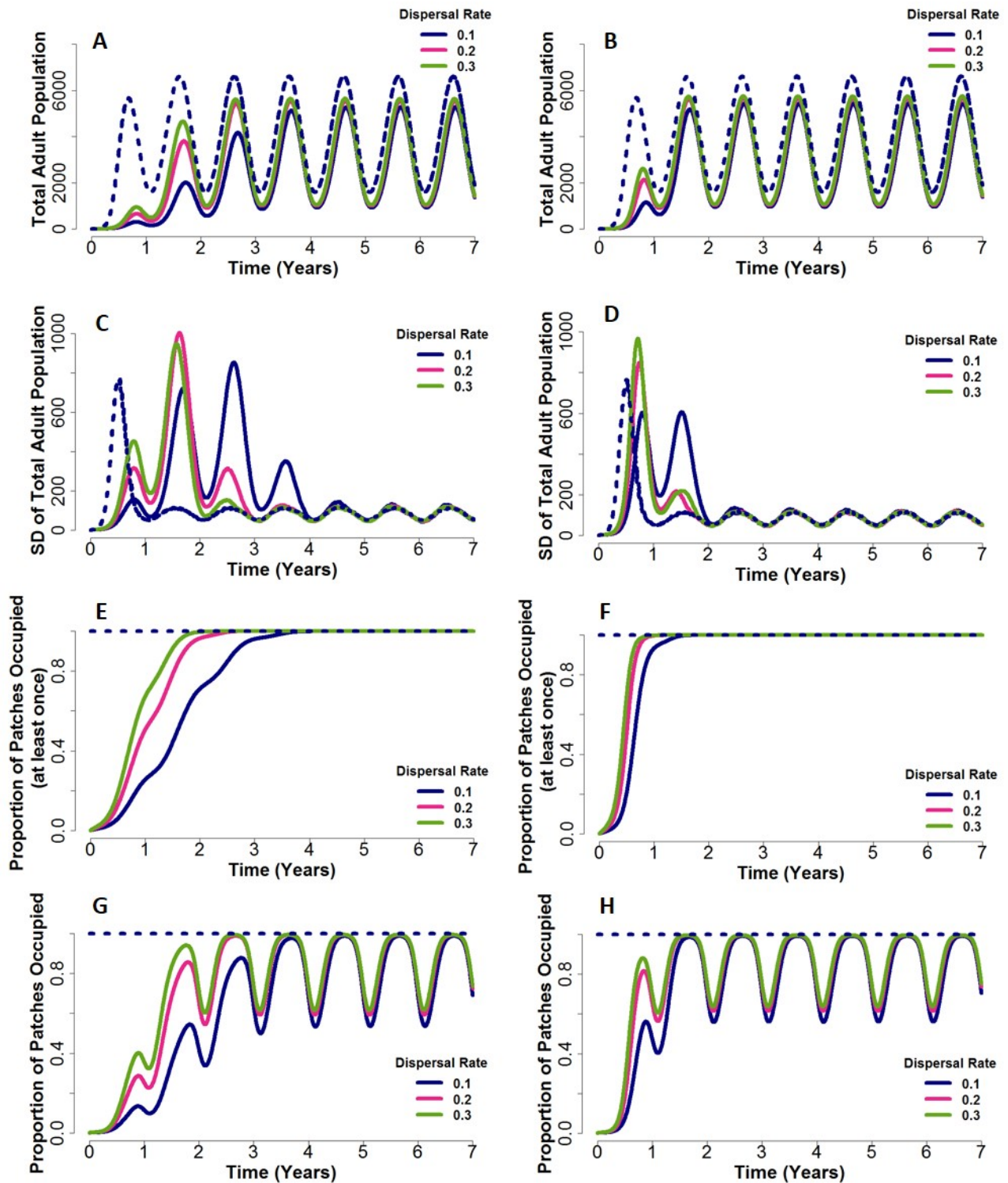


Figure 2.7: Impact of Dispersal Behaviour on Population Invasion. Population dynamics observed when a landscape with temporal variation in carrying capacity and a mean equilibrium larval population of 6 larvae per patch is seeded with 6 adult mosquitoes, and modelled as a single patch (dashed lines) or on a 32x32 grid (solid lines). A mean dispersal length of 1 patch (A,C,E,G) and 5 patches (B,D,F,H) was used, the amplitude and phase of seasonal variation in carrying capacity are 0.7 and 0.5 respectively. Results are compared with respect to mean total adult mosquito population size (A,B), the standard deviation of total adult mosquito population size (C,D), the mean proportion of patches which have been occupied at least once (E,F), and the mean proportion of patches occupied (G,H). For each scenario, the mean and variance were calculated across 1000 realisations of the stochastic model.

Invasion dynamics showed increased sensitivity to seasonal variation in carrying capacity in fragmented landscapes compared with the non-spatial single patch model, as the likelihood of sustained invasion upon seeding was more sensitive to the timing of seeding (Figure 2.8). For landscapes with a low mean carrying capacity, sustained invasion was least likely when seeding occurred prior to the onset of a seasonal trough in carrying capacity, and most likely when carrying capacity remained above the seasonal average immediately after seeding (Figure 2.8). Increasing the amplitude of seasonal increased the magnitude of these effects.

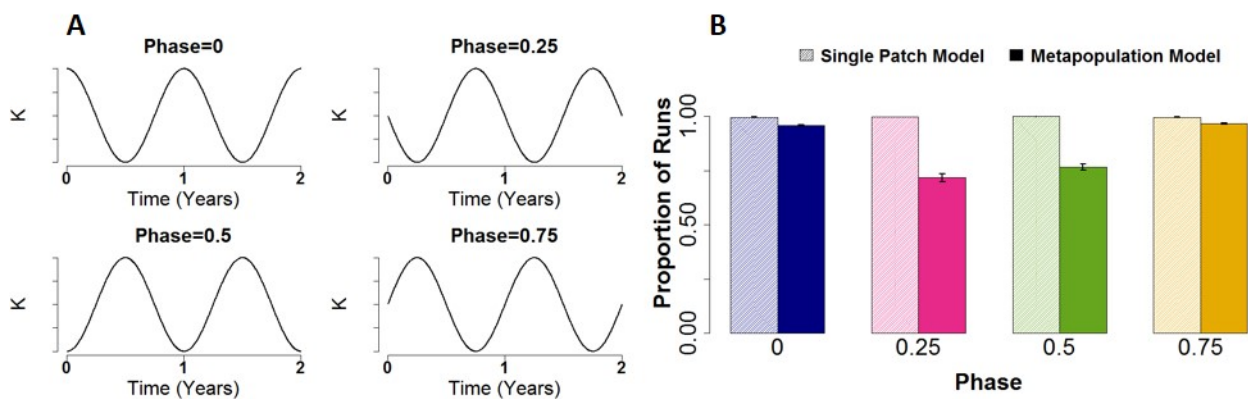


Figure 2.8: Timing of Population Invasion. Mean proportion of model runs which resulted in sustained invasion (final total adult population > 1) when a landscape with temporal variation in carrying capacity and mean a equilibrium larval population of 6 larvae per patch is seeded with 6 adult mosquitoes, and modelled as a single patch or on a 32×32 grid (with a dispersal rate of 0.08 per day and a mean dispersal length of 5 patches). The amplitude of seasonal variation in carrying capacity was 0.7, and seeding occurred when carrying capacity was at its seasonal peak (phase=0), mean value (phase=0.25, 0.75), or trough (phase=0.5). For each scenario, the mean was calculated across 1000 realisations of the stochastic model.

2.4 Discussion

In this chapter, we developed a stochastic metapopulation model of fine-scale *Aedes aegypti* population dynamics. We examined the impact of larval habitat fragmentation on mosquito population dynamics and explored the mechanisms which enable vector populations to persist in a fragmented landscape.

We found that fragmentation of larval populations can have a large impact on the dynamics observed, by leading to a reduction in population size and patch occupancy (compared with a single well-mixed population), with the largest reductions occurring when individual patches had low carrying capacities and thus a substantial risk of stochastic population extinction. The dispersal behaviour of adult mosquitoes played a key role in counterbalancing these effects, enabling increased local population persistence and allowing stability of the metapopulation as a whole to be maintained. Habitat fragmentation rendered successfully establishing a mosquito population in an unpopulated landscape considerably more difficult, with fragmentation reducing the likelihood of sustained invasion upon seeding, and the speed and extent of spatial population spread across the landscape strongly dependent on the frequency and range of adult mosquito dispersal.

These results suggest that using non-spatial models to represent the fine-scale dynamics of *Aedes aegypti* populations may substantially underestimate the stochastic volatility of those populations and the frequency at which local mosquito populations go extinct. This in turn may lead to over-estimates of vector population persistence and the speed at which *Aedes aegypti* populations are likely to invade unoccupied landscapes. The risk of extinction through stochastic effects is highest for small local populations and, given that density-dependent competition gives rise to non-linear dynamics during the larval stage of population growth, the dynamics observed when the fragmented structure of larval populations is explicitly represented cannot be exactly reproduced using a single patch (non-spatial) model. In a regime where local stochastic effects are substantial, total mosquito population size will be smaller (and population volatility larger) than predicted by a single patch model with the same total carrying capacity.

Before discussing the implications of these results further, we first seek to develop a fuller understanding of the effects of metapopulation structure on fine-scale *Aedes aegypti* population

dynamics by considering how spatial heterogeneity in the underlying landscape affects the dynamics observed and how the results we have obtained depend on the level of spatial granularity in our model. We thus proceed to explore these effects.

Chapter 3

Heterogeneous Landscapes

We showed in Chapter 2 that accounting for larval habitat fragmentation when modelling the dynamics of mosquito populations at fine spatial scales can have a large impact on the dynamics observed, but limited our analysis to spatially homogeneous landscapes. Here we extend the landscape model presented in Chapter 2 to allow for spatial heterogeneity in carrying capacity across patches, and explore how features of the underlying landscape influence fine-scale mosquito population dynamics. All other features of the metapopulation model remain unchanged and are as presented in Chapter 2.

3.1 Methods

3.1.1 Landscape Model

To compare the dynamics observed in landscapes with different levels of spatial heterogeneity in carrying capacity to those observed using the single patch model, we want total and mean carrying capacity across the landscape to remain fixed. We thus created spatially heterogeneous landscapes as follows.

To create a landscape with a fixed mean larval carrying capacity \bar{K}^* and a specified level of variability σ^2 around this mean value, we first draw a sequence of positive values X_{ij} from a log-normal distribution

$$X_{ij} \sim \text{logN}(\bar{K}^*, \sigma^2) \quad (3.1)$$

To keep the total carrying capacity across the landscape fixed, we apply a transformation of the

form aX_{ij}^b to the generated values, where the values of a and b are such that

$$\mathbb{E}[aX_{ij}^b] = \bar{K}^* \quad (3.2)$$

$$\text{Var}[aX_{ij}^b] = \sigma^2 \quad (3.3)$$

We then set $\bar{K}_{ij} = aX_{ij}^b$, where \bar{K}_{ij} denotes the mean carrying capacity of patch (i, j) across the year. Values of a and b such that equations (3.2) and (3.3) hold are found numerically using linear interpolation.

To create spatially heterogeneous landscapes with varying levels of spatial correlation (Figure 3.1) we use a similar approach to that adopted by Hancock *et al.* in [196]. An $n^2 \times n^2$ correlation matrix C with entries

$$C_{ij} = e^{-\alpha d} \quad (3.4)$$

is created, where d denotes the distance between a pair of patches, and α controls the degree of correlation between values, with very small values of α giving a high degree of correlation. Taking the Cholesky decomposition of C gives a matrix L such that $C = LL^T$. Thus for $X \sim N(0, I)$, we have that [224]:

$$\text{Corr}[LX] = \mathbb{E}[(LX)(LX)^T] = \mathbb{E}[L(XX^T)L^T] = L\mathbb{E}[XX^T]L^T = LL^T = C \quad (3.5)$$

Then, setting $Y = e^{LX}$, a similar approach to that described directly above by equations (3.2) and (3.3) is then used to transform the values of Y to give a landscape with a mean larval carrying capacity \bar{K}^* and variance σ^2 .

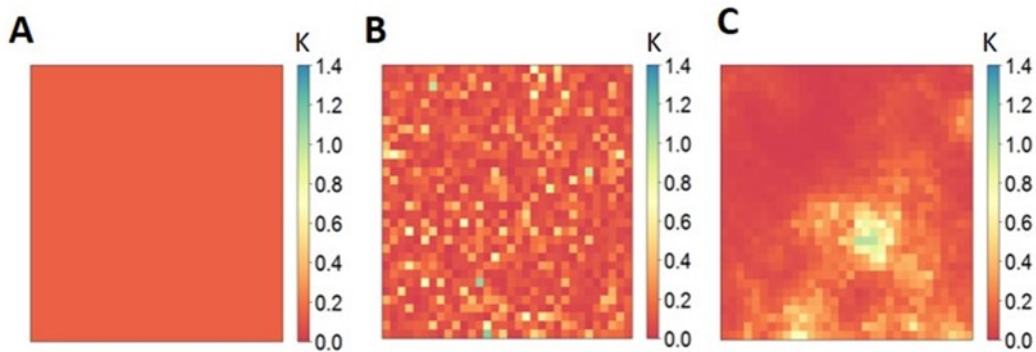


Figure 3.1: Example Landscapes. Examples of a landscape with a fixed total and mean carrying capacity: (A) homogeneous landscape, (B) heterogeneity in carrying capacity without clustering and (C) heterogeneity in carrying capacity and a high level of clustering across the landscape.

3.2 Results

3.2.1 Spatial Heterogeneity and Dispersal Dynamics

The impact of non-clustered spatial heterogeneity in carrying capacity across the landscape on the population dynamics observed was dependent both on the mean value of carrying capacity and the underlying dispersal dynamics. Increasing inter-patch variability, while keeping the total carrying capacity fixed, increases the risk of local stochastic extinction as a higher proportion of patches have low carrying capacities. However, this can have either positive or negative effects on overall population persistence, depending on the mean value of carrying capacity and the rate of dispersal. For landscapes with an established mosquito population, a low mean patch carrying capacity and a low rate of dispersal, increased spatial heterogeneity resulted in increases in total population size and patch occupancy compared with a spatially homogeneous landscape (Figure 3.2). This is because a small fraction of patches now have carrying capacities high enough to sustain local population persistence for an extended period. However, for higher values of mean patch carrying capacity, inter-patch variability increases the risk of stochastic extinction compared with a homogeneous landscape (Figure 3.2) - due to a higher proportion of patches having carrying capacities too low to allow local populations to persist.

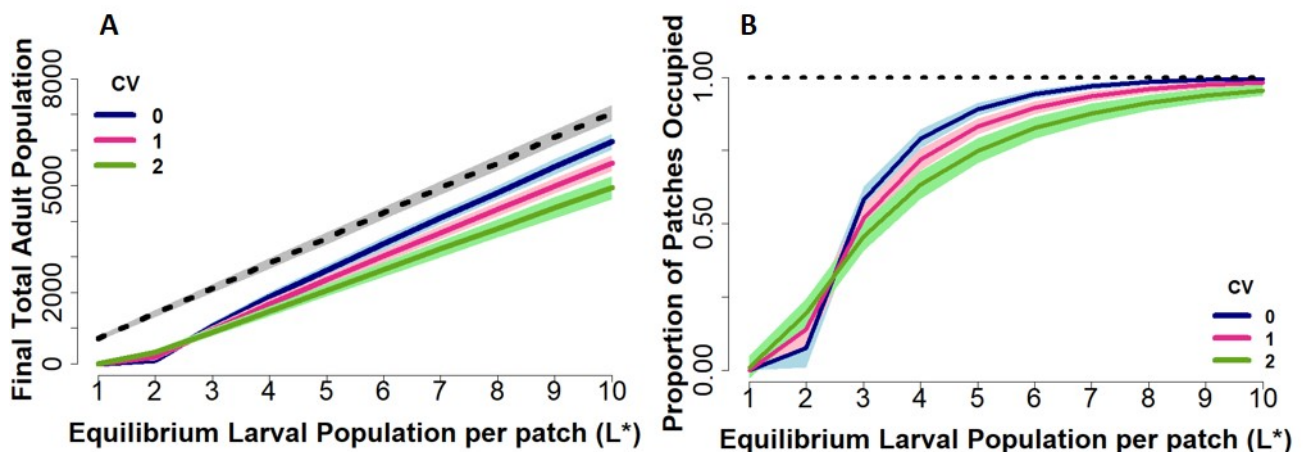


Figure 3.2: Impact of Fragmentation in Spatially Heterogeneous Landscapes. Mean final total population size and patch occupancy for a mosquito population modelled as a single patch and as a metapopulation on a 32x32 grid, using a dispersal rate of 0.08 per day and a mean dispersal distance of 5 patches. The initial population of each patch is at its deterministic equilibrium at the start of each simulation, and the dashed black line represent the results observed under the single patch model. The solid lines show the mean value, and the shaded areas show the 95% confidence interval. Figures (A) and (B) compare the single patch model to the metapopulation model with dispersal, for a heterogeneous landscape with the level of spatial heterogeneity in carrying capacity across patches characterised by the coefficient of variation (CV) and no temporal variation in carrying capacity. For each scenario, the mean was calculated across 1000 realisations of the stochastic model.

Population dynamics also showed non-monotonicity in relation to the dispersal rate. For established populations, with low between-patch variability, local persistence and thus overall population size was highest for high dispersal rates (Figures 3.3A,C). However, increasing between-patch variability resulted in reduced overall population size, with population size lowest for high dispersal rates due to dispersal-driven depopulation of patches with high carrying capacity (Figure 3.3). A similar pattern was observed with respect to patch occupancy for landscapes with very low mean carrying capacity (Figure 3.3B). However as mean carrying capacity increases, patch occupancy was less sensitive to changes in the dispersal rate as even patches with lower than mean carrying capacity were less vulnerable to local extinction (Figure 3.3D). Nonetheless, patch occupancy still decreased with increasing inter-patch variability (Figures 3.3B,D).

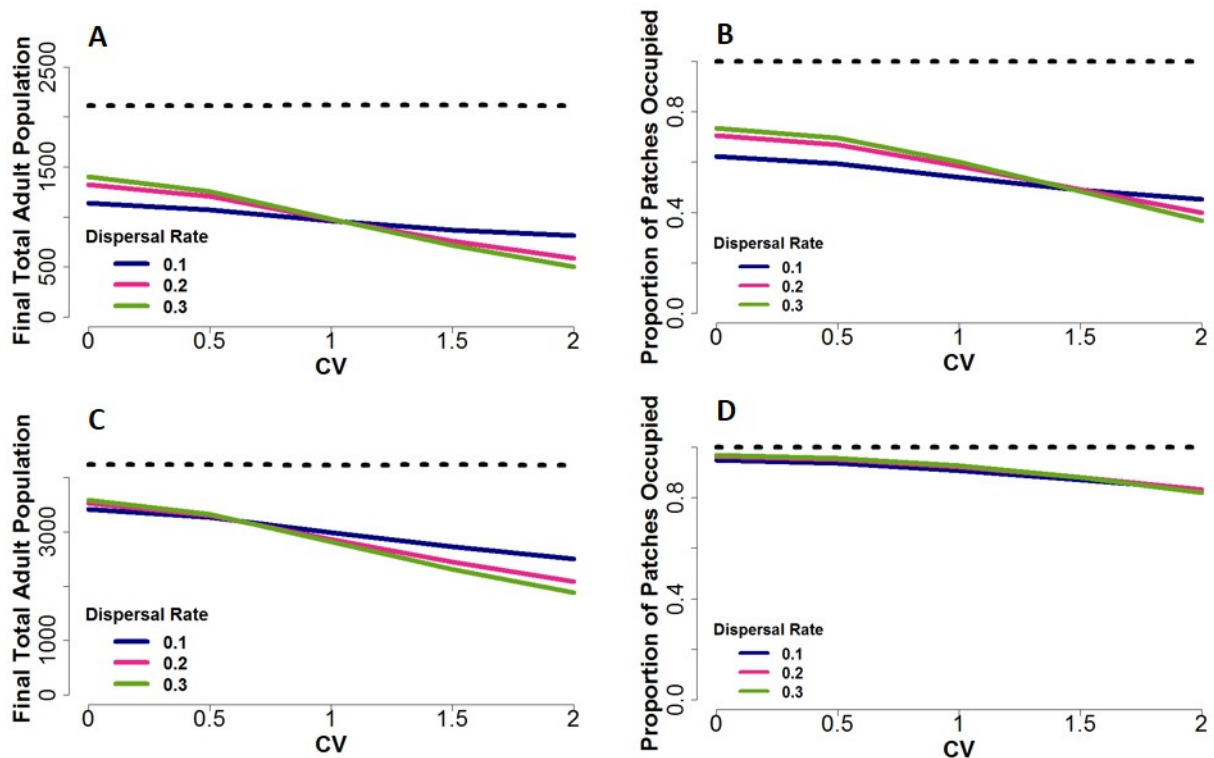


Figure 3.3: Spatial Heterogeneity and Dispersal. Population dynamics observed for an established mosquito population in landscapes with a varying degree of spatial heterogeneity, characterised by the coefficient of variation (CV), modelled as a single patch (dashed lines) or as a metapopulation on a 32x32 grid (solid lines). Figures (A,B) correspond to a landscape with an equilibrium mean larval population of 3 larvae per patch, while (C,D) correspond to a landscape with an equilibrium mean larval population of 6 larvae per patch. A mean dispersal distance of 5 patches was used. For each scenario, the mean was calculated across 1000 realisations of the stochastic model.

3.2.2 Spatial Heterogeneity and Invasion Dynamics

Spatial heterogeneity in carrying capacity across patches also had a large impact on population invasion. The likelihood of sustained invasion upon seeding decreased with increasing inter-patch variability, owing to an increased chance of seeding in an area of low carrying capacity (Figure 3.4A). Furthermore, while the speed of spatial spread increased monotonically with the dispersal rate, it decreased with increasing inter-patch variability as patches with low carrying capacity pose a barrier to local establishment and onwards spatial spread (Figure 3.4B). Increasing inter-patch variability therefore also led to reduced total population size and patch occupancy, particularly when dispersal was high local (Figures 3.4C,D)

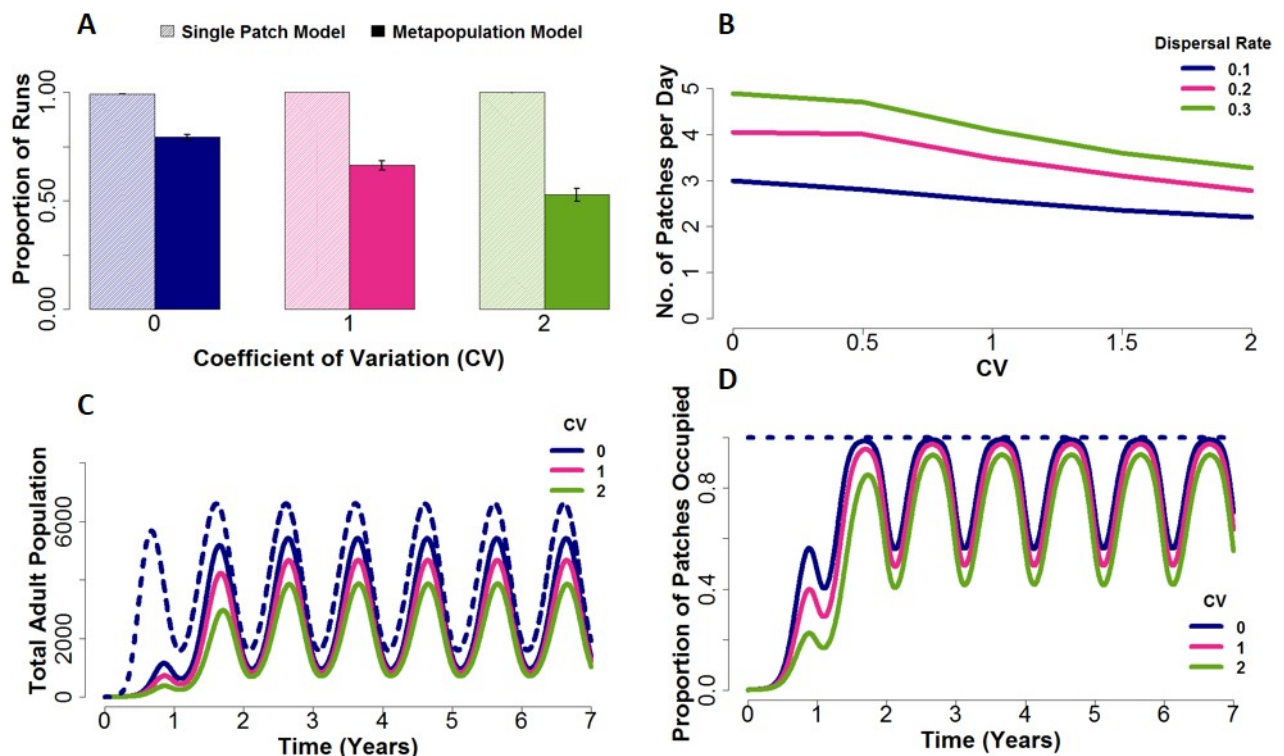


Figure 3.4: Invasion Dynamics in Spatially Heterogeneous Landscapes. Population dynamics observed when a landscape with spatial and temporal variation in carrying capacity and mean a equilibrium larval population of 6 larvae per patch is seeded with 6 adult mosquitoes, and modelled as a single patch (dashed lines) or on a 32x32 grid (solid lines). The level of spatial heterogeneity in carrying capacity across patches is characterised by the coefficient of variation (CV). A mean dispersal length of 5 patches was used, the amplitude and phase of seasonal variation in carrying capacity are 0.7 and 0.5 respectively. Results are compared with respect to the likelihood of sustained invasion (A), the speed of population spread across the landscape (B), mean total adult mosquito population size (C), and the mean proportion of patches occupied (D). Speed is characterised in terms of the average number of patches travelled per day, calculated by dividing the time taken until all patches have been occupied at least once by the number of patches in the metapopulation. For each scenario, the mean was calculated across 1000 realisations of the stochastic model.

3.2.3 Impact of Spatial Clustering

More realistic heterogeneous landscapes tend to show a high degree of local spatial correlation in carrying capacity, where patches with similar levels of carrying capacity are clustered together. Thus in a highly clustered landscape, the dispersal behaviour of the mosquito is critical to allowing mixing between areas of high and low carrying capacity, and hence is the key factor in driving the dynamics observed in these landscapes.

At high rates of dispersal and low mean dispersal length, increasing spatial correlation resulted in increases in the mean equilibrium population size (Figure 3.5A), but decreases in mean patch occupancy (Figure 3.5B). This arises from improved local population persistence in areas with high patch carrying capacity, but poorer local persistence in areas of low carrying capacity. As mean dispersal length is increased, more frequent dispersal from areas of high carrying capacity to areas of low carrying capacity occurs, and hence this improves local persistence in areas of low carrying capacity. However, while this in turn leads to increased patch occupancy (Figure 3.5B), it also leads to a reduction in mean total population size (Figure 3.5A), with behaviour tending towards that of a non-clustered landscape with the same level of heterogeneity in carrying capacity across patches.

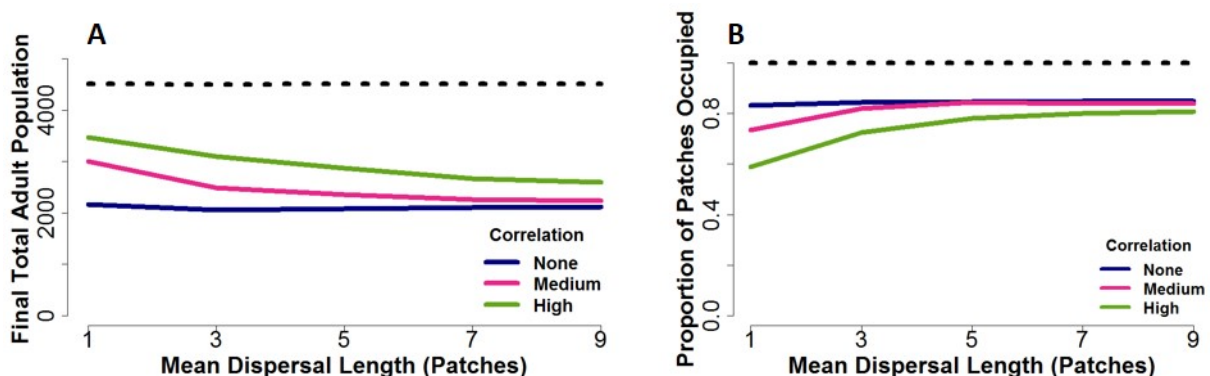


Figure 3.5: Spatial Correlation and Dispersal Length. Population dynamics observed in a spatially heterogeneous landscape comprised of 1024 patches, with a deterministic mean equilibrium larval population of 6 larvae per patch, spatial heterogeneity characterised by the coefficient of variation relative to this mean value, and no temporal variation in carrying capacity. A coefficient of variation of 2 and a dispersal rate of 0.3 per day was used. A medium and high correlation were defined as $\alpha=0.3$ and $\alpha=0.01$, respectively (Equation 3.4). The dashed black line describes the results obtained under the single patch model, and results are compared with respect to final total adult population size (A) and the proportion of patches occupied across the landscape (B). For each scenario, the mean was calculated across 1000 realisations of the stochastic model.

Population invasions into an unpopulated landscape more often result in early extinction and a lack of establishment in spatially correlated landscapes, due to the increased chance that

invasion will occur in an area of low carrying capacity (Figure 3.6A). Moreover, when dispersal is highly local, a high degree of spatial clustering substantially slows the speed of invasion, as local population establishment in areas of low carrying capacity becomes more difficult (Figure 3.6B). As we observed for established populations, this leads to increased population size compared with less correlated landscapes with the same level of spatial variability in carrying capacity, but also reduced patch occupancy (Figures 3.6C,D). As mean dispersal length increases, we again observe a reversal of this pattern.

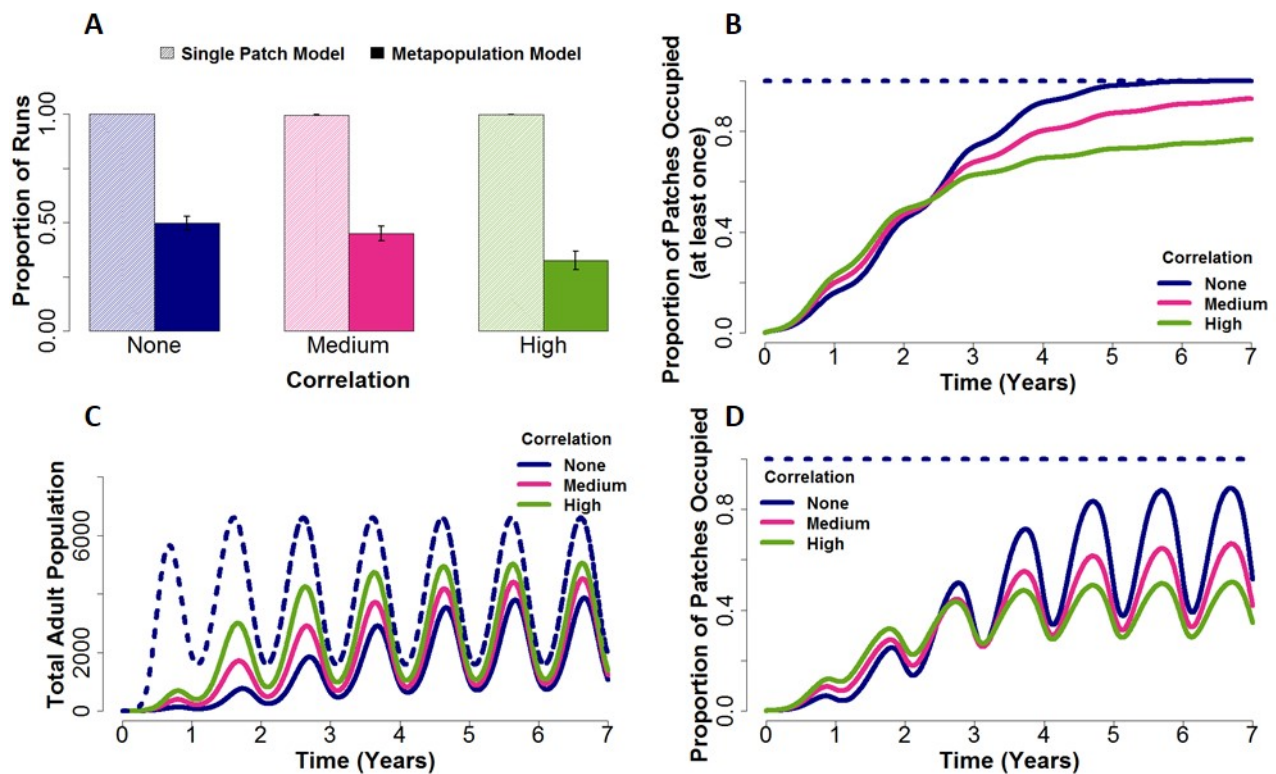


Figure 3.6: Spatial Correlation and Invasion Dynamics. Population dynamics observed when a single patch in a spatially heterogeneous landscape comprised of 1024 patches, with temporal variation in carrying capacity and a deterministic mean equilibrium larval population of 6 larvae per patch, is seeded with 6 adult mosquito population, and is modelled as a single patch (dashed lines) or as a metapopulation on a 32x32 grid (solid lines). A coefficient of variation of 2 and a dispersal rate of 0.3 per day was used. A medium and high correlation were defined as $\alpha=0.3$ and $\alpha=0.01$, respectively (Equation 3.4). The results are compared with respect to the mean proportion of models runs which resulted in sustained invasion (final total adult population >1) (A), the mean proportion of patches which have been occupied at least once (B), mean total adult mosquito population size (C), and the mean proportion of patches occupied across the landscape (D). A mean dispersal distance of 5 patches was used. For each scenario, the mean and variance were calculated across 1000 realisations of the stochastic model.

3.3 Discussion

As discussed in Chapter 1, *Aedes aegypti* is a highly adaptive species, breeding in a wide range of indoor and outdoor domestic habitats. Therefore, in any urban environment, larval carrying capacity will vary spatially in accordance with the size and availability of breeding habitats.

Understanding how heterogeneity in carrying capacity, combined with seasonal variation in mosquito abundance and the dispersal behaviour of the mosquito, shapes fine-scale mosquito population dynamics is thus an intrinsic part of understanding how vector populations persist in fragmented landscapes. In this chapter, we aimed to provide insight into these dynamics.

While local population extinction is a recurrent event in all fragmented landscapes with low mean carrying capacity, we observed that recovery from extinction was largely more difficult in spatially heterogeneous landscapes, with inter-patch variability reducing persistence of small local populations. This in turn resulted in a smaller total population sizes and reduced patch occupancy across the landscape (compared with a homogeneous landscape of similar carrying capacity). Successful population invasion into unoccupied landscapes also proved more challenging in spatially heterogeneous environments, with inter-patch variability reducing the likelihood of sustained invasion upon seeding and slowing the speed of spatial spread across the landscape. For highly local dispersal, spatial clustering of habitat of similar quality resulted in increased total population size, but at the cost of reduced patch occupancy across the landscape and a slower speed of invasion.

While potentially accounting for seasonal variation in carrying capacity, adopting a non-spatial approach to representing the fine-scale dynamics of vector populations does not account for the fact that larval populations across a landscape are likely to experience varying degrees of density-dependent competition, with areas of higher carrying capacity able to support larger larval populations and more densely populated areas subject to more intense competition. Our results illustrate the importance of these heterogeneities in driving fine-scale *Aedes aegypti* population dynamics, and thus suggest that, to gain a deeper insight and understanding of the drivers of vector population persistence at fine spatial scale, features of the underlying landscape need to be considered.

How mathematical models choose to represent a landscape however is determined by the level of spatial granularity in a model, and we now explore how the choice of spatial granularity affects the population dynamics observed when modelling *Aedes aegypti* populations at fine spatial scales.

Chapter 4

Spatial Granularity

In the previous two chapters we demonstrated the importance of habitat fragmentation, mosquito behaviour and features of the underlying landscape in shaping the fine-scale dynamics of *Aedes aegypti* populations. The question now remains of how the dynamics we have observed depend on the level of spatial granularity in our model. Would we observe similar dynamics at lower levels of spatial granularity? In this chapter, I address this question, and explore if the dynamics observed under the metapopulation model can be approximated using a non-spatial single patch model.

4.1 Methods

4.1.1 Varying Spatial Granularity

To model the effect of different levels of representation of spatial granularity, we need to ensure the dispersal range remains fixed as granularity is reduced. Thus, as the level of spatial granularity in the model is varied, the mean dispersal length and dispersal range (measured in units of patches) are adjusted accordingly. For example, if we move from a $n \times n$ to a $\frac{n}{2} \times \frac{n}{2}$ grid then, as the size of each patch is doubled, both the mean dispersal length and dispersal range are halved. All other model parameters remain fixed as spatial granularity is varied.

4.1.2 Single Patch Approximations

To recap, the deterministic dynamics for the non-spatial (single patch) model are described by the following set of equations:

$$\frac{dE(t)}{dt} = bgO(t) - \gamma_E E(t) - \mu_E E(t) \quad (4.1)$$

$$\frac{dL(t)}{dt} = \gamma_E E(t) - \gamma_L L(t) - \mu_L \left(1 + \left(\frac{L(t)}{K(t)}\right)^\Omega\right) L(t) \quad (4.2)$$

$$\frac{dA(t)}{dt} = \gamma_L L(t) - \mu_A A(t) \quad (4.3)$$

$$O(t) = g^{-1} A(t) \quad (4.4)$$

where $E(t)$, $L(t)$ and $A(t)$ denote the egg, larval and adult population at time t respectively, $K(t)$ denotes the larval carrying capacity at time t , $O(t)$ denotes the number of adult mosquitoes laying eggs at time t , Ω describes the strength of density dependence, b denotes the oviposition rate, g denotes the length of the gonotrophic cycle of adult female mosquitoes, and μ_E , μ_L and μ_A denote the egg, larval and adult mosquito mortality rate respectively.

We explored if the invasion dynamics observed under the metapopulation model could be approximated by varying parameters in the corresponding (non-spatial) single patch model whose values are not constrained by directly observed ecological processes - namely mean larval carrying capacity (\bar{K}), and the strength of density dependence (Ω). We then compared the results obtained using the metapopulation model and adjusted single patch model, and adopted a least squares approach to determine the combination of values of \bar{K} and Ω best approximating the metapopulation dynamics. The population characteristics we sought to approximate included the mean and variance of the equilibrium total adult mosquito population, and the time until the population reaches equilibrium (which acts as a proxy for the growth rate of the population).

More formally, for a homogeneous landscape where L_{ij}^* denotes the deterministic equilibrium larval population of each patch (i, j) in the metapopulation model, we allow \bar{K} and Ω to vary in the corresponding single patch model (irrespective of the value of L_{ij}^* and keeping all other parameter values fixed), denoting these varying parameters \bar{K}' and Ω' . If we wish to approximate the mean and variance of the equilibrium total adult mosquito population observed under the metapopulation model for example, we define the sum of squared errors associated with the approximation, $\epsilon(L_{ij}^*, \bar{K}', \Omega')$, as

$$\epsilon(L_{ij}^*, \bar{K}', \Omega') = \left[\frac{M(\bar{K}', \Omega') - M(L_{ij}^*)}{M(L_{ij}^*)} \right]^2 + \left[\frac{V(\bar{K}', \Omega') - V(L_{ij}^*)}{V(L_{ij}^*)} \right]^2 \quad (4.5)$$

where $M(L_{ij}^*)$ and $M(\bar{K}', \Omega')$ denote the mean equilibrium total adult mosquito population observed under the metapopulation model and adjusted single patch model respectively, and $V(L_{ij}^*)$ and $V(\bar{K}', \Omega')$ denote the variance of the equilibrium total adult mosquito population observed under the metapopulation model and adjusted single patch model respectively. The combination of (\bar{K}', Ω') which minimise this error is then selected as the best fitting values of \bar{K}' and Ω' .

We follow the same approach for all combinations of characteristics approximated.

4.2 Results

4.2.1 Varying Spatial Granularity

When modelling the dynamics of an established mosquito population or those of a newly seeded population, the dynamics observed were strongly dependent on the level of spatial granularity assumed in the model. As spatial granularity is reduced, this leads to an increase in patch size and thus in the carrying capacity of individual patches. For example, as we reduce spatial granularity in a 32x32 grid with a carrying capacity of 3 larvae per patch, we obtain a 16x16 grid with a carrying capacity of 12 larvae per patch, an 8x8 grid with a carrying capacity of 48 larvae per patch and so forth. Reducing spatial granularity therefore in turn reduces the probability of stochastic extinction in individual patches (Figures 4.1A,B). Thus in a context where dispersal rates were low to moderate, a reduction in the level of spatial granularity largely resulted in increases in long term mean population sizes, population persistence, and patch occupancy, with the behaviour of the metapopulation largely tending towards that of the single patch model as spatial granularity is further reduced (Figures 4.1C-F).

The largest differences between different levels of granularity were therefore observed for landscapes where, at the highest level of spatial granularity, individual patches had a low carrying capacity and thus a high probability of stochastic extinction. Changes to parameter values which improved population persistence, such as increasing equilibrium larval population size or the dispersal rate, reduced the magnitude of the differences observed between higher and lower levels of spatial granularity (Figure 4.1).

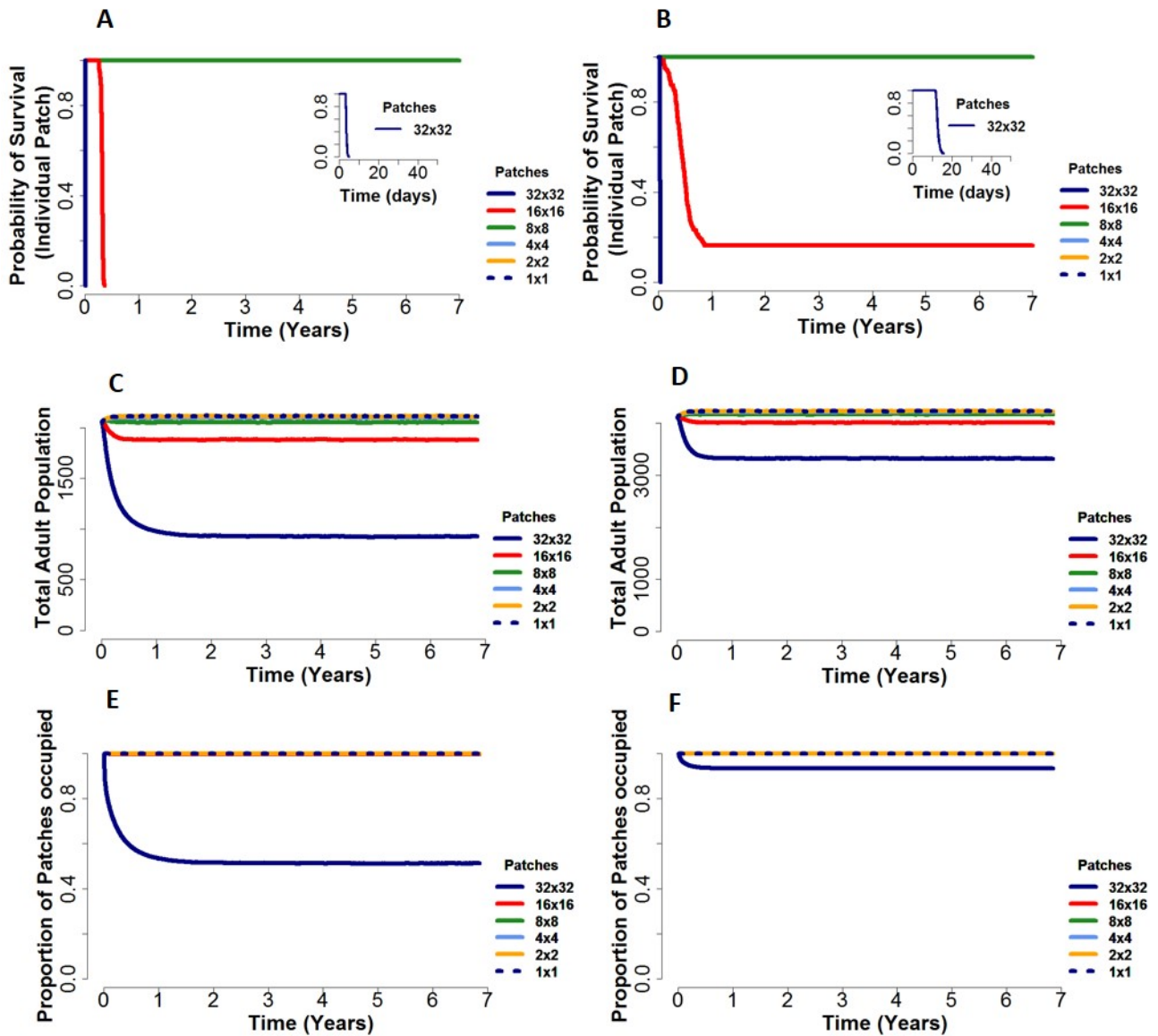


Figure 4.1: Modelling Established Populations at Different Levels of Spatial Granularity. Population dynamics observed when a homogeneous landscape with an equilibrium larval population (at the 32x32 level) of 3 (A,C,E) or 6 (B,D,F) larvae per patch is modelled at different levels of spatial granularity. A dispersal rate of 0.08 was used and mean dispersal length (at the 32x32 level) is 5 patches. The maximum dispersal range (at the 32x32 level) was set to 32 patches. Figures (A) and (B) are Kaplan-Meier curves showing the time to first extinction of an individual breeding site in the landscape. For each scenario, the mean was calculated across 1000 realisations of the stochastic model.

While behaviour of the metapopulation always tended towards that of the single patch model as spatial granularity is reduced for landscapes where a stable mosquito population was already established, this was not always the case for unoccupied landscapes newly seeded with a mosquito population. Here, the invasion dynamics observed depend heavily on both the level of spatial granularity in the model and the dispersal rate and kernel. Thus, a more complex picture emerges. For both low and high values of single patch carrying capacity, if dispersal across the landscape at the highest level of spatial granularity is very local then, as granularity is reduced, movement beyond the seeded patch becomes less likely. Therefore, at lower levels of granularity,

population spread and growth beyond the seeded patch may not occur, despite a very low risk of extinction through stochastic effects in neighbouring patches (Figure 4.2). Thus, behaviour tending towards the single patch model as granularity is reduced is not necessarily guaranteed, and relies on sufficient movement between patches at lower levels of granularity.

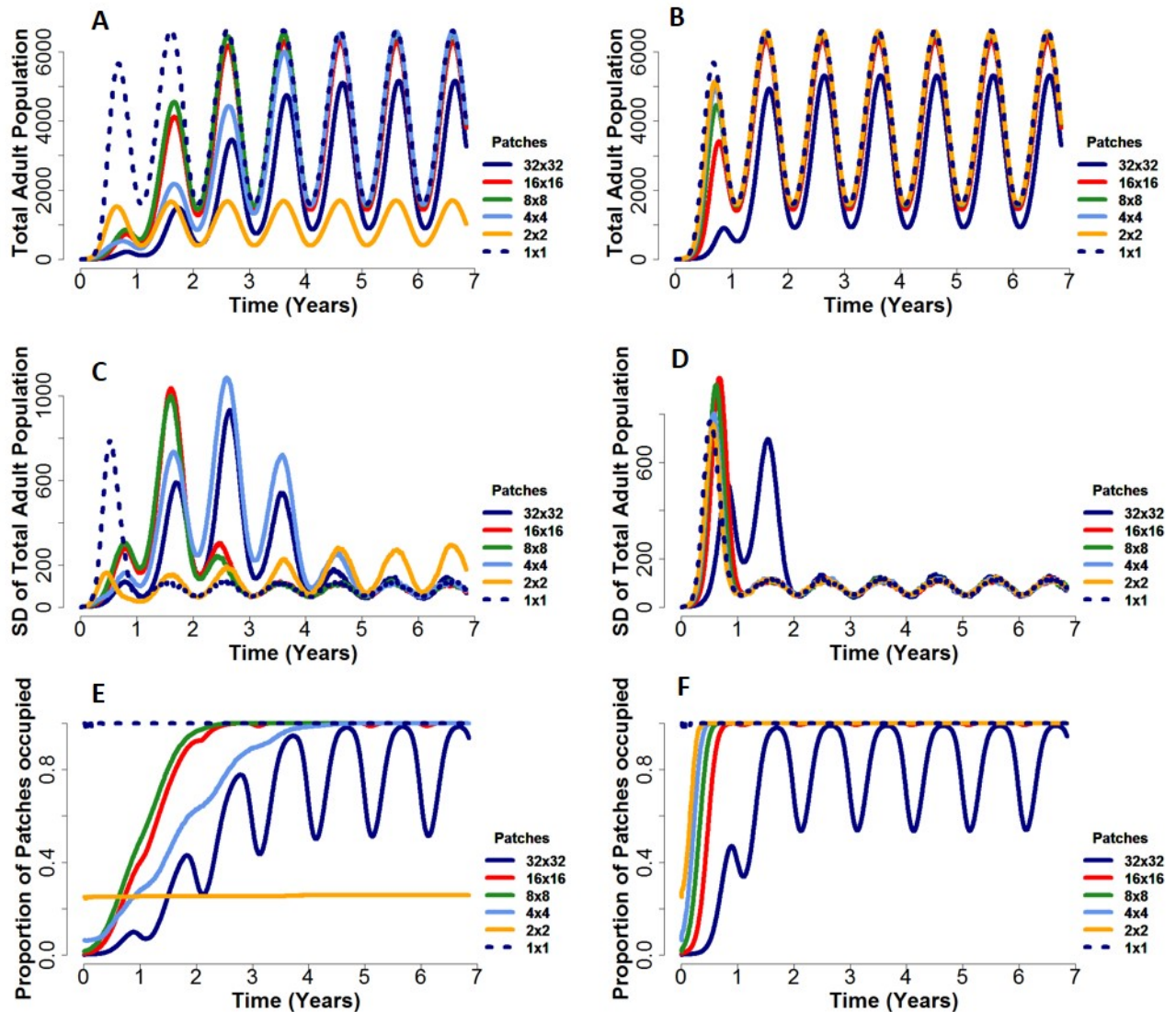


Figure 4.2: Modelling Invasion Dynamics at Different Levels of Spatial Granularity. Population dynamics observed when a landscape with temporal variation in carrying capacity and an equilibrium mean larval population of 6 larvae per patch (at the 32x32 level) is seeded with an adult population of 6 mosquitoes and modelled at different levels of spatial granularity. The dispersal rate was 0.08 per day. (A,C,E) correspond to dynamics observed when the mean dispersal length (at the 32x32 level) is 1 patch, and (B,D,E) correspond to the dynamics observed when the mean dispersal length (at the 32x32 level) is 5 patches. The maximum dispersal range (at the 32x32 level) was set to 32 patches. For each scenario, the mean and variance were calculated across 1000 realisations of the stochastic model.

4.2.2 Single Patch Approximations

We explored if the invasion population dynamics observed under the metapopulation model could be approximated by varying mean larval carrying capacity (\bar{K}) and the strength of density dependence (Ω) in the corresponding single patch model. To approximate the mean equilibrium total adult mosquito population size and growth rate observed under the metapopulation model, we first allowed \bar{K} alone to vary while keeping $\Omega = 1$ fixed (i.e. assuming density dependence remained linear). Reducing mean larval carrying capacity enabled us to closely approximate equilibrium population size (Figures 4.3A-B, 4.4A-B). However, owing to the rapid speed of population growth in the single patch model, this approach led us to overestimate the growth rate of the population and underestimate the variability in population size during the early stages of population growth (Figures 4.3C-D, 4.4C-D), particularly when equilibrium larval population size was small and movement across the landscape was limited.

Instead allowing both \bar{K} and Ω to vary resulted in a better approximation of the growth rate of the population (Figures 4.3A-D, 4.4A-D), with reducing both \bar{K} and Ω giving the best fitting combination of values for fragmented landscapes where individual patches have a low carrying capacity (Figure 4.5). This is because $\Omega < 1$ and reduced K results in higher larval mortality and thus slower population growth when larval density is low compared with single patch models where $\Omega = 1$ and K is larger. This in turn allowed us to better replicate the full temporal curve of population growth observed under the metapopulation model.

However, while this combined approach improved our approximation of the growth rate, we remained unable to capture the increase in variability during the early stages of population growth (Figures 4.3C-D, 4.4C-D). Furthermore, in some cases where the carrying capacity of individual patches was low, this led to an over-estimate of the variance of the equilibrium adult population (Figures 4.3C, 4.4C). Approximating the variance of the equilibrium adult population, in addition to the mean equilibrium adult population and the growth rate of the population, improved our estimate of the variance of the population but at the cost of then overestimating the speed of population growth (Figures 4.3E-H, 4.4E-H). Similar patterns were observed when approximating the mean and variance of the equilibrium adult population only, and not taking account of the growth rate.

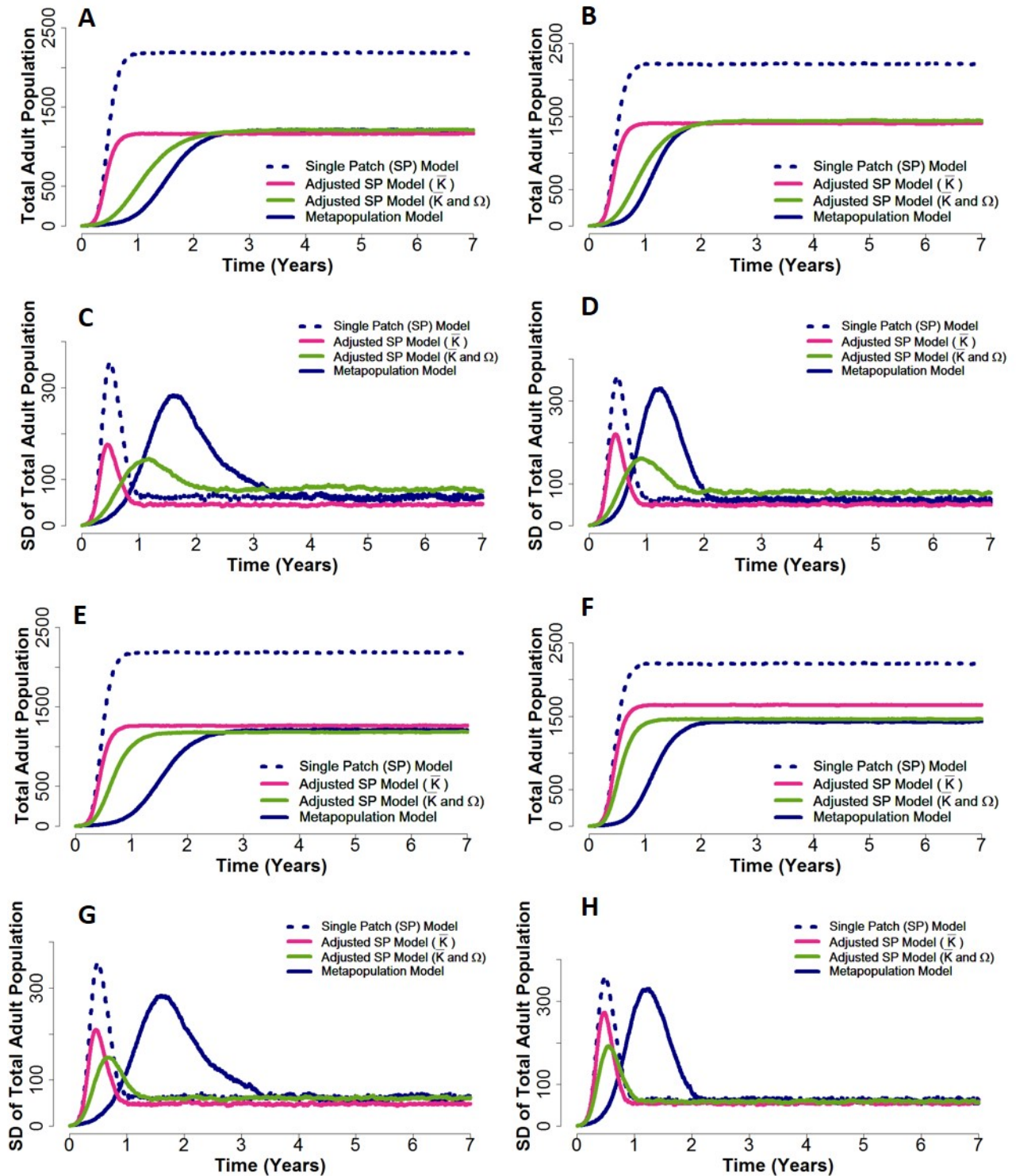


Figure 4.3: Single Patch Approximations - Example 1. Comparison of results obtained when we approximate the invasion dynamics observed when a homogeneous landscape comprised of 1024 patches, with an equilibrium larval population of 3 larvae per patch, is seeded with 3 adult mosquitoes. A mean dispersal length of 5 patches and for a dispersal rate of 0.10 (A,C,E,G) and 0.30 (B,D,F,H) was used. (A-D): We approximate mean equilibrium total adult mosquito population and the growth rate of the population. (E-H): We approximate the mean and variance of the total adult mosquito population in addition to the growth rate of the population. For each scenario, the mean and variance were calculated across 1000 realisations of the stochastic model.

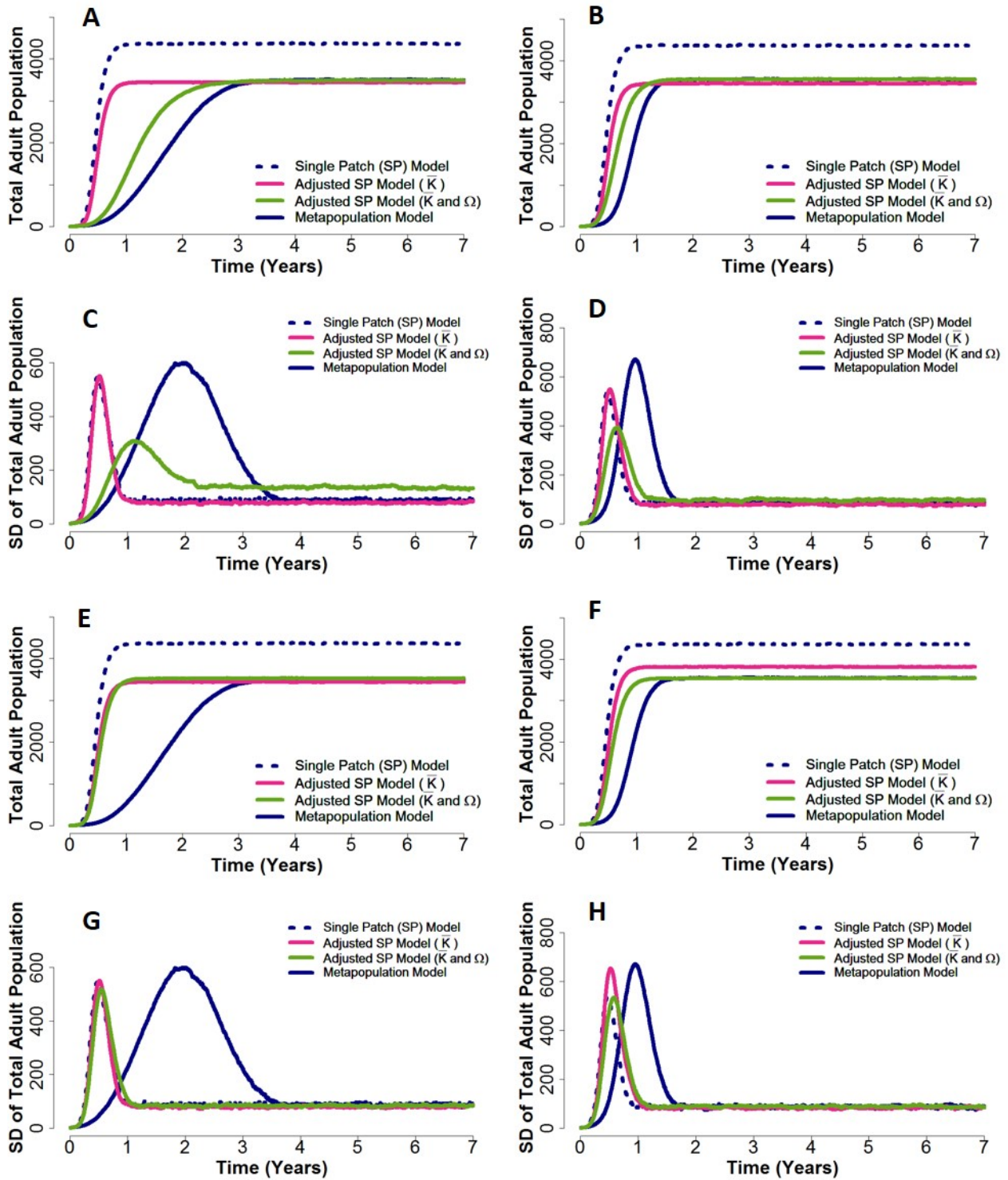


Figure 4.4: Single Patch Approximations - Example 2. Comparison of results obtained when we approximate the invasion dynamics observed when a homogeneous landscape comprised of 1024 patches, with an equilibrium larval population of 6 larvae per patch, is seeded with 6 adult mosquitoes. A dispersal rate of 0.1 and a mean dispersal length of 1 patch (A,C,E,G) and 5 patches (B,D,F,H) was used. (A-D): We approximate mean equilibrium total adult mosquito population and the growth rate of the population. (E-H): We approximate the mean and variance of the total adult mosquito population in addition to the growth rate of the population. For each scenario, the mean and variance were calculated across 1000 realisations of the stochastic model.

As expected, the largest adjustments to the single patch model were needed for fragmented landscapes where individual patches had a very low carrying capacity and where dispersal beyond the seeded patch was limited (Figure 4.5). Where changes to parameter values such as increasing the dispersal rate, the mean dispersal length or the equilibrium larval population size resulted in more rapid population growth and increased population size in the metapopulation model (and thus behaviour similar to the unadjusted single patch model) smaller adjustment to the single patch model were required. Thus we could more closely approximate the dynamics observed under the metapopulation model.

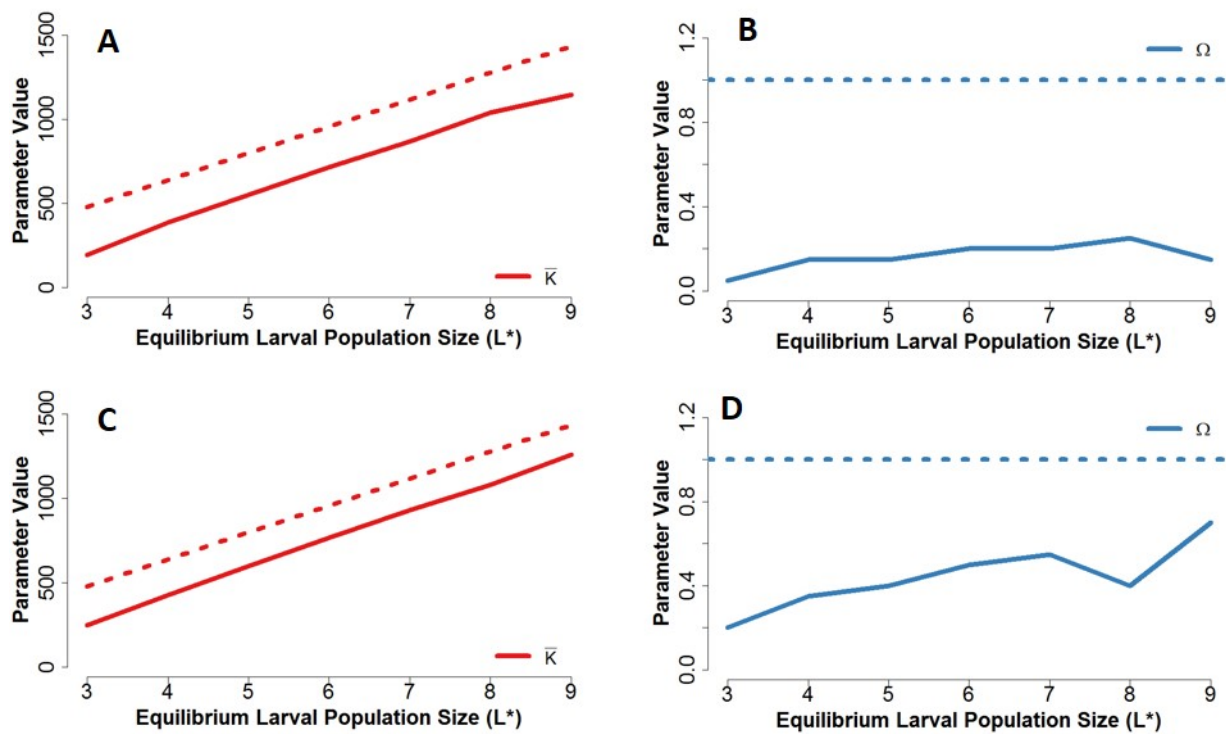


Figure 4.5: Single Patch Approximations - Magnitude of Adjustment. Example of difference between the best fitting values of \bar{K} and Ω in the adjusted single patch model (solid lines) and the corresponding values in the unadjusted single patch model (dashed lines). Here we approximate mean total population size and the growth rate of the population, and use a dispersal rate of 0.10. (A,B): Results corresponding to a mean dispersal length of 1 patch (C,D): Results corresponding to a mean dispersal length of 5 patches.

4.3 Discussion

When accounting for the fragmented structure of mosquito populations, the level of fidelity we have in representing this underlying spatial structure is determined by the level of spatial granularity in our metapopulation model. In the previous two chapters, we demonstrated the importance of this spatial structure to the fine-scale dynamics of *Aedes aegypti* populations, finding that larval habitat fragmentation, the dispersal behaviour of the mosquito and features of the underlying landscape combine to shape population dynamics at fine spatial scales. In this chapter, we found that the population dynamics we observed were heavily dependent on the level of spatial granularity represented in our model, as reductions in granularity reduced the risk of extinction through stochastic effects, thereby increasing population persistence, patch occupancy, and the speed of population spread across the landscape.

Approximating the dynamics observed at high levels of spatial granularity using the non-spatial single patch model is therefore difficult. Typically, as carrying capacity is an unmeasurable and quite theoretical concept, modellers calibrate models to reproduce observed population characteristics, such as population size or density. In that context, our results indicate that single patch models will underestimate population volatility, and over-estimate invasion speeds (e.g. following population troughs). We found that varying both carrying capacity and the strength of density-dependence allowed us better capture the dynamics observed in fragmented landscapes and, moreover, interestingly, found that stochastic volatility can be better captured by a single patch model if the intensity of density-dependence is assumed to be less than linear. However, even this adjustment is unable to capture the slower invasion dynamics and increased variability associated with the spatial structuring of the mosquito population when local populations are small and dispersal is limited.

As noted at the end of Chapter 2, our results suggest that using non-spatial models to represent the fine-scale dynamics of mosquito populations may substantially underestimate the stochastic volatility of those populations. However, given that these effects are greatest for landscapes where the carrying capacity of individual patches is low and adult mosquito dispersal is relatively local, assessing whether such effects are in fact relevant to real-world *Aedes aegypti* populations therefore requires consideration of what is the appropriate level of representation of spatial structure in these populations. The results obtained in this chapter suggest that, to capture

the impact of the fragmentation of larval breeding sites on fine-scale *Aedes aegypti* population dynamics in a meaningful way, models should aim to capture the population dynamics observed when modelling at a level of spatial granularity such that movement between patches is representative of the typical dispersal length of the mosquito. If granularity is reduced such that movement between patches goes beyond the typical dispersal length, the vulnerability of small local populations to extinction is masked by the increase in patch size and consequent reduction in the risk of extinction through stochastic effects, and thus we fail to observe the potential impact of habitat fragmentation with populations are small.

Field studies have shown that *Aedes aegypti* populations in dengue-endemic areas range between under 0.5 to over 3 adult females per person - namely in the range 2 to 20 per household, depending on household size [61, 220, 221], and furthermore can drop to very low numbers at the household level during seasonal troughs in mosquito abundance [221]. Empirical research has found that *Aedes aegypti* exhibit considerable spatial variation in abundance, even at the individual household level, with clustering among households of similar levels of carrying capacity often occurring [47, 59, 61, 220, 221, 225, 226]. In addition, mark-release-recapture experiments suggest the dispersal range of *Aedes aegypti* mosquitoes is in the range of 20-100 meters [75–77], with most released *Aedes aegypti* being recaptured in the house of release [75] and under 10% being captured more than 3 households away. Thus modelling at the individual household level seems appropriate for this species. Therefore, given these observations, the effects of larval habitat fragmentation and local dispersion described here may be highly relevant to the modelling of real-world *Aedes aegypti* populations.

These effects are also therefore likely to be of particular importance for the modelling of the potential impact of novel vector control measures. Indeed, recent analysis of the spread of the bacterium *Wolbachia* among local *Aedes aegypti* populations in northern Australia has shown that both the pattern and speed of spatial spread of *Wolbachia* is highly heterogeneous, largely owing to environmental factors, including fine-scale variation in *Aedes aegypti* population density [197]. The potential success of both populations modification and population suppression technologies relies on the successful integration of modified mosquito populations into wild-type *Aedes aegypti* populations. Hence, a deep understanding of fine-scale *Aedes aegypti* population dynamics is fundamental to understanding the likely impact of such approaches. Our results suggest that

underestimating the stochastic volatility of local populations, and failing to represent the underlying fragmented spatial structure of these populations at an appropriate level of spatial granularity, may lead to over-estimates of the speed of spatial spread of such technologies. Moreover, this may make it more difficult to identify potential barriers to local establishment and persistence, across a range of heterogeneous environments. This is in general agreement with dynamics observed by Hancock *et al.* who, using a 1-dimensional metapopulation model of the spread of *Wolbachia*, find that spatial heterogeneity may considerably slow the speed of spatial spread across a landscape [196]. Furthermore, in the context of population suppression approaches, understanding the role of spatial structure is likely to be an important factor in mitigating the risk of reduced efficacy owing to migration of wild-type mosquitoes from surrounding areas, and in assessing the speed at which the population may rebound once interventions have ceased.

It is important to note however that, while our results may be highly relevant for modelling *Aedes aegypti* populations, this may not necessarily be the case for models of other mosquito species as typical dispersal length varies between species. For example, measured mean dispersal distances are an order of magnitude further for *Anopheles gambiae* than *Aedes aegypti* - 500m or greater [227, 228] - meaning appropriate patch sizes (both in terms of dimension and population size) for modelling the fine-scale dynamics of these populations can be expected to be considerably larger - perhaps village level. Thus the effects of landscape heterogeneity, local stochastic extinction and reseeded predicted by our modelling to be significant for *Aedes aegypti* are likely to be less so for *Anopheles gambiae*. The exception might be in environments where *Anopheles gambiae* density is exceptionally low - for example during seasonal troughs in areas such as the Sahel [229, 230].

The work presented here also has several limitations. As discussed in Chapter 2, we assumed that density-dependent effects occur during the larval stage of mosquito development through changes in the larval mortality rate in accordance with larval density alone. However, density-dependent competition may also lead to longer larval development times or smaller adult females emerging from the breeding site [62, 64, 70], which in turn may reduce the oviposition rate of adult females [214]. Thus, the effects of density-dependent competition could instead, for example, been represented by varying the larval development rate or oviposition rate in our model in accordance with larval density.

For landscapes where *Aedes aegypti* populations are already established, we hypothesise that quantitatively similar equilibrium population dynamics would have been observed for alternative functional forms of density-dependence. For example, if we increase larval development times with increased larval density (rather than increasing the larval mortality rate), then this would also lead to fewer new adults emerging from the habitat at higher larval densities in a given timestep. Consequently, in subsequent timesteps, fewer eggs are laid and fewer new larvae develop. Thus, for a given landscape, these different forms of density dependence are likely to produce similar dynamics.

However, for landscapes where we're seeding a mosquito population, we hypothesise that alternative formulations of density-dependence may have a larger impact on the dynamics, compared with landscapes where an *Aedes aegypti* population is already established. For example, reducing the speed of larval development or the oviposition rate with increased larval density may in turn lead to a slower speed of population spread across the landscape, as it may take longer for populations to become established in individual patches. Consequently, this may also lead to a potentially longer period of population instability during the early stages of population growth, particularly when the dispersal rate across the landscape is low. However, overall, our results suggest that the primary driver of the dynamics observed is the increased risk of local extinction through stochastic effects, arising from larval habitat fragmentation. Hence, we hypothesise that changing the functional form of density-dependence used in our model is unlikely to have a large impact on the results obtained and key patterns observed.

Our results concerning approximating metapopulation dynamics using the non-spatial single patch model, by varying both carrying capacity and the strength of density-dependence, may also depend on the functional form of density-dependence adopted. Alternative formulations of density-dependence may have improved or worsened our approximations, however we have not explored this here.

In addition, although appropriate values for model parameters were sourced where possible from the existing literature, the model presented was not explicitly fitted to entomological data. We have also assumed that larval development times and the lifespan of adult mosquitoes are

exponentially distributed, however the rate at which mosquito larvae develop is temperature dependent [64] and older adult mosquitoes may experience increased mortality [231, 232]. Finally, as we consider the dynamics of *Aedes aegypti* populations alone, the extent to which our results may affect models of dengue transmission, which consider larval population dynamics, is unknown. A model which incorporates both vector and disease dynamics would offer much greater insight into the potential impact of larval population fragmentation on the fine-scale transmission dynamics of dengue.

In conclusion, our work highlights the importance of choices made about representations of the spatial structure of larval populations when modelling the dynamics of *Aedes aegypti* populations at fine spatial scales. Our results demonstrate that, for low mosquito population densities, adopting a non-spatial approach to model the fine-scale dynamics of *Aedes aegypti* larval populations may substantially underestimate the stochastic volatility of mosquito populations and over-estimate the speed of population invasion and growth. Accounting for the fragmented structure of larval populations allows us to better capture the dynamics of density-dependent competition, and understand how the level of connectivity between local populations and features of the underlying landscape shape *Aedes aegypti* population dynamics at fine spatial scales. Our results indicate that the individual household level is likely to be an appropriate level of spatial granularity for models to adopt to represent the fine-scale dynamics of *Aedes aegypti* populations.

Chapter 5

Project *Wolbachia* Singapore: Data & Model Development

In Chapters 5 and 6, I move to addressing the second aim of this thesis - namely to develop an inferential framework which allows us to calibrate a stochastic model of *Aedes aegypti* population dynamics against entomological data, while accounting for the highly variable nature of mosquito trapping data. I then use this framework to explore the results of a small-scale field study of IIT conducted in Singapore.

5.1 Introduction

With its tropical climate and high levels of urbanisation, Singapore provides an ideal setting for dengue transmission. Dengue is thus endemic in Singapore, with all four serotypes co-circulating and a high degree of viral diversity within serotypes [233, 234]. However, despite these favourable conditions for transmission, dengue seroprevalence in Singapore is low compared with other countries in Southeast Asia such as Thailand and Vietnam where dengue is hyperendemic. Analysis of serology data collected during recent vaccine trials estimated a seroprevalence rate of 48.7% among adults aged 18-45 in Singapore, compared with 94.5% among the same age group in Vietnam [235].

The relatively low level of dengue transmission in Singapore can largely be attributed to the intensive vector control measures which have been in place since the late 1960's. Following the first reported case of dengue haemorrhagic fever in Singapore in 1966, a multifaceted active vector control strategy was introduced which combined vector surveillance, source reduction,

legal enforcement and education of the public on the risks associated with breeding *Aedes aegypti* mosquitoes. This in turn resulted in a drop in the premises index (defined as the proportion of inspected premises found to have containers with *Aedes aegypti* larvae or pupae) from approximately 50% in 1966 to less than 5% in 1973 [82, 236]. Consequently, incidence of dengue also dropped dramatically during this period.

Although intensive vector control efforts have been sustained and the premises index remains below 1% [236], there has been a resurgence of dengue in Singapore since the late 1980's [82, 237]. Dengue epidemics now occur approximately every 5-6 years, with the size of outbreaks increasing in recent years [236, 238]. The largest outbreak to date occurred in 2013-2014, resulting in a total of 22,170 cases in 2013 and 18,338 cases in 2014, corresponding to an incidence rate of 410.6 and 335 per 100,000 population in 2013 and 2014 respectively [236]. The number of cases reported was approximately 1.7 times the number reported during the previous largest outbreak which occurred in 2005 [236, 238].

Several hypotheses have been proposed to explain this resurgence. One reason suggested is that, as a consequence of the long period of low transmission in the 1970's and early 1980's following successes in vector control, herd immunity among the population is low, thereby leaving the adult population more susceptible to outbreaks of dengue [82]. Indeed, dengue now predominantly affects the adult population in Singapore [238, 239]. The highest incidence of dengue during outbreaks in 2005, 2007 and 2013-2014 was observed in older age groups [236, 238, 240], and the median age of infection increased from 14 in 1973 to 37 in 2007 [238, 241]. Recent outbreaks have been caused by switches in the predominant circulating serotype (primarily between DENV1 and DENV2) [239], and seroprevalence surveys have shown that previous exposure to dengue is low among young adults in Singapore [242].

Another hypothesis is that the location of dengue transmission in Singapore has changed, with transmission now often occurring outside of the home environment [82, 237, 243]. As noted above, dengue now predominantly affects the adult population. Incidence of dengue has also been greater in males than females during recent outbreaks [236, 238, 240]. In addition, a substantial rise in seroconversion has been observed in children aged 6 and above which coincides with the age children typically start school in Singapore [243].

Several other environmental, social and immunological factors have also been suggested as possible contributing factors to the resurgence of dengue in Singapore. Increased travel, urbanisation and human population density may have facilitated increased virus transmission [236], and the high degree of diversity within virus serotypes may allow for selection of strains with higher fitness [234]. Recent years have also seen a change in emphasis from vector surveillance to early case detection [82].

In light of this resurgence, new vector control tools are sought to improve dengue control in Singapore and, since 2012, the National Environment Agency (NEA) in Singapore has focused on exploring the use of *Wolbachia* as a tool for vector population suppression. This in turn has led to the creation of Project *Wolbachia* Singapore which, through a series of field studies, aims to examine whether releasing *Wolbachia*-infected male *Aedes aegypti* can be used to suppress the *Aedes aegypti* population in Singapore. The first small-scale field study (Phase 1) testing this approach began in October 2016, and here we analyse the results of this study by calibrating a model of IIT against the detailed entomological data collected during this study.

In this chapter, I describe the Phase 1 study design and the data collected over the course of this study. I then describe the model of IIT developed, and the inferential methods used to calibrate the model against the mosquito trapping data collected during the study. Model fitting results using simulated data are presented at the end this chapter, and results using the Phase 1 field study data are presented and discussed in Chapter 6.

5.2 Phase 1 Field Study

Phase 1 of Project *Wolbachia* Singapore began in October 2016, with the aim of exploring if the *Aedes aegypti* population in Singapore could be suppressed through releasing *Wolbachia*-infected male *Aedes aegypti* into the urban environment. This small-scale study involved the release of male *Aedes aegypti*, transinfected with the *wAlbB* *Wolbachia* strain (isolated from *Aedes albopictus*), into residential blocks in two areas of the city, Tampines and Yishun (Figure 5.1).

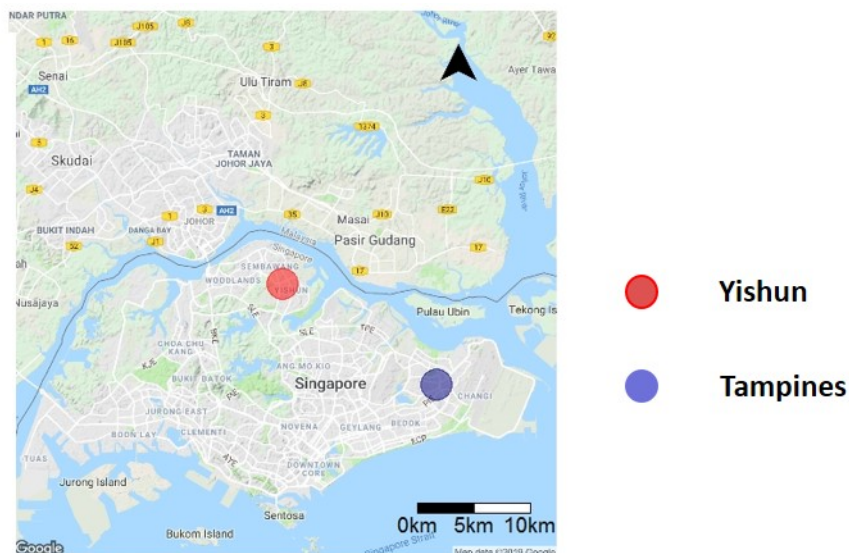


Figure 5.1: Project *Wolbachia* Phase 1 - Study Sites. *Wolbachia*-infected male *Aedes Aegypti* were released in Tampines and Yishun.

5.2.1 Release Strategy

In Tampines, *Wolbachia*-infected males were released weekly for a period of 31 weeks, from October 2016 to May 2017, across 29 residential blocks (Figure 5.2A). The number of *Wolbachia*-infected males released per week varied during the release period, ranging from 9,814 when releases commenced to 46,061 at the end of the release period. This resulted in a total release size of 579,735 *Wolbachia*-infected males (Figure 5.3A). The corresponding control site was comprised of 21 residential blocks.

In Yishun, a slightly different release strategy was adopted, as releases of *Wolbachia*-infected males were performed only in a subset of 10 of the 35 residential blocks at the release site (Figure 5.2B). Thus, compared with Tampines, fewer *Wolbachia*-infected males were released over a smaller area. This approach was adopted to test the dispersal of *Wolbachia*-infected males beyond the boundary of where releases occurred. Therefore, although releases only occurred across 10 blocks, data was collected from all 35 residential blocks at the release site. The corresponding control site was comprised of 29 residential blocks.

Releases in Yishun also began later than in Tampines. Three initial single releases of 3,500 *Wolbachia*-infected males took place at three different residential blocks in November and December 2016, and January 2017 (Figure 5.3B). The aim of these releases was to test the

longevity and vertical dispersal range of *Wolbachia*-infected males. Bi-weekly releases of *Wolbachia*-infected males across all 10 residential blocks subsequently began in February 2017, and continued for a period of 15 weeks. 10,500 *Wolbachia*-infected males in total per week were released during this period, and the release size remained constant (Figure 5.3B). A total of 216,900 *Wolbachia*-infected males were thus released in Yishun. In both Tampines and Yishun, all *Wolbachia*-infected males were released at the ground floor level.

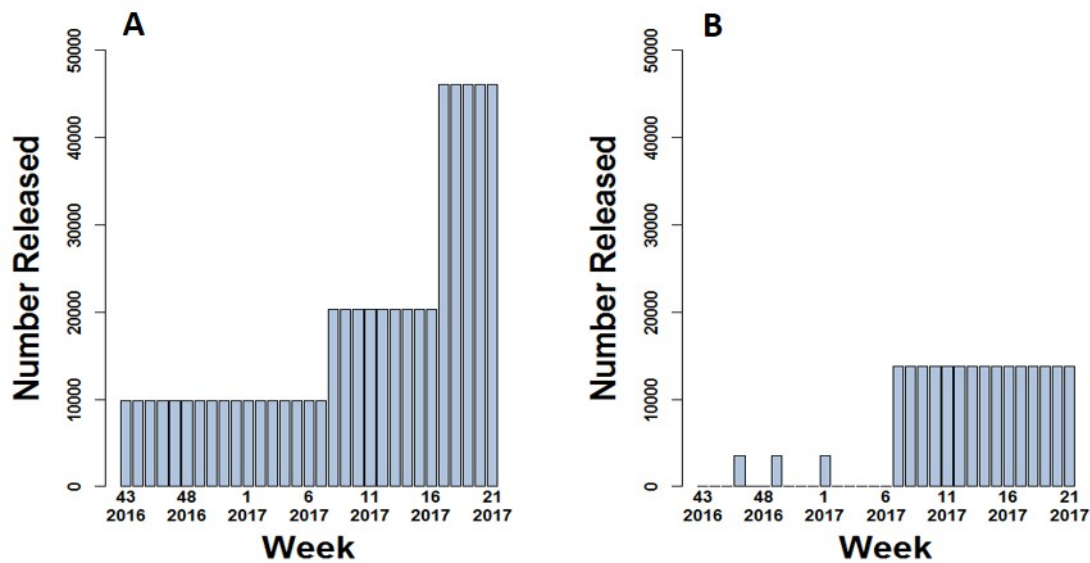


Figure 5.2: Release Sizes Number of *Wolbachia*-infected male *Aedes aegypti* released in Tampines (A) and Yishun (B) during the Phase 1 field study.

	Tampines (Control)	Tampines (Release)	Yishun (Control)	Yishun (Release)
Number of <i>Wolbachia</i> -infected Males Released	-	579,735	-	216,900
Number of Releases	-	31	-	18
Frequency of Releases	-	Weekly	-	Bi-weekly
Number of Residential Blocks	21	29	29	35 (10)
Number of Gravitraps (adults)	145	182	218	243 (73)
Number of Ovitrap (eggs)	78	95	14	66 (28)

Table 5.1: Phase 1 Summary. Overview of the Phase 1 study. For the Yishun release site the values in brackets correspond to the number of residential blocks and traps in the area where *Wolbachia*-infected males were released.

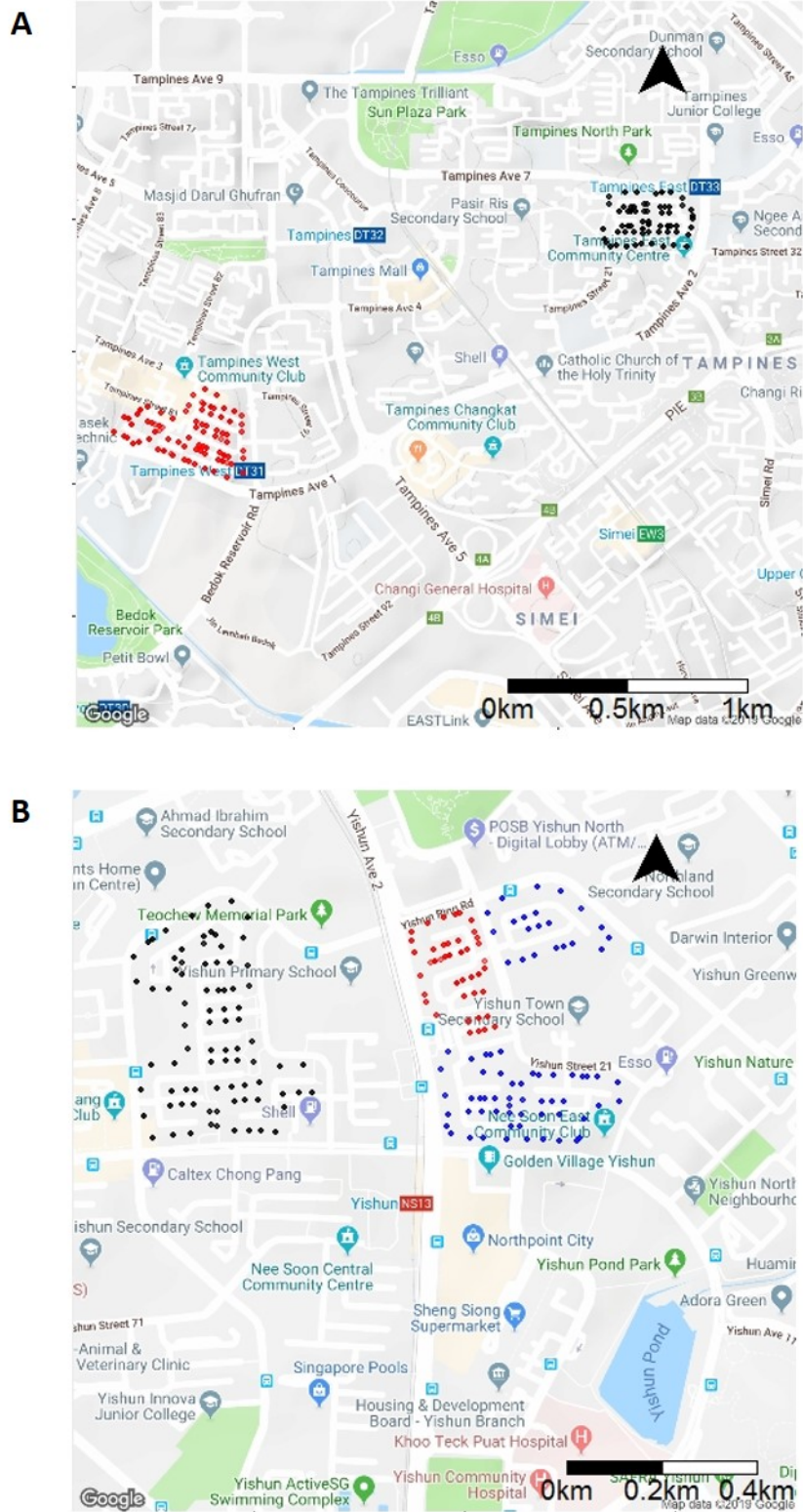


Figure 5.3: Residential Blocks Location of Gravitraps in residential blocks at the Tampines (A) and Yishun (B) study sites. Here, black represents Gravitraps in residential blocks at the control site and red represents Gravitraps in residential blocks at the release site, into which *Wolbachia*-infected males were released. The blue dots at the Yishun release site correspond to Gravitraps in residential blocks in areas which were monitored but where *Wolbachia* releases did not occur.

5.2.2 Data Collected

Detailed entomological data was collected across all sites, with the full entomological dataset we received comprising of:

- Egg Data - weekly counts of the number of hatching (viable) and non-hatching (nonviable) *Aedes aegypti* eggs per trap, per residential block
- Adult Mosquito Data - weekly counts of the number of wild-type and *Wolbachia*-infected *Aedes aegypti* males, and wild-type *Aedes aegypti* females per trap, per residential block
- Release Sizes - number of *Wolbachia*-infected male *Aedes aegypti* released per residential block per week for each release site

In both Tampines and Yishun, Gravitraps (which trap adult mosquitoes) were placed in each residential block at the control and release sites, while ovitraps were placed in a subset of residential blocks at each site. The location of traps varied between blocks, depending on the size of the block. However, in all residential blocks, traps were placed on lower, middle and upper floors of the block (typically on floors 2, 6 and 11). Trapping data was collected weekly and recorded at the individual trap level. Egg trapping data was collected over a shorter period compared with adult mosquito trapping data and, in addition, data collection began at different time points for each site.

Nonviable eggs were collected at both control and release sites as eggs laid may fail hatch for reasons other than CI. Other environmental and physiological reasons such as an insufficient level of submergence, changes in temperature or the presence of other micro-organisms in the water [48] may also lead to eggs not hatching. However, as expected, very low number of nonviable eggs were collected at control sites. Plots of the Gravitraps and ovitraps data aggregated across residential blocks for each site are presented in Figure 5.4 below. For ease of comparison, we present the data for weeks where we have data for corresponding control and release sites in this figure.

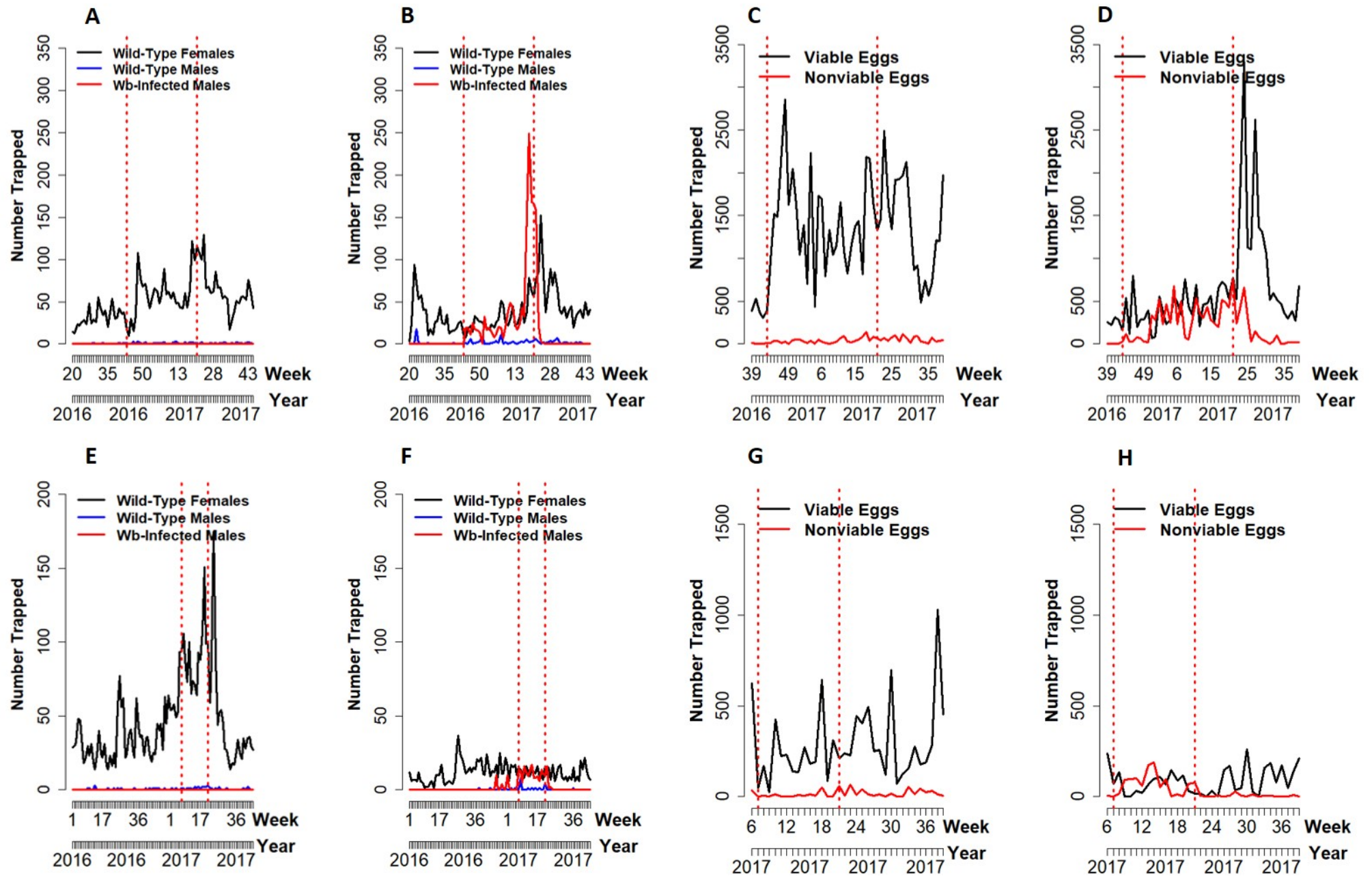


Figure 5.4: Aggregated Trapping Data. A-D: Gravitrapp and ovitrapp data aggregated across residential blocks for the Tampines control (A,C) and release (B,D) sites. E-H: Gravitrapp and ovitrapp data aggregated across residential blocks for the Yishun control (E,G) and release (F,H) sites. For each location, the dashed red lines show the period when *Wolbachia*-infected males were released. The data for the Yishun release site corresponds to the area where *Wolbachia*-infected males were released only.

Considerable differences were observed between the number of wild-type *Aedes aegypti* males and females trapped, with very few wild-type males trapped in both Tampines and Yishun (Figure 5.4, 5.9, 5.10). This pattern was consistent across all control and release sites (Figure 5.4, 5.9, 5.10). However, a very low trapping rate for adult males was not unexpected as Gravitraps have been designed to primarily attract female *Aedes aegypti* (using hay-infused water) [244]. Nonetheless, wild-type male mosquitoes were trapped at all sites, and *Wolbachia*-infected males were successfully trapped at both release sites. In Tampines 0.26% (1480/579,735) of the *Wolbachia*-infected males released were subsequently trapped, while 0.12% (260/216,900) were subsequently trapped in Yishun. Of those trapped in Yishun, 81% (211/260) were trapped within the area where releases occurred.

During the release periods, the majority of wild-type and *Wolbachia*-infected males were trapped on lower floors in both Tampines and Yishun (Figure 5.5). The distribution of trapped females was more evenly spread across lower, middle and upper floors, however, the majority of females were also trapped on lower floors during the release period at both release sites (Figures 5.5A,D). The distribution of trapped females across floors was similar at control and release sites, in both Tampines and Yishun (Figures 5.5A,D). There was a greater variability between control and releases sites in the distribution of trapped wild-type males across floors (Figures 5.5B,E). However, as very few wild-type males were trapped (Figure 5.4), the sample size is very small.

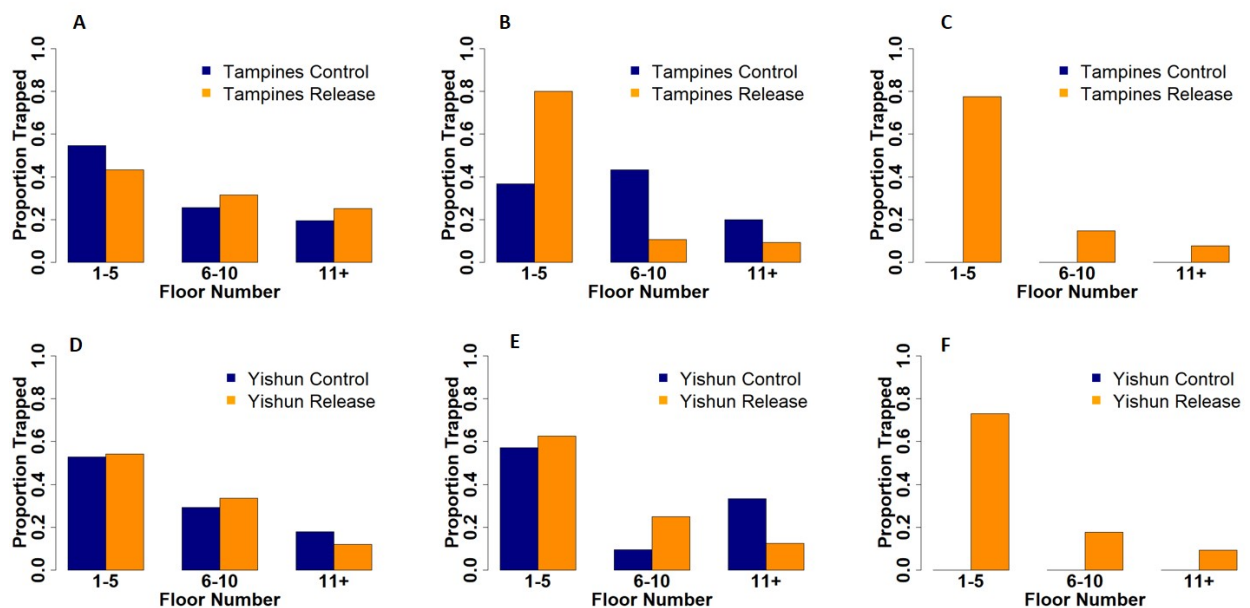


Figure 5.5: Distribution of Adult Mosquitoes Trapped across Floors Proportion of wild-type adult females (A,D), wild-type males (B,E) and *Wolbachia*-infected males (C,F) trapped on lower, middle and upper floors of residential blocks during the release period at both study sites.

At both Tampines and Yishun, the mean number of adult females trapped per residential block varied temporally, and between control and release sites (Figures 5.6, 5.7, 5.8). Figures 5.7 and 5.8 compare the number of adult mosquitoes trapped per block and the proportion of viable eggs among eggs trapped per block at control and releases sites in Tampines 5.7 and Yishun 5.8, before, during and after the release period.

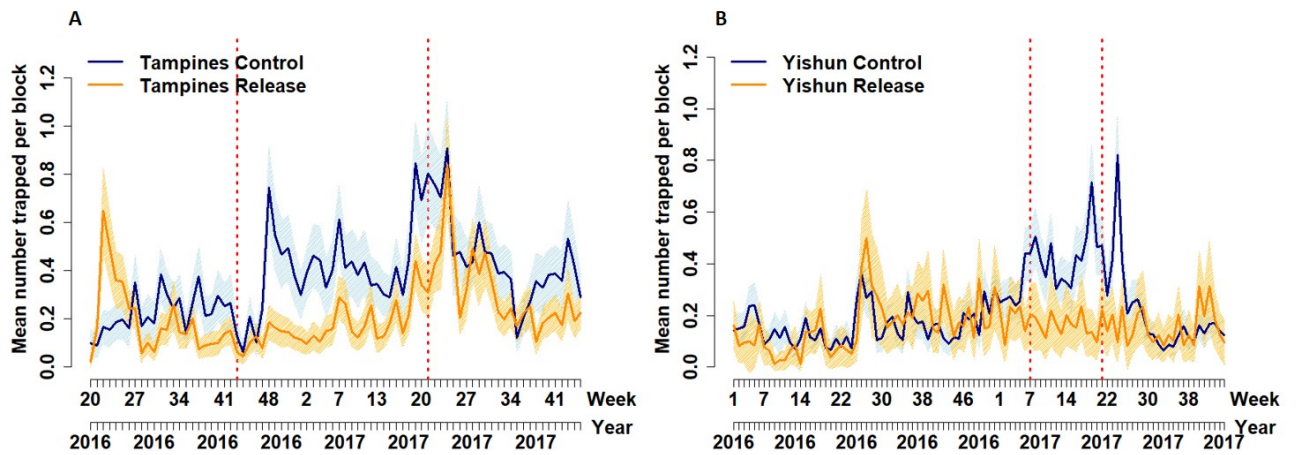


Figure 5.6: Mean Number of Adult Females Trapped per Block Temporal variation in the mean number of adult females trapped per block at the Tampines (A) and Yishun (B) study sites. The solid lines show the mean number trapped, and the shaded areas shows the 95% confidence interval.

For both study areas, the mean number of adult females trapped per residential block and the mean proportion of viable eggs per block was lower during the release period at the release site compared with the control site (Figures 5.7 A2,D2, 5.8 A2,D2), with larger differences in Yishun compared with Tampines. In Tampines, the mean number of adult females trapped per block was typically slightly higher at the control site compared with the release site both before and after the release period (Figures 5.7 A1,A3), while in Yishun this was broadly similar between control and release sites during these periods (Figures 5.8 A1,A3). However, for both study areas, there was substantial temporal variation in patterns observed in the adult and egg trapping data (Figures 5.7, 5.8). For example, the mean proportion of viable eggs among eggs trapped per block ranged from 0 to 1 during the release period at Yishun (Figure 5.8 D2).

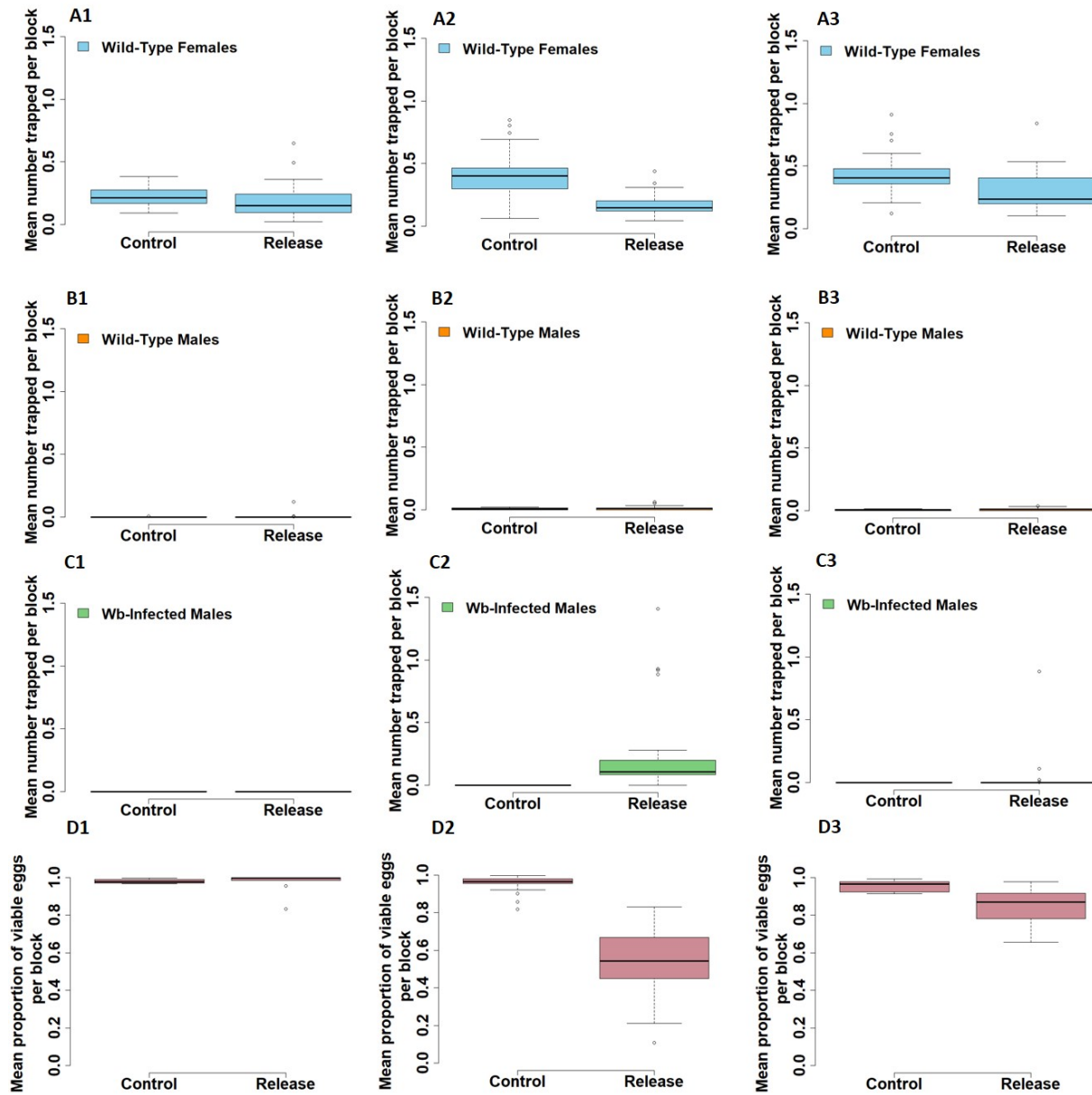


Figure 5.7: Trapping Data-Tampines Box-whisker plots summarising the temporal variability in the trapping data collected at the Tampines control and release sites before (column 1), during (column 2) and after (column 3) the release period. The solid line in each box represents the median value and the coloured region represents the interquartile range.

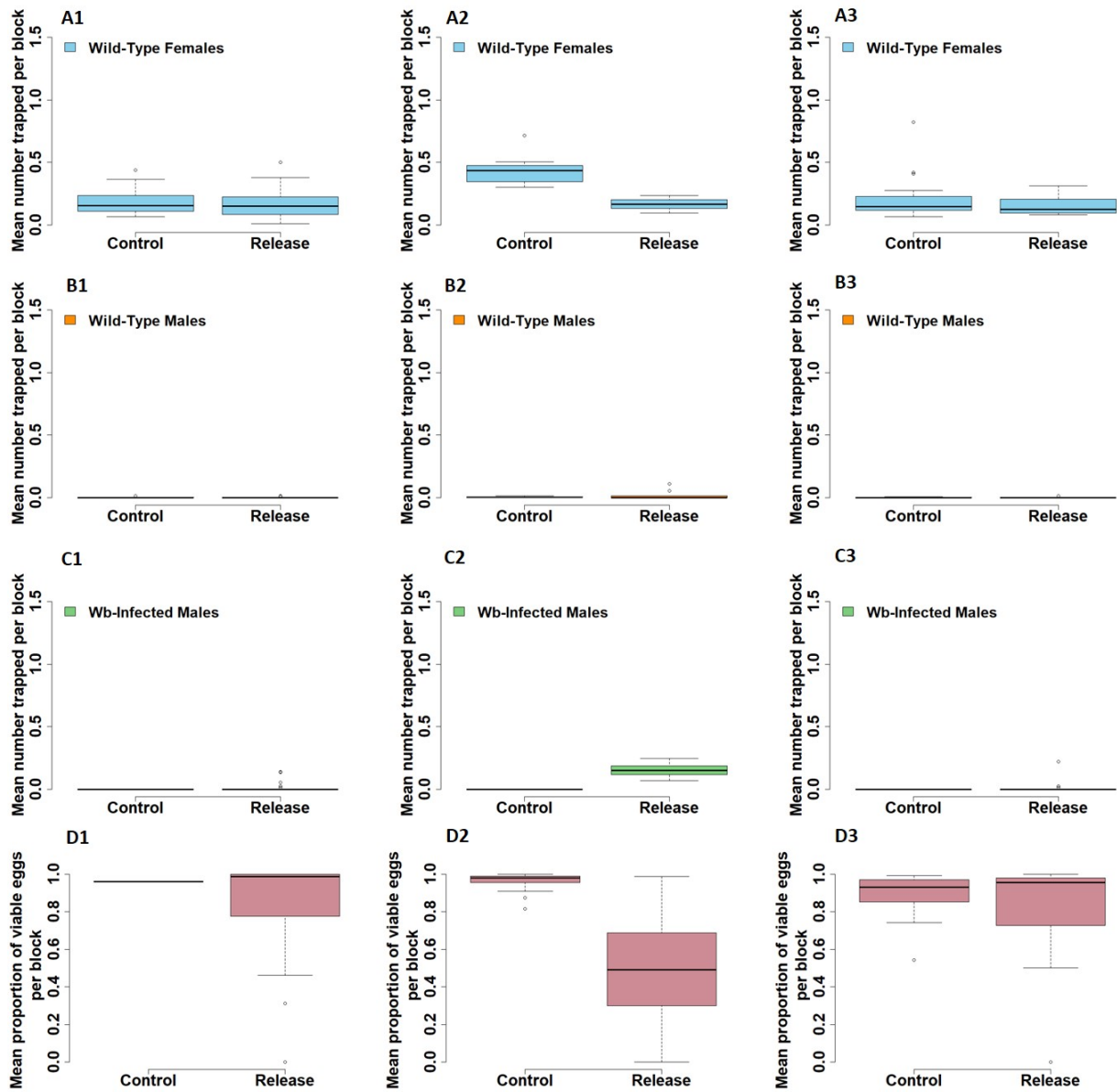


Figure 5.8: Trapping Data-Yishun Box-whisker plots summarising the temporal variability in the trapping data collected at the Yishun control and release sites before (column 1), during (column 2) and after (column 3) the release period. The solid line in each box represents the median value and the coloured region represents the interquartile range. The data presented for the Yishun release site corresponds to the residential blocks into which *Wolbachia*-infected males were released.

In addition to temporal variability, substantial inter-block variation in the number of eggs and adult mosquitoes trapped was also evident in the data collected at all sites. Summaries of the inter-block variation in the data collected in both Tampines and Yishun are presented Figures 5.9 and 5.10 below.

In both Tampines and Yishun, the median number of wild-type females trapped per residential block per week was typically below 10. As noted above, very few (if any) wild-type males were trapped during the study period. Larger numbers of *Wolbachia*-infected males were trapped compared with wild-type males, with the median number of *Wolbachia*-infected males trapped highest following the largest releases.

Across both control and release sites, the median number of viable eggs trapped per block per week typically remained below 200. As expected, few nonviable eggs were trapped at both control sites, with the median number trapped per block per week typically below 5. Some larger observations were observed at both control sites. Generally, a higher median number of nonviable eggs was observed at the release sites compared with the corresponding control sites.

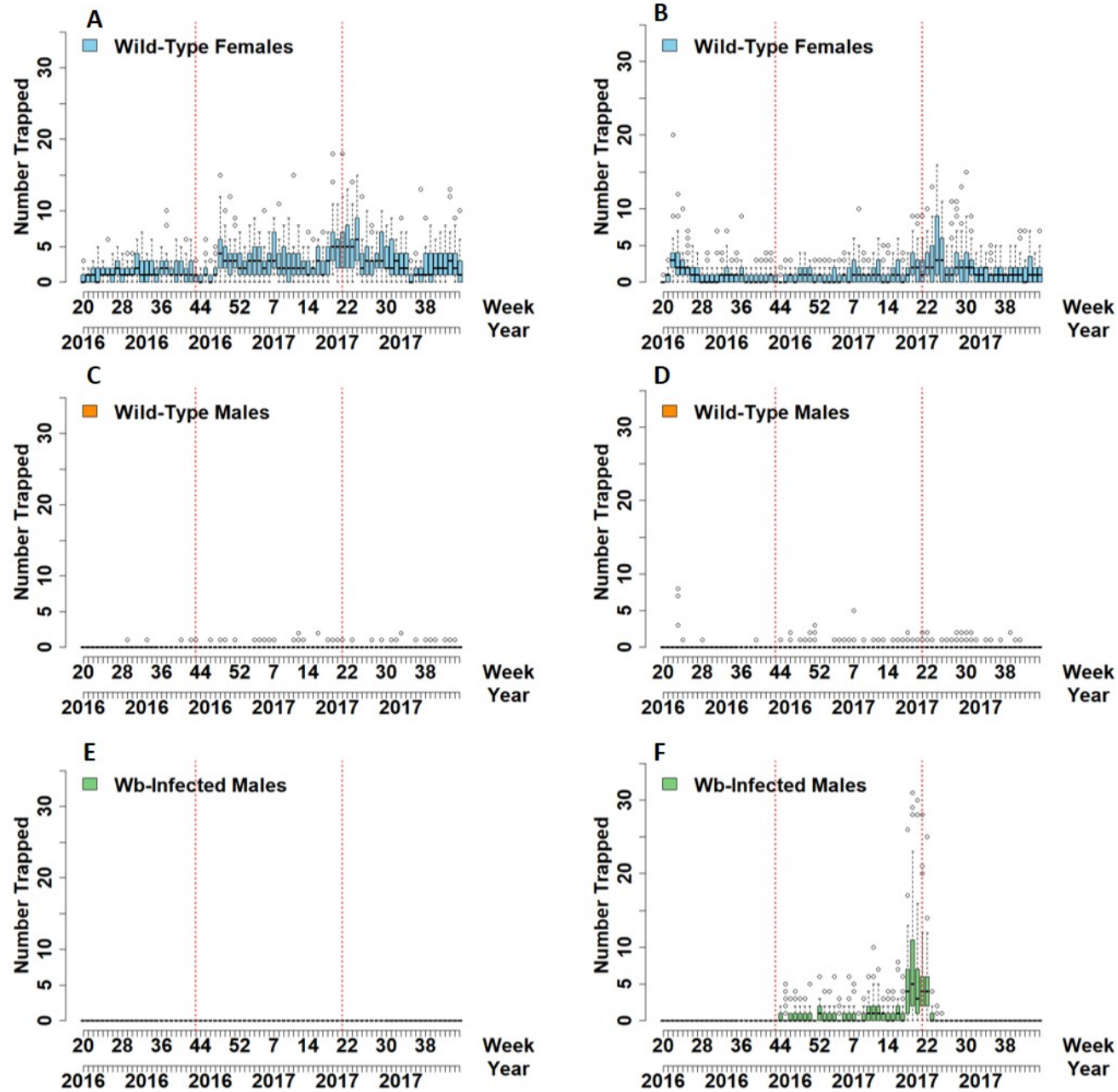


Figure 5.9: Inter-block variability-Tampines Box-whisker plots summarising the inter-block variability in the weekly trapping data collected at the Tampines control (left column) and release site (right column). The solid line in each box represents the median value and the coloured region represents the interquartile range. The dashed red lines show the period when *Wolbachia*-infected males were released.

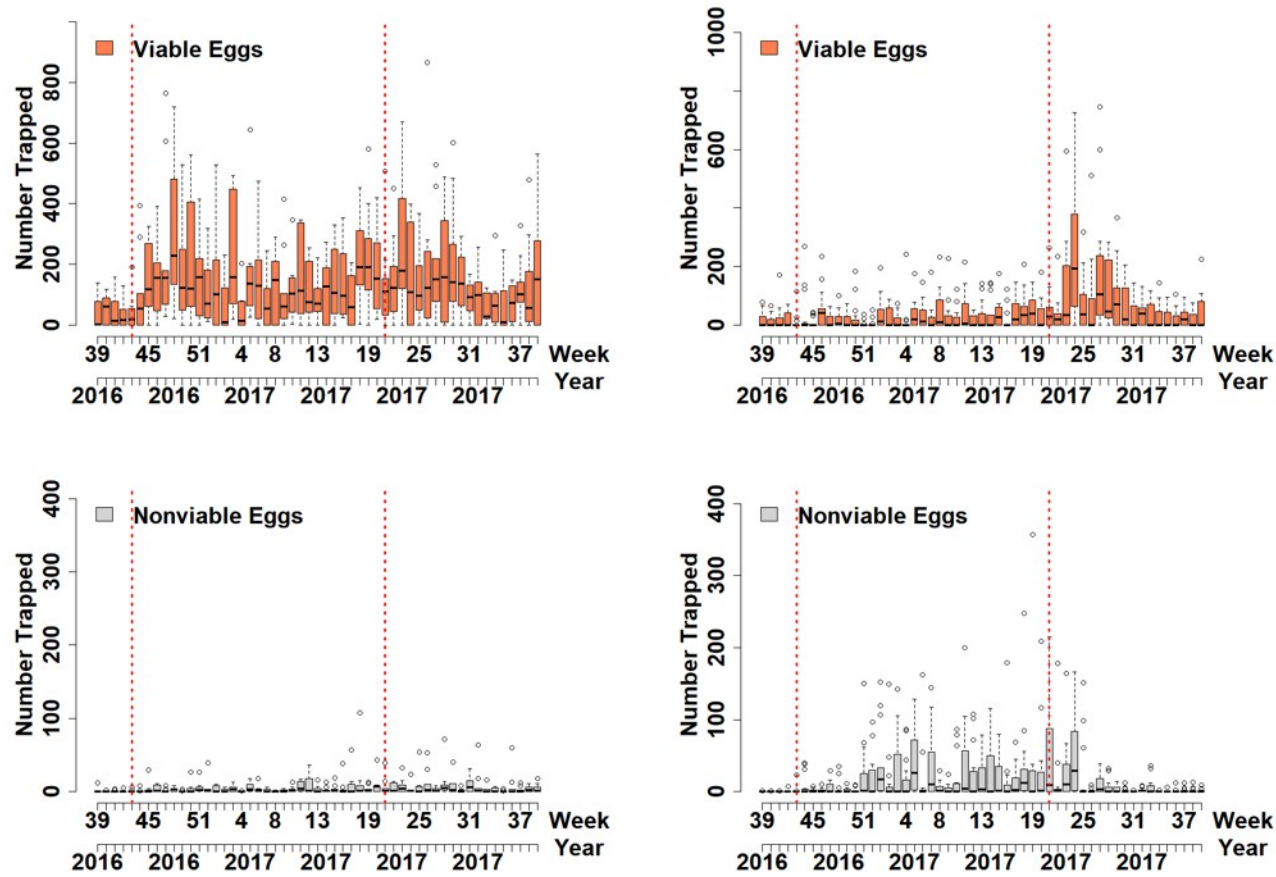


Figure 5.9 (Continued): Inter-block variability-Tampines Box-whisker plots summarising the inter-block variability in the weekly trapping data collected at the Tampines control (left column) and release site (right column). The solid line in each box represents the median value and the coloured region represents the interquartile range. The dashed red lines show the period when *Wolbachia*-infected males were released.

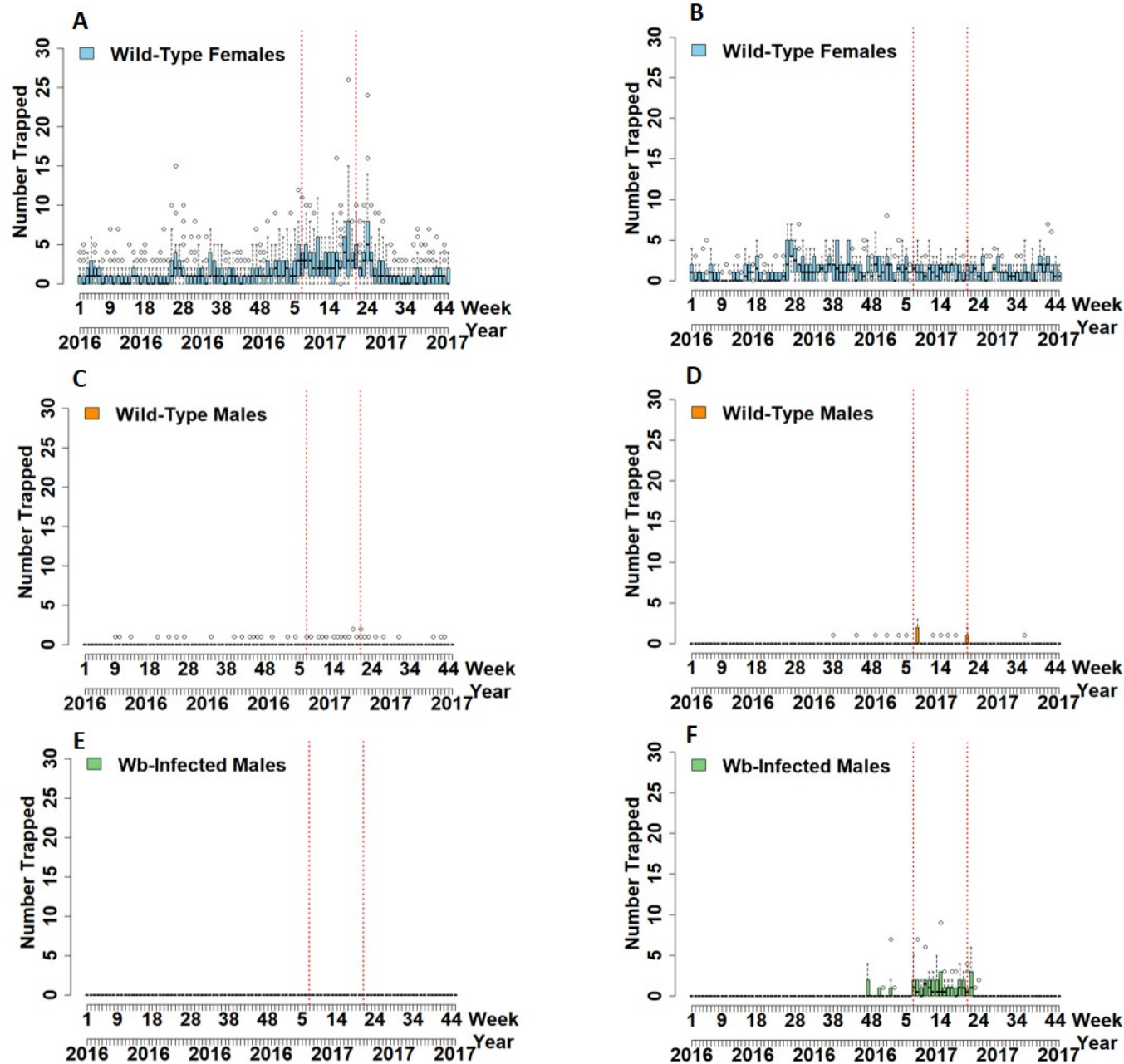


Figure 5.10: Inter-block variability-Yishun Box-whisker plots summarising the inter-block variability in the weekly trapping data collected at the Yishun control (left column) and release site (right column). The solid line in each box represents the median value and the coloured region represents the interquartile range. The data presented for the release site corresponds to the blocks into which *Wolbachia*-infected males were released. The dashed red lines show the period when *Wolbachia*-infected males were released.

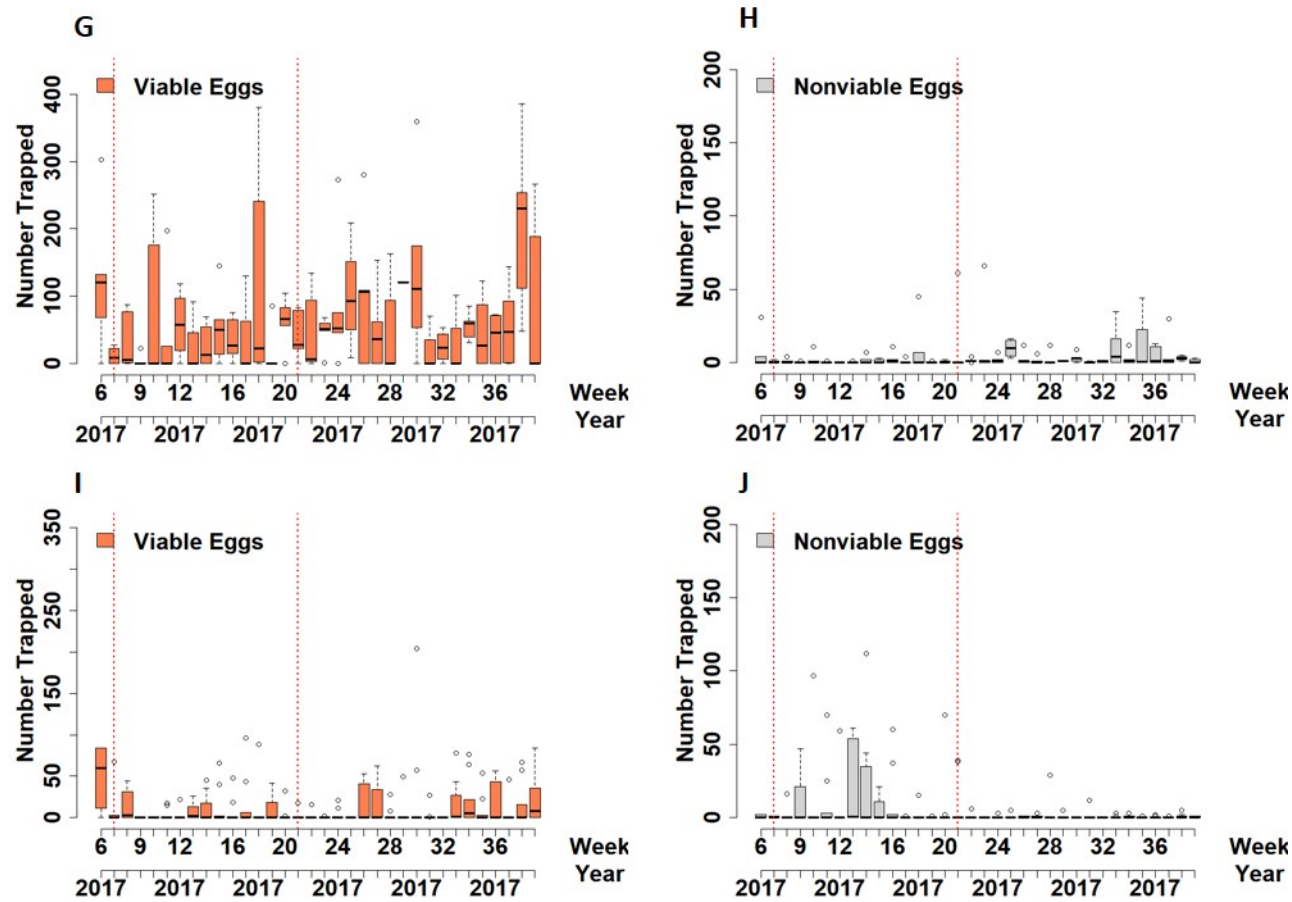


Figure 5.10 (Continued): Inter-block variability-Yishun Box-whisker plots summarising the inter-block variability in the weekly trapping data collected at the Yishun control (left column) and release site (right column). The solid line in each box represents the median value and the coloured region represents the interquartile range. The data presented for the release site corresponds to the blocks into which *Wolbachia*-infected males were released. The dashed red lines show the period when *Wolbachia*-infected males were released.

5.3 Model Structure

To model the impact of the release of *Wolbachia*-infected male *Aedes aegypti* on local wild-type *Aedes aegypti* population dynamics, we extended the stochastic model of *Aedes aegypti* population dynamics presented in Chapter 2. A simple schematic of the model is provided below (Figure 5.11), and the dynamics of the model are as follows.

Following mating with a wild-type male (M^{WT}), a wild-type female (F^{WT}) lay eggs at a rate b . A proportion η of these eggs may be nonviable (for reasons other than CI), and thus only viable eggs mature to become larvae, at a daily rate γ_E . Larvae subsequently develop into (wild-type) adult males and females at a daily rate γ_L . We assume that, on average, an equal proportion of larvae hatch as wild-type male and female adult mosquitoes.

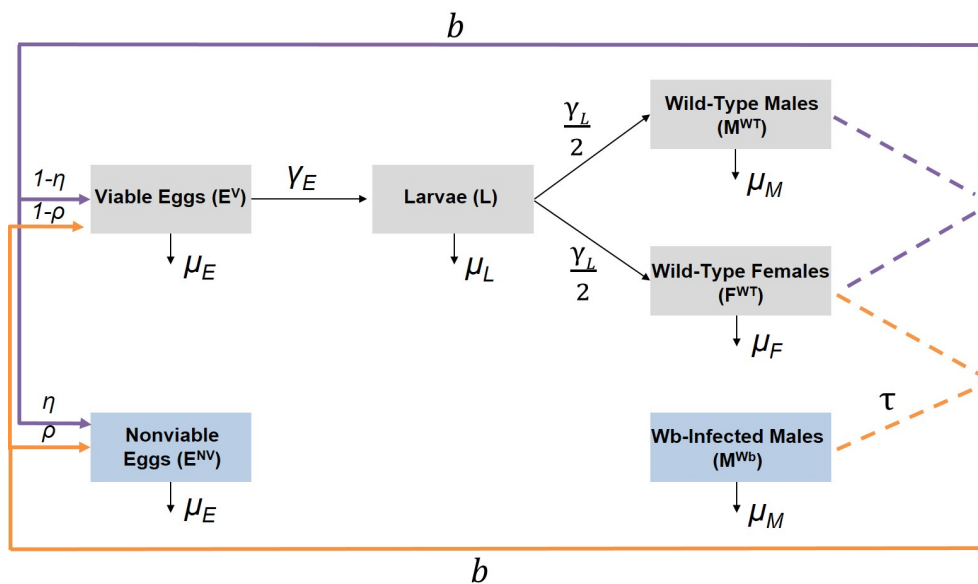


Figure 5.11: Schematic of Model of IIT

We do not assume that *Wolbachia*-infected males are necessarily equally as competitive at finding mates as wild-type males. Thus we allow the relative mating competitiveness of *Wolbachia*-infected males to vary via the parameter $\tau \in [0, 1]$, where $\tau = 1$ describes the scenario where wild-type and *Wolbachia*-infected males are equally competitive. The likelihood of a wild-type female mating with a *Wolbachia*-infected male is therefore determined by the relative frequency of *Wolbachia*-infected males in the population of competitive males which is given by:

$$\frac{\tau M^{Wb}}{M^{WT} + \tau M^{Wb}} \quad (5.1)$$

When a wild-type female mates with a *Wolbachia*-infected male, she also lays eggs at a rate b . The proportion of these eggs which are viable is now determined by the relative reduction in the egg hatch rate owing to incompatible matings between *Wolbachia*-infected males and wild-type females, represented by the parameter $\rho \in [0, 1]$. When $\rho = 1$ all eggs produced following mating between a wild-type female and *Wolbachia*-infected male are nonviable. Based on laboratory and field observations (personal communication with NEA Singapore), we assume that wild-type males and *Wolbachia*-infected males have the same daily mortality rate.

The deterministic dynamics of a local *Aedes aegypti* population in patch (i, j) at time t are hence described by the following set of equations:

$$\frac{dE_{ij}^V(t)}{dt} = bgO_{ij}(t) \left[\frac{(1-\eta)M_{ij}^{WT}(t) + (1-\rho)\tau M_{ij}^{Wb}(t)}{M_{ij}^{WT}(t) + \tau M_{ij}^{Wb}(t)} \right] - \gamma_E E_{ij}^V(t) - \mu_E E_{ij}^V(t) \quad (5.2)$$

$$\frac{dE_{ij}^{NV}(t)}{dt} = bgO_{ij}(t) \left[\frac{\eta M_{ij}^{WT}(t) + \rho\tau M_{ij}^{Wb}(t)}{M_{ij}^{WT}(t) + \tau M_{ij}^{Wb}(t)} \right] - \mu_E E_{ij}^{NV}(t) \quad (5.3)$$

$$\frac{dL_{ij}(t)}{dt} = \gamma_E E_{ij}^V(t) - \gamma_L L_{ij}(t) - \mu_L \left(1 + \left(\frac{L_{ij}(t)}{K_{ij}(t)} \right)^\Omega \right) L_{ij}(t) \quad (5.4)$$

$$\frac{dM_{ij}^{WT}(t)}{dt} = \frac{\gamma_L}{2} L_{ij}(t) - \mu_M M_{ij}^{WT}(t) \quad (5.5)$$

$$\frac{dF_{ij}^{WT}(t)}{dt} = \frac{\gamma_L}{2} L_{ij}(t) - \mu_F F_{ij}^{WT}(t) \quad (5.6)$$

$$\frac{dM_{ij}^{Wb}(t)}{dt} = R_{ij}^{Wb}(t) - \mu_M M_{ij}^{Wb}(t) \quad (5.7)$$

$$O_{ij}(t) = g^{-1} F_{ij}^{WT}(t) \quad (5.8)$$

where $E_{ij}^V(t)$, $E_{ij}^{NV}(t)$, $L_{ij}(t)$, $F_{ij}^{WT}(t)$, $M_{ij}^{WT}(t)$, and $M_{ij}^{Wb}(t)$ denote the number of viable eggs, nonviable eggs, larvae, wild-type adult females, wild-type adult males, and *Wolbachia*-infected adult males in the patch at time t respectively. $R_{ij}^{Wb}(t)$ denotes the number of *Wolbachia*-infected males released into patch (i, j) at time t , $K_{ij}(t)$ denotes the larval carrying capacity of the patch at time t , and Ω describes the strength of density dependence. $O_{ij}(t)$ denotes the number of wild-type females laying eggs in the patch at time t , b denotes the oviposition rate, g denotes the length of the gonotrophic cycle of wild-type adult female mosquitoes. γ_E and γ_L denote the development rate of viable eggs and larvae respectively. μ_E , μ_L , μ_F and μ_M denote the egg, larval, adult female, and adult male mosquito mortality rate respectively.

The basic mosquito reproduction number, R_M , for this model is given by

$$R_M = b \frac{\gamma_E}{\gamma_E + \mu_E} \frac{\gamma_L}{\gamma_L + \mu_L} \frac{1}{2\mu_F} \quad (5.9)$$

This differs from our equation for R_M in Chapter 2 (Equation 2.5) owing to the inclusion of male mosquitoes in our model. Here $\frac{b}{2\mu_F}$ describes the average number of eggs laid by a female over the course of her lifetime, while the terms $\frac{\gamma_E}{\gamma_E + \mu_E}$ and $\frac{\gamma_L}{\gamma_L + \mu_L}$ account for mortality during the egg and larval stage respectively when determining the average number of females produced.

While in Chapters 2-4 we used our equation for R_M to obtain the value of b , here we instead fix the value of b and use our equation for R_M to obtain the value of μ_L . We chose to implement the model in this way as an estimate of the oviposition rate (b) of adult female *Aedes aegypti* in Singapore was provided to us by NEA Singapore. The density-independent larval mortality rate (μ_L) however was unknown.

The model is fitted at the release site level (i.e. modelling four patches), with trapping data aggregated across all residential blocks at a given site. Given the typically short dispersal length of *Aedes aegypti* [75–77] and the distance between study sites (Figure 5.3), we assume dispersal between patches does not occur. In addition, we assume adult mosquitoes do not disperse outside of the modelled population, and hence do not account for immigration of wild-type adult mosquitoes from surrounding areas.

To approximate the continuous time dynamics described by equations 5.2-5.8 above, we implemented a discrete time stochastic version of this model as detailed below. We chose a timestep of one day ($\delta t = 1$) as this allowed us to complete model runs in a computationally feasible timeframe, and similar results were observed for a timestep of one half of a day ($\delta t = 0.5$).

The model was implemented as follows:

Egg Population

At time t , the number of wild-type females mating with wild-type males ($C^{WT}(t)$) and the number mating with *Wolbachia*-infected males ($C^{Wb}(t)$) is given by

$$C^{WT}(t) = F^{WT}(t) \left(\frac{M^{WT}(t)}{M^{WT}(t) + \tau M^{Wb}(t)} \right) \quad (5.10)$$

$$C^{Wb}(t) = F^{WT}(t) \left(\frac{\tau M^{Wb}(t)}{M^{WT}(t) + \tau M^{Wb}(t)} \right) \quad (5.11)$$

For a timestep $\delta t = 1$, we then draw the number of these females laying eggs at time t following a cross of each type ($O^{WT}(t), O^{Wb}(t)$) from a Binomial distribution

$$O^{WT}(t) \sim Bin(C^{WT}(t), g^{-1}) \quad (5.12)$$

$$O^{Wb}(t) \sim Bin(C^{Wb}(t), g^{-1}) \quad (5.13)$$

and the total number of new eggs laid at time t ($Q^{WT}(t), Q^{Wb}(t)$) from a Poisson distribution

$$Q^{WT}(t) \sim Poisson(bgO^{WT}(t)\delta t) \quad (5.14)$$

$$Q^{Wb}(t) \sim Poisson(bgO^{Wb}(t)\delta t) \quad (5.15)$$

Of those eggs laid, we determine the number which are viable according to the cross type as follows:

$$H^{WT}(t) \sim Bin(Q^{WT}(t), 1 - \eta) \quad (5.16)$$

$$H^{Wb}(t) \sim Bin(Q^{Wb}(t), 1 - \rho) \quad (5.17)$$

where $H^{WT}(t)$ and $H^{Wb}(t)$ denote the number of viable eggs laid from wild-type and *Wolbachia* crosses respectively. Thus the total number of new viable (N_V^E) and new nonviable eggs (N_{NV}^E) at time t is given by

$$N_V^E(t) = H^{WT}(t) + H^{Wb}(t) \quad (5.18)$$

$$N_{NV}^E(t) = (Q^{WT}(t) - H^{WT}(t)) + (Q^{Wb}(t) - H^{Wb}(t)) \quad (5.19)$$

Similarly to that described in Chapter 2 (Equations (2.8)-(2.11)) we use a competing hazards approach to determine the number of new larvae (N^L) and deaths of viable eggs (D_V^E) at time t as follows:

$$h_V^E(t) = \gamma_E + \mu_E \quad (5.20)$$

$$p_V^E(t) = 1 - e^{(-h_V^E(t)\delta t)} \quad (5.21)$$

$$T_V^E(t) \sim \text{Bin}(E^V(t), p_V^E(t)) \quad (5.22)$$

$$N^L(t) \sim \text{Bin}\left(T_V^E(t), \frac{\gamma_E}{h_V^E(t)}\right) \quad (5.23)$$

$$D_V^E(t) = T_V^E(t) - N^L(t) \quad (5.24)$$

where $h_V^E(t)$ describes the total hazard of leaving the viable egg population at time t , $p_V^E(t)$ describes the probability of leaving the viable egg population at time t , and $T_V^E(t)$ denotes the total number of viable eggs leaving the patch at time t . The number of deaths of nonviable eggs at time t ($D_{NV}^E(t)$) is given by

$$D_{NV}^E(t) \sim \text{Bin}(E^{NV}(t), \mu_E \delta t) \quad (5.25)$$

The number of viable and nonviable eggs at time $(t + 1)$ is therefore given by

$$E^V(t + 1) = E^V(t) + N_V^E(t) - N^L(t) - D_V^E(t) \quad (5.26)$$

$$E^{NV}(t + 1) = E^{NV}(t) + N_{NV}^E(t) - D_{NV}^E(t) \quad (5.27)$$

Larval Population

We determine the total number of new wild-type adult mosquitoes ($N^A(t)$) and the number of larval deaths ($D^L(t)$) at time t using a similar competing hazards approach. We have

$$h^L(t) = \gamma_L + \mu_L \left(1 + \left(\frac{L(t)}{K(t)}\right)^\Omega\right) \quad (5.28)$$

$$p^L(t) = 1 - e^{(-h^L(t)\delta t)} \quad (5.29)$$

$$T^L(t) \sim \text{Bin}(L(t), p^L(t)) \quad (5.30)$$

$$N^A(t) \sim \text{Bin}\left(T^L(t), \frac{\gamma_L}{h^L(t)}\right) \quad (5.31)$$

$$D^L(t) = T^L(t) - N^A(t) \quad (5.32)$$

where $h^L(t)$ denotes the total hazard of leaving the larval population at time t , $p^L(t)$ denotes the probability of leaving the larval population at time t , $T^L(t)$ denotes the total number of larvae leaving the patch at time t , and $N^A(t)$ denotes the total number of new wild-type adult mosquitoes at time t . We assume larvae are equally likely to develop as adult males and females, and thus the number of new wild-type adult females ($N_F^A(t)$) and males ($N_M^A(t)$) is given by

$$N_F^A(t) \sim \text{Bin}(N^A(t), .5) \quad (5.33)$$

$$N_M^A(t) = N^A(t) - N_F^A(t) \quad (5.34)$$

The larval population in patch (i, j) at time $(t + 1)$ is therefore given by

$$L(t + 1) = L(t) + N^L(t) - N^A(t) - D^L(t) \quad (5.35)$$

Adult Mosquito Population

As we assume that there is no dispersal between patches, and that mosquitoes do not disperse beyond the modelled population, the hazard of an adult mosquito leaving the population in a given patch is given by their mortality rate. Thus, we determine the number of deaths of wild-type females (D_F^A), wild-type males (D_M^A) and *Wolbachia*-infected males (D_{Wb}^A) at time t as follows:

$$D_F^A(t) \sim \text{Bin}(F^{WT}(t), 1 - e^{(\mu_F \delta t)}) \quad (5.36)$$

$$D_M^A(t) \sim \text{Bin}(M^{WT}(t), 1 - e^{(\mu_M \delta t)}) \quad (5.37)$$

$$D_{Wb}^A(t) \sim \text{Bin}(M^{Wb}(t), 1 - e^{(\mu_M \delta t)}) \quad (5.38)$$

Here, for example, $1 - e^{(\mu_F \delta t)}$ describes the probability of leaving the adult female population in a given timestep. Therefore the number of wild-type males, wild-type females and *Wolbachia*-infected males at time $t + 1$ is given by

$$F^{WT}(t + 1) = F^{WT}(t) + N_F^A(t) - D_F^A(t) \quad (5.39)$$

$$M^{WT}(t + 1) = M^{WT}(t) + N_M^A(t) - D_M^A(t) \quad (5.40)$$

$$M^{Wb}(t + 1) = R^{Wb}(t) - D_{Wb}^A(t) \quad (5.41)$$

where $R^{Wb}(t)$ denotes the number of *Wolbachia*-infected males released at time t .

5.3.1 Landscape Model

We assume that all patches have the same seasonal profile in carrying capacity, and estimate temporal heterogeneity in carrying capacity using a cubic spline function, with the knots or cutpoints of the spline occurring at evenly spaced intervals across the time series. At the beginning of the time series, the value of the spline function is set to 1, and thus values of the spline function at subsequent time points describe the change in the seasonal profile relative to this initial starting point (Figure 5.12).

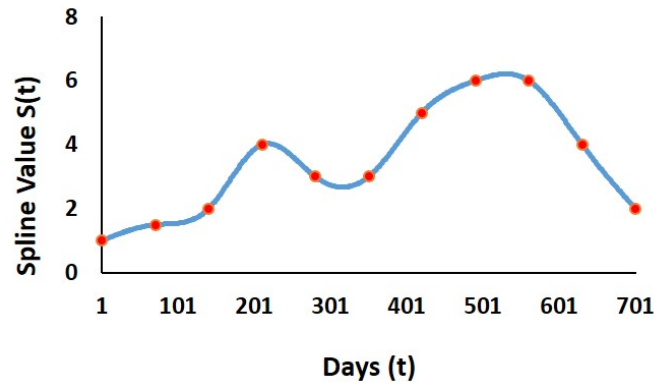


Figure 5.12: Example of Spline Function

Although the seasonal profile remains fixed across patches, we allow overall carrying capacity to vary between patches by fitting a local scaling factor κ_{ij} (unique to each patch) to the time series data. The deterministic equilibrium larval population of patch (i, j) at time t is given by

$$L_{ij}^*(t) = \kappa_{ij}S(t) \quad (5.42)$$

where $S(t)$ denotes the value of the spline function at time t . Therefore, we set $K_{ij}(t)$, the carrying capacity of patch (i, j) at time t , as

$$K_{ij}(t) = \frac{L_{ij}^*}{\frac{\gamma_L}{\mu_L} \left(\frac{b(1-\eta)\gamma_E}{2\mu_F(\gamma_E + \mu_E)} - 1 \right) - 1} \quad (5.43)$$

$$= \frac{\kappa_{ij}S(t)}{\frac{\gamma_L}{\mu_L} \left(\frac{b(1-\eta)\gamma_E}{2\mu_F(\gamma_E + \mu_E)} - 1 \right) - 1} \quad (5.44)$$

5.4 Model Fitting

To fit the model to the trial data, we use a particle Markov Chain Monte Carlo (MCMC) approach. The primary advantage of adopting this approach, compared with other MCMC methods for Bayesian inference, is that it allows us to directly fit a stochastic model to the trapping data [245, 246]. Here, we model both the underlying mosquito population dynamics and the trapping process itself, with the aim of providing more robust estimates of model parameters and the impact of the *Wolbachia* releases on wild-type female population size..

Before presenting details of the particle MCMC algorithm used, we briefly discuss the motivation for the development of particle MCMC methods. Our aim is not to provide a full, technical background to the development of these techniques, as this is beyond the scope of this thesis, but rather to provide some intuition of why these methods have been developed and how the algorithm we employ works.

5.4.1 Particle MCMC

Motivation

First consider a model with parameters θ . Given a corresponding dataset y , we wish to make inferences about θ and therefore our goal is to determine the posterior distribution $p(\theta|y)$, which describes the probability of θ given y . From Bayes' Theorem, we have

$$p(\theta|y) \propto p(y|\theta)p(\theta) \tag{5.45}$$

where $p(y|\theta)$ describes the likelihood of observing the data y given parameters θ , and $p(\theta)$ denotes the prior distribution on θ [247].

While the posterior distribution $p(\theta|y)$ can be computed analytically for some simple models, for more complex models, $p(\theta|y)$ is usually not analytically tractable. MCMC methods however allow us to explore the posterior distribution, by constructing a Markov chain which converges to the posterior distribution, through sampling from the distribution $p(y|\theta)p(\theta)$ ($\propto p(\theta|y)$). One such MCMC method is the Metropolis-Hastings algorithm [248] which proceeds as follows:

Box 5.1: Metropolis-Hastings Algorithm [248]

1. At iteration k , propose a new parameter value θ^* according to the proposal distribution $q(\theta^*|\theta_k)$, where θ_k denotes the current parameter value
2. Calculate the acceptance ratio α

$$\alpha = \min\left(1, \frac{p(y|\theta^*)p(\theta^*)q(\theta_k|\theta^*)}{p(y|\theta_k)p(\theta_k)q(\theta^*|\theta_k)}\right) \tag{5.46}$$

3. Draw a random number $u \in [0, 1]$ and
 - if $u \leq \alpha$, accept θ^* and set $\theta_{k+1} = \theta^*$
 - if $u > \alpha$, reject θ^* and set $\theta_{k+1} = \theta_k$
4. Repeat steps 1-3 above.

Suppose now that our dataset y is comprised of a set of discrete time observations, generated by an underlying Markov process x , which cannot be directly observed - namely, we have a hidden Markov model or partially observed Markov process. The system we model in this work is an example of this kind of process as our trapping data ($y = \{y_t\}_{t=1}^T$) consists of a sequence of observations at discrete time points, which have been generated by the underlying dynamics of the whole mosquito population ($x = \{x_t\}_{t=1}^T$) - a process we cannot directly observe but can simulate using our model (Figure 5.13).

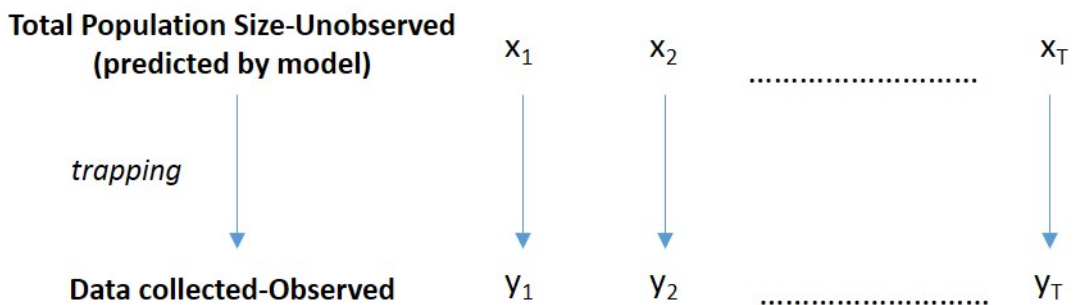


Figure 5.13: Illustration of Hidden Markov Model

Given y , we now wish to make inferences about both model parameters θ and the underlying process generating the data, x . Therefore we seek to describe the full joint posterior distribution $p(\theta, x|y)$, where

$$p(\theta, x|y) \propto p(x|y, \theta)p(y|\theta)p(\theta) \quad (5.47)$$

The marginal likelihood $p(y|\theta)$ is now given by

$$p(y|\theta) = \int_X p(y|x, \theta)p(x|\theta)dx \quad (5.48)$$

where X denotes the set of all possible model trajectories or outcomes for a given θ . Ideally we would like to construct a Markov chain which converges to the joint posterior distribution $p(\theta, x|y)$ by sampling from the distribution $p(x|y, \theta)p(y|\theta)p(\theta)$. However, our ability to sample from this distribution now depends on the structure of the underlying model.

If the underlying model is deterministic, then for any fixed set of parameter values θ , each model run will result in the same trajectory. Thus, for θ fixed, we have $|X| = 1$ and $p(x|\theta) = 1$. If however the underlying model is stochastic, then even if parameter values θ remain fixed, each model run will produce a different set of model outcomes. The total number of possible model trajectories is unknown and possibly very large ($|X| \gg 1$), thereby making consideration of all possible model trajectories computationally infeasible. Thus $p(x|\theta)$ is unknown, and exact calculation of the marginal likelihood $p(y|\theta)$ is not possible.

Particle MCMC algorithms provide a computationally feasible way of approximating the marginal likelihood of a given set of observations for hidden Markov models ($p(y|\theta)$), thereby allowing us to directly fit stochastic models to time series data [245]. In particular, the particle marginal Metropolis-Hastings (PMMH) particle MCMC algorithm [245] targets the full joint posterior distribution $p(\theta, x|y)$, which in turn enables us to make inferences about both θ and x .

The PMMH particle MCMC Algorithm

The PMMH particle MCMC algorithm [245] extends the traditional Metropolis-Hastings algorithm [248] (Box 5.1 above) by embedding a bootstrap particle filter after step 1 of the algorithm. Having proposed a new parameter value θ^* , this additional step creates a corresponding proposed

model trajectory x^* , and the pair (θ^*, x^*) are then subsequently jointly accepted (or rejected), thus allowing us to explore the full joint posterior distribution $p(\theta, x|y)$.

A comprehensive proof and discussion of why this approach works is provided by Andrieu *et al* [245]. Briefly, however, the ability of the algorithm to target the full joint posterior distribution $p(\theta, x|y)$ (rather than just the marginal posterior distribution $p(\theta|y)$) relies on how values of θ and x are proposed.

The acceptance ratio in the Metropolis-Hastings algorithm for sampling from the joint posterior distribution $p(\theta, x|y)$ is given by

$$\frac{p(\theta^*, x^*|y)q((\theta, x)|(\theta^*, x^*))}{p(\theta, x|y)q((\theta^*, x^*)|(\theta, x))} \quad (5.49)$$

If the trajectory x^* is proposed by considering both θ^* and the data y , this allows us to decompose the proposal distribution $q((\theta^*, x^*)|(\theta, x))$ as follows

$$q((\theta^*, x^*)|(\theta, x)) = q(\theta^*|\theta)p(x^*|y, \theta^*) \quad (5.50)$$

Therefore, the acceptance ratio now becomes

$$\frac{p(\theta^*, x^*|y)q((\theta, x)|(\theta^*, x^*))}{p(\theta, x|y)q((\theta^*, x^*)|(\theta, x))} = \frac{p(\theta^*, x^*|y)q(\theta|\theta^*)p(x|y, \theta)}{p(\theta, x|y)q(\theta^*|\theta)p(x^*|y, \theta^*)} \quad (5.51)$$

$$= \frac{p(\theta^*, x^*|y)q(\theta|\theta^*)p(\theta, x|y)p(\theta^*|y)}{p(\theta, x|y)q(\theta^*|\theta)p(\theta^*, x^*|y)p(\theta|y)} \quad (5.52)$$

$$= \frac{p(\theta^*|y)q(\theta|\theta^*)}{p(\theta|y)q(\theta^*|\theta)} \quad (5.53)$$

as $p(\theta, x|y) = p(x|y, \theta)p(\theta|y)$. Thus, if x^* is generated in this way, sampling from the full joint posterior distribution $p(\theta, x|y)$ is reduced to sampling from the marginal distribution $p(\theta|y)$ ($\propto p(y|\theta)p(\theta)$). The particle filtering approach enables us to generate a sample trajectory from $p(x^*|y, \theta)$ and to approximate the marginal likelihood $p(y|\theta^*)$, enabling us to sample from $p(\theta|y)$ and consequently $p(\theta, x|y)$ [245].

This trajectory x^* is created by comparing different trajectories simulated by the model (with fixed parameters θ^*) to the data y at each observation point $t \in [1, T]$. Each ‘particle’ in the algorithm corresponds to a single model trajectory, and thus the number of particles used in the algorithm

corresponds to the number of trajectories compared. A simple schematic illustrating this process, for a model with four particles, is provided in Figure 5.14 below.

At time $t - 1$, we run the model forward to time t . For each particle, the likelihood of observing the data y_t , given the value of the trajectory at time t , x_t , is calculated and the particles are weighted according to their likelihood values. Particles values x_t are then resampled (with replacement) using the normalised weights, and particles with lower likelihood values are thus filtered out as the algorithm progresses. In addition, as we resample particle values with replacement, the total number of particles used remains fixed at all times. The algorithm proceeds in this way until the final observation, at which point a sample model trajectory x^* is selected based on the normalised weights of the final set of particles. This trajectory is then used to give an estimate of the marginal likelihood $p(y|\theta)$ across the whole time series.

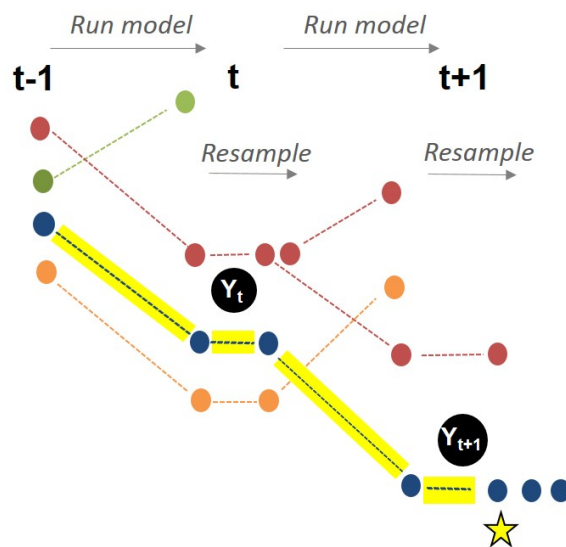


Figure 5.14: Schematic of Particle Filtering Illustration of particle filtering with four particles (each represented by a different colour). At time $t - 1$ we run the model forward to time t . Particle values are weighted according to the likelihood of observing y_t (the data at time t) given the particle value, and resample (with replacement) using the normalised weights. Here, the green particle is furthest away from the data y_t and hence has a lower likelihood value than other particles. Thus it is filtered out, and we now have two of the red particles. We run the model forward to time $t + 1$ and repeat this process. If time $t + 1$ is the final time step, we pick a sample trajectory based on the normalised weights at time $t + 1$ (here the first blue particle), and then use this trajectory to obtain an estimate of the marginal likelihood across the whole time series.

The full details of the algorithm are provided in Box 5.2 below. I coded the algorithm in C++, with parallelisation of code enabled at the particle filtering step to aid computational efficiency. Samples of the code I wrote to implement the particle filtering step are provided in Appendix B.

We next discuss how we implemented this algorithm to fit our model of IIT against the trapping data collected.

Box 5.2: Particle Marginal Metropolis-Hastings (PMMH) Algorithm [245]

Suppose we have a partially observed Markov process with a set of observations $y_{t=1\dots T}$, a corresponding state space model $x_{t=0\dots T}$ with parameters θ , and N particles. The algorithm proceeds as follows:

1. At iteration k , propose a new parameter value θ^* according to the proposal distribution $q(\theta^*|\theta_k)$, where θ_k denotes the current parameter value
2. Use a bootstrap particle filter to create a corresponding model trajectory x^* and estimate of the marginal likelihood $p(y|\theta^*)$, letting $\hat{p}(y|\theta^*)$ denote this estimate, as follows:
 - (a) At $t = 0$, initialise each particle, letting x_0^n denote the initial value of particle n , $n = 1\dots N$. Assume all particles have equal weight, and thus set $w_0^n = \frac{1}{N}$, where w_0^n denotes the weight of particle n at time 0.
 - (b) For each particle, run the model forward to the next time step. Calculate $p(y_t|x_t^n, \theta^*)$, the likelihood of observing the data y_t given the value of particle n at time t , x_t^n , and θ^* .
 - (c) Calculate the normalised weight of each particle at time t , w_t^n :

$$w_t^n = \frac{p(y_t|x_t^n, \theta^*)}{\sum_{n=1}^N p(y_t|x_t^n, \theta^*)} \quad (5.54)$$

- (d) For each particle n , resample the particle index according to the distribution of weights $i \sim \mathcal{F}(\cdot|w_t)$ and set $x_t^n = x_t^i$.
- (e) Propagate each particle forward to the next time step and repeat steps (b)-(d).
- (f) At time T , draw an index j from the final set of particle weights, $j \sim \mathcal{F}(\cdot|w_T)$ and use this sample trajectory to obtain $\hat{p}(y|\theta^*)$ as follows:

$$\hat{p}(y|\theta^*) = \prod_{t=1}^T p(y_t|x_t^{\beta_j(t)}, \theta^*) \quad (5.55)$$

where $\beta_j(t)$ denotes the ancestor of index j at time t .

3. Calculate the acceptance ratio α

$$\alpha = \min\left(1, \frac{\hat{p}(y|\theta^*)p(\theta^*)q(\theta_k|\theta^*)}{\hat{p}(y|\theta_k)p(\theta_k)q(\theta^*|\theta_k)}\right) \quad (5.56)$$

4. Draw a random number $u \in [0, 1]$ and

- if $u \leq \alpha$, accept θ^* (and x^*) and set $\theta_{k+1} = \theta^*$
- If $u > \alpha$, reject θ^* (and x^*) and set $\theta_{k+1} = \theta_k$

5. Repeat steps 1-4 above.

5.4.2 Proposing Parameter Values

Given that we're estimating both the underlying mosquito population dynamics and the trapping process, many parameters in our model are strongly correlated. Thus, to account for this correlation, we use a multivariate Normal distribution to propose new parameter values. Parameter values are therefore updated as a single block. At iteration k , we draw our proposed parameter values θ^* as follows

$$\theta^* \sim \mathcal{N}(\theta_k, \sigma^2 C_k) \quad (5.57)$$

where θ_k denotes the current vector of parameter values, and the matrix $\sigma^2 C_k$ denotes the covariance matrix of the proposal distribution, which is composed of a scaling factor σ^2 and a positive definite matrix C_k . The parameter σ^2 can be thought of as determining the size of the covariance matrix, while the matrix C_k determines the shape of the distribution.

Ideally, we would like C_k to be the true covariance matrix (Σ) of θ . However, the true underlying covariance structure is unknown, and hence we approximate Σ by learning the covariance structure as the algorithm progresses, letting $\hat{\Sigma}_k$ denote our approximation of Σ at iteration k . We assume parameters are not correlated for the first 5000 iterations of the algorithm, and account for the covariance structure from this point onwards. Computing the covariance matrix at each iteration is very computationally intensive and so, to aid computational efficiency, we subsequently calculate the covariance matrix every 1000 iterations, using a maximum of the previous 500,000

iterations. We therefore set

$$\hat{\Sigma}_k = \begin{cases} I, & k < 5000 \\ \frac{1}{k-k_0-1} \sum_{i=k_0}^k (\theta_i - \bar{\theta})(\theta_i - \bar{\theta})^\top, & k \geq 5000 \text{ \& } k \bmod 1000 = 0 \\ \hat{\Sigma}_{k-1} & \text{otherwise} \end{cases} \quad (5.58)$$

where $k_0 = \max(0, k - 500000)$ and I denotes the identity matrix. In addition, to ensure C_k is always positive definite, we set

$$C_k = \hat{\Sigma}_k + \frac{0.001^2}{k} I \quad (5.59)$$

The scaling factor σ^2 is tuned to give a desired acceptance rate r using a Robbins-Monro algorithm developed by Garthwaite *et. al* [249]. This algorithm searches for the optimal scaling factor needed to give an acceptance rate r by adjusting the scaling factor at each iteration in accordance with how parameter values are updated. Namely, at iteration $k + 1$, σ is marginally increased if proposed parameter values θ^* are accepted, or else is marginally decreased if proposed parameter values are rejected. We implement this algorithm by setting

$$\sigma_{k+1} = \begin{cases} \sigma_k + s(1-r)/k & \text{if } \theta^* \text{ is accepted} \\ \sigma_k - sr/k & \text{if } \theta^* \text{ is rejected} \end{cases} \quad (5.60)$$

where

$$s = \sigma_k \left[\left(1 - \frac{1}{d}\right) \frac{(2\pi)^{1/2} e^{\alpha^2/2}}{2\alpha} + \frac{1}{dr(1-r)} \right] \quad (5.61)$$

and d denotes the dimension of our proposal distribution, $\alpha = -\Phi^{-1}(r/2)$, and $\Phi(\cdot)$ denotes the cumulative distribution function of the Normal distribution [249].

5.4.3 Likelihood Function

In any environment, the likelihood of successfully trapping mosquitoes is highly variable and trapping data is therefore often over-dispersed. To allow for over-dispersion in the entomological data collected during the Phase 1 study, we assume observations y_t are distributed according to a BetaBinomial distribution

$$y_t \sim \text{BetaBin}(x_t, p, \alpha, \beta) \quad (5.62)$$

where x_t denotes total population size at t as predicted by the model, p denotes the average proportion trapped, and α and β determine the level of over-dispersion in p . This distribution can be decomposed as

$$y_t \sim \text{Bin}(x_t, p) \quad (5.63)$$

$$p \sim \text{Beta}(\alpha, \beta) \quad (5.64)$$

and, hence this distribution is the logical extension of the Binomial distribution to allow for over-dispersion. The likelihood of observing y_t given x_t is given by

$$\mathcal{L} = \binom{x_t}{y_t} \frac{B(x_t + \alpha, x_t - y_t + \beta)}{B(\alpha, \beta)} \quad (5.65)$$

where B denotes the Beta function with standard arguments α and β .

To gain a more intuitive understanding of the variability in the trapping process, we re-parameterise the Beta function describing the distribution of p in terms of its mean (m) and variance (v). We have that

$$m = \mathbb{E}[p] = \frac{\alpha}{\alpha + \beta} \quad (5.66)$$

$$v = \text{Var}[p] = \frac{\alpha\beta}{(\alpha + \beta)^2(\alpha + \beta + 1)} \quad (5.67)$$

$$= m(1 - m) \left(\frac{1}{\alpha + \beta + 1} \right) \quad (5.68)$$

where $\psi = \frac{1}{\alpha + \beta + 1}$ is the over-dispersion parameter, with larger values of ψ giving increased variability in p . This gives

$$\alpha = m \left(\frac{1}{\psi} - 1 \right) \quad (5.69)$$

$$\beta = (1 - m) \left(\frac{1}{\psi} - 1 \right) \quad (5.70)$$

Setting $m = p$, the likelihood \mathcal{L} of observing the data y_t given our model prediction x_t is therefore given by

$$\mathcal{L} = \binom{x_t}{y_t} \frac{B(x_t + p(\frac{1}{\psi} - 1), x_t - y_t + (1 - p)(\frac{1}{\psi} - 1))}{B(p(\frac{1}{\psi} - 1), (1 - p)(\frac{1}{\psi} - 1))} \quad (5.71)$$

We fit our model using both the adult mosquito and egg trapping data collected. At time t , we calculate \mathcal{L} for each part of the population s for which trapping data is available. The total likelihood at time t is then calculated by taking the product of the likelihood for each of these parts, and is therefore given by

$$\mathcal{L} = \prod_{s \in S} \mathcal{L}(s) \quad (5.72)$$

$$= \prod_{s \in S} \binom{x_t(s)}{y_t(s)} \frac{B(x_t(s) + p(s)(\frac{1}{\psi(s)} - 1), x_t(s) - y_t(s) + (1 - p(s))(\frac{1}{\psi(s)} - 1))}{B(p(s)(\frac{1}{\psi(s)} - 1), (1 - p(s))(\frac{1}{\psi(s)} - 1))} \quad (5.73)$$

If only adult mosquito data is available at time t then $S = \{F^{WT}, M^{WT}, M^{Wb}\}$, while if both adult and egg data is available, $S = \{F^{WT}, M^{WT}, M^{Wb}, E^V, E^{NV}\}$. Taking wild-type females for example, $x_t(F^{WT})$ and $y_t(F^{WT})$ denote the total number of wild-type females predicted by the model and trapped at time t respectively. $p(F^{WT})$ and $\psi(F^{WT})$ denote the mean proportion of wild-type females trapped and the over-dispersion in this trapping rate respectively.

The total log-likelihood at time t is given by

$$\log \mathcal{L} = \sum_{s \in S} \log(\mathcal{L}(s)) \quad (5.74)$$

5.5 Testing with Simulated Data

To explore how well parameter values of our model can be estimated using our model fitting approach, we calibrate the model against a dataset of simulated values and compare estimates obtained against the true parameter values.

5.5.1 Generating the Simulated Data

As far as possible, we simulated data to mimic the trapping data collected during the Phase 1 field study. Thus, using our model of IIT, we simulated data for a landscape comprised of four patches, where we have two control and two release sites. The number of *Wolbachia*-infected males released increases over time in one release site, and remains constant in the other. We generate trapping data for both adult mosquitoes and eggs as follows:

For a fixed set of parameter values, we run the model once to generate a sample trajectory x of the whole mosquito population. From this trajectory, we then generate weekly trapping data by sampling from a Binomial distribution with parameters determined by x and the relevant trapping distribution. For example, to generate the number of wild-type females trapped at time t ($y_t(F^{WT})$) for a single patch, we draw $y_t(F^{WT})$ from a Binomial distribution

$$y_t(F^{WT}) \sim \text{Bin}(x_t(F^{WT}), \tilde{p}(F^{WT})) \quad (5.75)$$

where $x_t(F^{WT})$ denotes the total number of wild-type females predicted by the model at time t and $\tilde{p}(F^{WT})$ denotes the mean proportion trapped at time t . This is drawn from a Beta distribution with mean $p(F^{WT})$ and an over-dispersion parameter $\psi(F^{WT})$. We adopt a similar approach with respect to generating trapping data for wild-type and *Wolbachia*-infected males, and viable and nonviable eggs.

We simulate data over a period of 95 weeks, and allow the model to run-in for 5 weeks, giving a total time period of 100 weeks. Seasonal variation in mosquito abundance is determined using a spline function as described in section 5.2.1 above, and cutpoints of the spline are placed 10 weeks apart. Therefore we have 11 cutpoints in total $c_{1..11}$, with $c_1 = 1$. All sites have the same seasonal profile in carrying capacity and thus cutpoint values remain fixed across sites. Each site however has a unique multiplier κ which scales the spline function to give an overall measure

of carrying capacity. Mean trapping proportions vary between (but not within) control-release pairs, and we allow different mean trapping proportions for wild-type females, wild-type males and *Wolbachia*-infected males. Viable and nonviable eggs are trapped at the same mean rate. The over-dispersion parameter with respect to the mean proportions trapped varies between eggs and adult mosquitoes, but remains the same for all adult mosquitoes and across sites.

5.5.2 Reducing Correlation

To help reduce correlation between parameter values when fitting the model, we choose one control-release pair as a reference pair (with parameter values corresponding to this pair denoted with superscript 1). The mean trapping proportions and multipliers for the spline function for the remaining pair (denoted with superscript 2) are then determined by scaling the corresponding values for the reference pair. Thus, we have

$$p^2(F^{WT}) = s_f p^1(F^{WT}), \quad p^2(M^{WT}) = s_m p^1(M^{WT}), \quad p^2(M^{Wb}) = s_{wb} p^1(M^{Wb}), \quad (5.76)$$

$$p^2(E) = s_e p^1(E), \quad \kappa_c^2 = s_c \kappa_c^1, \quad \kappa_r^2 = s_r \kappa_r^1 \quad (5.77)$$

where κ_c^1 and κ_r^1 denote the multipliers of the spline function for the control and release site of the reference pair respectively, and parameters s denote the different relevant scaling factors.

Within the reference pair of sites we estimate the mean proportions of wild-type and *Wolbachia*-infected males trapped relative to the mean proportion of wild-type females trapped, and the multiplier of the spline function for the release site relative to that of the control site. Namely, for the reference pair we have

$$p^1(F^{WT}) = p_f, \quad p^1(M^{WT}) = \lambda_m p_f, \quad p^1(M^{Wb}) = \lambda_{wb} p_f, \quad (5.78)$$

$$p^1(E) = p_e, \quad \kappa_c^1 = \kappa_c, \quad \kappa_r^1 = \lambda_r \kappa_c \quad (5.79)$$

where parameters λ denote the relevant scaling factors for within the reference pair of sites.

Using this approach allows us to fit all four sites together with a mixture of local and global parameter values, reducing the correlation between parameter values as much as possible.

Here we estimated model parameters using $N = 50$ particles, running the chains for 4,000,000

iterations. We chose to use 50 particles as this provided similar estimates of model parameter values and the likelihood function to runs with more particles ($N = 100$, $N = 150$), while allowing us to complete model runs within a computationally feasible timeframe. Uniform prior distributions were used for all parameters, and all parameters were fitted on a \log_{10} scale. Parameter samples from the posterior distribution were obtained using the last 500,000 iterations of each chain, thinned by a factor of 100, giving a total sample size of 5000 values for each parameter. Fits of the model to the simulated trapping data were generated using 1000 parameter sets sampled from the posterior distributions. For each of these parameter sets, one model run was performed.

5.5.3 Results

Results of this calibration exercise are presented in Figures 5.15-5.20 below. Figure 5.15 shows the posterior distribution for each parameter, and Figure 5.16 shows the underlying correlation structure. Figures 5.17-5.20 show the fits of the model to the simulated data using parameter values sampled from the posterior distribution.

Good estimates of parameter values were obtained, with the majority of true parameter values lying within the 95% credible interval of samples from the posterior distributions (Figure 5.15). We were unable to recover a very precise estimate of the basic mosquito reproduction number R_M , with estimates of this parameter spanning a large range of values. Strong correlation between the cutpoints and multipliers of the spline function and the mean proportion of adult mosquitoes trapped was observed (Figure 5.16), however good estimates of the true values for these parameters were obtained.

Importantly, the algorithm provided good estimates of the over-dispersion parameters (ψ, ψ_e) , indicating that we were able to capture variability in the simulated trapping data for both adult mosquitoes and eggs well.

A good fit of the model to the simulated data was thus obtained, with the data within the 95% posterior predicted intervals at almost all time points (Figures 5.17-5.20). The egg hatch rate (defined as the proportion of viable eggs among the total number of eggs trapped at a given time point) was not used in the model fitting process, and was estimated based on our samples from the posterior distribution. We observe that this was also captured well by the model (Figures

5.17-5.20).

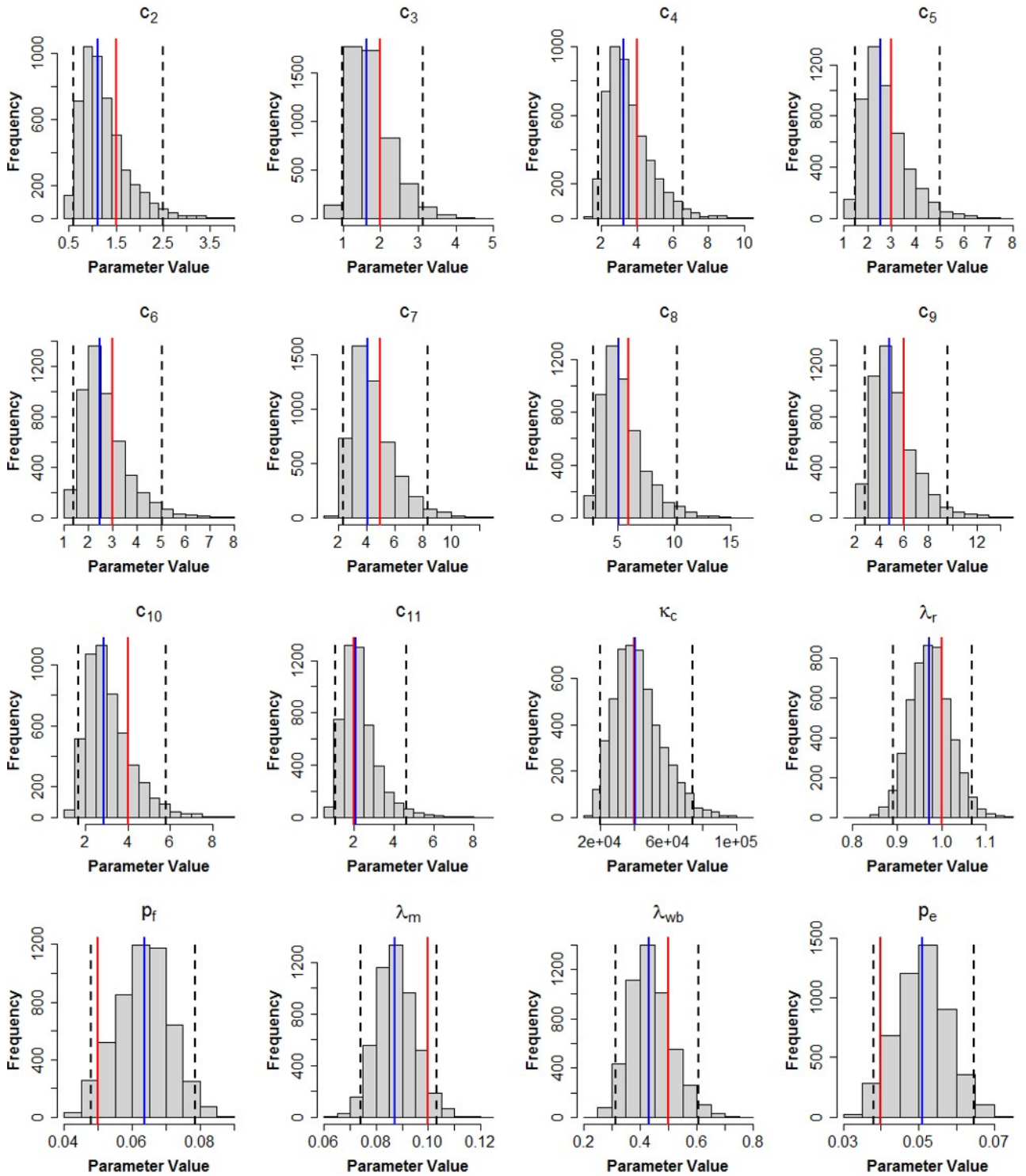


Figure 5.15: Posterior Parameter Distributions Histograms of the posterior distributions for all estimated parameters. For each parameter, 5000 values from the posterior distribution were sampled. The solid blue line shows the posterior median, the dashed black lines show the 95% credible interval, and the solid red line show the true parameter value.

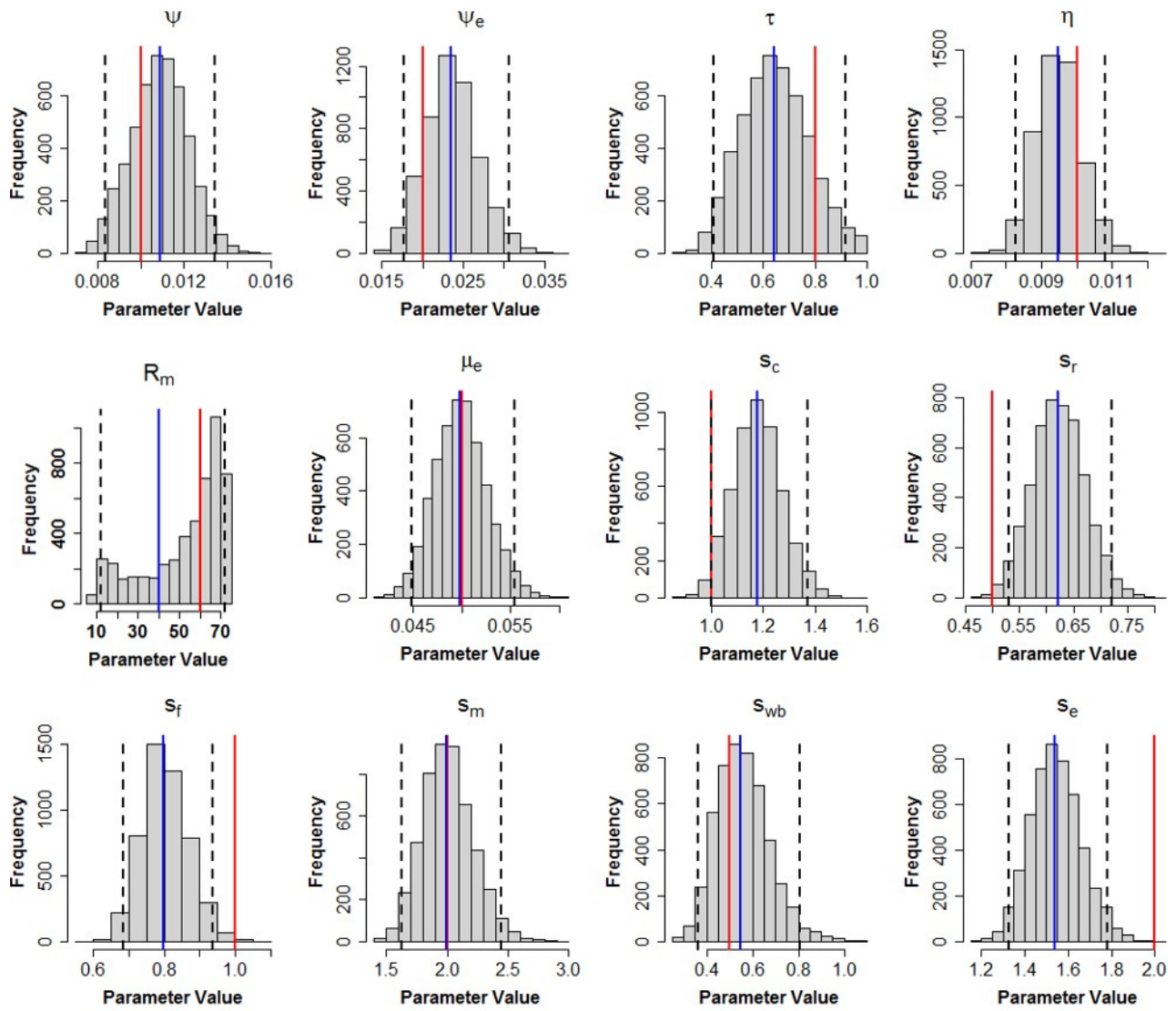


Figure 5.15 (Continued): Posterior Parameter Distributions Histograms of the posterior distributions for all estimated parameters. For each parameter, 5000 values from the posterior distribution interval were sampled. The solid blue line shows the posterior median, the dashed black lines show the 95% credible interval, and the solid red line show the true parameter value.

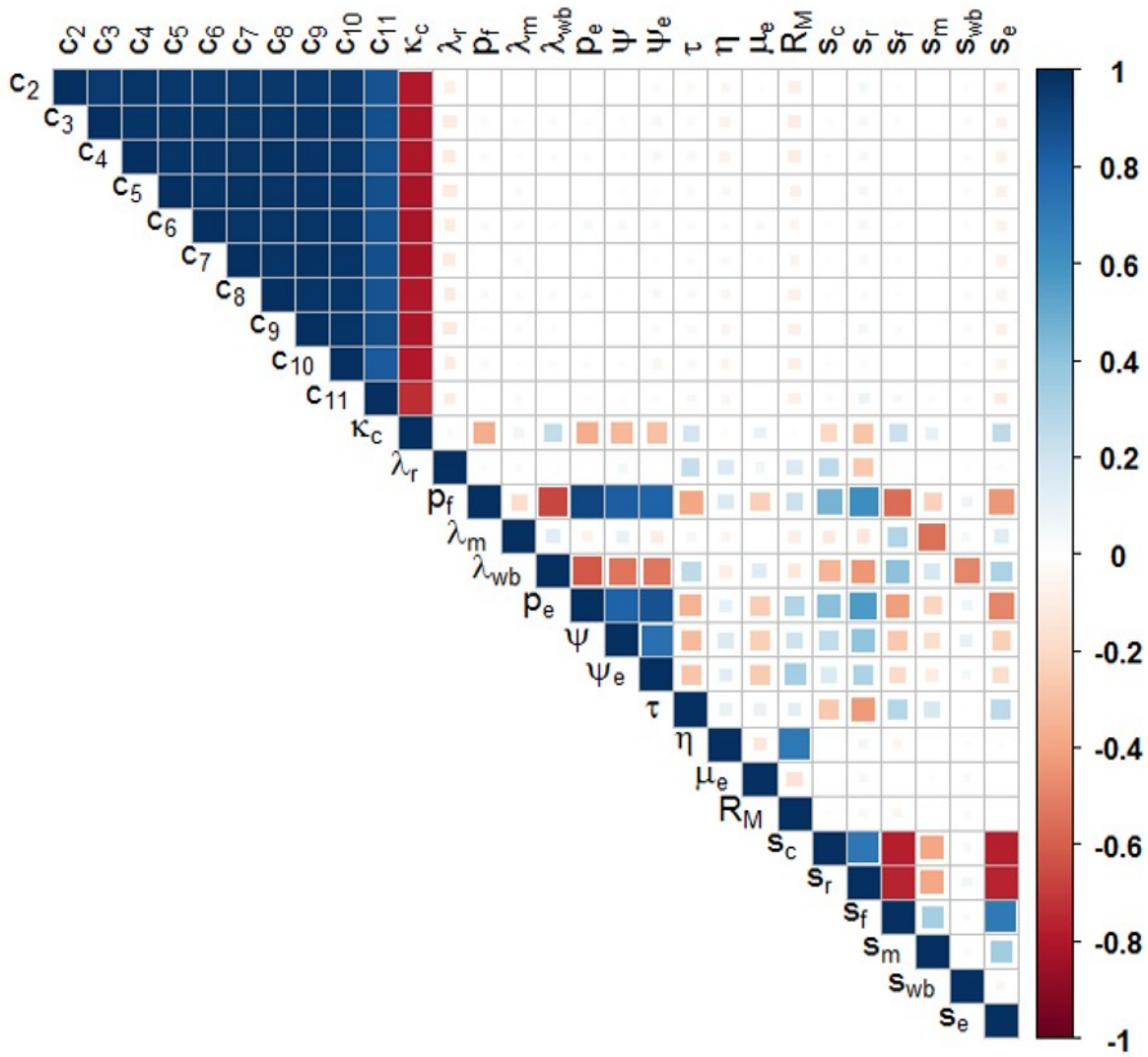


Figure 5.16: Correlation Structure Underlying correlation structure of estimate parameter values. Dark blue squares indicate pairs of parameter values which are strongly positively correlated with one another, while dark red squares indicate pairs of parameter values which are strongly negatively correlated with one another.

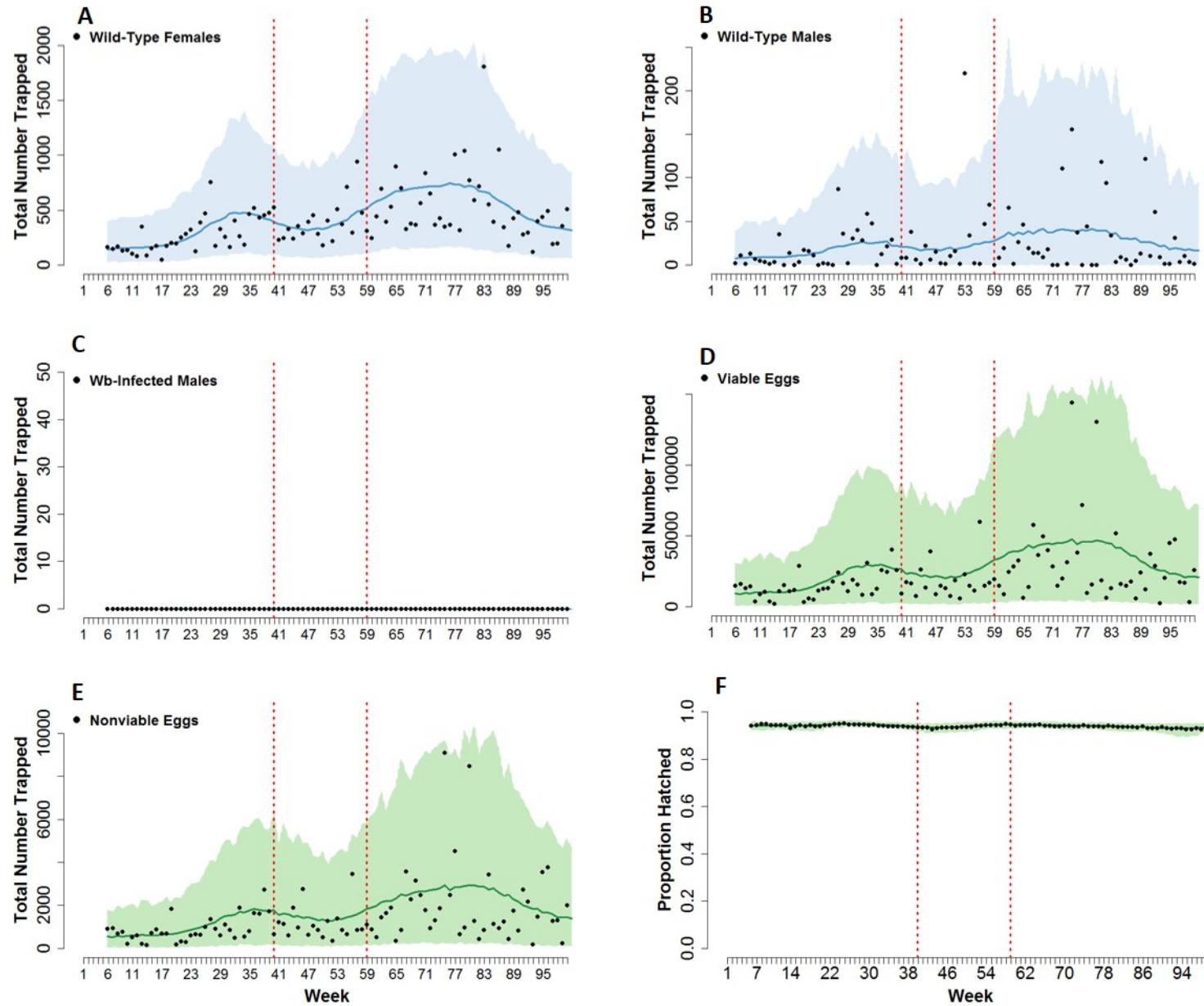


Figure 5.17: Control Site 1 Fits of the model to the simulated trapping data for the first control site. Observed data are shown in black, and the solid line and shaded area show the posterior median and 95% posterior predictive interval respectively. The dashed red lines show the period when *Wolbachia*-infected males were released. Figure F shows the estimated egg hatch rate.

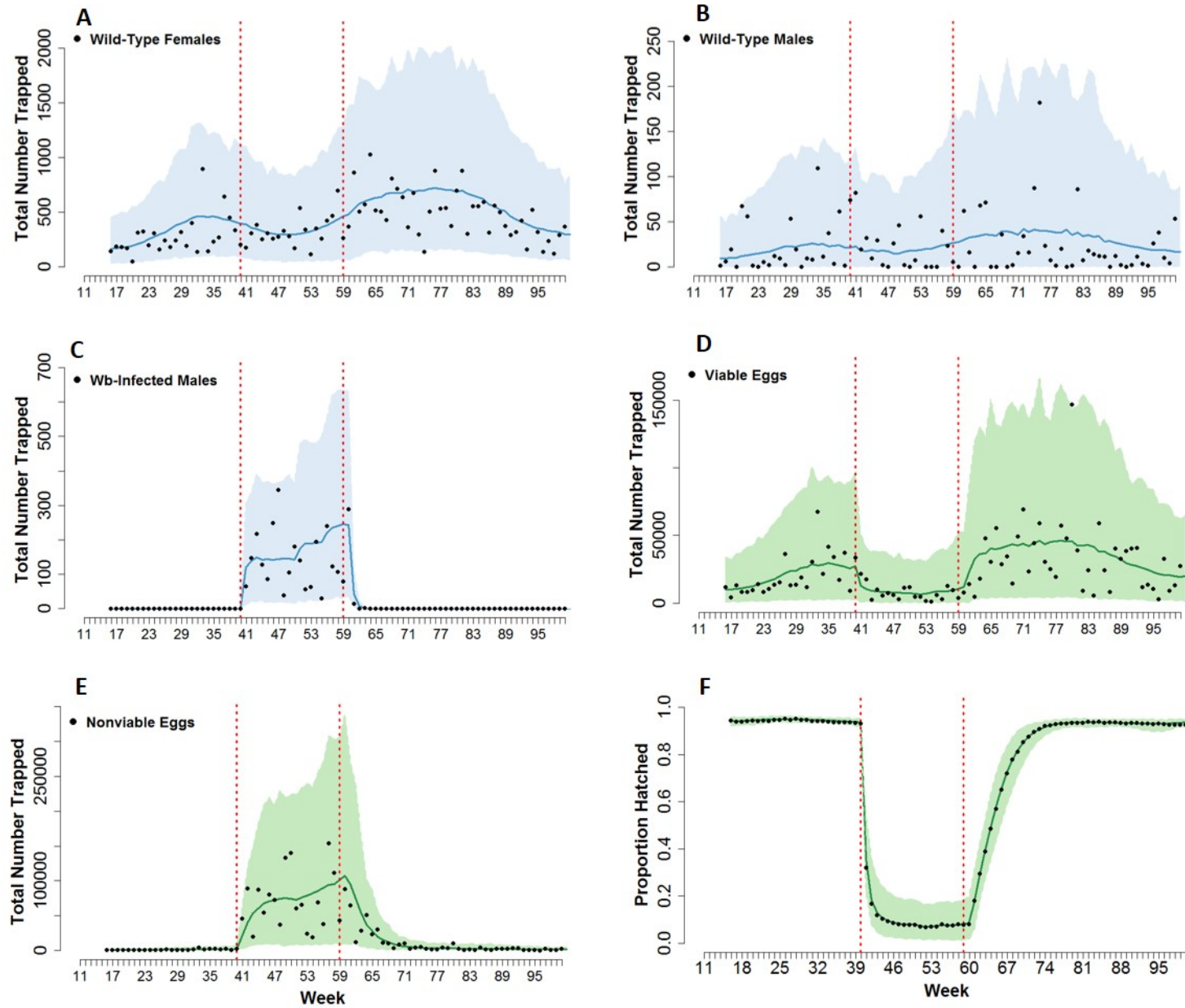


Figure 5.18: Release Site 1 Fits of the model to the simulated trapping data for the first release site. Observed data are shown in black, and the solid line and shaded area show the posterior median and 95% posterior predictive interval respectively. The dashed red lines show the period when *Wolbachia*-infected males were released. Figure F shows the estimated egg hatch rate.

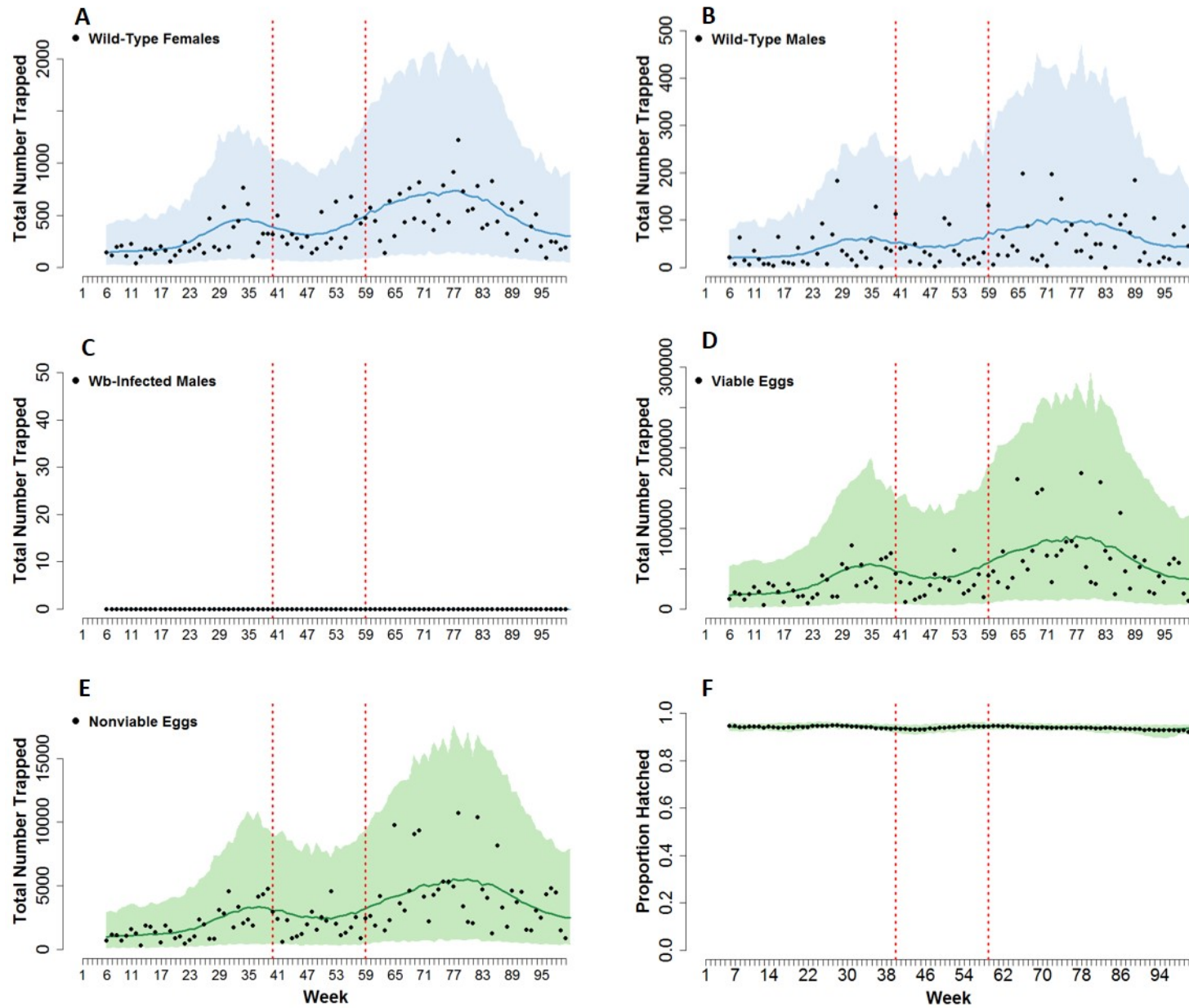


Figure 5.19: Control Site 2 Fits of the model to the simulated trapping data for the second control site. Observed data are shown in black, and the solid line and shaded area show the posterior median and 95% posterior predictive interval respectively. The dashed red lines show the period when *Wolbachia*-infected males were released. Figure F shows the estimated egg hatch rate.

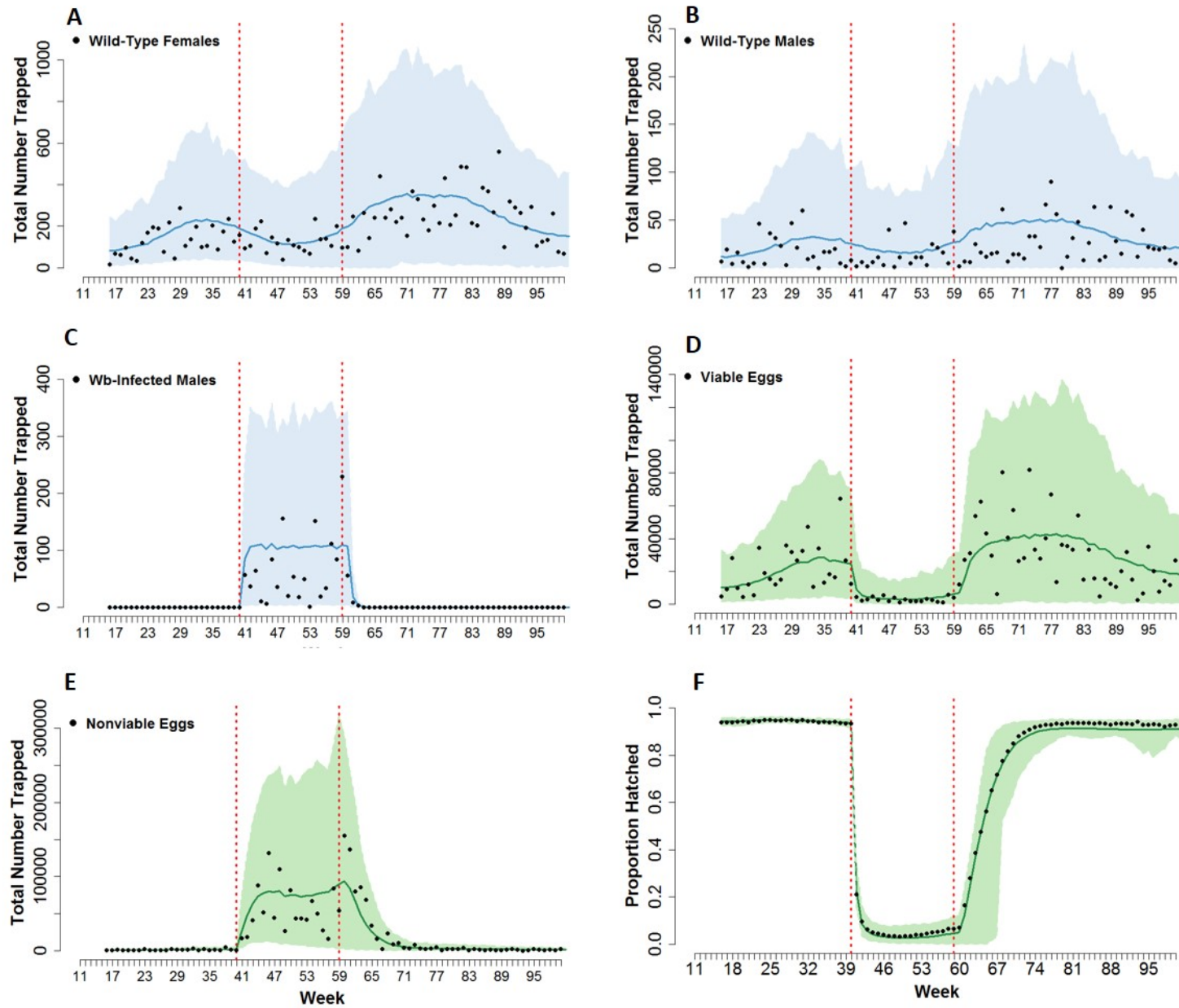


Figure 5.20: Release Site 2 Fits of the model to the simulated trapping data for the second release site. Observed data are shown in black, and the solid line and shaded area show the posterior median and 95% posterior predictive interval respectively. The dashed red lines show the period when *Wolbachia*-infected males were released. Figure F shows the estimated egg hatch rate.

5.6 Discussion

In this chapter, we described the first field study testing *Wolbachia* as a tool for *Aedes aegypti* population suppression undertaken in Singapore, and the data collected over the course of this study. We described the model of IIT developed to explore the results of this study, and the inferential approach developed to calibrate the model against the entomological data collected. We concluded by presenting results for testing the model with simulated data.

While we obtained good estimates of the majority of model parameters, it was difficult to achieve a precise estimate of the mosquito reproduction number R_M , with the 95% posterior credible interval spanning a large range of values. We hypothesise that, even with simulated egg and adult mosquito trapping data, it is difficult to robustly estimate R_M (in addition to many other model parameters) owing to density-dependent mortality during the larval stage of mosquito development. Nonetheless, the true value for R_M was contained within the 95% credible interval for estimates of this parameter. Furthermore, good fits of the model to the data were obtained, with the model able to capture well the variability in the simulated trapping data.

We now proceed to exploring the results obtained from calibrating the model against the data collected during the Phase 1 study.

Chapter 6

Project *Wolbachia* Singapore: Phase 1

Results

In Chapter 5, I described the Phase 1 field study of IIT conducted in Singapore, the model of IIT developed and the approach we use to calibrate the model against mosquito trapping data. Here, I present the results of fitting the model to the trapping data collected during the field study and discuss the insight gained from these results.

6.1 Methods

We calibrated our model of IIT against the adult mosquito and egg data collected during the Phase 1 study using a particle MCMC approach as described in Chapter 5. All four sites were fitted together and, when examining the dynamics at the Yishun release site, we restricted our analysis to the area where *Wolbachia*-infected males were released. We aimed to describe both the underlying dynamics of the full *Aedes aegypti* population at each site, and the level of variability in the trapping process. We considered the dynamics across a period of 100 weeks from January 2016 to October 2017. Cutpoints of the spline function were placed 10 weeks apart, giving a total of 11 cutpoints. When fitting the model to the data, Tampines was chosen as the reference control-release pair.

We sought to estimate

- the cutpoints and multipliers of the spline function
- the mean sampling proportions and corresponding over-dispersion parameters

- the mean proportion of eggs which are nonviable (not from CI)
- the egg mortality rate
- the basic mosquito reproduction number
- the mating competitiveness of *Wolbachia*-infected males

Thus, taking the different scaling factors into account, we estimated values for 28 parameters in total: $c_{2\dots 11}$, κ_C , p_f , p_e , ψ , ψ_e , η , μ_E , R_M , τ , $\lambda_{-m,r,wb}$, $s_{-c,r,f,m,wb,e}$. Uniform prior distributions were used for all parameters.

Values of the remaining model parameters were fixed, as described in Table 6.1 below. These values were chosen where possible to reflect the dynamics of wild-type *Aedes aegypti* populations in Singapore, and were determined in consultation with NEA Singapore. The adult mortality rate differs between males and females as adult females are typically observed to have a longer lifespan than wild-type adult males in Singapore. A similar pattern has been observed in several MRR studies of *Aedes aegypti*, conducted across a variety of settings [76, 77, 223, 250].

Parameter	Description	Value	Reference
b	Mean number of eggs laid by a female <i>Aedes aegypti</i>	25/day (based on estimate of 100 eggs per gonotrophic cycle)	[99]
g	Length of gonotrophic cycle	4 days	[251]
$\frac{1}{\gamma_E}$	Mean egg development time	3 days	[48]
$\frac{1}{\gamma_L}$	Mean larval development time	7 days	[48, 64, 68, 99]
μ_M	Adult male mortality rate	0.25/day	[223]
μ_F	Adult female mortality rate	0.15/day	[77, 223, 250]
ρ	Degree of CI	0.99	[97]
Ω	Strength of density dependence	1	-

Table 6.1: Fixed Model Parameter Values.

The particle MCMC algorithm was implemented using 50 particles, and the MCMC chains were run for 5 million iterations. Parameter values were sampled from the posterior distribution using

the final 500,000 iterations of each chain, thinned by a factor of 100. This gave an overall sample size of 5000 for each parameter value. Posterior predictive intervals were generated using 1000 parameter sets sampled from the posterior distribution of each parameter. For each of these parameter sets, one model run was performed.

6.2 Results

We adopted a number of different approaches when calibrating the model against the trapping data. We first included the basic mosquito reproduction number R_M in the set of estimated parameter values, and then tested sensitivity of estimated parameter values to different values of R_M by calibrating the model against the data for different fixed values of R_M . We also explored whether mating competitiveness of *Wolbachia*-infected males varied between the Tampines and Yishun.

6.2.1 Estimating the Basic Mosquito Reproduction Number

Results corresponding to the model where R_M is included in the set of estimated parameter values are presented in Figures 6.1-6.7 below. The posterior distributions of estimated parameter values are shown in Figure 6.1. Estimates of the wild-type adult female population size at both control sites and the variability in the underlying trapping process are presented in Figures 6.2 and 6.3. Fits of the model to the trapping data for both Tampines and Yishun are presented in Figures 6.4-6.7.

We obtained a very low estimate of R_M (posterior median 1.26, 95% CrI 1.21-1.33) (Figure 6.1) and, consequently, estimated a low wild-type adult female mosquito population size for both Tampines and Yishun. We estimated a maximum adult female population size of approximately 1,000 mosquitoes across the study period for both control sites (Figures 6.2,6.3). In order to fit the model to the data given these low estimates of population size, we therefore also estimated that, on average, a relatively large proportion of wild-type females were trapped at both sites with a high degree of variability in the trapping process.

In Tampines, we estimated that approximately 9% of wild-type females were trapped per week on average, with the proportion of females trapped ranging from 2%-20% approximately (Figure 6.2). As expected given the pattern observed in the trapping data, we estimated that a considerably

smaller proportion of wild-type males were trapped compared with wild-type females, with approximately 0.5% of wild-type males trapped per week on average (approximate range 0%-4%). A larger trapping rate was estimated for *Wolbachia*-infected males, with approximately 1% trapped per week on average (approximate range 0%-5%). A high degree of variability was also estimated for the egg trapping process, with approximately 2% of eggs laid trapped per week on average and the proportion of eggs trapped ranging from 0%-10%.

We estimated that, on average, a larger proportion of wild-type females were trapped in Yishun compared with Tampines, with approximately 16% of wild-type females trapped per week on average (approximate range 6%-30%) (Figure 6.3). Similarly to Tampines, we estimated a smaller proportion of wild-type males and *Wolbachia*-infected males were trapped in Yishun compared with wild-type females (Figure 6.3). However, we estimated a slightly smaller proportion of *Wolbachia*-infected males were trapped on average in Yishun compared with Tampines (.5%) (Figure 6.3). This is in agreement with the pattern observed in the trapping data. In addition, we estimated a smaller proportion of eggs were trapped on average in Yishun compared with Tampines.

We estimated a small proportion of eggs were non-viable for reasons other than CI (posterior median .67%, 95% CrI 0.5%-0.7%), and estimated a daily egg mortality rate of approximately .06 (95% CrI .055-.068) (Figure 6.1). We also estimated that there was substantial seasonal variation in mosquito abundance. This is shown by changes in the values of the cutpoints of the spline function used to determine seasonal variation in mosquito abundance (Figures 6.1-6.3).

Interestingly, we estimated that the mating competitiveness of the *Wolbachia*-infected males released was very low, with an estimated median proportion 0.22% of *Wolbachia*-infected males mating with wild-type female (95% CrI .18%-.24%). Here, we assumed mating competitiveness did not differ between Tampines and Yishun.

Under this parameter regime, we obtained a good fit of the model to the data across all sites, with the majority of data points lying within the 95% posterior predictive interval (Figures 6.4-6.7). The observed egg hatch rate was not used in the model fitting process, and thus was estimated using the trapping data simulated by the model when generating posterior predictive intervals. Here,

we obtained a good fit to the hatch rate observed at both control sites (Figures 6.4, 6.6). However we obtained a poorer fit to the hatch rate observed during the release period was obtained for both release sites (Figures 6.5, 6.7).

Although a good fit of the model to the data was obtained, the estimates of the weekly trapping rates for wild-type females obtained are unrealistically large. Furthermore, when fitting the model to the data, we did not model trapping mosquitoes as removing mosquitoes from the population. Had the trapping process been modelled in this way, such high trapping rates would have substantially affected the population dynamics. Thus, we explored sensitivity of parameter estimates to the value of R_M to gain a better understanding of the wild-type mosquito population size, the variability in the trapping process and the likely impact of the *Wolbachia* releases on the wild-type population.

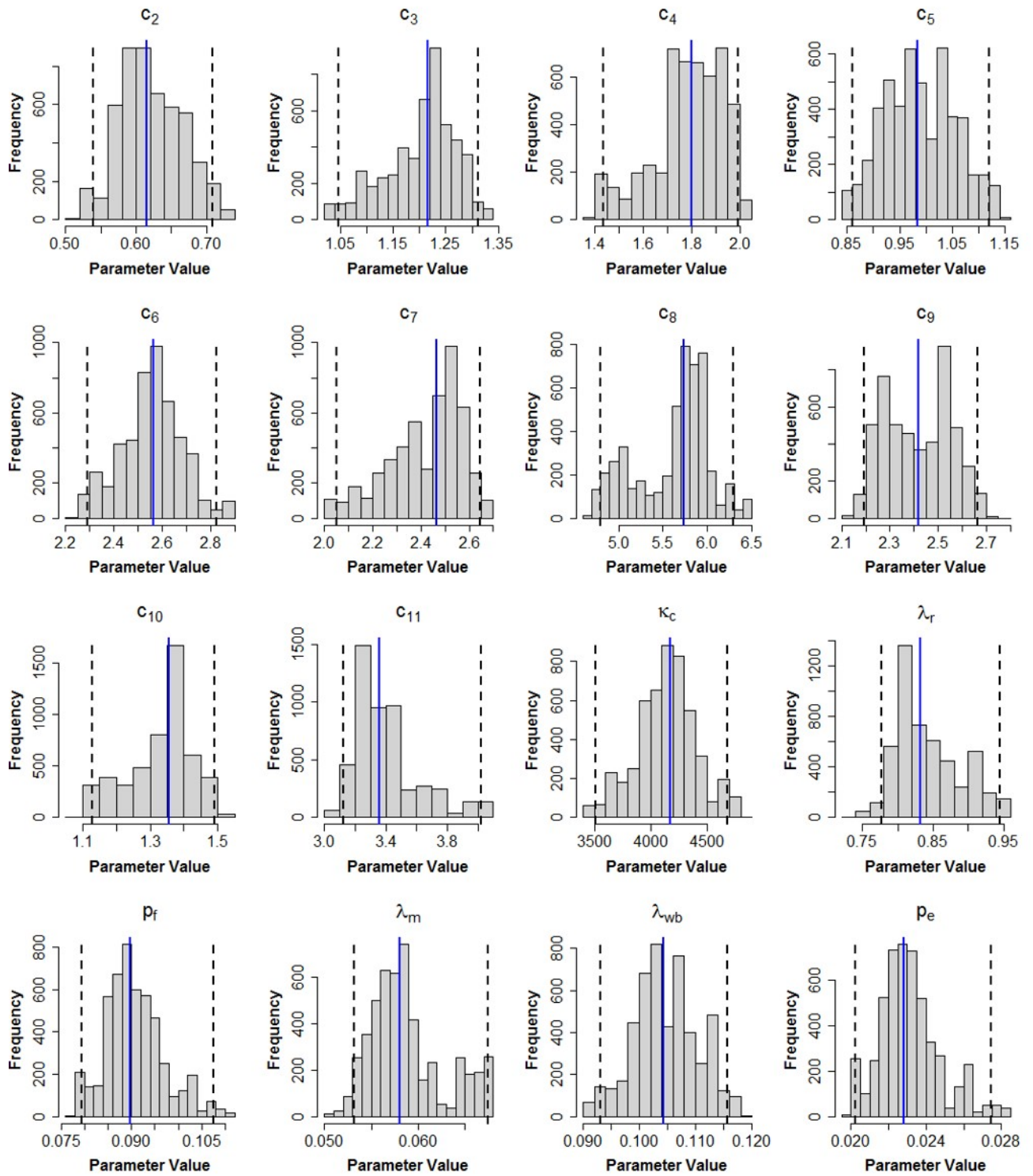


Figure 6.1: Posterior Parameter Distributions Histograms of the posterior distributions for all estimated parameters (when fitting R_M). For each parameter, 5000 values from the posterior distribution were sampled. The solid blue line shows the posterior median, and the dashed black lines show the 95% credible interval.

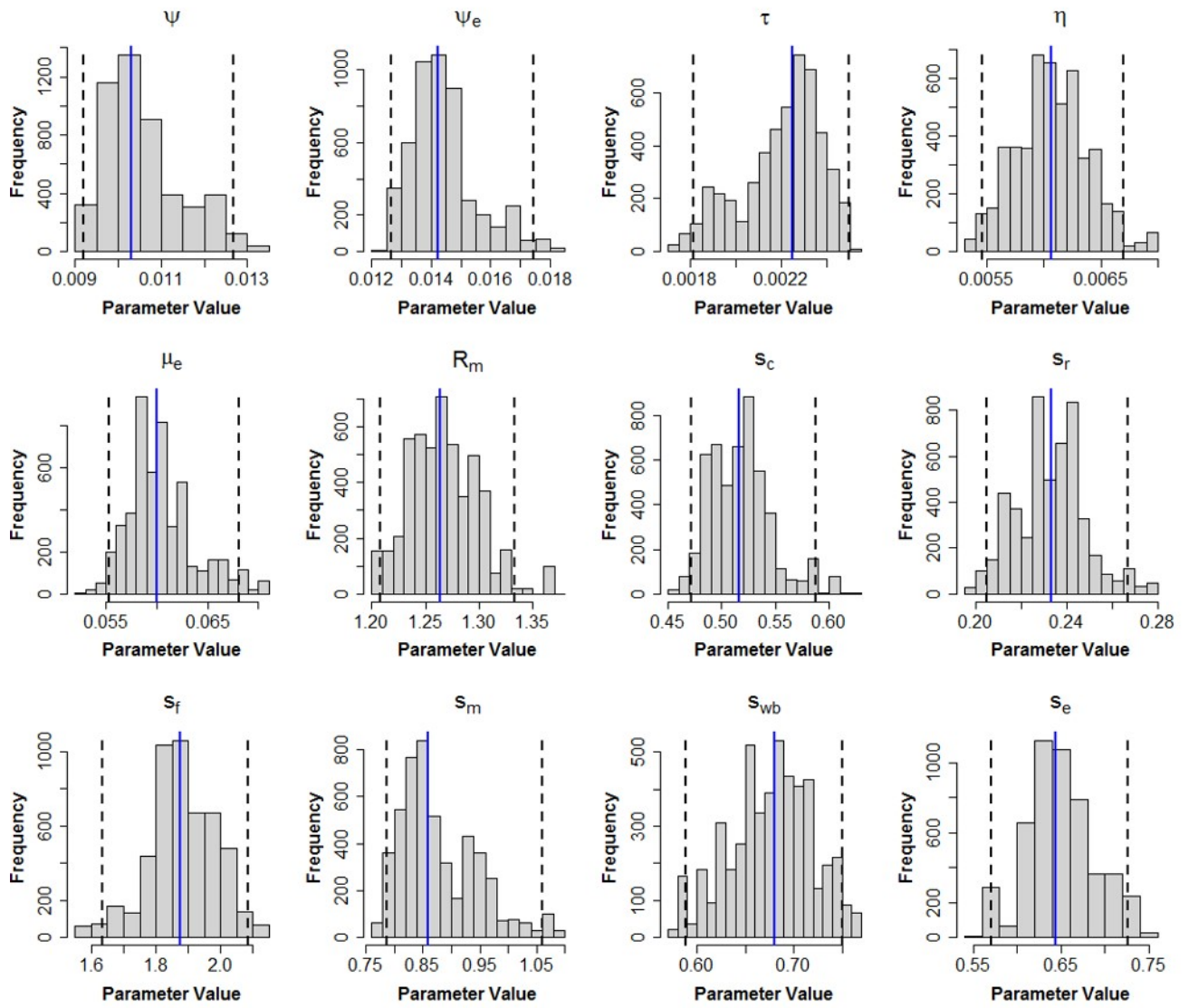


Figure 6.1 (Continued): Posterior Parameter Distributions Histograms of the posterior distributions for all estimated parameters (when fitting R_M). The solid blue line shows the posterior median, and the dashed black lines show the 95% credible interval.

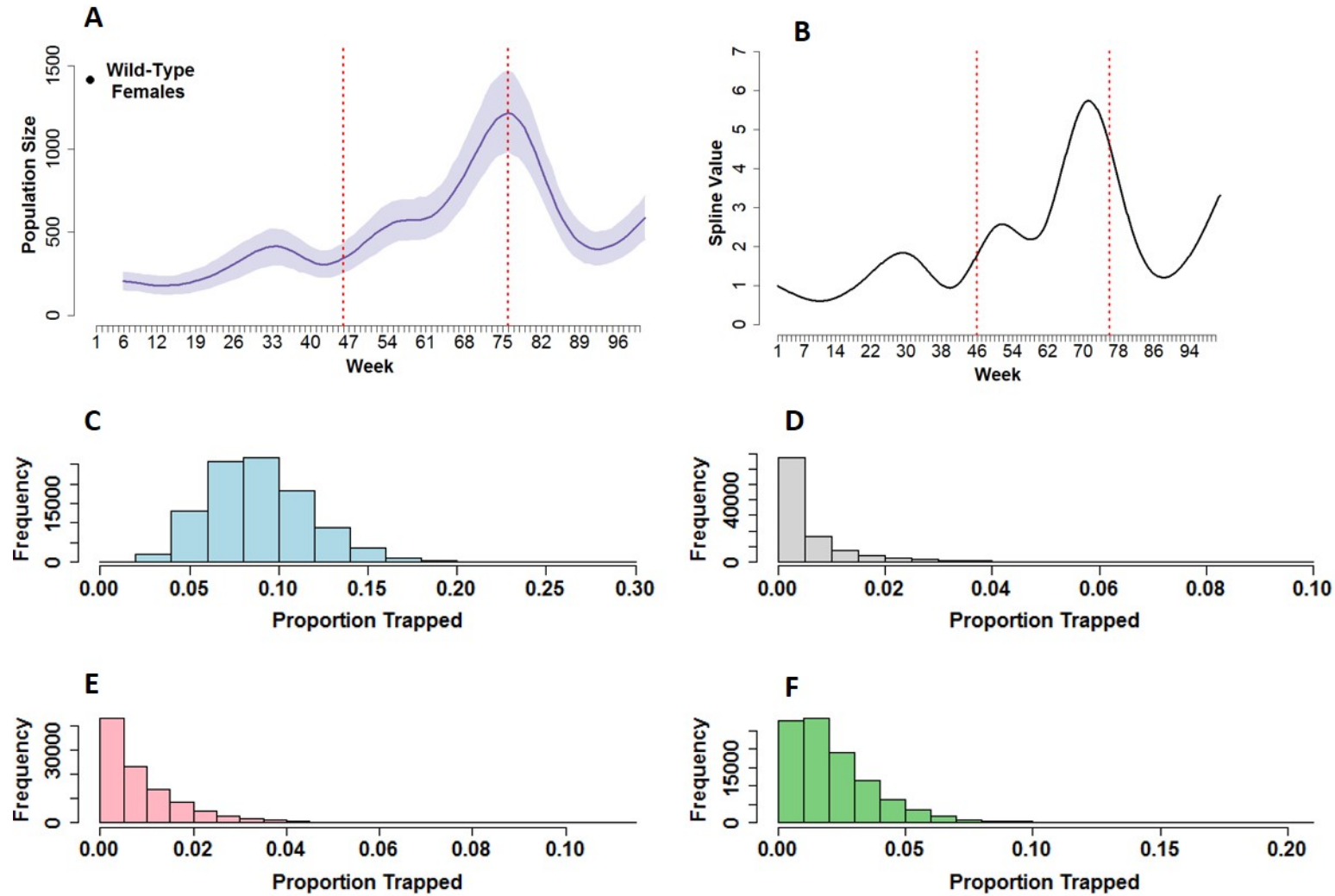


Figure 6.2: Population Size & Trapping - Tampines (A) Estimated total wild-type female population size for the Tampines control site. The solid line and shaded area show the posterior median and 95% posterior predictive interval respectively (based on 1000 simulations using samples from the posterior distribution). (B) Estimated spline function. (C-F) Histograms of the estimated distribution of the proportion of wild-type females (C), wild-type males (D), *Wolbachia*-infected males (E) and eggs (F) trapped in Tampines.

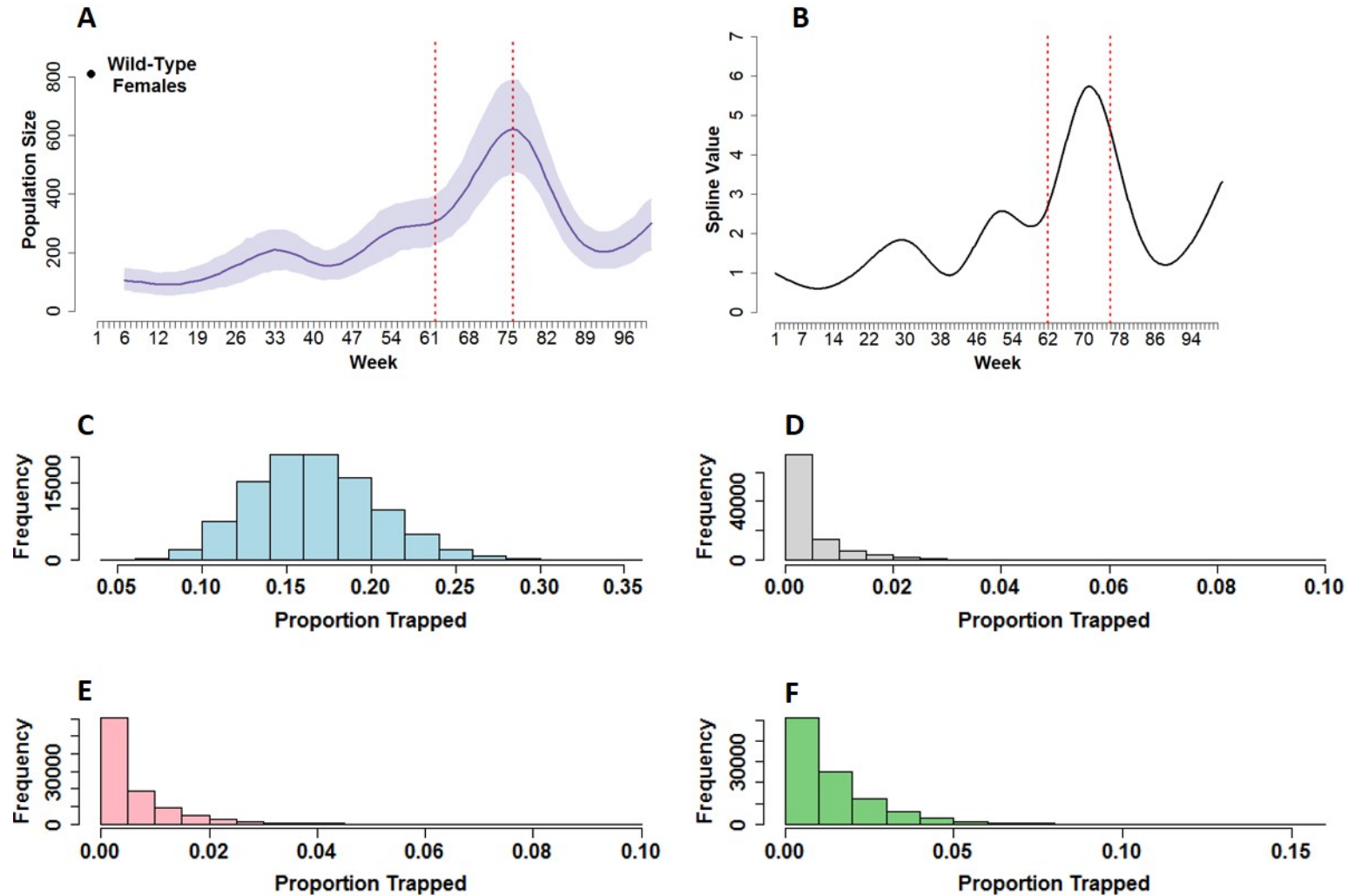


Figure 6.3: Population Size & Trapping -Yishun(A) Estimated total wild-type female population size for the Yishun control site. The solid line and shaded area show the posterior median and 95% posterior predictive interval respectively (based on 1000 simulations using samples from the posterior distribution).(B) Estimated spline function. (C-F) Histograms of the estimated distribution of the proportion of wild-type females (C), wild-type males (D), *Wolbachia*-infected males (E) and eggs (F) trapped in Yishun.

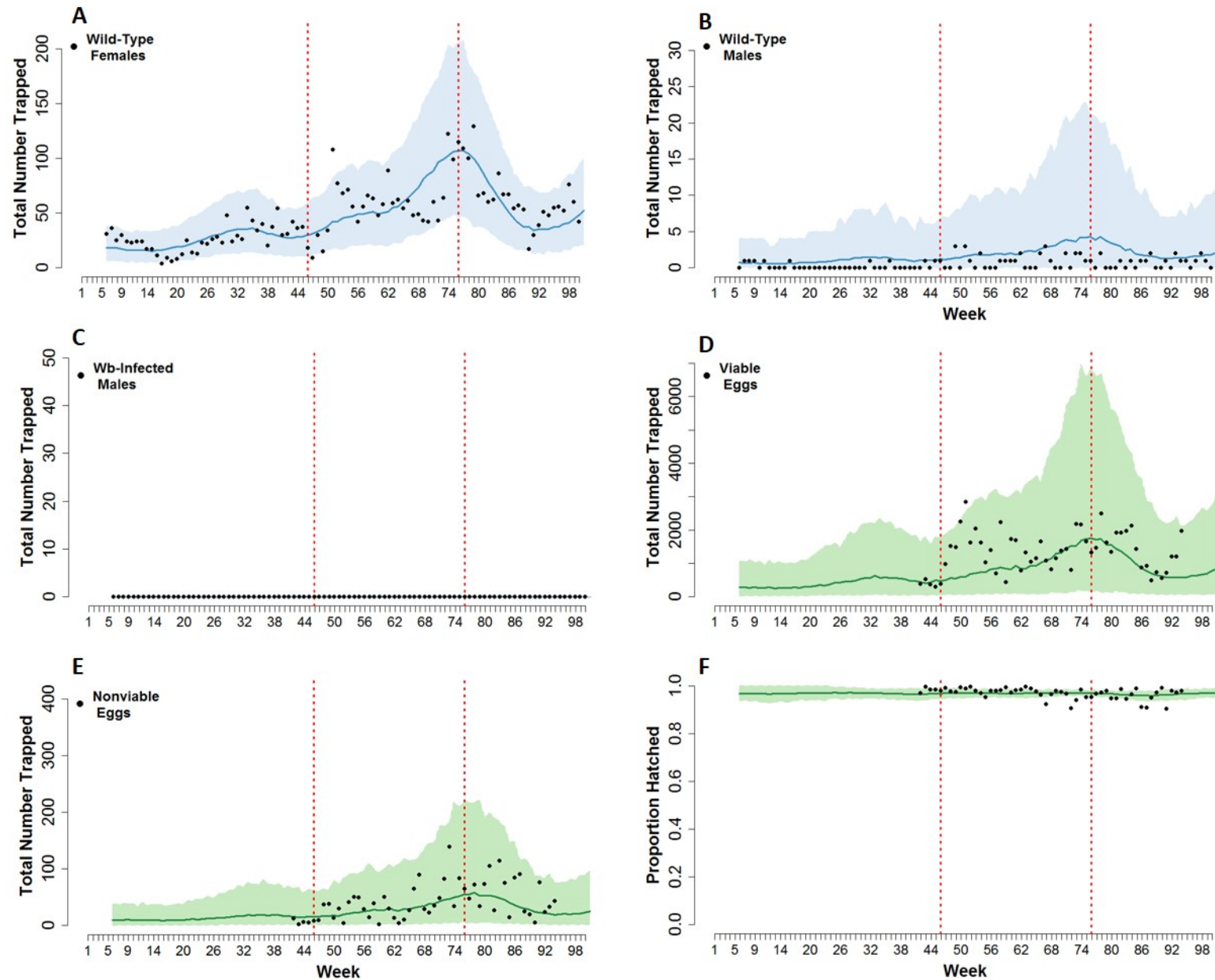


Figure 6.4: Tampines-Control Site (fitting R_M) Fits of the model to the trapping data collected at the Tampines control site. Observed data are shown in black, and the solid line and shaded area show the posterior median and 95% posterior predictive interval respectively. The dashed red lines show the period when *Wolbachia*-infected males were released. Figure F shows the estimated egg hatch rate.

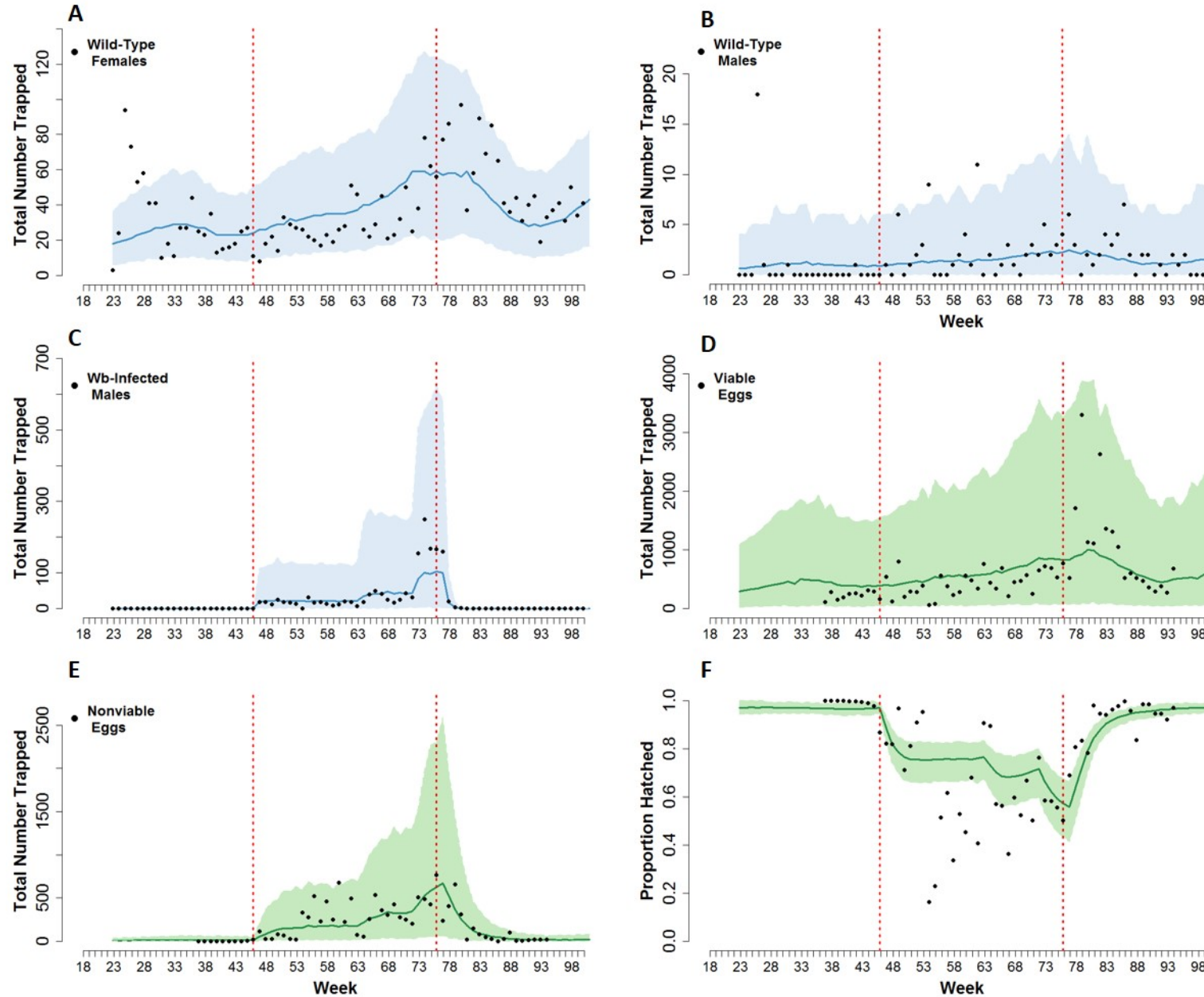


Figure 6.5: Tampines-Release Site (fitting R_M) Fits of the model to the trapping data collected at the Tampines release site. Observed data are shown in black, and the solid line and shaded area show the posterior median and 95% posterior predictive interval respectively. The dashed red lines show the period when *Wolbachia*-infected males were released. Figure F shows the estimated egg hatch rate.

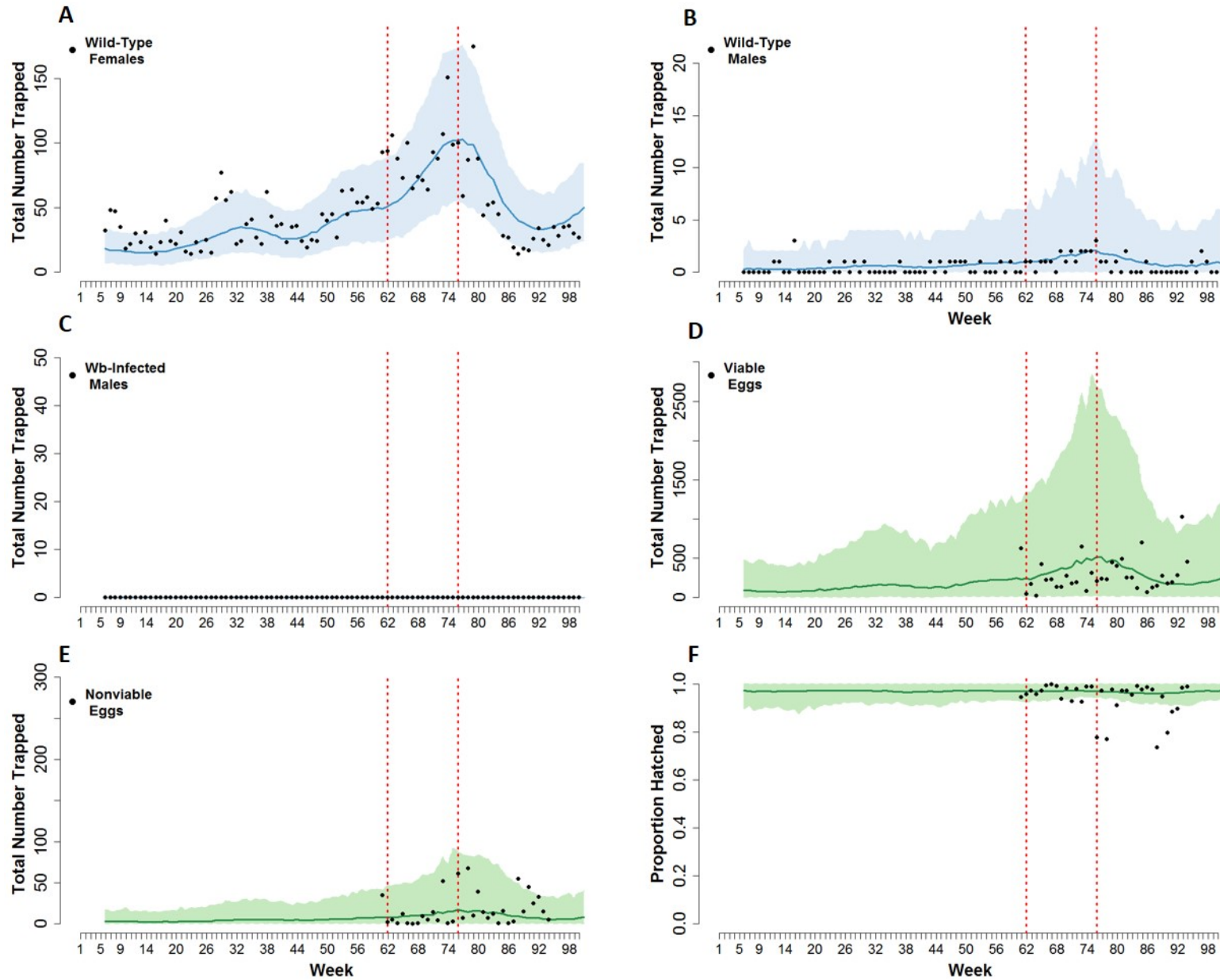


Figure 6.6: Yishun-Control Site (fitting R_M) Fits of the model to the trapping data collected at the Yishun control site. Observed data are shown in black, and the solid line and shaded area show the posterior median and 95% posterior predictive interval respectively. The dashed red lines show the period when *Wolbachia*-infected males were released. Figure F shows the estimated egg hatch rate.

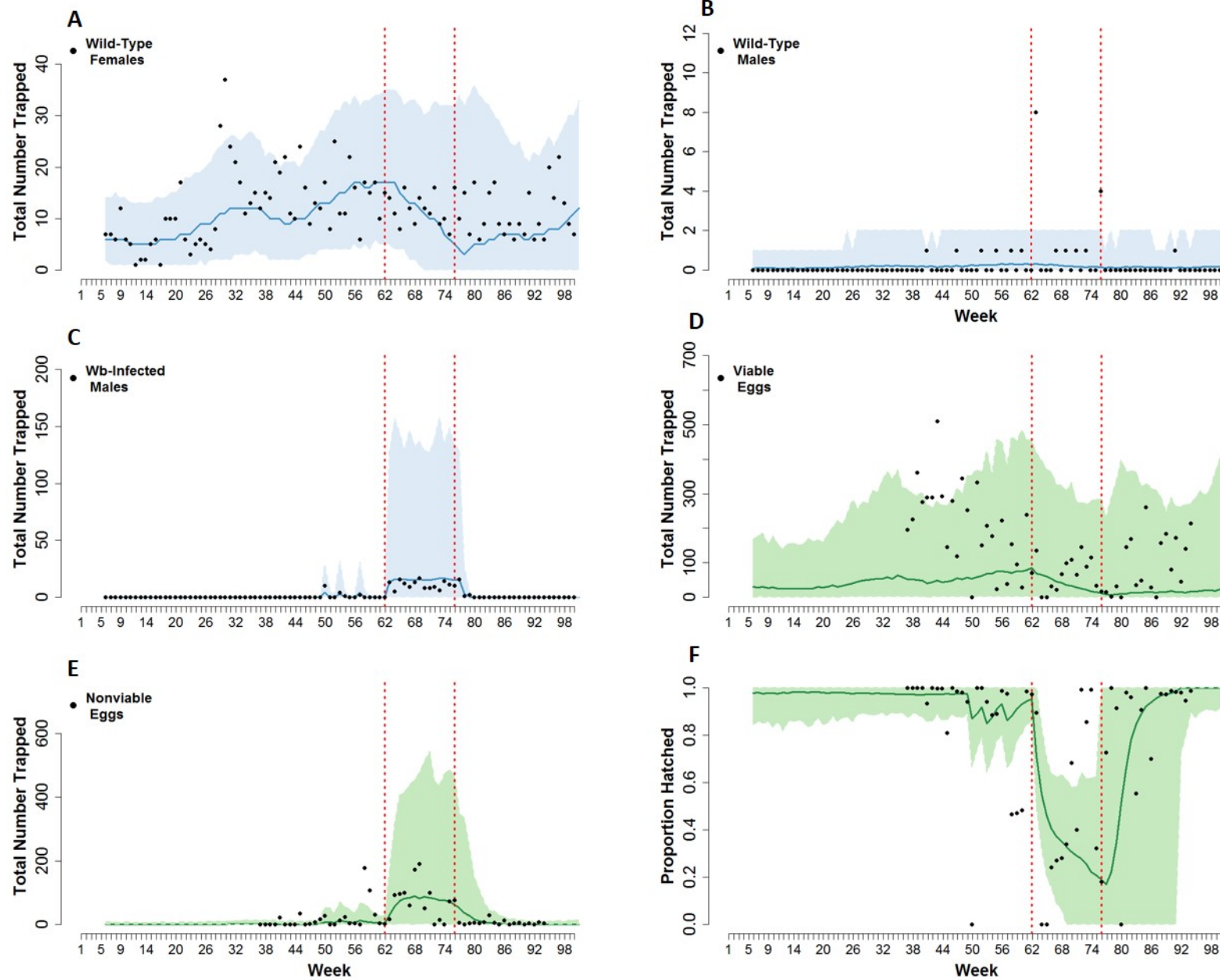


Figure 6.7: Yishun-Release Site (fitting R_M) Fits of the model to the trapping data collected at the Yishun release site. Observed data are shown in black, and the solid line and shaded area show the posterior median and 95% posterior predictive interval respectively. The dashed red lines show the period when *Wolbachia*-infected males were released. Figure F shows the estimated egg hatch rate.

6.2.2 Sensitivity to the Basic Mosquito Reproduction Number

Given the very low estimate of the basic mosquito reproduction number and high estimates of the trapping rates obtained in the previous section, we tested sensitivity of posterior parameter estimates to the value of the basic mosquito reproduction number by fixing the value of R_M at a range of different values ($R_M = 1.5, 5, 12$), and subsequently calibrating the model against the trapping data. A summary of the parameter estimates obtained for different values of R_M are presented in Table 6.2. Corresponding estimates of total wild-type adult female population size and the proportion of adults and eggs trapped in Tampines and Yishun are shown in Figures 6.10 and 6.11 below. Fits of the model to the data for $R_M = 12$ are presented in Figures 6.12-15.

In agreement with the results obtained in the previous section, we observed that the log-likelihood was largest when $R_M = 1.5$ (Figure 6.8). Considerably lower values of log-likelihood were obtained for $R_M = 5, 12$ compared with $R_M = 1.5$, however we observed little difference in the log-likelihood values obtained for $R_M = 5$ and $R_M = 12$ (Figure 6.8).

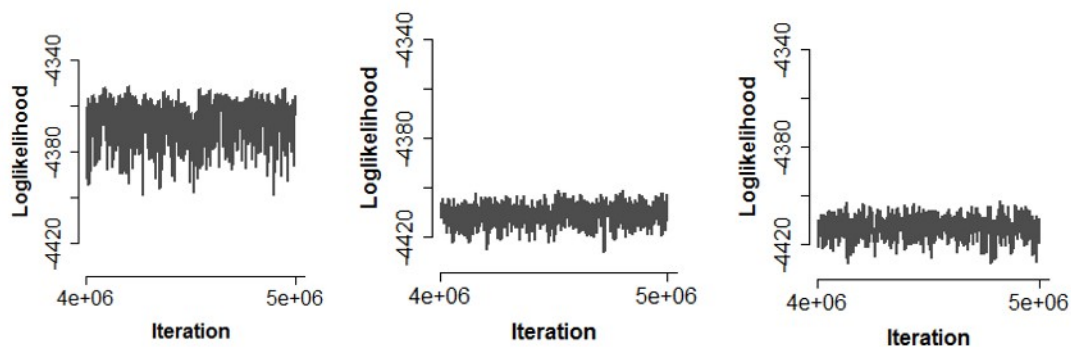


Figure 6.8: Comparison of Log-likelihood Log-likelihood values observed when fitting the model to the data for (A) $R_M=1.5$, (B) $R_M=5$ and (C) $R_M=12$.

The largest differences in estimates of parameter values were also observed when moving from $R_M = 1.5$ to $R_M = 5$. We observed a large increase in total wild-type adult female population size and a substantial reduction in both the mean trapping rates and the variability in the trapping process when moving between these parameter regimes. For example, for $R_M = 1.5$ we estimated a maximum wild-type adult female mosquito population size for the Tampines control site of approximately 1,000 mosquitoes, and estimated approximately 10% of wild-type females were trapped per week on average in Tampines, with the proportion trapped ranging from 3%-20% approximately (Figure 6.10). In contrast, for $R_M = 5$, we estimated a maximum wild-type

adult female mosquito population size for the Tampines control site of approximately 12,000 mosquitoes, and estimated approximately 1.5% of wild-type females were trapped per week on average in Tampines, with the proportion trapped ranging from 0.5%-3% approximately (Figure 6.10). For $R_M = 5$, we also estimated a lower proportion of wild-type males, *Wolbachia*-infected males and eggs were trapped on average in Tampines, compared with $R_M = 1.5$ (Figure 6.10). A similar pattern was observed for Yishun when moving from $R_M = 1.5$ to larger values (Figure 6.11).

For the majority of model parameters, similar estimates of parameter values were obtained for $R_M = 5$ and $R_M = 12$ (Table 6.2). Although differences in the estimates of the multipliers of the spline function were observed when moving between larger values of R_M , estimates of the wild-type adult female mosquito population size and the variability in the trapping process remained broadly similar for $R_M = 5$ and $R_M = 12$ (Figure 6.9). For larger values of R_M , we also estimated less seasonal variability in mosquito abundance as smaller differences were observed between the estimated values of the cutpoints of the spline function, compared with for very low values of R_M (Table 6.2). In addition, for larger values of R_M , we estimated that, on average, a smaller proportion of adult mosquitoes and eggs were trapped in Yishun compared with Tampines.

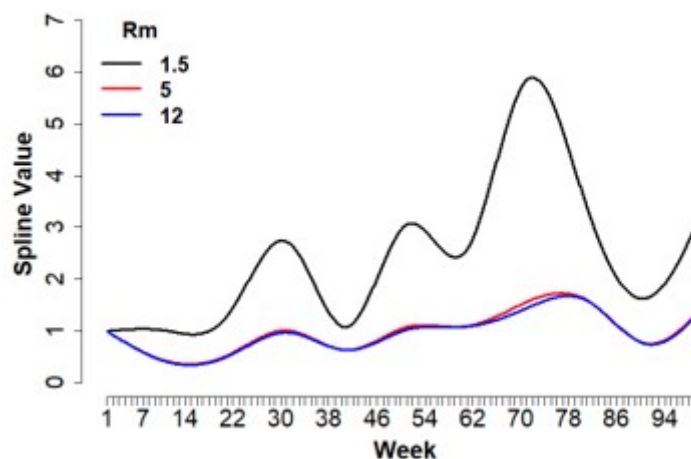


Figure 6.9: Spline Function (fixed R_M) Estimated spline function for different fixed values of R_M .

For all values of R_M , we estimated approximately 1% of eggs were non-viable for reasons other than CI, and a daily egg mortality rate of approximately 0.10 (Table 6.2). Although slightly higher estimates of mating competitiveness were obtained for larger values of R_M , estimates of the mating competitiveness of *Wolbachia*-infected males, overall, remained very low. For $R_M = 1.5$

we estimated approximately 0.4% of *Wolbachia*-infected males mated successfully with wild-type females, while for $R_M = 5$ and $R_M = 12$ this value increased to approximately 3% (Table 6.2).

Despite having lower log-likelihood values, a good fit of the model to the data was still obtained for larger values of R_M (Figures 6.12-15). Posterior predictive intervals were wider compared with model fits for very low values of R_M , however we obtained a better fit to the observed egg hatch rate during the release periods for both Tampines and Yishun for larger values of R_M (Figures 6.13, 6.15).

Parameter	Description	Prior	$R_M = 1.5$	$R_M = 5$	$R_M = 12$
c_2	Cutpoint of Spline Function	U [0.001,20]	1.01 (0.81, 1.11)	0.42 (0.26, 0.69)	0.41 (0.23, 0.80)
c_3	Cutpoint of Spline Function	U [0.001,20]	1.29 (1.09, 1.46)	0.53 (0.37,0.79)	0.50 (0.33, 0.82)
c_4	Cutpoint of Spline Function	U [0.001,20]	2.72 (2.34, 2.91)	1.01 (0.68, 1.62)	0.97 (0.58, 1.79)
c_5	Cutpoint of Spline Function	U [0.001,20]	1.08 (0.90, 1.20)	0.63 (0.43, 0.99)	0.63 (0.39, 1.10)
c_6	Cutpoint of Spline Function	U [0.001,20]	3.05 (2.68, 3.37)	1.08 (0.74, 1.65)	1.02 (0.62, 1.80)
c_7	Cutpoint of Spline Function	U [0.001,20]	2.57 (2.27, 2.88)	1.09 (0.75, 1.68)	1.09 (0.66, 1.87)
c_8	Cutpoint of Spline Function	U [0.001,20]	5.84 (4.54, 6.33)	1.56 (1.05, 2.43)	1.44 (0.87, 2.59)
c_9	Cutpoint of Spline Function	U [0.001,20]	3.40 (2.76, 3.75)	1.60 (1.11, 2.49)	1.59 (0.97, 2.78)
c_{10}	Cutpoint of Spline Function	U [0.001,20]	1.63 (1.30, 1.79)	0.76 (0.51, 1.17)	0.75 (0.46, 1.29)
c_{11}	Cutpoint of Spline Function	U [0.001,20]	3.50 (2.88, 3.81)	1.55 (0.92,2.69)	1.49 (0.81, 2.71)
κ_c	Multiplier of Spline Function (Tampines control site)	U [0.001,1000000]	3,018 (2,698,3,245)	56,722 (29,700,101,391)	65,960 (30,659,146,786)
λ_r	Scaling Factor (Tampines release site)	U [0.001,1000]	0.89 (0.83,1.01)	0.73 (0.65,0.82)	0.71 (0.63,0.79)
p_f	Mean proportion of wild-type females sampled (Tampines)	U [0,1]	0.097 (0.088,0.119)	0.014 (0.008,0.026)	0.013 (0.007,0.025)
p_e	Mean proportion of eggs sampled (Tampines)	U [0,1]	0.026 (0.024,0.031)	0.004 (0.002,0.007)	0.003 (0.002,0.007)

ψ	Over-dispersion parameter (adult mosquitoes)	U [0.00001, 1]	0.010 (0.009,0.012)	0.002 (0.001,0.003)	0.002 (0.001,0.003)
ψ_e	Over-dispersion parameter (eggs)	U [0.00001, 1]	0.014 (0.013,0.016)	0.002 (0.001,0.004)	0.002 (0.001,0.004)
μ_e	Egg mortality rate	U [0.001, .25]	0.098 (0.081,0.114)	0.103 (0.069,0.217)	0.096 (0.064,0.161)
η	Degree of non-viability among eggs laid (not from CI)	U [0, 1]	0.010 (0.008,0.010)	0.010 (0.007,0.017)	0.009 (0.006,0.015)
τ	Mating competitiveness of <i>Wolbachia</i> -infected males	U [0, 1]	0.0040 (0.0036,0.0043)	0.031 (0.015,0.115)	0.032 (0.013,0.075)
λ_m	Scaling Factor (Tampines)	U [0, 10]	0.055 (0.042,0.061)	0.054 (0.042,0.068)	0.054 (0.042,0.067)
λ_{wb}	Scaling Factor (Tampines)	U [0, 10]	0.101 (0.085,0.109)	0.536 (0.311,0.932)	0.591 (0.313,1.071)
s_c	Scaling Factor (Yishun control site)	U [0, 1000]	0.95 (0.87, 1.21)	1.13 (0.82, 1.52)	1.20 (0.90, 1.61)
s_r	Scaling Factor (Yishun release site)	U [0, 1000]	0.35 (0.31, 0.38)	0.46 (0.33, 0.62)	0.49 (0.37, 0.67)
s_f	Scaling Factor (Yishun)	U [0, 10]	1.09 (0.89, 1.19)	0.86 (0.65, 1.18)	0.81 (0.62, 1.07)
s_m	Scaling Factor (Yishun)	U [0, 10]	0.66 (0.53, 0.71)	0.59 (0.40, 0.87)	0.56 (0.38, 0.82)
s_{wb}	Scaling Factor (Yishun)	U [0, 10]	0.60 (0.48, 0.67)	0.53 (0.37, 0.75)	0.52 (0.37, 0.75)
s_e	Scaling Factor (Yishun)	U [0, 10]	0.43 (0.40, 0.48)	0.41 (0.32, 0.53)	0.39 (0.31, 0.49)

Table 6.2: Sensitivity to R_M . Summary of posterior estimates of parameter values for the model with different fixed values of R_M . The median posterior estimate is reported with the 95% credible interval in brackets.

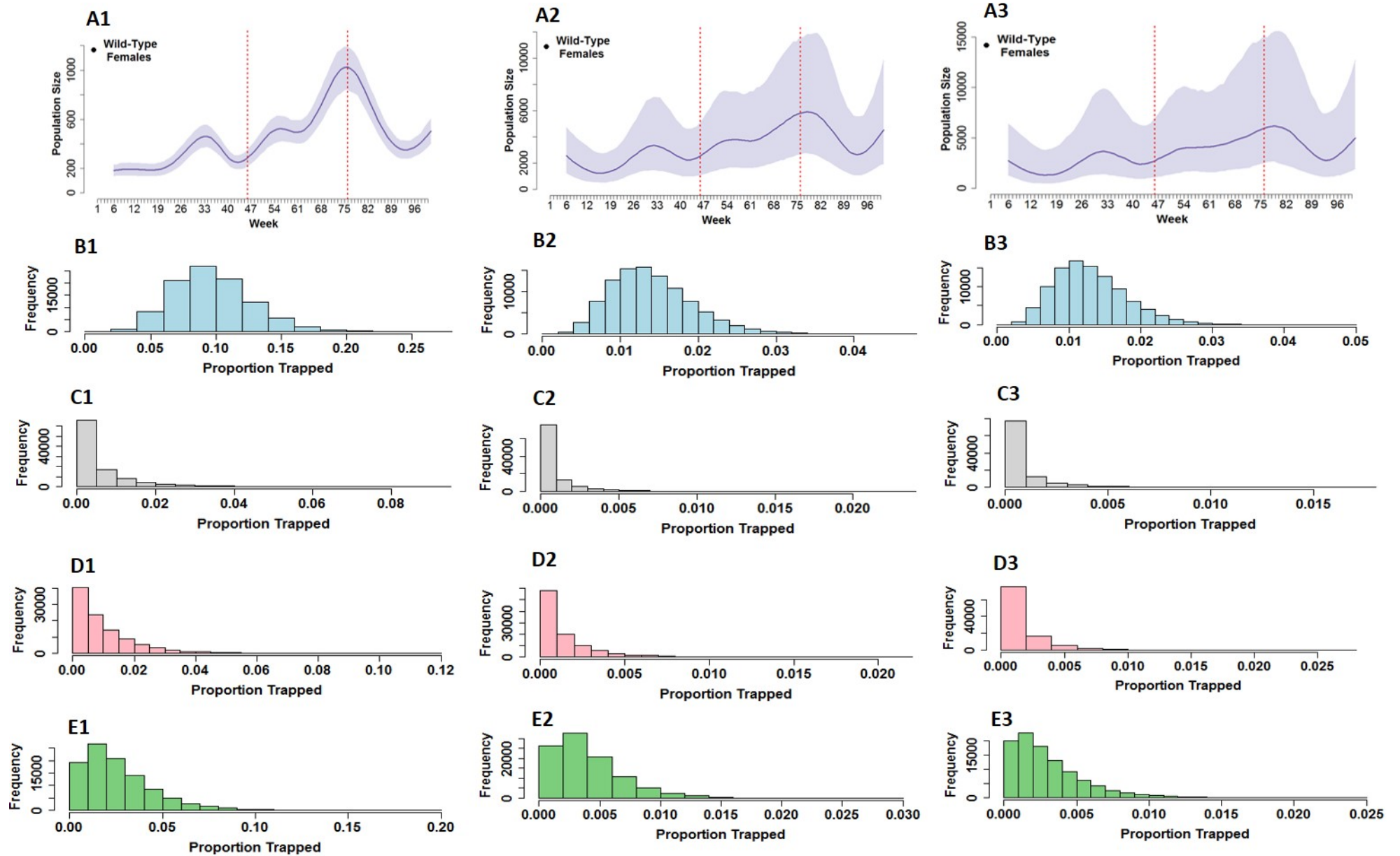


Figure 6.10: Population Size & Trapping (fixed R_M)-Tampines Comparison of estimated total wild-type female population size and trapping rates for the Tampines control site. Figures in columns 1,2 and 3 correspond to $R_M = 1.5$, $R_M = 5$, and $R_M = 12$ respectively. The solid line and shaded area in (A1-A3) show the posterior median and 95% posterior predictive interval respectively (based on 1000 simulations using samples from the posterior distribution). (B1-E3) Histograms of the estimated distribution of the proportion of wild-type females (B1-B3), wild-type males (C1-C3), *Wolbachia*-infected males (D1-D3) and eggs (E1-E3) trapped in Tampines.

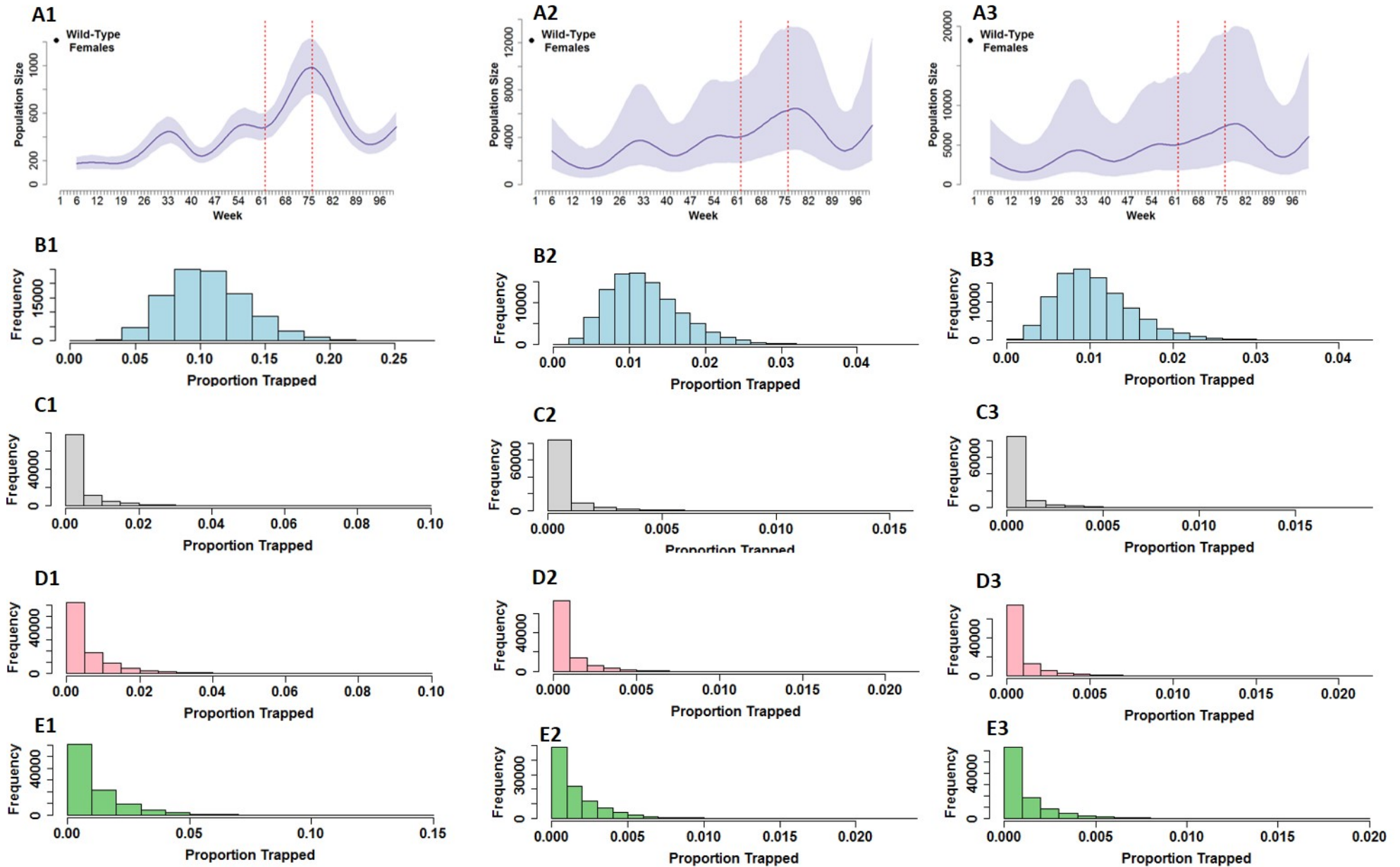


Figure 6.11: Population Size & Trapping (fixed R_M)-Yishun Comparison of estimated total wild-type female population size and trapping rates for the Yishun control site. Figures in columns 1,2 and 3 correspond to $R_M = 1.5$, $R_M = 5$, and $R_M = 12$ respectively. The solid line and shaded area in (A1-A3) show the posterior median and 95% posterior predictive interval respectively (based on 1000 simulations using samples from the posterior distribution). (B1-E3) Histograms of the estimated distribution of the proportion of wild-type females (B1-B3), wild-type males (C1-C3), *Wolbachia*-infected males (D1-D3) and eggs (E1-E3) trapped in Yishun.

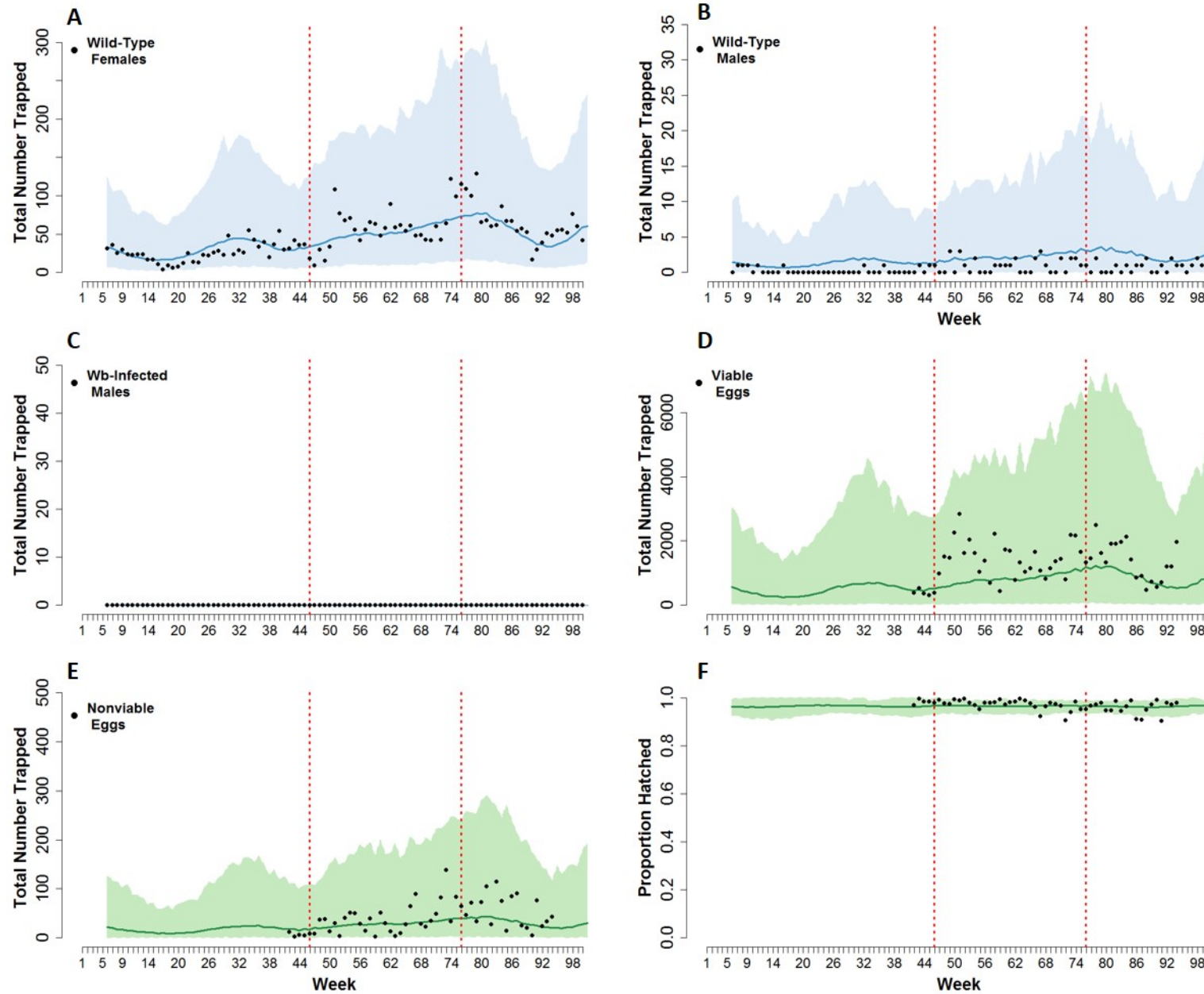


Figure 6.12: Tampines-Control Site ($R_M = 12$) Fits of the model to the trapping data collected at the Tampines control site. Observed data are shown in black, and the solid line and shaded area show the posterior median and 95% posterior predictive interval respectively. The dashed red lines show the period when *Wolbachia*-infected males were released. Figure F shows the estimated egg hatch rate.

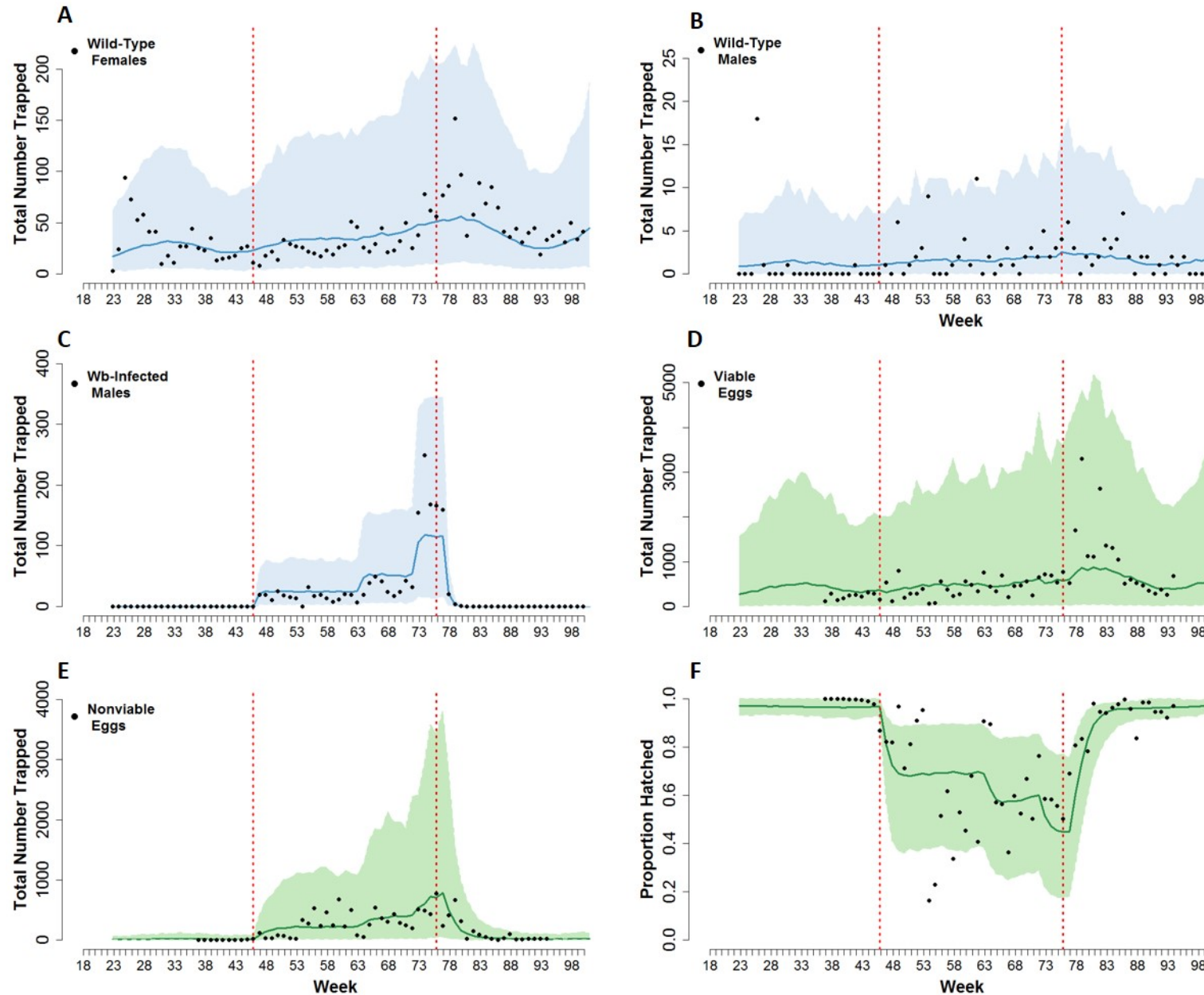


Figure 6.13: Tampines-Release Site ($R_M = 12$) Fits of the model to the trapping data collected at the Tampines release site. Observed data are shown in black, and the solid line and shaded area show the posterior median and 95% posterior predictive interval respectively. The dashed red lines show the period when *Wolbachia*-infected males were released. Figure F shows the estimated egg hatch rate.

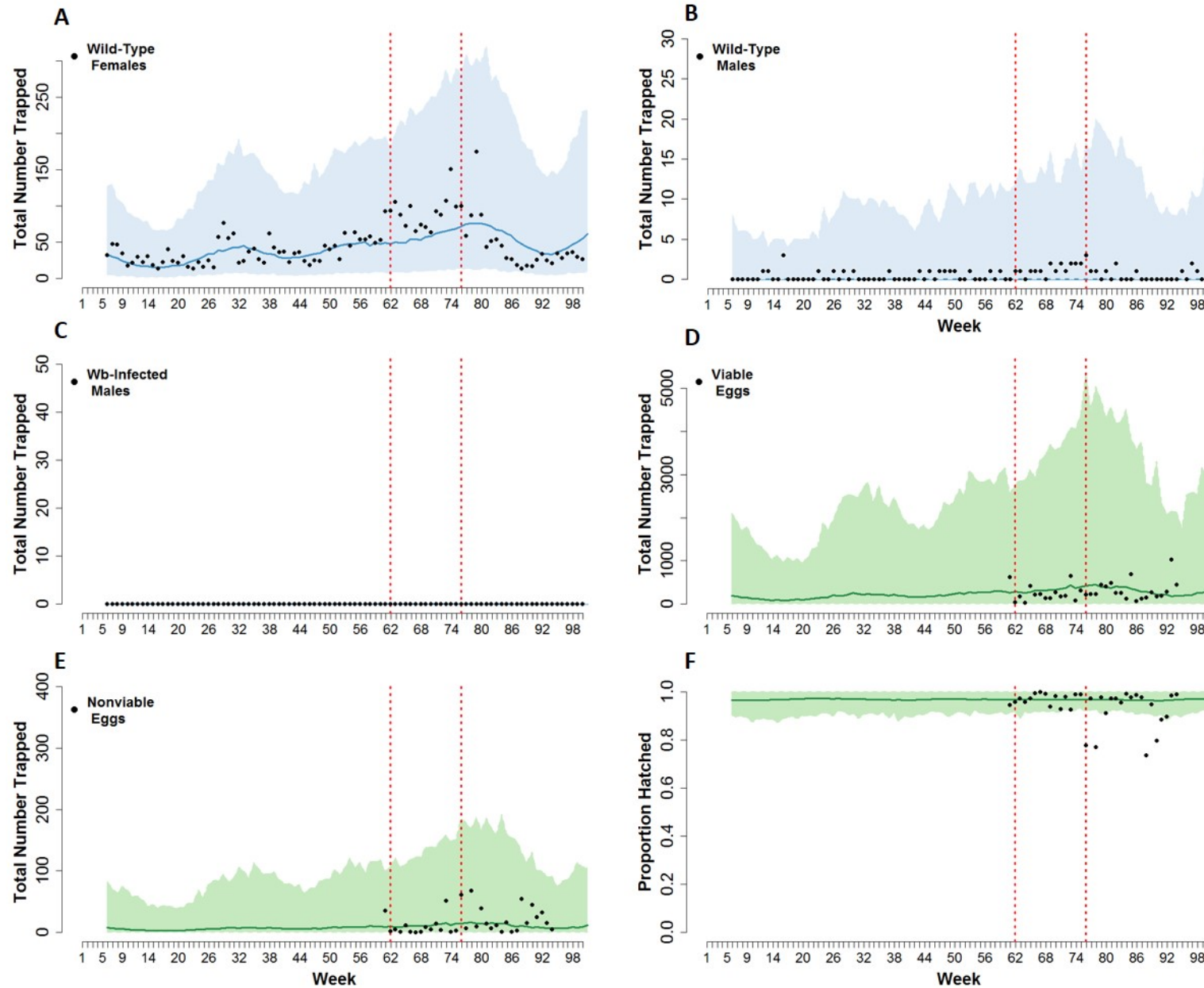


Figure 6.14: Yishun-Control Site ($R_M = 12$) Fits of the model to the trapping data collected at the Yishun control site. Observed data are shown in black, and the solid line and shaded area show the posterior median and 95% posterior predictive interval respectively. The dashed red lines show the period when *Wolbachia*-infected males were released. Figure F shows the estimated egg hatch rate.

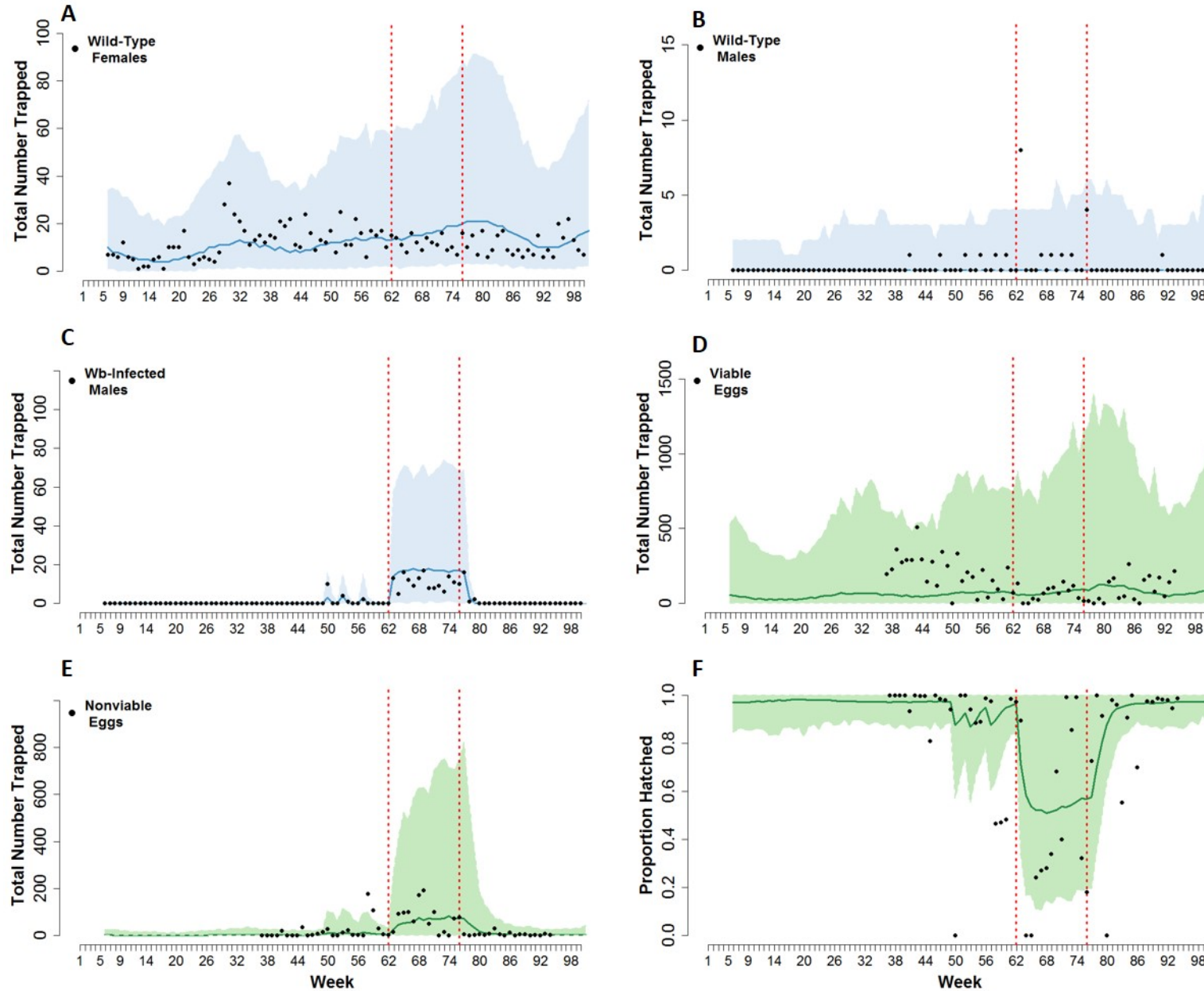


Figure 6.15: Yishun-Release Site ($R_M = 12$) Fits of the model to the trapping data collected at the Yishun Release site. Observed data are shown in black, and the solid line and shaded area show the posterior median and 95% posterior predictive interval respectively. The dashed red lines show the period when *Wolbachia*-infected males were released. Figure F shows the estimated egg hatch rate.

6.2.3 Mating Competitiveness

We tested whether the mating competitiveness of *Wolbachia*-infected males varied between release sites by allowing the parameter τ to vary between sites when fitting the model to the data. We let τ^1 and τ^2 denote the mating competitiveness of *Wolbachia*-infected males released in Tampines and Yishun respectively. As in the previous section, results for $R_M = 5$ and $R_M = 12$ were similar, and here we discuss the results for the model where $R_M = 12$ remains fixed.

We observed considerable differences in estimates of the mating competitiveness of *Wolbachia*-infected males released in Tampines and Yishun, with substantially greater mating competitiveness estimated for Yishun (posterior median 18.5%, 95% CrI 5.1%-44%) compared with Tampines (3.1%, 95% CrI 1.4%-8.1%) (Figure 6.16). Furthermore, allowing mating competitiveness to vary between sites also resulted in slightly higher mean log-likelihood values (Figure 6.16).

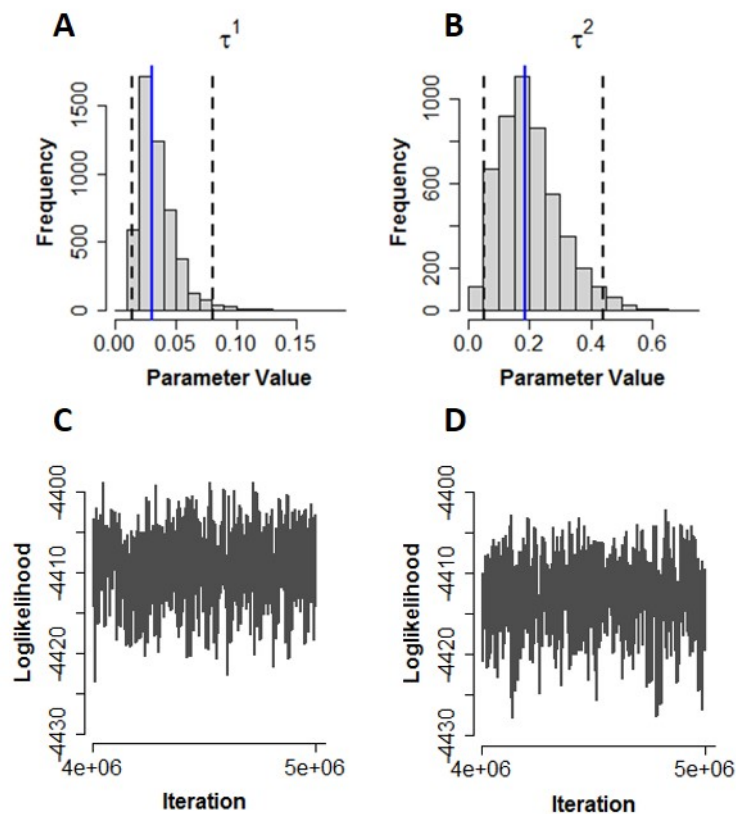


Figure 6.16: Mating Competitiveness (A-B) Posterior estimates of mating competitiveness for Tampines (A) and Yishun (B) for the model where $R_M=12$ is fixed. The solid blue line shows the posterior median, and the dashed black lines show the 95% credible interval. (C-D) Log-likelihood values of model where $R_M=12$ is fixed when mating competitiveness is estimated locally (C) or globally (D).

The majority of posterior estimates for other parameter values remained largely unchanged when fitting τ locally (Table 6.3). We estimated a higher daily egg mortality rate when mating competitiveness was fitted locally (posterior median .133, 95% CrI .083-.231) compared with globally (posterior median .096, 95% CrI .064-.161). Slight differences in the multipliers of the spline function were also observed, however estimates of total wild-type adult female size remained broadly similar. Estimates of the mean trapping rates and level of variability in the trapping process for both adult mosquitoes and eggs also remained similar under both scenarios (Table 6.3).

Given our estimate of mating competitiveness for Tampines was similar to that obtained when mating competitiveness was estimated globally (Table 6.3), fits of the model to the trapping data collected at Tampines remained largely unchanged when τ was estimated locally (Figures 6.17, 6.18). However, for Yishun, a higher estimate of mating competitiveness resulted in wider posterior predictive intervals for the number of nonviable eggs at the Yishun release site (Figure 6.20). This in turn resulted in a better fit to the hatch rate observed during the release period at the Yishun release site (Figure 6.20).

Parameter	Description	Prior	τ - global	τ - local
c_2	Cutpoint of Spline Function	U [0.001,20]	0.41 (0.23,0.80)	0.41 (0.24,0.84)
c_3	Cutpoint of Spline Function	U [0.001,20]	0.50 (0.33,0.82)	0.49 (0.34,0.87)
c_4	Cutpoint of Spline Function	U [0.001,20]	0.97 (0.58,1.79)	0.97 (0.61,1.84)
c_5	Cutpoint of Spline Function	U [0.001,20]	0.63 (0.39,1.10)	0.62 (0.40,1.13)
c_6	Cutpoint of Spline Function	U [0.001,20]	1.02 (0.62,1.80)	1.00 (0.65,1.86)
c_7	Cutpoint of Spline Function	U [0.001,20]	1.09 (0.66,1.87)	1.07 (0.68,2.00)
c_8	Cutpoint of Spline Function	U [0.001,20]	1.44 (0.87,2.59)	1.50 (0.96,2.75)
c_9	Cutpoint of Spline Function	U [0.001,20]	1.59 (0.97,2.78)	1.57 (1.02,2.86)
c_{10}	Cutpoint of Spline Function	U [0.001,20]	0.75 (0.46,1.29)	0.75 (0.49,1.39)
c_{11}	Cutpoint of Spline Function	U [0.001,20]	1.49 (0.81,2.71)	1.45 (0.86,2.74)
κ_c	Multiplier of Spline Function (Tampines control site)	U [0.001,1000000]	65,960 (30,659,146,786)	53,135 (22,002,120,609)
λ_r	Scaling Factor (Tampines release site)	U [0.001,1000]	0.71 (0.63,0.79)	0.72 (0.64,0.80)
p_f	Mean proportion of wild-type females sampled (Tampines)	U [0,1]	0.013 (0.007,0.025)	0.014 (0.008,0.030)
p_e	Mean proportion of eggs sampled (Tampines)	U [0,1]	0.003 (0.002,0.007)	0.004 (0.002,0.010)
ψ	Over-dispersion parameter (adult mosquitoes)	U [0.00001,1]	0.002 (0.001,0.003)	0.002 (0.001,0.004)
ψ_e	Over-dispersion parameter (eggs)	U [0.00001,1]	0.002 (0.001,0.004)	0.002 (0.001,0.006)
μ_e	Egg mortality rate	U [0.001, .25]	0.096 (0.064,0.161)	0.133 (0.083,0.231)

η	Degree of non-viability among eggs laid (not from CI)	U [0,1]	0.009 (0.006,0.015)	0.012 (0.008,0.018)
τ^1	Mating competitiveness of <i>Wolbachia</i> -infected males (Tampines)	U [0,1]	0.032 (0.013,0.075)	0.031 (0.014,0.081)
τ^2	Mating competitiveness of <i>Wolbachia</i> -infected males (Yishun)	U [0,1]	0.032 (0.013,0.075)	0.185 (0.051,0.440)
λ_m	Scaling Factor (Tampines release site)	U [0,10]	0.054 (0.042,0.067)	0.054 (0.042,0.068)
λ_{wb}	Scaling Factor (Tampines release site)	U [0,10]	0.591 (0.313, 1.071)	0.528 (0.256, 0.949)
s_c	Scaling Factor (Yishun release site)	U [0,1000]	1.20 (0.90,1.61)	1.19 (0.90,1.57)
s_r	Scaling Factor (Yishun release site)	U [0,1000]	0.49 (0.37,0.67)	0.50 (0.38,0.67)
s_f	Scaling Factor (Yishun release site)	U [0,10]	0.81 (0.62,1.07)	0.83 (0.63,1.08)
s_m	Scaling Factor (Yishun release site)	U [0,10]	0.56 (0.38,0.82)	0.57 (0.39,0.84)
s_{wb}	Scaling Factor (Yishun release site)	U [0,10]	0.52 (0.37,0.75)	0.54 (0.37,0.77)
s_e	Scaling Factor (Yishun release site)	U [0,10]	0.39 (0.31,0.49)	0.37 (0.29,0.47)

Table 6.3: Estimating Mating Competitiveness. Summary of posterior estimates of parameter values for the model where $R_M = 12$ is fixed and mating competitiveness is estimated globally or locally. The median posterior estimate is reported with the 95% credible interval in brackets.

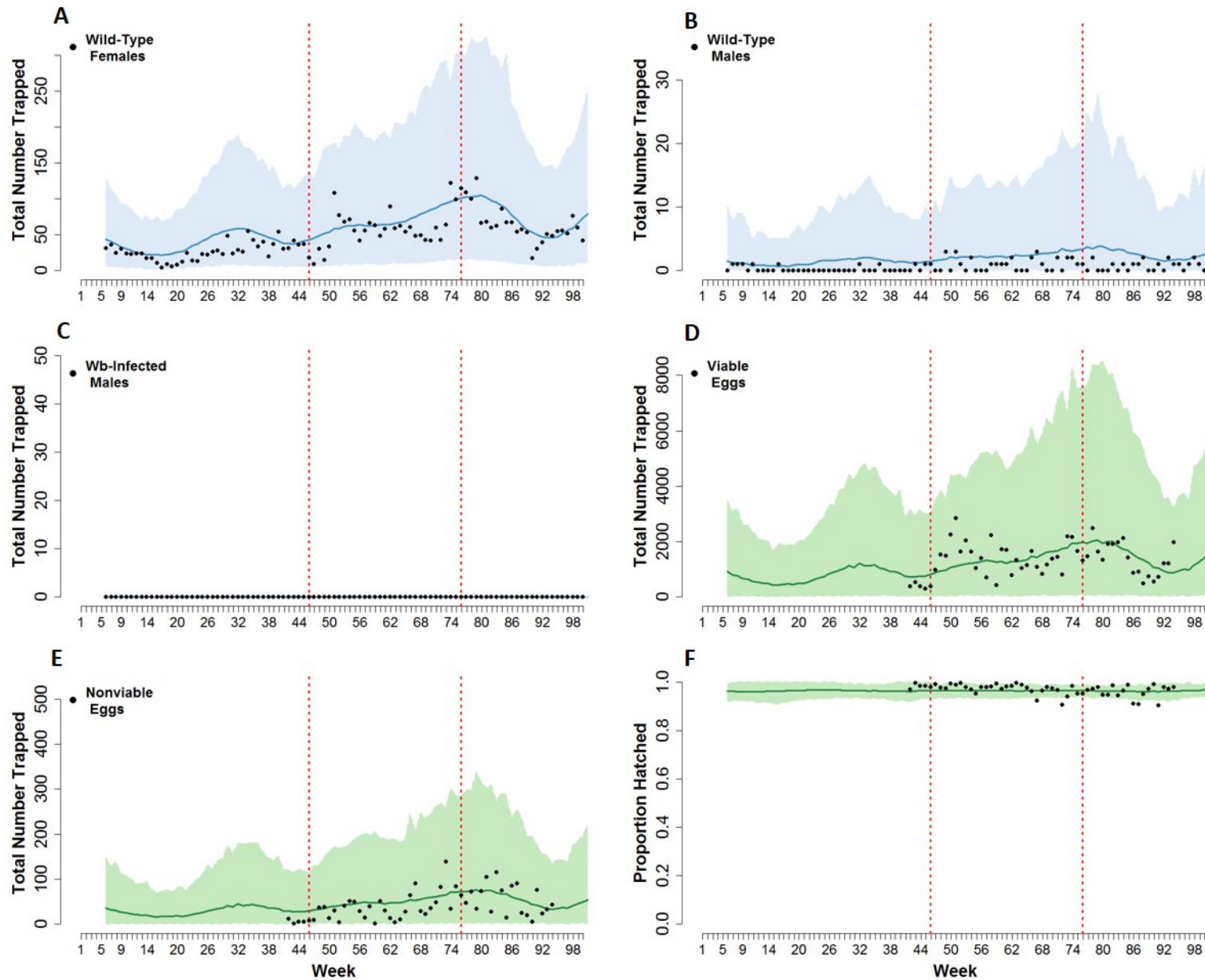


Figure 6.17: Tampines-Control Site ($R_M = 12$, τ local) Fits of the model to the trapping data collected at the Tampines control site. Observed data are shown in black, and the solid line and shaded area show the posterior mean and 95% posterior predictive interval respectively. The dashed red lines show the period when *Wolbachia*-infected males were released. Figure F shows the estimated egg hatch rate.

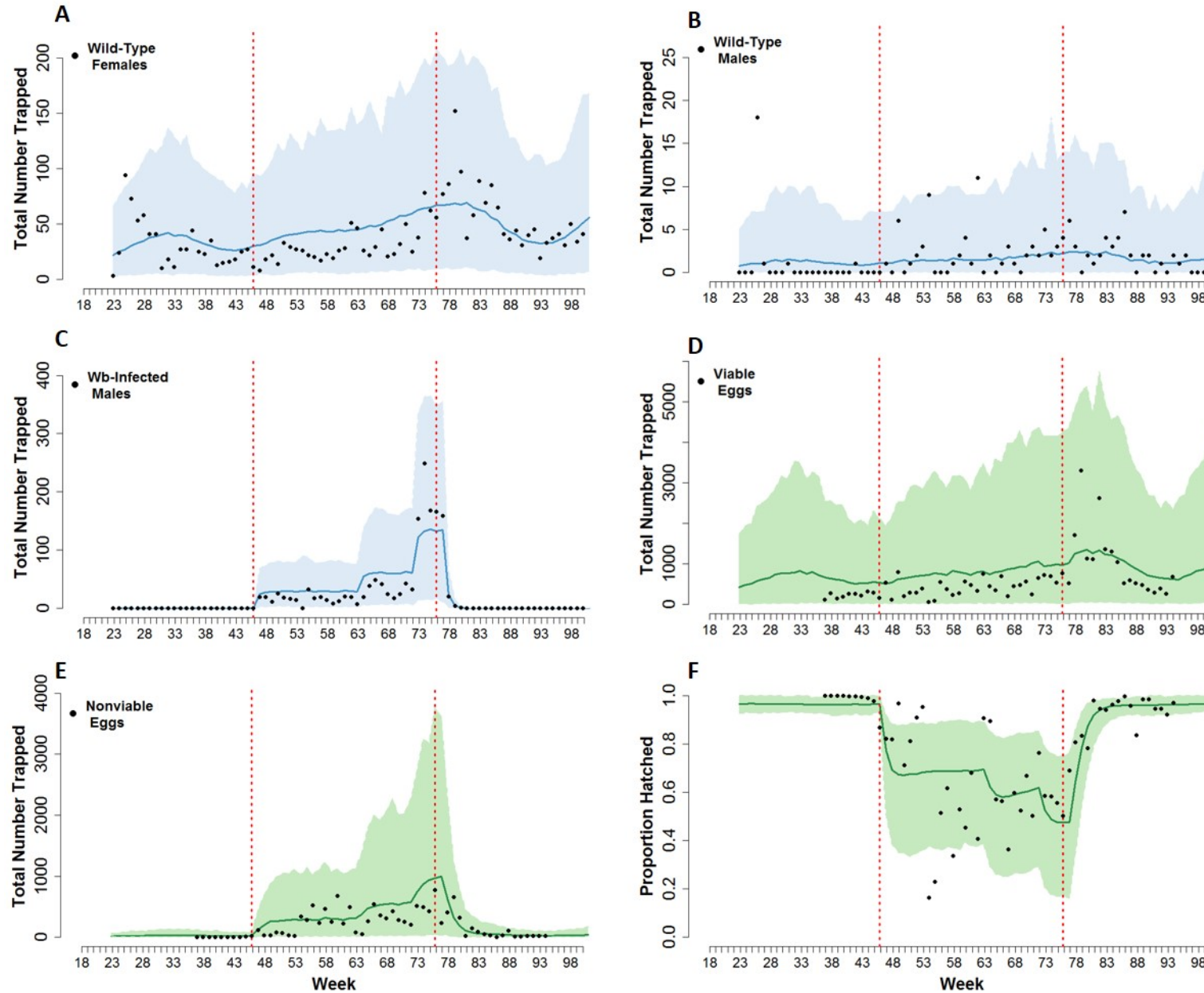


Figure 6.18: Tampines-Release Site ($R_M = 12$, τ local) Fits of the model to the trapping data collected at the Tampines release site. Observed data are shown in black, and the solid line and shaded area show the posterior median and 95% posterior predictive interval respectively. The dashed red lines show the period when *Wolbachia*-infected males were released. Figure F shows the estimated egg hatch rate.

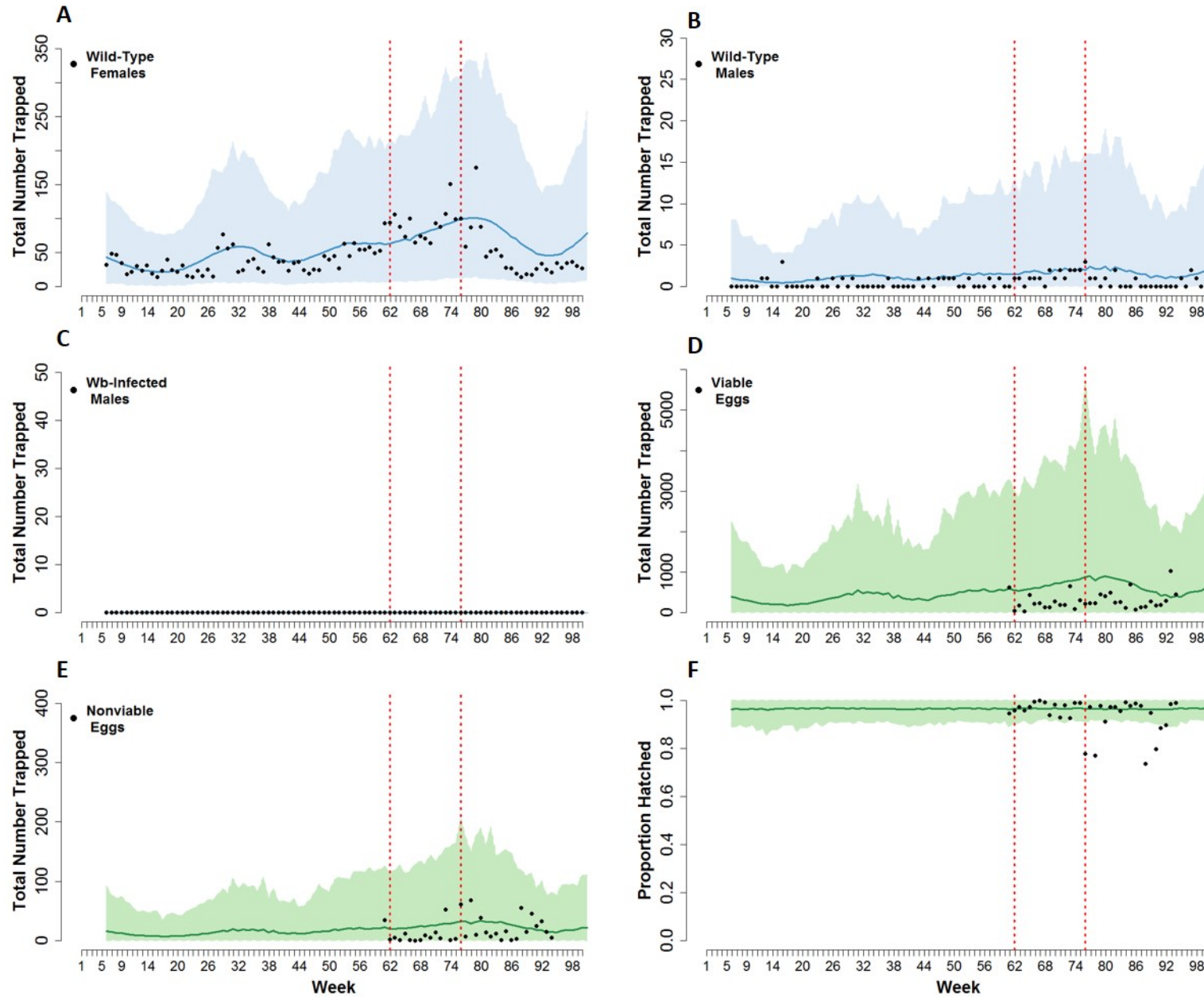


Figure 6.19: Yishun-Control Site ($R_M = 12$, τ local) Fits of the model to the trapping data collected at the Yishun control site. Observed data are shown in black, and the solid line and shaded area show the posterior median and 95% posterior predictive interval respectively. The dashed red lines show the period when *Wolbachia*-infected males were released. Figure F shows the estimated egg hatch rate.

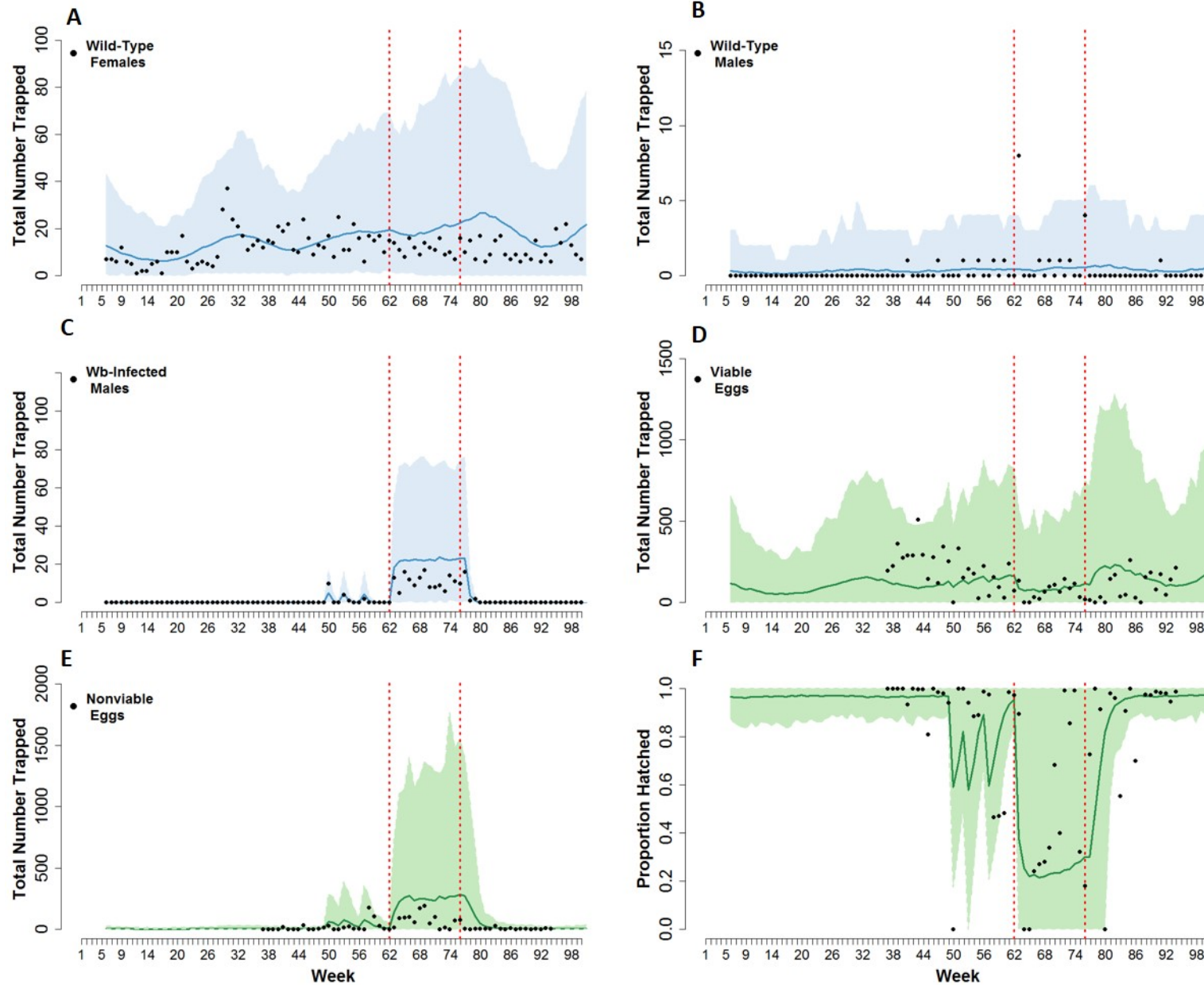


Figure 6.20: Yishun-Release Site ($R_M = 12$, τ local) Fits of the model to the trapping data collected at the Yishun release site. Observed data are shown in black, and the solid line and shaded area show the posterior median and 95% posterior predictive interval respectively. The dashed red lines show the period when *Wolbachia*-infected males were released. Figure F shows the estimated egg hatch rate.

6.2.4 Simulating Counterfactual Release Scenarios

To gain further insight into the likely impact of the *Wolbachia* releases on the wild-type *Aedes aegypti* population at the release sites, we simulated the dynamics of the full wild-type adult female *Aedes aegypti* population at both the Tampines and Yishun release sites using posterior estimates of parameter values, for a range of different scenarios. We first simulated the dynamics for the scenario where no *Wolbachia*-infected males were released. Then, to assess the likely impact of different release strategies, we simulated the dynamics for the scenarios where (i) releases occurred over a longer period, (ii) larger numbers of *Wolbachia*-infected males were released and (iii) *Wolbachia*-infected males released showed greater mating competitiveness.

For each scenario, we simulated the dynamics for different fixed values of R_M ($R_M = 1.5, 5, 12$) using posterior median estimates of parameter values obtained when the calibrating the model against the data, allowing mating competitiveness of *Wolbachia*-infected males to vary between sites.

Generally, we observed that the estimated impact of the *Wolbachia* releases on wild-type adult female population size under each scenario was dependent on the value of R_M and the mating competitiveness of *Wolbachia*-infected males, with greater impact observed for lower values of R_M and higher values of mating competitiveness.

For Tampines, we estimated that, owing to very low levels of mating competitiveness, the *Wolbachia* releases which took place had a small impact on total wild-type adult female population size for $R_M = 1.5$ and very little impact for $R_M = 5$ and $R_M = 12$ (Figure 6.21). As we obtained larger posterior estimates of mating competitiveness for Yishun for $R_M = 5$ and $R_M = 12$, we estimated the *Wolbachia* releases had a larger impact on wild-type adult female population size at Yishun compared with Tampines. However, overall, the estimated impact on wild-type adult female population size remained low (Figure 6.21).

Owing to higher posterior estimates of mating competitiveness, we found that increasing the number of *Wolbachia*-infected males released had the largest impact for Yishun (Figure 6.22). We estimated that, for all values of R_M , scaling the number of *Wolbachia*-infected males released three-fold or more may have led to suppression of the wild-type adult female population in

Yishun. However, for Tampines, scaling the releases sizes by the same factor only had a large effect when $R_M = 1.5$, owing to the much lower level of mating competitiveness (Figure 6.21). For $R_M = 12$, we estimated that increasing the number of *Wolbachia*-infected males released only had a marginal effect on the wild-type adult female population in Tampines. A larger effect was estimated for $R_M = 5$ compared with $R_M = 12$, however the size of the estimated impact remained small (Figure 6.21).

The impact of increasing the length of the release period also differed between release sites according to differences in estimates of mating competitiveness. For Tampines, we estimated that extending the release period by 20 weeks was likely only to have a considerable impact on wild-type adult female population size when $R_M = 1.5$ (Figure 6.21). However, for Yishun, we estimated this would have a large impact on population size for both $R_M = 1.5$ and $R_M = 5$, and a small impact for $R_M = 12$ (Figure 6.22).

For both Tampines and Yishun we estimated that, had the *Wolbachia*-infected males released shown greater mating competitiveness, the number of *Wolbachia*-infected males released and the length of the release periods were likely to have been sufficient to suppress the wild-type adult female population at both sites (Figure 6.23). The estimated level of mating competitiveness required to achieve this was dependent on the value of R_M , with a higher level of mating competitiveness needed for larger values of R_M .

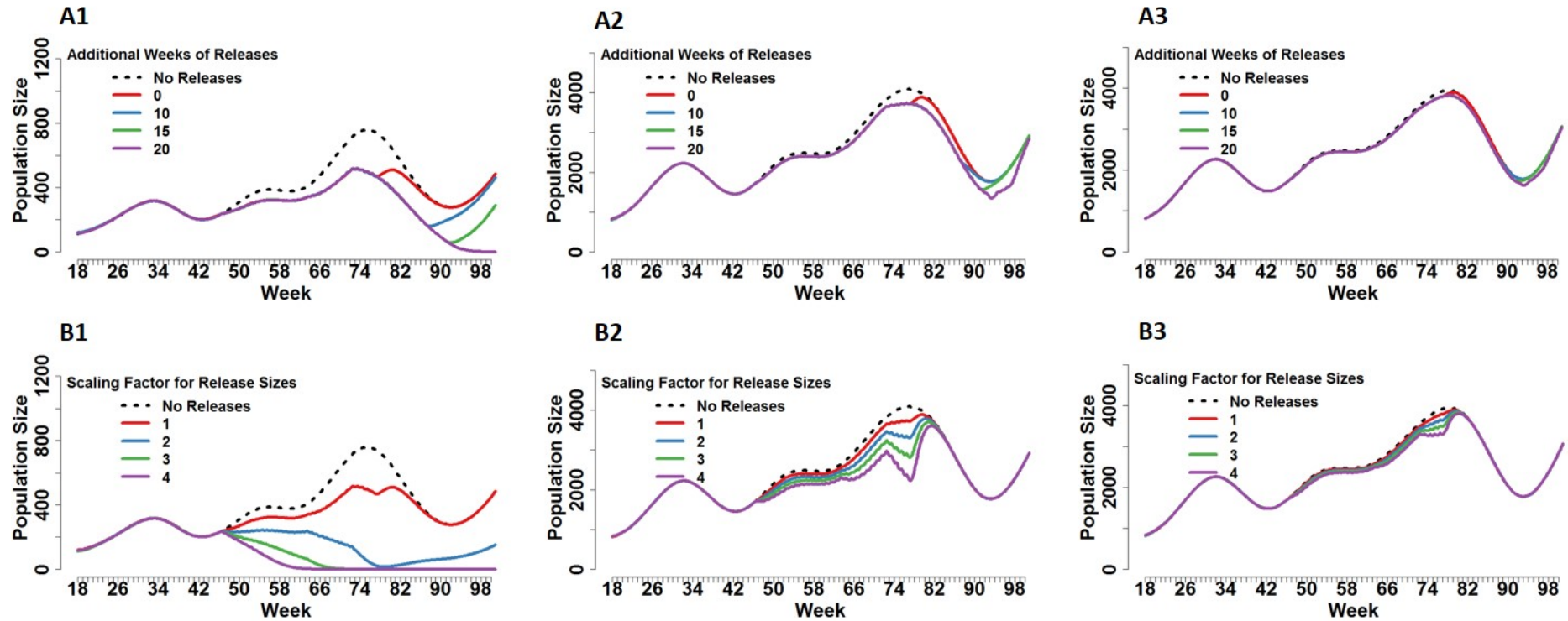


Figure 6.21: Simulating Counterfactual Release Scenarios - Tampines Simulated mean wild-type adult female population size for the Tampines release site under different release scenarios, for different values of R_M . Columns 1, 2, and 3 show the results corresponding to $R_M = 1.5$, $R_M = 5$, and $R_M = 12$ respectively. In each figure, the dashed black line shows the simulated mean population size if no releases had occurred and the red line shows the simulated mean population size given the *Wolbachia* releases actually performed. Thus, the difference between these two lines shows the estimated actual impact on wild-type adult female population size for each value of R_M . Figures (A1-A3) show the results of extending the release period (keeping the size of releases fixed at the number released in the final week of the actual release period (46,061)). Figures (B1-B3) show the results of scaling the release sizes across the whole release period by a constant factor (here the simulated release period is the same as the actual release period). For each scenario, the mean is calculated across 1000 realisations of the stochastic model (using posterior median estimates of parameter values).

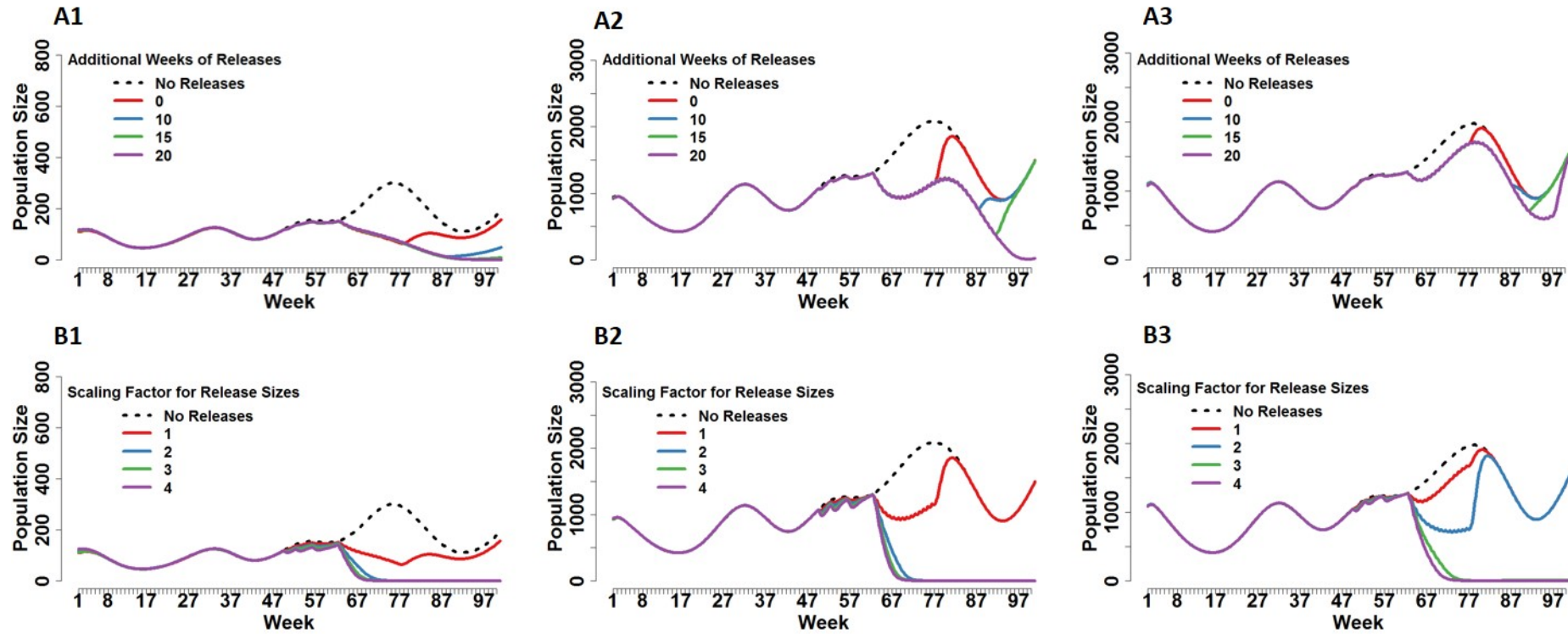


Figure 6.22: Simulating Counterfactual Release Scenarios - Yishun Simulated mean wild-type adult female population size for the Yishun release site under different release scenarios, for different values of R_M . Columns 1,2, and 3 show the results corresponding to $R_M = 1.5$, $R_M = 5$, and $R_M = 12$ respectively. In each figure, the dashed black line shows the simulated mean population size if no releases had occurred and the red line shows the simulated mean population size given the *Wolbachia* releases actually performed. Thus, the difference between these two lines shows the estimated actual impact on wild-type adult female population size for each value of R_M . Figures (A1-A3) show the results of extending the release period (keeping the size of releases fixed at the number released in the final week of the actual release period (10,500)). Figures (B1-B3) show the results of scaling the release sizes across the whole release period by a constant factor (here the simulated release period is the same as the actual release period). For each scenario, the mean is calculated across 1000 realisations of the stochastic model (using posterior median estimates of parameter values).

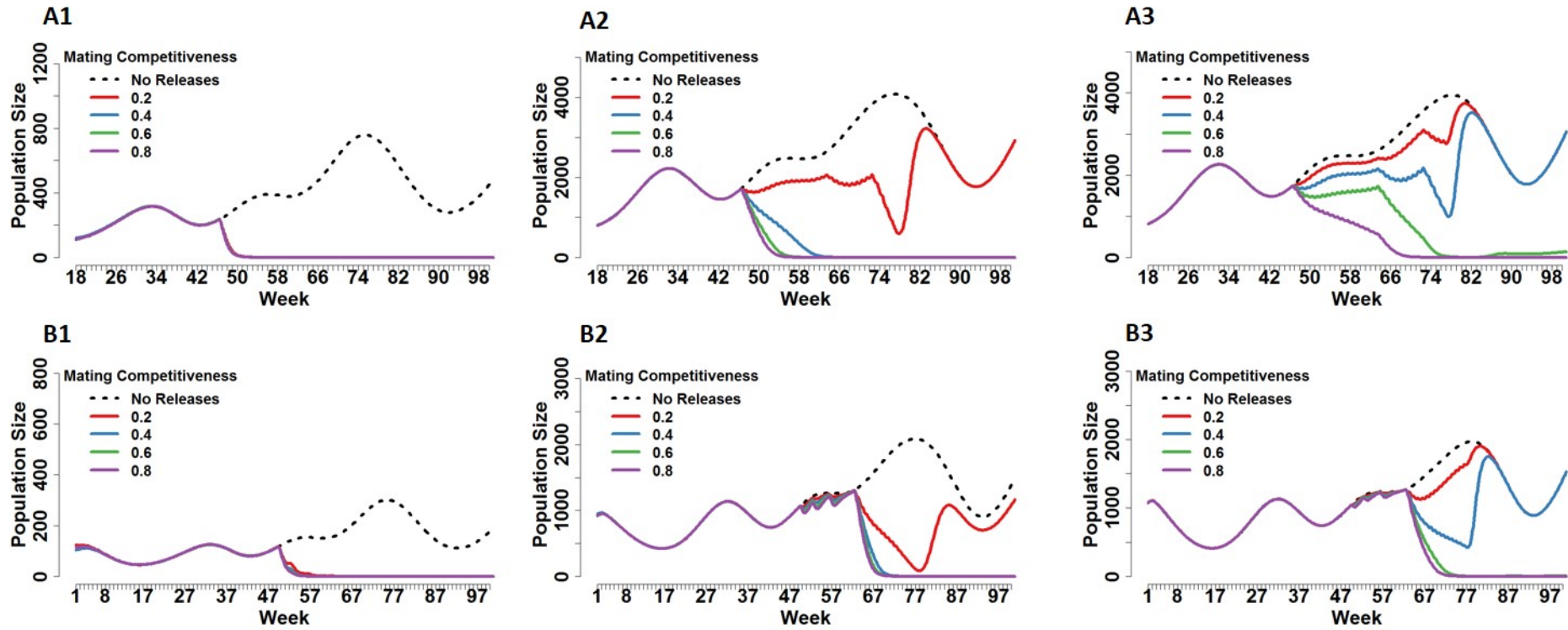


Figure 6.23: Simulating Counterfactual Release Scenarios - Mating Competitiveness Simulated wild-type adult female population size for the Tampines (top row) and Yishun (bottom row) release sites for different values of R_M , given different levels of mating competitiveness of *Wolbachia*-infected males. Columns 1,2, and 3 show the results corresponding to $R_M = 1.5$, $R_M = 5$, and $R_M = 12$ respectively. In each figure, the dashed black line shows the simulated population size if no releases had occurred. For all other scenarios, no changes to the size of releases or length of the release period were made. For each scenario, the mean is calculated across 1000 realisations of the stochastic model (using posterior median estimates of parameter values for all parameters other than τ).

6.3 Discussion

Through a series of small-scale field studies, Project *Wolbachia* Singapore aims to establish if *Wolbachia* can be used as a tool for *Aedes aegypti* population suppression in the urban environment of Singapore. Here we analysed the results of the first study testing this approach in Singapore by calibrating a stochastic model of IIT against the detailed entomological trapping data collected across all study sites. Using advanced model fitting techniques, we estimated the overall *Aedes aegypti* population size and the level of variability in the trapping process, with the goal of gaining a deeper understanding of the impact of the release of *Wolbachia*-infected male *Aedes aegypti* on local wild-type *Aedes aegypti* population dynamics.

Our estimates of total mosquito population size and the proportion of the population captured during the trapping process were dependent on the value of the basic mosquito reproduction number, R_M . When estimating R_M during the model fitting process, we observed that the log-likelihood was highest for very low values of R_M (just above 1) resulting in a very low estimate of total wild-type female population size (maximum population size < 1000 approximately) and relatively large estimates of the mean proportion of wild-type females captured during the trapping process (10%-15% per week). However, we question whether these estimated values are in fact biologically plausible for a number of reasons.

First, the Tampines and Yishun control sites were comprised of 21 and 29 residential blocks respectively. Residential blocks in these areas typically contain 100 households, giving a total of 2,000-3,000 households at each control site approximately. An estimated total wild-type female population size of 1000 mosquitoes say would therefore imply an estimate of 0.33-0.5 wild-type female *Aedes aegypti* per household. Based on data collected through household inspections and other vector surveillance systems, NEA Singapore currently estimate an average *Aedes aegypti* population size of 1 adult female mosquito per house. Thus, even our largest estimates of wild-type adult female population size R_M fall considerable below this value. Second, when modelling the trapping process, we do not consider trapped mosquitoes as being removed from the population. Therefore, trapping a high proportion of wild-type females does not reduce overall wild-type adult female population size. However, in reality, if the wild-type adult female population size is very low, then trapping and therefore removing 10%-15% of the population each week on average over a many months would likely have a substantial impact on overall population

size. While removal trapping has led to successes in the control of some vector species (e.g. the tsetse fly [252]), results of field studies examining the use of mass trapping for *Aedes aegypti* population control have largely been inconsistent [253–256]. For example, field studies testing the use of lethal ovitraps for *Aedes aegypti* control conducted in Brazil [256] and Australia [254] both reported a significant reduction in adult female mosquito abundance in areas where this intervention was employed. However, the results of both of these studies were inconsistent, as some areas showed no decline in abundance following application of this intervention [254, 256].

Our results suggest that, in the absence of greater power to estimate the basic mosquito reproduction number R_M , the model favours a low overall total population size and a high level of over-dispersion in the trapping process, as this allows us to obtain a very precise fit of the model to trapping data with narrow posterior predictive intervals.

For larger fixed values of R_M , similar estimates of both adult mosquito population size and the variability in the trapping process were obtained. We estimated a mean wild-type adult female population size of approximately 2,000-5,000 mosquitoes for the Tampines and Yishun control sites, with approximately 1% of wild-type females and 0.5% of eggs trapped per week on average. As the true underlying mosquito population size is unknown, it is difficult to assess the accuracy of our estimates of population size. However, our estimates of wild-type adult female population size for larger values of R_M are broadly consistent with those obtained by NEA Singapore.

The estimated impact of the *Wolbachia* releases on the wild-type adult female population at both release sites was also dependent on the value of R_M . For larger values of R_M , our results suggest that the *Wolbachia* releases performed had only a marginal, temporary impact on the wild-type adult female *Aedes aegypti* population in both Tampines and Yishun. Our results indicate that there was a small decline in the wild-type adult female population at the Yishun release site during the release period, but that the impact on the wild-type adult female population at the Tampines release site was negligible. A slightly larger impact was estimated for very low values of R_M . However, we nonetheless conclude that the release of *Wolbachia*-infected males did not result in suppression of the wild-type adult female *Aedes aegypti* population at either release site.

Our results suggest that the primary reason why greater suppression of the wild-type adult female population was not achieved was poor mating competitiveness of the *Wolbachia*-infected *Aedes aegypti* males released. The value of mating competitiveness estimated by the model indicates how well the *Wolbachia*-infected males integrated into local wild-type *Aedes aegypti* populations. Thus, consistently low estimates of mating competitiveness, suggest that the *Wolbachia*-infected males released did not integrate well among the local wild-type populations.

It is difficult to know exactly why better integration was not achieved as several factors may have contributed to this. Singapore is highly urbanised environment, and residential blocks in both Tampines and Yishun typically contain 11 or 12 floors. However, in both areas, all *Wolbachia*-infected males were released at the ground floor level. Thus successful integration of the *Wolbachia*-infected males into the wild-type population in upper floors was dependent upon the vertical dispersal behaviour of the released males. Although *Aedes aegypti* are known to possess a typically short horizontal dispersal range [53, 75, 77], little is known about the vertical dispersal range of the species. The trapping data for both release sites shows that the majority of *Wolbachia*-infected males trapped were captured on lower floors. However, a very small proportion of the *Wolbachia*-males released were subsequently trapped, and one could argue that the majority of wild-type males and females were also trapped on lower floors. Furthermore, the traps used to capture adult mosquitoes were designed to primarily attract adult females. Therefore it is difficult to fully understand to what extent environmental challenges played a role in hindering better integration.

Another possible reason is that the majority of *Wolbachia*-infected males died quickly following release and, crucially, before having the opportunity to mate with wild-type females. Longevity of *Wolbachia*-infected male *Aedes aegypti* in the field has been investigated by NEA Singapore, and they estimated a daily probability of survival of 78% for *Wolbachia*-infected males (personal communication with NEA). These survival estimates therefore suggest that a high level of mortality of *Wolbachia*-infected males is unlikely to have been the primary cause of poor integration.

Adult mosquito dispersal may also have played a role, in a number of different ways. Upon release, *Wolbachia*-infected males may have dispersed beyond the release site into neighbouring

areas. On the other hand, the impact of the *Wolbachia* releases on wild-type adult female population size may have been lessened by the migration of previously mated wild-type females from neighbouring areas. However, trapping data was not collected from areas neighbouring the study sites, and thus we do not know how large a role dispersal between the release sites and neighbouring areas played in determining the level of suppression achieved. Our results also suggest that releases in both Tampines and Yishun occurred during a period when the wild-type *Aedes aegypti* population was increasing. Thus increases in wild-type population size may have counteracted decreases owing to the release of *Wolbachia*-infected males, thereby lessening the impact of the *Wolbachia* releases.

The frequency of releases may also have been a contributing factor. We estimated a higher level of mating competitiveness in Yishun where *Wolbachia*-infected males were largely released bi-weekly, compared with Tampines where releases were performed weekly. This may have allowed for better integration of *Wolbachia*-infected males into the local wild-type population. Some theoretical modelling studies of population suppression measures have suggested that smaller, more frequent releases may be more effective than less frequent, larger releases [174, 193]. However, this has not yet been demonstrated in the field, and thus caution is required when drawing inferences between the increased mating competitiveness estimated for Yishun and the increased frequency of releases. Furthermore, it is important to consider that releases at Yishun were performed across a smaller number of residential blocks compared with Tampines, as this may also have affected the level of integration among wild-type *Aedes aegypti* populations.

Several other field studies have been undertaken to explore the potential impact of mosquito population suppression technologies. However, given differences between the species targeted, the environments where trials have been conducted, and the release strategies employed, it is difficult to directly compare the results obtained here with those of other studies. Furthermore, the work presented here is the first to model the trapping process when estimating the impact of a vector population suppression strategy.

Successful suppression of *Culex pipiens* populations was achieved during the first field study of IIT in Myanmar in the 1967, however this study was conducted in a small rural area [109]. Small scale field studies targeting *Aedes albopictus* populations conducted in suburban areas

of northern Italy (using SIT) [121] and Kentucky (using IIT) [113], reported a reduction in hatch rate of 18%-68% [121] and approximately 40% [113] respectively. A recent field study of IIT in French Polynesia, targeting *Aedes polynesiensis* populations, reported an estimated mating competitiveness of 68% for *Wolbachia*-infected males. However, in this study, the *Wolbachia* releases were performed on three small isolated islands with no human inhabitants [111], thus constituting a very different field setting to the highly urbanised, densely populated environment of Singapore. Low mating competitiveness has been estimated for transgenic *Aedes aegypti* males released during field trials conducted in the Cayman Islands (6%) [123] and Brazil (3%) [124] to assess the potential impact of the RIDL technology. Nonetheless, these trials reported suppression of the wild-type population by 82% [123] and 78% [124] respectively based on changes in the proportion of ovitraps containing eggs.

Given the high level of urbanisation and existing high levels of vector control, Singapore is a unique environment, and thus extrapolation of the results presented here to other settings may not be valid. However, some more general insights applicable to assessing the impact of novel vector control measures can be drawn from the work presented here. First, our results illustrate the importance of accounting for underlying variability in the trapping process when estimating the likely impact of a particular control measure as, given mosquito trapping data is often highly over-dispersed, estimates of impact based on trapping data alone may not be fully indicative of the estimated impact at the population level. Understanding the size of the existing wild-type population (and in particular the mosquito reproduction number), in addition to the level of variability in the trapping process, is likely to be of critical importance to gaining a deeper understanding of the likely impact of these measures and to disentangling stochastic noise from real impacts on the population. This is likely to be particularly important in settings where intermediate levels of vector control are achieved as, in the absence of a clear, large proportional decline in mosquito abundance, measuring the impact on the intervention on the size of the vector population may be very challenging given the highly stochastic nature of mosquito trapping data, and natural, climate-driven temporal fluctuations in mosquito abundance. In addition, our results highlight that successful integration of modified populations into local wild-type populations is fundamental for the success of these measures, in particular as increasing the size of releases or length of the release period is unlikely to compensate for poor mating competitiveness. However, achieving high levels of mating competitiveness of modified mosquitoes is also likely to be one of

the main challenges in successfully implementing these measures.

The work presented here also has several limitations. When calibrating the model against the trapping data, we aggregated the data to the release site level. A fully spatially explicit stochastic model which accounts for adult mosquito dispersal and the dynamics of local populations at the individual residential block level would offer greater insight into the impact of the *Wolbachia*-releases on local wild-type populations. It would also allow us to better statistically characterise spatial heterogeneity in *Aedes aegypti* populations, and to assess how very fine-scale spatial heterogeneity in *Aedes aegypti* populations may have affected the level of suppression achieved. In addition, we modelled the population at each site as a closed population. In reality, dispersal of adult mosquitoes to and from surrounding areas may have affected the level of population suppression observed. As mentioned earlier, we also did not consider trapping as a removal process and this may have hindered our ability to estimate the basic reproduction number. We also assumed density-dependence during the larval stage of population growth was linear (i.e. $\Omega = 1$). However, the strength of density-dependence among larval populations is unknown, and assuming different values of Ω may have led to different estimates of parameter values when calibrating the model against the trapping data. When trying to estimate R_M , we found that the model favours a low overall total population size and a high level of over-dispersion in the trapping process. Therefore, we hypothesise that, changing the strength of density-dependence (while keeping R_M fixed) may, for example, allow the model to behave in a similar way. Consequently, this may result in lower estimates of wild-type population size and higher estimates of the trapping proportions. However, a full understanding of the effect of varying Ω requires further investigation. We also assumed that development and mortality rates are not temperature dependent, and that each site had the same seasonal profile in carrying capacity. Individual sites however may experience different levels of seasonal fluctuation in carrying capacity, and development and mortality rates of *Aedes aegypti* may vary with changes in temperature [64, 231, 232].

In conclusion, using advanced Bayesian inference techniques, we have calibrated a stochastic model of *Aedes aegypti* population dynamics against the entomological data collected during the Phase 1 field study, while allowing for variability in the trapping data. This has allowed us to estimate both the size of the wild-type *Aedes aegypti* population and the level of variability in the

trapping process, thereby providing us with a deeper understanding of the impact of the release of *Wolbachia*-infected male *Aedes aegypti* on local *Aedes aegypti* populations.

6.4 Acknowledgements

We would like to thank NEA Singapore, and in particular Prof. Lee Ching Ng and her team, for generously sharing their data from the Phase 1 study with us and for many insightful discussions.

Chapter 7

Discussion

Recent years have seen much progress in the development of novel vector control measures for *Aedes aegypti* populations. As more and more field studies testing these technologies across a wide range of different environments are undertaken, one of the major challenges going forward, from a mathematical modelling perspective, is how to rigorously estimate the likely impact of these interventions on local *Aedes aegypti* populations. While mathematical models of novel vector control measures developed to date provide valuable theoretical insights into some of the likely challenges associated with successfully implementing these measures, improved models of fine-scale *Aedes aegypti* population dynamics are needed to realistically model the likely impact of these measures on real *Aedes aegypti* populations. Spatially explicit stochastic models of fine-scale *Aedes aegypti* population dynamics which have been rigorously fitted to, and validated against, high quality entomological data are the ultimate goal. However, development of these models is challenging, not least because it requires careful consideration of what is an appropriate level of spatial granularity for models to adopt when representing fine-scale *Aedes aegypti* population dynamics, and an inferential framework which allows for the highly variable nature of mosquito trapping data. In this thesis, we began to address this challenge by examining the role of spatial structure in shaping the dynamics of *Aedes aegypti* populations at fine spatial scales, and by using advanced Bayesian inference techniques to calibrate a stochastic model of *Aedes aegypti* population dynamics against detailed entomological data.

7.1 Summary of Key Findings

In Chapters 2-4 of this thesis we developed a stochastic metapopulation model of fine-scale *Aedes aegypti* population dynamics, and explored how the dispersal behaviour of the mosquito,

features of the underlying landscape, and the level of spatial granularity in our model affected the dynamics observed. We considered the dynamics for landscapes where an established mosquito population exists and for landscapes where mosquitoes are seeded into an otherwise unoccupied landscape. We found that, for low mosquito population densities, larval habitat fragmentation can have a large impact on the dynamics observed, leading to reductions in population size and the level of habitat occupancy across a landscape. Furthermore, both the dispersal behaviour of adult mosquitoes and features of the underlying landscape played key roles in driving the dynamics observed at fine spatial scales.

Importantly, we found that using non-spatial models to represent the fine-scale dynamics of *Aedes aegypti* populations may substantially underestimate the stochastic volatility of these populations and the frequency at which local populations go extinct. Through examining the dynamics observed at different levels of spatial granularity, we concluded that, to capture the fine-scale dynamics of *Aedes aegypti* populations in a meaningful way, the individual household level may be an appropriate level of spatial granularity for models to adopt when modelling the dynamics of *Aedes aegypti* populations at fine spatial scales. Adopting a lower level of granularity may fail to capture the adverse effects of larval habitat fragmentation on *Aedes aegypti* populations, and consequently underestimate the vulnerability of local populations to extinction when populations are small.

In Chapter 5, we extended the model developed in Chapters 2-4 to a model of IIT and, using particle MCMC methods, developed a framework to enable us to calibrate a stochastic model of *Aedes aegypti* population dynamics against detailed entomological data, while allowing for the highly variable nature of mosquito trapping data. In Chapter 6 we then used this approach to examine the results of a small-scale field study testing *Wolbachia* as a tool for *Aedes aegypti* population suppression conducted in Singapore, by calibrating our model of IIT against the entomological data collected during the study. Modelling the trapping process, in addition to the underlying mosquito population dynamics, allowed us to account for variability in the trapping data when estimating parameter values and the likely impact of the *Wolbachia* releases on local *Aedes aegypti* populations. While our estimates of the size of the impact were dependent on the value of the basic mosquito reproduction number, we concluded that, overall, the *Wolbachia* releases had little impact on the size of the wild-type *Aedes aegypti* female population, and that suppression

of local *Aedes aegypti* populations at the release sites was not achieved. Our results indicated that this was primarily owing to poor integration of the *Wolbachia*-infected *Aedes aegypti* males released among local wild-type *Aedes aegypti* populations.

7.2 Implications of Research

The research presented here has several important implications for modelling the fine-scale dynamics of *Aedes aegypti* populations and the likely impact of novel vector control measures.

As *Aedes aegypti* primarily breed in domestic urban habitats and typically have a short dispersal length [75–77], local populations of *Aedes aegypti* across any given landscape are often both highly fragmented and highly spatially heterogeneous [47, 59, 61, 220, 221, 225, 226]. However, while several very detailed models of fine-scale *Aedes aegypti* population dynamics have been developed [165, 168, 171], the impact of breeding site fragmentation on *Aedes aegypti* population dynamics at fine spatial scales is poorly understood. By exploring the dynamics of *Aedes aegypti* populations at different levels of spatial granularity, the analysis presented in Chapters 2-4 of this thesis contributes to our understanding of the importance of spatial structure and fine-scale spatial heterogeneity in mosquito population density in shaping the dynamics of *Aedes aegypti* populations at fine spatial scales. Furthermore, the model developed is flexible and could be used to explore the dynamics of different mosquito species, across a variety of settings.

While life cycles, types of habitat and dispersal behaviour varies between different species, the results presented in Chapters 2-4 are broadly consistent with those of other modelling and empirical studies exploring the effects of habitat fragmentation on species persistence and distribution across a landscape [143, 146–152, 154, 208]. In line with these studies, our results highlight the vulnerability of small local populations to extinction, and illustrate how local population persistence is not only a function of individual patch size, but also of the level of connectivity between local populations and the composition of the fragmented landscape [143, 146–154, 156, 208].

Moreover, our results indicate that for species, like *Aedes aegypti*, with a typically small dispersal range and/or a low propensity to disperse [75–77], the adverse effects of habitat fragmentation on species persistence and distribution across a landscape are likely to be more pronounced

(e.g. Figures 2.4, 2.7) as dispersal provides a mechanism through which metapopulations can persist in a balance between extinction and colonization. While the model presented in Chapters 2-4 was not calibrated against entomological data, the importance of limitations in dispersal to local and metapopulation persistence has been demonstrated elsewhere for a variety of different species [146, 148, 149, 152, 154–157, 257]. For example, empirical studies of metapopulations of the butterfly species *Plebejus argus* in northern Wales have shown that, within its typical dispersal range (< 1km), small local populations experience a high rate of population turnover as unoccupied, suitable habitat is typically quickly recolonized by the species [149, 257]. However, colonization of unoccupied, potential habitat at greater distances is hindered by limitations in its dispersal range, thereby limiting distribution of the species across the landscape [149, 257]. In addition, infrequent dispersal has been suggested as a possible contributing factor to the decline of an American pika metapopulation in Bodie, California [154, 155]. As discussed in Chapter 1, the northern half of this metapopulation has remained stable for several decades, while the population in the southern half declined and failed to recover during the study period, despite potentially suitable habitat being available [154, 155]. Smith *et. al* suggest that the low rate of recolonization of suitable habitat in the southern half of the metapopulation is potentially owing to the low propensity of this species to disperse [155].

Our results also showed that fine-scale *Aedes aegypti* dynamics were heavily influenced by spatial heterogeneity in carrying capacity across a landscape (which can be thought of as spatial variation in habitat quality), with local persistence more difficult to achieve in areas of low quality. Habitat quality has been shown to be an important factor in metapopulation persistence, particularly in the context of butterfly metapopulations [209, 210, 258]. Perhaps one of the most interesting examples of the interaction between habitat quality and metapopulation persistence is the expansion and re-establishment of metapopulations of the *Hesperia comma* butterfly species in Britain. Following a long period of population decline, metapopulations of the species have recovered, owing to improved habitat quality and availability [210]. Another example is metapopulations of the Glanville fritillary butterfly in Finland [209]. Recent modelling of the long-term dynamics of these metapopulations has suggested that both habitat quality and the spatial configuration of habitats of different quality are key drivers of local population persistence for this species, and species distribution across the landscape [209].

Our results also indicate that spatial correlation in habitat quality is most likely to have the largest impact on population persistence and patch occupancy when the typical dispersal length of a species is small. While other theoretical modelling studies have largely focused on exploring the effects of spatial correlation in habitat loss on species persistence rather than the effects of spatial correlation in habitat quality on metapopulation dynamics more generally [259, 260], these studies have also concluded that the effects of spatial correlation in habitat quality will depend on the dispersal range of the species, with species having a small dispersal range likely to most affected [259, 260].

The analysis presented in Chapters 2-4 differs from existing metapopulation models of *Aedes aegypti* population dynamics, and those of other species, as we explicitly model and compare the dynamics of the same metapopulation at different levels of spatial granularity. This allows us to gain a deeper understanding of the importance of model choice in how to represent and account for metapopulation structure. This analysis is of particular importance for the development of spatially explicit models of novel vector control measures, as we have identified the individual household is likely to be an appropriate level of spatial granularity for models to adopt to capture the fine-scale dynamics of *Aedes aegypti* populations. In addition, beyond exploring the impact of novel vector control measures, our work may also have important implications for mathematical models of dengue transmission, which consider larval population dynamics. Typically these models use a non-spatial approach to model the dynamics of larval populations [204–206]. However, our results suggest that using a non-spatial approach may underestimate the volatility of *Aedes aegypti* populations when population densities are low. This in turn may have important implications for estimates of transmission intensity and disease dynamics.

The work presented in Chapter 6 is the first to estimate the likely impact of a vector population suppression strategy on *Aedes aegypti* populations by calibrating a stochastic model of *Aedes aegypti* population dynamics against the detailed entomological data collected during a field study. Thus, it represents an important step forward in the development of methods to rigorously estimate the likely impact of novel vector control measures. Our work shows that the highly variable nature of mosquito trapping data can be accounted for when estimating the likely impact of these measures, and moreover that, by doing so, additional insights into key factors such as size of existing wild-type *Aedes aegypti* populations and the mating competitiveness of modified

mosquito populations can be gained. In addition, while local *Aedes aegypti* population dynamics will vary across different settings, the model fitting approach developed here is flexible and can be applied to estimate the likely impact of different vector control measures across a range of different settings. Furthermore, the model developed here could easily be extended to include *Wolbachia*-infected females, and hence be used to explore the impact of population replacement strategies.

While we found it difficult to obtain a biologically plausible estimate of the basic mosquito reproduction number R_M for *Aedes aegypti* populations in Singapore, our results nonetheless highlight the critical importance of R_M in estimating the likely impact of vector suppression technologies. In settings where R_M is high, larger reductions in the egg hatching rate will be required to suppress vector populations compared with settings where R_M is low. Thus similar levels of reduction in the egg hatch rate may not translate to similar levels of vector population suppression in different settings. Consequently, understanding what level of reduction in the egg hatching rate is required to have a substantial impact on vector population size, requires an understanding of R_M .

7.3 Limitations and Future Work

The work presented in this thesis has several key limitations. The analysis presented in Chapters 2-4 is based on simulations from a theoretical model of fine-scale *Aedes aegypti* population dynamics which has not been calibrated against entomological data. Thus, while we believe this work provides important insights into role of spatial structure in shaping the dynamics of *Aedes aegypti* populations at fine spatial scales, it is important to recognise that the dynamics of real-world fragmented *Aedes aegypti* populations and of density-dependent competition are likely to be highly complex. Thus, theoretical modelling studies are likely to be unable to fully capture these dynamics. Calibrating the model against fine-scale entomological data may offer additional insights into the effects of larval habitat fragmentation and metapopulation structure on fine-scale *Aedes aegypti* population dynamics. In addition, our model does not consider some important aspects of *Aedes aegypti* ecology, such as aestivation and overwintering mechanisms [54].

The extent to which the results presented in Chapters 2-4 may affect models of dengue transmission, which use a non-spatial approach to represent the dynamics of larval *Aedes*

aegypti populations, is also unknown. A model which incorporates both vector and disease dynamics, ideally calibrated against fine-scale entomological and epidemiological data, is required to understand the potential impact on larval habitat fragmentation on the fine-scale transmission dynamics of dengue.

When calibrating our model of IIT against the entomological data collected during the small-scale field study of IIT undertaken in Singapore, we were unable to obtain a robust estimate of the basic mosquito reproduction number, R_M . However, we also struggled to obtain a precise estimate of R_M (in addition to good estimates of other model parameter values), when testing the inferential framework using simulated entomological data in Chapter 5. This suggests that it is particularly difficult to robustly estimate R_M , in addition to a large number of other model parameters. We hypothesise that this is most likely owing to density-dependence during the larval stage of population growth.

The importance of R_M to assessing the impact of novel vector control measures has also been highlighted in the context of exploring the potential impact of utilising homing endonuclease genes (HEGs) for malaria control [261, 262]. Mathematical modelling has shown that the potential impact of this technology will also depend on R_M , with more HEGs needed to eliminate vector populations for higher values of R_M [261, 262]. Given the difficulties in obtaining robust estimates of R_M , we adopted a similar approach to that used elsewhere [261] by testing sensitivity of our results in Chapter 6 to different values of the reproduction number. However, ideally we would like to have a better understanding of the basic mosquito reproduction number in Singapore, as this in turn would allow us to provide more robust estimates of the impact of the *Wolbachia* releases on local *Aedes aegypti* populations.

When fitting the model to the data, we aggregated the trapping data across residential blocks for each study site. We chose to aggregate the data when fitting the model in the first instance as this reduced the substantial computational challenges associated with calibrating the model against the data using a pMCMC inferential framework. This, in turn, allowed us to test the ability of the framework estimate parameter values within a computationally feasible timeframe. In addition, aggregating the data did not hinder our ability, in an overall sense, to estimate the impact of the *Wolbachia* releases on local *Aedes aegypti* population dynamics. However, we recognize that

aggregating the data placed limitations on the depth of our analysis, and the insight that could be drawn therefrom. Fitting the model to the data at the individual residential block level would allow us to statistically characterise fine-scale spatial heterogeneity in *Aedes aegypti* population density, and to explore how this heterogeneity affected the level of suppression achieved in the release areas. Furthermore, it would allow us to explore the role of adult mosquito dispersal (both horizontal and vertical) in driving the results observed, thereby perhaps providing deeper insight into why greater levels of suppression and better integration of *Wolbachia*-infected males among wild-type populations were not achieved.

Indeed, our analysis in Chapters 2-4 indicates that the fragmented spatial structure of *Aedes aegypti* populations is likely to play an important role in determining the impact of novel vector control measures. We observed how the fine-scale dynamics of *Aedes aegypti* populations are shaped by the dispersal behaviour of the mosquito and spatial variation in carrying capacity across a landscape. Thus the impact of the Phase 1 *Wolbachia* releases is likely to have varied between residential blocks at both release sites, owing to the underlying spatial heterogeneity in wild-type *Aedes aegypti* population density between residential blocks (Figures 5.9, 5.10). For example, a greater degree of population suppression may have been achieved in blocks with lower densities of wild-type *Aedes aegypti*. However, this would also have depended on the dispersal behaviour of the mosquito, and level of integration of *Wolbachia*-infected males among wild-type populations in individual blocks. The results presented in Chapters 2-4 highlighted the importance of limitations in the dispersal range of *Aedes aegypti* to the spread and distribution of the species across a landscape. Furthermore, our analysis in Chapters 3 and 4 suggests that the spatial configuration of residential blocks may also have played a role in determining the impact of the *Wolbachia* releases on wild-type population density in individual blocks, as the population dynamics in individual blocks are likely to be influenced by those in neighbouring blocks. Consequently, higher levels of suppression may have been achieved in residential blocks at the centre of the release sites, as the dynamics within these blocks may have been affected less by migration of wild-type adult females to and from neighbouring areas beyond the boundary of the release site, owing to the typically short dispersal length of *Aedes aegypti* [75–77].

Future work will build on the work presented in this thesis by addressing these limitations. We aim to calibrate a fully spatially explicit model of IIT against the entomological data collected in

Singapore, by fitting the model of IIT developed here at the individual residential block level. This however represents a considerable computational challenge, owing to the number of residential blocks at each site and the computationally intensive nature of particle MCMC methods. Fitting the model at a higher level of spatial resolution will require estimation of more parameters and consequently may be necessary to increase the number of particles used in the fitting algorithm. The addition of fine-scale spatial structure, more parameters and potentially more particles will come at the expense of computational speed, and thus dealing with these computational challenges is likely to be one of the most demanding aspects of this work.

In addition to providing further insights into the impact of the *Wolbachia* releases on local *Aedes aegypti* populations, we hope that fitting the model at a higher level of spatial granularity will allow us gain a deeper understanding of the role breeding site fragmentation and the underlying landscape in shaping the dynamics of real-world *Aedes aegypti* populations at fine spatial scales, thereby building on the theoretical results presented in Chapters 2-4 of this thesis.

Last, further avenues of model development could be explored. One possible avenue would be to incorporate rainfall and temperature data into the model. This may offer additional insights into the role of climatic conditions in driving temporal heterogeneity in *Aedes aegypti* abundance in Singapore. The model could also be extended to include dengue disease dynamics. However, whether the inclusion of disease dynamics may help capture the spatial behaviour of *Aedes aegypti* is likely to depend on the epidemiological data available that could be used to parameterize the model.

Transmission of dengue has been shown to be both highly spatially and temporally focal [16, 220, 263, 264]. For example, using phylogeographic methods, Salje *et. al* estimated that, in Bangkok, Thailand, 60% of dengue cases occurring less than 200 metres apart come from the same transmission chain, compared with 3% occurring 1km-5km apart [263]. These focal patterns of dengue transmission are primarily driven by patterns in human movement, patterns in population immunity and the short dispersal range of *Aedes aegypti* [16, 263]. Thus, knowledge of the fine-scale distribution of dengue cases may provide insight into the spatial behaviour of the *Aedes aegypti*. However, the majority of dengue infections are asymptomatic [9, 10, 12], with recent estimates suggesting 65% of dengue infections are subclinical [12]. Therefore, while clinical

incidence data would provide some information on the spatial distribution of cases, the information it may provide on the spatial behaviour of the vector and spatial variation in transmission intensity is likely to be limited. Serological data, combined with matching entomological data, is likely to be more informative than incidence data of the spatial behaviour of the vector as it provides a fuller picture of infection history, serotype diversity and levels of immunity within a population, thereby perhaps helping to capture fine-scale spatial heterogeneity in transmission intensity, and consequently helping to characterise fine-scale spatial heterogeneity in vector density.

7.4 Conclusions

Novel vector control measures for *Aedes aegypti* populations represent an exciting new form of dengue control. Progress in the development and testing of these measures presents new challenges for modelling the dynamics of *Aedes aegypti* populations, as estimating the likely impact of these measures on real-world vector populations will require spatially explicit models of fine-scale *Aedes aegypti* population dynamics, calibrated against high quality entomological data. The work presented in this thesis begins to address the challenge of developing such models, and thus is an important first step in this endeavour.

Bibliography

- [1] NEA Singapore, *Risk assessment for the use of male Wolbachia-carrying Aedes aegypti for suppression of the Aedes aegypti mosquito population*, 2016. [Online]. Available: <https://www.nea.gov.sg/docs/default-source/resource/2016-08-24-risk-assessment-for-the-use-of-wolbachia-carrying-aedes-males.pdf>.
- [2] NEA Singapore, *Secondary impact assessment on the use of Wolbachia technology to suppress Aedes aegypti population*, 2016. [Online]. Available: <https://www.nea.gov.sg/docs/default-source/resource/part-i.pdf>.
- [3] J. P. Messina, O. J. Brady, T. W. Scott, C. Zou, D. M. Pigott, K. A. Duda, S. Bhatt, L. Katzelnick, R. E. Howes, K. E. Battle, *et al.*, "Global spread of dengue virus types: Mapping the 70 year history," *Trends in Microbiology*, vol. 22, no. 3, pp. 138–146, 2014.
- [4] WHO 2012, *Global Strategy for Dengue Prevention and Control 2012-2020*. [Online]. Available: <http://www.who.int/denguecontrol/9789241504034/en/>.
- [5] D. J. Gubler, "Dengue, Urbanization and Globalization: The Unholy Trinity of the 21st Century," *Tropical Medicine and Health*, vol. 39, no. 4, S3–S11, 2011.
- [6] G. La Ruche, Y Souarès, A Armengaud, F Peloux-Petiot, P Delaunay, P Desprès, A Lenglet, F Jourdain, I Leparç-Goffart, F Charlet, *et al.*, "First two autochthonous dengue virus infections in metropolitan France, September 2010," *Eurosurveillance*, vol. 15, no. 39, pp. 1–5, 2010.
- [7] I Gjenero-Margan, B Aleraj, D Krajcar, V Lesnikar, A Klobučar, I Pem-Novosel, S Kurečić-Filipović, S Komparak, R Martić, S Duričić, *et al.*, "Autochthonous dengue fever in Croatia, August-September 2010.," *Eurosurveillance*, vol. 16, no. 9, p. 19805, 2011.
- [8] M. Chan, M. M. A. Johansson, M. Guzman, S. Halstead, H Artsob, P Buchy, J Farrar, W. Black, K. Bennett, N Gorrochotegui-Escalante, *et al.*, "The Incubation Periods of Dengue Viruses," *PLoS ONE*, vol. 7, no. 11, e50972, 2012.

- [9] S. B. Halstead, "Dengue," *The Lancet*, vol. 370, no. 9599, pp. 1644–1652, 2007.
- [10] C. P. Simmons, J. J. Farrar, v. V. C. Nguyen, B. Wills, N. van Vinh Chau, and B. Wills, "Dengue.," *New England Journal of Medicine*, vol. 366, no. 15, pp. 1423–32, 2012.
- [11] WHO 2018, *Dengue and Severe Dengue Factsheet*. [Online]. Available: <http://www.who.int/news-room/fact-sheets/detail/dengue-and-severe-dengue>.
- [12] H. Salje, D. A. T. Cummings, I. Rodriguez-Barraquer, L. C. Katzelnick, J. Lessler, C. Klungthong, B. Thaisomboonsuk, A. Nisalak, A. Weg, D. Ellison, *et al.*, "Reconstruction of antibody dynamics and infection histories to evaluate dengue risk," *Nature*, p. 1, 2018.
- [13] A. B. Sabin, "Research on dengue during world war II," *American Journal of Tropical Medicine and Hygiene*, vol. 1, no. 1, pp. 30–50, 1952.
- [14] M. OhAinle, A. Balmaseda, A. R. Macalalad, Y. Tellez, M. C. Zody, S. Saborío, A. Nuñez, N. J. Lennon, B. W. Birren, A. Gordon, *et al.*, "Dynamics of dengue disease severity determined by the interplay between viral genetics and serotype-specific immunity," *Science Translational Medicine*, vol. 3, no. 114, 114ra128, 2011.
- [15] N. G. Reich, S. Shrestha, A. A. King, P. Rohani, J. Lessler, S. Kalayanarooj, I.-K. Yoon, R. V. Gibbons, D. S. Burke, and D. A. T. Cummings, "Interactions between serotypes of dengue highlight epidemiological impact of cross-immunity," *Journal of The Royal Society Interface*, vol. 10, no. 86, p. 20130414, 2013.
- [16] H. Salje, J. Lessler, T. P. Endy, F. C. Curriero, R. V. Gibbons, A. Nisalak, S. Nimmannitya, S. Kalayanarooj, R. G. Jarman, S. J. Thomas, *et al.*, "Revealing the microscale spatial signature of dengue transmission and immunity in an urban population.," *Proceedings of the National Academy of Sciences*, vol. 109, no. 24, pp. 9535–8, 2012.
- [17] M. G. Guzman and S. Vazquez, "The complexity of antibody-dependent enhancement of dengue virus infection," *Viruses*, vol. 2, no. 12, pp. 2649–2662, 2010.
- [18] L. C. Katzelnick, L. Gresh, M. E. Halloran, J. C. Mercado, G. Kuan, A. Gordon, A. Balmaseda, and E. Harris, "Antibody-dependent enhancement of severe dengue disease in humans," *Science*, vol. 358, no. 6365, pp. 929–932, 2017.
- [19] P. S. Wikramaratna, C. P. Simmons, S. Gupta, and M. Recker, "The effects of tertiary and quaternary infections on the epidemiology of dengue," *PLoS ONE*, vol. 5, no. 8, e12347, 2010.

- [20] R. V. Gibbons, S. Kalanarooj, R. G. Jarman, A. Nisalak, D. W. Vaughn, T. P. Endy, M. P. Mammen, and A. Srikiatkachorn, "Analysis of repeat hospital admissions for dengue to estimate the frequency of third or fourth dengue infections resulting in admissions and dengue hemorrhagic fever, and serotype sequences," *American Journal of Tropical Medicine and Hygiene*, vol. 77, no. 5, pp. 910–913, 2007.
- [21] S. Olkowski, B. M. Forshey, A. C. Morrison, C. Rocha, S. Vilcarrero, E. S. Halsey, T. J. Kochel, T. W. Scott, and S. T. Stoddard, "Reduced risk of disease during postsecondary dengue virus infections," *The Journal of Infectious Diseases*, vol. 208, no. 6, pp. 1026–1033, 2013.
- [22] S. Bhatt, P. W. Gething, O. J. Brady, J. P. Messina, A. W. Farlow, C. L. Moyes, J. M. Drake, J. S. Brownstein, A. G. Hoen, O. Sankoh, *et al.*, "The global distribution and burden of dengue," *Nature*, vol. 496, no. 7446, pp. 504–507, 2013.
- [23] J. D. Stanaway, D. S. Shepard, E. A. Undurraga, Y. A. Halasa, L. E. Coffeng, O. J. Brady, S. I. Hay, N. Bedi, I. M. Bensenor, C. A. Castañeda-Orjuela, *et al.*, "The global burden of dengue: an analysis from the Global Burden of Disease Study 2013," *The Lancet Infectious Diseases*, vol. 16, no. 6, pp. 712–723, 2016.
- [24] D. S. Shepard, E. A. Undurraga, M. Betancourt-Cravioto, M. G. Guzmán, S. B. Halstead, E. Harris, R. N. Mudin, K. O. Murray, R. Tapia-Conyer, and D. J. Gubler, "Approaches to Refining Estimates of Global Burden and Economics of Dengue," *PLoS Neglected Tropical Diseases*, vol. 8, no. 11, e3306, 2014.
- [25] R. C. Reiner, S. T. Stoddard, B. M. Forshey, A. A. King, A. M. Ellis, A. L. Lloyd, K. C. Long, C. Rocha, S. Vilcarrero, H. Astete, *et al.*, "Time-varying, serotype-specific force of infection of dengue virus," *Proceedings of the National Academy of Sciences*, vol. 111, no. 26, E2694–E2702, 2014.
- [26] E. A. Undurraga, Y. A. Halasa, and D. S. Shepard, "Use of Expansion Factors to Estimate the Burden of Dengue in Southeast Asia: A Systematic Analysis," *PLoS Neglected Tropical Diseases*, vol. 7, no. 2, e3306, 2013.
- [27] K. B. Anderson, T. P. Endy, and S. J. Thomas, "The dynamic role of dengue cross-reactive immunity: changing the approach to defining vaccine safety and efficacy," *The Lancet Infectious Diseases*, 2018.

- [28] J. Deen, "The Dengue Vaccine Dilemma: Balancing the Individual and Population Risks and Benefits," *PLoS Medicine*, vol. 13, no. 11, e1002182, 2016.
- [29] WHO 2018, *Questions and Answers on Dengue Vaccines*. [Online]. Available: http://www.who.int/immunization/research/development/dengue_q_and_a/en/.
- [30] A. Sabchareon, D. Wallace, C. Sirivichayakul, K. Limkittikul, P. Chanthavanich, S. Suvannadabba, V. Jiwariyavej, W. Dulyachai, K. Pengsaa, T. A. Wartel, *et al.*, "Protective efficacy of the recombinant, live-attenuated, CYD tetravalent dengue vaccine in Thai schoolchildren: A randomised, controlled phase 2b trial," *The Lancet*, vol. 380, no. 9853, pp. 1559–1567, 2012.
- [31] L. Villar, G. H. Dayan, L. Arredondo-García, D. M. Rivera, R. Cunha, C. Deseda, H. Reynales, M. S. Costa, J. O. Morales-Ramírez, G. Carrasquilla, *et al.*, "Efficacy of a Tetravalent Dengue Vaccine in Children in Latin America," *New England Journal of Medicine*, vol. 372, no. 8, p. 141 103 114 505 002, 2014.
- [32] M. R. Capeding, N. H. Tran, S. R. S. Hadinegoro, H. I. H. M. Ismail, T. Chotpitayasunondh, M. N. Chua, C. Q. Luong, K. Rusmil, D. N. Wirawan, R. Nallusamy, *et al.*, "Clinical efficacy and safety of a novel tetravalent dengue vaccine in healthy children in Asia: A phase 3, randomised, observer-masked, placebo-controlled trial," *The Lancet*, vol. 384, no. 9951, pp. 1358–1365, 2014.
- [33] S. R. Hadinegoro, J. L. Arredondo-García, M. R. Capeding, C. Deseda, T. Chotpitayasunondh, R. Dietze, H. Hj Muhammad Ismail, H. Reynales, K. Limkittikul, D. M. Rivera-Medina, *et al.*, "Efficacy and Long-Term Safety of a Dengue Vaccine in Regions of Endemic Disease," *New England Journal of Medicine*, vol. 373, no. 13, pp. 1195–1206, 2015.
- [34] N. M. Ferguson, I. Rodríguez-Barraquer, I. Dorigatti, L. Mier-Y-Teran-Romero, D. J. Laydon, and D. A. T. Cummings, "Benefits and risks of the Sanofi-Pasteur dengue vaccine: Modeling optimal deployment," *Science*, vol. 353, no. 6303, pp. 1033–1036, 2016.
- [35] WHO, "Dengue position paper," *Weekly Epidemiological Record*, July 2016.
- [36] S. Sridhar, A. Luedtke, E. Langevin, M. Zhu, M. Bonaparte, T. Machabert, S. Savarino, B. Zambrano, A. Moureau, A. Khromava, *et al.*, "Effect of Dengue Serostatus on Dengue Vaccine Safety and Efficacy," *New England Journal of Medicine*, vol. 379, no. 4, 2018.

- [37] WHO 2018, *Revised SAGE recommendation on use of dengue vaccine*. [Online]. Available: http://www.who.int/immunization/diseases/dengue/revised_SAGE_recommendations_dengue_vaccines_apr2018/en/.
- [38] K. S. Vannice, A. Durbin, and J. Hombach, "Status of vaccine research and development of vaccines for dengue," *Vaccine*, vol. 34, no. 26, pp. 2934–2938, 2016.
- [39] J. E. Osorio, C. D. Partidos, D. Wallace, and D. T. Stinchcomb, "Development of a recombinant, chimeric tetravalent dengue vaccine candidate," *Vaccine*, vol. 33, no. 50, pp. 7112–7120, 2015.
- [40] B. D. Kirkpatrick, S. S. Whitehead, K. K. Pierce, C. M. Tibery, P. L. Grier, N. A. Hynes, C. J. Larsson, B. P. Sabundayo, K. R. Talaat, A. Janiak, *et al.*, "The live attenuated dengue vaccine TV003 elicits complete protection against dengue in a human challenge model," *Science Translational Medicine*, vol. 8, no. 330, 330ra36, 2016.
- [41] S. S. Whitehead, A. P. Durbin, K. K. Pierce, D. Elwood, B. D. McElvany, E. A. Fraser, M. P. Carmolli, C. M. Tibery, N. A. Hynes, M. Jo, *et al.*, "In a randomized trial, the live attenuated tetravalent dengue vaccine TV003 is well-tolerated and highly immunogenic in subjects with flavivirus exposure prior to vaccination," *PLoS Neglected Tropical Diseases*, vol. 11, no. 5, e0005584, 2017.
- [42] X. Sáez-Llorens, V. Tricou, D. Yu, L. Rivera, J. Jimeno, A. C. Villarreal, E. Dato, S. Mazara, M. Vargas, M. Brose, *et al.*, "Immunogenicity and safety of one versus two doses of tetravalent dengue vaccine in healthy children aged 2-17 years in Asia and Latin America: 18-month interim data from a phase 2, randomised, placebo-controlled study," *The Lancet Infectious Diseases*, vol. 18, no. 2, pp. 162–170, 2017.
- [43] J. E. Osorio, I. D. Velez, C. Thomson, L. Lopez, A. Jimenez, A. A. Haller, S. Silengo, J. Scott, K. L. Boroughs, J. L. Stovall, *et al.*, "Safety and immunogenicity of a recombinant live attenuated tetravalent dengue vaccine (DENVax) in flavivirus-naive healthy adults in Colombia: A randomised, placebo-controlled, phase 1 study," *The Lancet Infectious Diseases*, vol. 14, no. 9, pp. 830–838, 2014.
- [44] *Efficacy, Safety and Immunogenicity of Takeda's Tetravalent Dengue Vaccine (TDV) in Healthy Children*, <https://clinicaltrials.gov/ct2/show/NCT02747927>.
- [45] *Phase III Trial to Evaluate Efficacy and Safety of a Tetravalent Dengue Vaccine*, <https://clinicaltrials.gov/ct2/show/NCT02406729>.

- [46] H. M. Giles and D. A. Warrell, *Essential Malariology*, Arnold. 2002.
- [47] A. C. Morrison, K. Gray, A. Getis, H. Astete, M. Sihuincha, D. Focks, D. Watts, J. D. Stancil, J. G. Olson, P. Blair, *et al.*, “Temporal and Geographic Patterns of *Aedes aegypti* (Diptera: Culicidae) Production in Iquitos, Peru,” *Journal of Medical Entomology*, vol. 41, no. 6, pp. 1123–1142, 2004.
- [48] S. Christophers, *Aedes aegypti (L.) the Yellow Fever Mosquito: its Life History, Bionomics and Structure*. Rickard. 1960.
- [49] C. Pant and M. Yasuno, “Field studies on the gonotrophic cycle of *Aedes aegypti* in Bangkok, Thailand,” *Journal of Medical Entomology*, vol. 10, no. 2, pp. 219–223, 1973.
- [50] F. V. S. de Abreu, M. M. Morais, S. P. Ribeiro, and Á. E. Eiras, “Influence of breeding site availability on the oviposition behaviour of *Aedes aegypti*,” *Memórias do Instituto Oswaldo Cruz*, vol. 110, no. 5, pp. 669–676, 2015.
- [51] J. D. Edman, T. W. Scott, A. Costero, A. C. Morrison, L. C. Harrington, and G. G. Clark, “*Aedes aegypti* (diptera: Culicidae) movement influenced by availability of oviposition sites,” *Journal of Medical Entomology*, vol. 35, no. 4, pp. 578–583, 1998.
- [52] R. Chowdhury, V. Chowdhury, S. Faria, M. M. Huda, R. Laila, I. Dhar, N. P. Maheswary, and A. P. Dash, “How dengue vector *Aedes albopictus* (Diptera: Culicidae) survive during the dry season in Dhaka City, Bangladesh?” *Journal of Vector Borne Diseases*, vol. 51, no. 3, pp. 179–87, 2014.
- [53] M Trpis, “Dry season survival of *Aedes aegypti* eggs in various breeding sites in the Dar es Salaam area, Tanzania.,” *Bulletin of the World Health Organization*, vol. 47, no. 3, pp. 433–7, 1972.
- [54] D. F. A. Diniz, C. M. R. De Albuquerque, L. O. Oliva, M. A. V. De Melo-Santos, and C. F. J. Ayres, “Diapause and quiescence: Dormancy mechanisms that contribute to the geographical expansion of mosquitoes and their evolutionary success,” *Parasites & Vectors*, vol. 10, no. 1, p. 310, 2017.
- [55] G. Lacour, L. Chanaud, G. L’Ambert, and T. Hance, “Seasonal Synchronization of Diapause Phases in *Aedes albopictus* (Diptera: Culicidae),” *PLoS ONE*, vol. 10, no. 12, e0145311, 2015.

- [56] C. Paupy, H. Delatte, L. Bagny, V. Corbel, and D. Fontenille, "Aedes albopictus, an arbovirus vector: From the darkness to the light," *Microbes and Infection*, vol. 11, no. 14-15, pp. 1177–1185, 2009.
- [57] M. Q. Benedict, R. S. Levine, W. A. Hawley, and L. P. Lounibos, "Spread of The Tiger: Global Risk of Invasion by The Mosquito *Aedes albopictus*," *Vector-Borne and Zoonotic Diseases*, vol. 7, no. 1, pp. 76–85, 2007.
- [58] M. U. Kraemer, M. E. Sinka, K. A. Duda, A. Q. Mylne, F. M. Shearer, C. M. Barker, C. G. Moore, R. G. Carvalho, G. E. Coelho, W. Van Bortel, *et al.*, "The global distribution of the arbovirus vectors *Aedes aegypti* and *Ae. albopictus*," *eLife*, vol. 4, e08347, 2015.
- [59] R. Barrera, M. Amador, and G. G. Clark, "Ecological factors influencing *Aedes aegypti* (Diptera: Culicidae) productivity in artificial containers in Salinas, Puerto Rico.," *Journal of Medical Entomology*, vol. 43, no. 3, pp. 484–492, 2006.
- [60] A. Morrison, M. Sihuincha, J. Stancil, E. Zamora, H. Astete, J. Olson, C. Vidal-Ore, and T. Scott, "*Aedes aegypti* (diptera: Culicidae) production from non-residential sites in the amazonian city of Iquitos, Peru," *Annals of Tropical Medicine & Parasitology*, vol. 100, no. sup1, pp. 73–86, 2006.
- [61] A. Getis, A. C. Morrison, K. Gray, and T. W. Scott, "Characteristics of the spatial pattern of the dengue vector, *Aedes aegypti*, in Iquitos, Peru," *American Journal of Tropical Medicine and Hygiene*, vol. 69, no. 5, pp. 494–505, 2003.
- [62] R. K. Walsh, L. Facchinelli, J. M. Ramsey, J. G. Bond, and F. Gould, "Assessing the impact of density dependence in field populations of *Aedes aegypti*," *Journal of Vector Ecology*, vol. 36, no. 2, pp. 300–307, 2011.
- [63] C. G. Moore and B. R. Fisher, "Competition in mosquitoes. density and species ratio effects on growth, mortality, fecundity, and production of growth retardant," *Annals of the Entomological Society of America*, vol. 62, no. 6, pp. 1325–1331, 1969.
- [64] W. Tun-Lin, T. R. Burkot, and B. H. Kay, "Effects of temperature and larval diet on development rates and survival of the dengue vector *Aedes aegypti* in north Queensland, Australia," *Medical and Veterinary Entomology*, vol. 14, no. 1, pp. 31–37, 2000.
- [65] M. Legros, A. L. Lloyd, Y. Huang, and F. Gould, "Density-Dependent Intraspecific Competition in the Larval Stage of *Aedes aegypti* (Diptera: Culicidae): Revisiting the Current Paradigm," *Journal of Medical Entomology*, vol. 46, no. 3, pp. 409–419, 2009.

- [66] T. Southwood, G Murdie, M Yasuno, R. J. Tonn, and P. Reader, "Studies on the life budget of *Aedes aegypti* in Wat Samphaya, Bangkok, Thailand," *Bulletin of the World Health Organization*, vol. 46, no. 2, p. 211, 1972.
- [67] R. K. Walsh, C. L. Aguilar, L. Facchinelli, L. Valerio, J. M. Ramsey, T. W. Scott, A. L. Lloyd, and F. Gould, "Regulation of *Aedes aegypti* population dynamics in field systems: Quantifying direct and delayed density dependence," *American Journal of Tropical Medicine and Hygiene*, vol. 89, no. 1, pp. 68–77, 2013.
- [68] J. Couret, E. Dotson, and M. Q. Benedict, "Temperature, larval diet, and density effects on development rate and survival of *Aedes aegypti* (Diptera: Culicidae)," *PLoS ONE*, vol. 9, no. 2, e87468, 2014.
- [69] M. Reiskind and L. Lounibos, "Effects of intraspecific larval competition on adult longevity in the mosquitoes *Aedes aegypti* and *Aedes albopictus*," *Medical and Veterinary Entomology*, vol. 23, no. 1, pp. 62–68, 2009.
- [70] P. Agnew, M. Hide, C. Sidobre, and Y. Michalakakis, "A minimalist approach to the effects of density-dependent competition on insect life-history traits," *Ecological Entomology*, vol. 27, no. 4, pp. 396–402, 2002.
- [71] J. Arrivillaga and R. Barrera, "Food as a limiting factor for *Aedes aegypti* in water-storage containers.," *Journal of the Society for Vector Ecology*, vol. 29, no. 1, pp. 11–20, 2004.
- [72] M. Service, "Mosquito (diptera: Culicidae) dispersal-the long and short of it," *Journal of Medical Entomology*, vol. 34, no. 6, pp. 579–588, 1997.
- [73] A. Ponlawat and L. C. Harrington, "Blood Feeding Patterns of *Aedes aegypti* and *Aedes albopictus* in Thailand," *Journal of Medical Entomology*, vol. 42, no. 5, pp. 844–849, 2005.
- [74] C. A. Guerra, R. C. Reiner, T Perkins, S. W. Lindsay, J. T. Midega, O. J. Brady, C. M. Barker, W. K. Reisen, L. C. Harrington, W. Takken, *et al.*, "A global assembly of adult female mosquito mark-release-recapture data to inform the control of mosquito-borne pathogens," *Parasites & Vectors*, vol. 7, no. 1, p. 276, 2014.
- [75] L. C. Harrington, T. W. Scott, K. Lerdthusnee, R. C. Coleman, A. Costero, G. G. Clark, J. J. Jones, S. Kitthawee, P. Kittayapong, R. Sithiprasasna, *et al.*, "Dispersal of the dengue vector *Aedes aegypti* within and between rural communities," *American Journal of Tropical Medicine and Hygiene*, vol. 72, no. 2, pp. 209–220, 2005.

- [76] M Trpis and W Hausermann, "Dispersal and other population parameters of *Aedes aegypti* in an African village and their possible significance in epidemiology of vector-borne diseases," *American Journal of Tropical Medicine and Hygiene*, vol. 35, no. 6, pp. 1263–1279, 1986.
- [77] L. E. Muir and B. H. Kay, "*Aedes aegypti* survival and dispersal estimated by mark-release-recapture in northern Australia," *American Journal of Tropical Medicine and Hygiene*, vol. 58, no. 3, pp. 277–282, 1998.
- [78] N. A. Honório, W. d. C. Silva, P. J. Leite, J. M. Gonçalves, L. P. Lounibos, and R. Lourenço-de Oliveira, "Dispersal of *Aedes aegypti* and *Aedes albopictus* (Diptera: Culicidae) in an urban endemic dengue area in the State of Rio de Janeiro, Brazil," *Memórias do Instituto Oswaldo Cruz*, vol. 98, no. 2, pp. 191–198, 2003.
- [79] N. L. Achee, F. Gould, T. A. Perkins, R. C. Reiner, A. C. Morrison, S. A. Ritchie, D. J. Gubler, R. Teyssou, and T. W. Scott, "A Critical Assessment of Vector Control for Dengue Prevention," *PLoS Neglected Tropical Diseases*, vol. 9, no. 5, e0003655, 2015.
- [80] WHO 2017, *Global vector control response 2017-2030*. [Online]. Available: <http://www.who.int/vector-control/publications/global-control-response/en/>.
- [81] D. J. Gubler, "Epidemic dengue/dengue hemorrhagic fever as a public health, social and economic problem in the 21st century," *Trends in Microbiology*, vol. 10, no. 2, pp. 100–103, 2002.
- [82] E. E. Ooi, K. T. Goh, and D. J. Gubler, "Dengue prevention and 35 years of vector control in Singapore," *Emerging Infectious Diseases*, vol. 12, no. 6, pp. 887–893, 2006.
- [83] J. A. Gessa and R. F. Gonzalez, "Application of environmental management principles in the programme for eradication of *Aedes (Stegomyia) aegypti* (Linnaeus, 1752) in the Republic of Cuba, 1984," *Bull Pan Am Health Organ*, vol. 20, no. 2, pp. 186–193, 1986.
- [84] E. Esu, A. Lenhart, L. Smith, and O. Horstick, "Effectiveness of peridomestic space spraying with insecticide on dengue transmission; Systematic review," *Tropical Medicine and International Health*, vol. 15, no. 5, pp. 619–631, 2010.
- [85] H. Ranson, J. Burhani, N. Lumjuan, and W. C. Black IV, "Insecticide resistance in dengue vectors," *TropIKA. net [online]*, vol. 1, no. 1, 2010.

- [86] S. Marcombe, R. B. Mathieu, N. Pocquet, M. A. Riaz, R. Poupardin, S. Sélior, F. Darriet, S. Reynaud, A. Yébakima, V. Corbel, *et al.*, “Insecticide resistance in the dengue vector *Aedes aegypti* from martinique: Distribution, mechanisms and relations with environmental factors,” *PLoS ONE*, vol. 7, no. 2, e30989, 2012.
- [87] Z. H. Amelia-Yap, C. D. Chen, M. Sofian-Azirun, and V. L. Low, “Pyrethroid resistance in the dengue vector *Aedes aegypti* in Southeast Asia: present situation and prospects for management,” *Parasites & Vectors*, vol. 11, no. 1, p. 332, 2018.
- [88] C. L. Moyes, J. Vontas, A. J. Martins, L. C. Ng, S. Y. Koou, I. Dusfour, K. Raghavendra, J. Pinto, V. Corbel, J.-P. P. David, *et al.*, “Contemporary status of insecticide resistance in the major *Aedes* vectors of arboviruses infecting humans,” *PLoS Neglected Tropical Diseases*, vol. 11, no. 7, e0005625, 2017.
- [89] G. Kourí, M. G. Guzmán, L. Valdés, I. Carbonel, D. del Rosario, S. Vázquez, J. Laferte, J. Delgado, and M. V. Cabrera, “Reemergence of dengue in Cuba: A 1997 epidemic in Santiago de Cuba,” *Emerging infectious diseases*, vol. 4, no. 1, p. 89, 1998.
- [90] J. H. Werren, L. Baldo, and M. E. Clark, “*Wolbachia*: Master manipulators of invertebrate biology,” *Nature Reviews Microbiology*, vol. 6, no. 10, p. 741, 2008.
- [91] R. Zug and P. Hammerstein, “Still a host of hosts for *Wolbachia* : Analysis of recent data suggests that 40% of terrestrial arthropod species are infected,” *PLoS ONE*, vol. 7, no. 6, e38544, 2012.
- [92] I. Dorigatti, C. McCormack, G. Nedjati-Gilani, and N. M. Ferguson, “Using *Wolbachia* for Dengue Control: Insights from Modelling,” *Trends in Parasitology*, vol. 34, no. 2, pp. 102–113, 2018.
- [93] P. Kittayapong, V. Baimai, S. L. O’Neill, P. Kitrayapong, V. Baimai, and S. L. O’Neill, “Field prevalence of *Wolbachia* in the mosquito vector *Aedes albopictus*,” *American Journal of Tropical Medicine and Hygiene*, vol. 66, no. 1, pp. 108–111, 2002.
- [94] M. Hertig, “The rickettsia, *Wolbachia pipientis* (gen. et sp. n.) and associated inclusions of the mosquito, *Culex pipiens*,” *Parasitology*, vol. 28, no. 04, pp. 453–486, 1936.
- [95] Z. Xi, C. C. Khoo, and S. L. Dobson, “*Wolbachia* establishment and invasion in an *Aedes aegypti* laboratory population,” *Science*, vol. 310, no. 5746, pp. 326–328, 2005.

- [96] K.-T. Min and S. Benzer, “*Wolbachia*, normally a symbiont of *Drosophila*, can be virulent, causing degeneration and early death,” *Proceedings of the National Academy of Sciences*, vol. 94, no. 20, pp. 10 792–10 796, 1997.
- [97] C. J. McMeniman, R. V. Lane, B. N. Cass, A. W. Fong, M. Sidhu, Y.-F. Wang, and S. L. O’Neill, “Stable introduction of a life-shortening *Wolbachia* infection into the mosquito *Aedes aegypti*,” *Science*, vol. 323, no. 5910, pp. 141–144, 2009.
- [98] P. E. Cook, C. J. McMeniman, and S. L. O’Neill, “Modifying Insect Population Age Structure to Control Vector-Borne Disease,” in *Transgenesis and the Management of Vector-Borne Disease*, Springer New York, 2008, pp. 126–140.
- [99] T. Walker, P. H. Johnson, L. A. Moreira, I. Iturbe-Ormaetxe, F. D. Frentiu, C. J. McMeniman, Y. S. Leong, Y. Dong, J. Axford, P. Kriesner, *et al.*, “The *wMel* *Wolbachia* strain blocks dengue and invades caged *Aedes aegypti* populations,” *Nature*, vol. 476, no. 7361, p. 450, 2011.
- [100] L. A. Moreira, I. Iturbe-Ormaetxe, J. A. Jeffery, G. Lu, A. T. Pyke, L. M. Hedges, B. C. Rocha, S. Hall-Mendelin, A. Day, M. Riegler, *et al.*, “A *Wolbachia* Symbiont in *Aedes aegypti* Limits Infection with Dengue, Chikungunya, and Plasmodium,” *Cell*, vol. 139, no. 7, pp. 1268–1278, 2009.
- [101] A. A. Hoffmann, B. L. Montgomery, J. Popovici, I. Iturbe-Ormaetxe, P. H. Johnson, F. Muzzi, M. Greenfield, M. Durkan, Y. S. Leong, Y. Dong, *et al.*, “Successful establishment of *Wolbachia* in *Aedes* populations to suppress dengue transmission.,” *Nature*, vol. 476, no. 7361, pp. 454–7, 2011.
- [102] A. A. Hoffmann, I. Iturbe-Ormaetxe, A. G. Callahan, B. L. Phillips, K. Billington, J. K. Axford, B. Montgomery, A. P. Turley, and S. L. O’Neill, “Stability of the *wMel* *Wolbachia* infection following invasion into *Aedes aegypti* populations,” *PLoS neglected tropical diseases*, vol. 8, no. 9, e31115, 2014.
- [103] F. D. Frentiu, T. Zakir, T. Walker, J. Popovici, A. T. Pyke, A. van den Hurk, E. A. McGraw, and S. L. O’Neill, “Limited Dengue Virus Replication in Field-Collected *Aedes aegypti* Mosquitoes Infected with *Wolbachia*,” *PLoS Neglected Tropical Diseases*, vol. 8, no. 2, e2688, 2014.
- [104] T. H. Nguyen, H. Le Nguyen, T. Y. Nguyen, S. N. Vu, N. D. Tran, T. N. Le, Q. M. Vien, T. C. Bui, H. T. Le, S. Kutcher, *et al.*, “Field evaluation of the establishment potential of

- wMelPop *Wolbachia* in Australia and Vietnam for dengue control,” *Parasites & Vectors*, vol. 8, no. 1, p. 563, 2015.
- [105] *Applying Wolbachia to Eliminate Dengue*. [Online]. Available: <https://clinicaltrials.gov/ct2/show/NCT03055585>.
- [106] *World Mosquito Program*, <http://www.eliminatedengue.com/vn>.
- [107] E. Callaway, “Rio fights Zika with biggest release yet of bacteria-infected mosquitoes,” *Nature*, vol. 539, no. 7627, pp. 17–18, 2016.
- [108] S. L. O’Neill, P. A. Ryan, A. P. Turley, G. Wilson, K. Retzki, I. Iturbe-Ormaetxe, Y. Dong, N. Kenny, C. J. Paton, S. A. Ritchie, *et al.*, “Scaled deployment of *Wolbachia* to protect the community from *Aedes* transmitted arboviruses,” *Gates Open Research*, vol. 2, 2018.
- [109] H. Laven, “Eradication of *Culex pipiens fatigans* through cytoplasmic incompatibility,” *Nature*, vol. 216, no. 5113, pp. 383–384, 1967.
- [110] E. Marris, “Bacteria could be key to freeing South Pacific of mosquitoes,” *Nature*, vol. 548, no. 7665, pp. 17–18, 2017.
- [111] L. O’Connor, C. Plichart, A. C. Sang, C. L. Brelsfoard, H. C. Bossin, and S. L. Dobson, “Open Release of Male Mosquitoes Infected with a *Wolbachia* Biopesticide: Field Performance and Infection Containment,” *PLoS Neglected Tropical Diseases*, vol. 6, no. 11, e1797, 2012.
- [112] *MosquitoMate - Debug Fresno*. [Online]. Available: <http://www.arcgis.com/apps/MapJournal/index.html?appid=0586437f5b69477fbad9f3774047420a>.
- [113] J. W. Mains, C. L. Brelsfoard, R. I. Rose, and S. L. Dobson, “Female adult *Aedes albopictus* suppression by *Wolbachia*-infected male mosquitoes,” *Scientific Reports*, vol. 6, no. 1, p. 33846, 2016.
- [114] *Debug Project: Wrapping up Debug Fresno 2017*. [Online]. Available: <https://blog.debug.com/2017/11/wrapping-up-debug-fresno-2017.html>.
- [115] *Debug Project: Debug Innisfail achieves strong suppression*. [Online]. Available: <https://blog.debug.com/2018/07/debug-innisfail-achieves-strong.html>.
- [116] CSIRO, *Studying mosquitoes to stop the spread of disease*. [Online]. Available: <https://www.csiro.au/en/Research/BF/Areas/Protecting-Animal-and-Human-Health/InsectBorneDisease/Innisfail-project>.

- [117] NEA, *Project Wolbachia - Singapore*. [Online]. Available: <https://www.nea.gov.sg/corporate-functions/resources/research/wolbachia-aedes-mosquito-suppression-strategy/project-wolbachia-singapore>.
- [118] W. Klassen and C. F. Curtis, "History of the sterile insect technique," in *Sterile Insect Technique: Principles and Practice in Area-Wide Integrated Pest Management*, Springer, 2005, pp. 3–36.
- [119] R. S. Lees, J. R. Gilles, J. Hendrichs, M. J. Vreysen, and K. Bourtzis, "Back to the future: the sterile insect technique against mosquito disease vectors," *Current Opinion in Insect Science*, vol. 10, pp. 156–162, 2015.
- [120] R. Bellini, A. Albieri, F. Balestrino, M. Carrieri, D. Porretta, S. Urbanelli, M. Calvitti, R. Moretti, and S. Maini, "Dispersal and Survival of *Aedes albopictus* (Diptera: Culicidae) Males in Italian Urban Areas and Significance for Sterile Insect Technique Application," *Journal of Medical Entomology*, vol. 47, no. 6, pp. 1082–1091, 2010.
- [121] R. Bellini, A. Medici, A. Puggioli, F. Balestrino, and M. Carrieri, "Pilot Field Trials With *Aedes albopictus* Irradiated Sterile Males in Italian Urban Areas," *Journal of Medical Entomology*, vol. 50, no. 2, pp. 317–325, 2013.
- [122] H. Phuc, M. H. Andreasen, R. S. Burton, C. C. Vass, M. J. Epton, G. Pape, G. Fu, K. C. Condon, S. Scaife, C. A. Donnelly, *et al.*, "Late-acting dominant lethal genetic systems and mosquito control," *BMC Biology*, vol. 5, no. 1, p. 11, 2007.
- [123] A. F. Harris, A. R. McKemey, D. Nimmo, Z. Curtis, I. Black, S. A. Morgan, M. N. Oviedo, R. Lacroix, N. Naish, N. I. Morrison, *et al.*, "Successful suppression of a field mosquito population by sustained release of engineered male mosquitoes," *Nature Biotechnology*, vol. 30, no. 9, pp. 828–830, 2012.
- [124] D. O. Carvalho, A. R. McKemey, L. Garziera, R. Lacroix, C. A. Donnelly, L. Alphey, A. Malvasi, and M. L. Capurro, "Suppression of a field population of *Aedes aegypti* in Brazil by sustained release of transgenic male mosquitoes," *PLoS Neglected Tropical Diseases*, vol. 9, no. 7, e0003864, 2015.
- [125] M. R. Wise de Valdez, D. Nimmo, J. Betz, H.-F. Gong, A. A. James, L. Alphey, and W. C. Black, "Genetic elimination of dengue vector mosquitoes," *Proceedings of the National Academy of Sciences*, vol. 108, no. 12, pp. 4772–4775, 2011.

- [126] L. Facchinelli, L. Valerio, J. M. Ramsey, F. Gould, R. K. Walsh, G. Bond, M. A. Robert, A. L. Lloyd, A. A. James, L. Alphey, *et al.*, “Field Cage Studies and Progressive Evaluation of Genetically-Engineered Mosquitoes,” *PLoS Neglected Tropical Diseases*, vol. 7, no. 1, 2013.
- [127] D. Zhang, R. S. Lees, Z. Xi, K. Bourtzis, and J. R. Gilles, “Combining the sterile insect technique with the incompatible insect technique: III-robust mating competitiveness of irradiated triple *Wolbachia*-infected *Aedes albopictus* males under semi-field conditions,” *PloS one*, vol. 11, no. 3, e0151864, 2016.
- [128] S. A. Ritchie and B. J. Johnson, “Advances in vector control science: Rear-and-release strategies show promise-but don’t forget the basics,” *Journal of Infectious Diseases*, vol. 215, no. suppl_2, S103–S108, 2017.
- [129] D. Zhang, X. Zheng, Z. Xi, K. Bourtzis, and J. R. Gilles, “Combining the sterile insect technique with the incompatible insect technique: I-impact of *Wolbachia* infection on the fitness of triple- and double-infected strains of *Aedes albopictus*,” *PLoS ONE*, vol. 10, no. 4, e0121126, 2015.
- [130] D. Zhang, R. S. Lees, Z. Xi, J. R. Gilles, and K. Bourtzis, “Combining the sterile insect technique with *Wolbachia* -based approaches: II - A safer approach to *Aedes albopictus* population suppression programmes, designed to minimize the consequences of inadvertent female release,” *PLoS ONE*, vol. 10, no. 8, e0135194, 2015.
- [131] S. Naish, P. Dale, J. S. Mackenzie, J. McBride, K. Mengersen, and S. Tong, “Climate change and dengue: A critical and systematic review of quantitative modelling approaches,” *BMC Infectious Diseases*, vol. 14, no. 1, p. 167, 2014.
- [132] L. Xu, L. C. Stige, K.-S. Chan, J. Zhou, J. Yang, S. Sang, M. Wang, Z. Yang, Z. Yan, T. Jiang, *et al.*, “Climate variation drives dengue dynamics,” *Proceedings of the National Academy of Sciences*, vol. 114, no. 1, pp. 113–118, 2017.
- [133] P.-C. Wu, J.-G. Lay, H.-R. Guo, C.-Y. Lin, S.-C. Lung, and H.-J. Su, “Higher temperature and urbanization affect the spatial patterns of dengue fever transmission in subtropical Taiwan,” *Science of The Total Environment*, vol. 407, no. 7, pp. 2224–2233, 2009.
- [134] D. J. Gubler, “Dengue and dengue hemorrhagic fever.,” *Clinical Microbiology Reviews*, vol. 11, no. 3, pp. 480–96, 1998.

- [135] R. C. Reiner, T. A. Perkins, C. M. Barker, T. Niu, L. F. Chaves, A. M. Ellis, D. B. George, A. Le Menach, J. R. C. Pulliam, D. Bisanzio, *et al.*, “A systematic review of mathematical models of mosquito-borne pathogen transmission: 1970-2010.” *Journal of the Royal Society, Interface*, vol. 10, no. 81, p. 20120921, 2013.
- [136] R. Levins, “Some Demographic and Genetic Consequences of Environmental Heterogeneity for Biological Control,” *Bulletin of the Entomological Society of America*, vol. 15, no. 3, pp. 237–240, 1969.
- [137] M. Gilpin, “Metapopulation dynamics: Empirical and theoretical investigations,” *Academic Press*, 2012.
- [138] I. Hanski, “Metapopulation dynamics,” *Nature*, vol. 396, no. 6706, pp. 41–49, 1998.
- [139] I. Hanski and M. Gilpin, “Metapopulation dynamics: brief history and conceptual domain,” *Biological Journal of the Linnean Society*, vol. 42, no. 1-2, pp. 3–16, 1991.
- [140] S. Harrison, “Local extinction in a metapopulation context : an empirical evaluation,” *Biological Journal of the Linnean Society*, vol. 42, pp. 73–88, 1991.
- [141] I. Hanski, “Metapopulation theory, its use and misuse,” *Basic and Applied Ecology*, vol. 5, no. 3, pp. 225–229, 2004.
- [142] I. Hanski and O. Ovaskainen, “Metapopulation theory for fragmented landscapes,” *Theoretical Population Biology*, vol. 64, no. 1, pp. 119–127, 2003.
- [143] I. Hanski, M. E. Gilpin, and D. E. McCauley, “Metapopulation biology,” *Elsevier*, vol. 454, 1997.
- [144] S. A. Boorman and P. R. Levitt, “Group selection on the boundary of a stable population,” *Theoretical Population Biology*, vol. 4, no. 1, pp. 85–128, 1973.
- [145] O. Ovaskainen and M. Saastamoinen, “Frontiers in Metapopulation Biology: The Legacy of Ilkka Hanski,” *Annual Review of Ecology, Evolution, and Systematics*, vol. 49, pp. 231–252, 2018.
- [146] J. Hill, C. Thomas, and O. Lewis, “Effects of Habitat Patch Size and Isolation on Dispersal by *Hesperia comma* Butterflies: Implications for Metapopulation Structure,” *The Journal of Animal Ecology*, vol. 65, no. 6, p. 725, 1996.
- [147] C. Thomas and S. Harrison, “Spatial Dynamics of a Patchily Distributed Butterfly Species,” *The Journal of Animal Ecology*, vol. 61, no. 2, p. 437, 2006.

- [148] S. Harrison, "Long-distance dispersal and colonization in the bay checkerspot butterfly, *Euphydryas editha bayensis*," *Ecology*, vol. 70, no. 5, pp. 1236–1243, 1989.
- [149] C. D. Thomas, "Spatial dynamics of a patchily distributed butterfly species," *Journal of Animal Ecology*, vol. 61, no. 2, pp. 437–446, 1992.
- [150] M. Baguette and N. Schtickzelle, "Local population dynamics are important to the conservation of metapopulations in highly fragmented landscapes," *Journal of Applied Ecology*, vol. 40, no. 2, pp. 404–412, 2003.
- [151] I. Hanski, "A practical model of metapopulation dynamics," *Journal of Animal Ecology*, vol. 63, no. 1, pp. 151–162, 2014.
- [152] P. Stacey and M. Taper, "Environmental Variation and the Persistence of Small Populations," *Ecological Applications*, vol. 2, no. 1, pp. 18–29, 1992.
- [153] R. L. Schooley and L. C. Branch, "Spatial heterogeneity in habitat quality and cross-scale interactions in metapopulations," *Ecosystems*, vol. 10, no. 5, pp. 846–853, 2007.
- [154] A. Moilanen, A. T. Smith, and I. Hanski, "Long-term dynamics in a metapopulation of the American pika," *The American Naturalist*, vol. 152, no. 4, pp. 530–542, 1998.
- [155] A. T. Smith and J. D. Nagy, "Population resilience in an American pika (*Ochotona princeps*) metapopulation," *Journal of Mammalogy*, vol. 96, no. 2, pp. 394–404, 2015.
- [156] J. Worthington Wilmer, C. Elkin, C. Wilcox, L. Murray, D. Niejalke, and H. Possingham, "The influence of multiple dispersal mechanisms and landscape structure on population clustering and connectivity in fragmented artesian spring snail populations," *Molecular Ecology*, vol. 17, no. 16, pp. 3733–3751, 2008.
- [157] J. Dunham and B. Rieman, "Metapopulation structure of bull trout: Influences of physical, biotic, and geometrical landscape characteristics," *Ecological Applications*, vol. 9, no. 2, pp. 642–655, 1999.
- [158] S. Nee, "How populations persist," *Nature*, vol. 367, no. 6459, pp. 123–124, 1994.
- [159] I. Hanski, "Single-species metapopulation dynamics: concepts, models and observations," *Biological Journal of the Linnean Society*, vol. 42, pp. 17–38, 1991.
- [160] S. Nee and R. M. May, "Dynamics of Metapopulations - Habitat Destruction and Competitive Coexistence," *Journal of Animal Ecology*, vol. 61, no. 1, pp. 37–40, 1992.

- [161] B Grenfell, "(Meta)population dynamics of infectious diseases," *Trends in Ecology & Evolution*, vol. 12, no. 10, pp. 395–399, 1997.
- [162] M. J. Keeling, O. N. Bjørnstad, and B. T. Grenfell, "Metapopulation dynamics of infectious diseases," in *Ecology, Genetics and Evolution of Metapopulations*, Elsevier, 2004, pp. 415–445.
- [163] M. Keeling and C. Gilligan, "Metapopulation dynamics of bubonic plague," *Nature*, vol. 407, no. 6806, p. 903, 2000.
- [164] T. A. Perkins, T. W. Scott, A. Le Menach, and D. L. Smith, "Heterogeneity, Mixing, and the Spatial Scales of Mosquito-Borne Pathogen Transmission," *PLoS Computational Biology*, vol. 9, no. 12, e1003327, 2013.
- [165] K. Magori, M. Legros, M. E. Puentes, D. A. Focks, T. W. Scott, A. L. Lloyd, and F. Gould, "Skeeter Buster: A Stochastic, Spatially Explicit Modeling Tool for Studying *Aedes aegypti* Population Replacement and Population Suppression Strategies," *PLoS Neglected Tropical Diseases*, vol. 3, no. 9, e508, 2009.
- [166] D. A. Focks, D. G. Haile, E. Daniels, and G. A. Mount, "Dynamic Life Table Model for *Aedes aegypti* (Diptera: Culicidae): Simulation Results and Validation," *Journal of Medical Entomology*, vol. 30, no. 6, pp. 1018–1028, 1993.
- [167] M. Legros, K. Magori, A. C. Morrison, C. Xu, T. W. Scott, A. L. Lloyd, and F. Gould, "Evaluation of Location-Specific predictions by a detailed simulation model of *Aedes aegypti* populations," *PLoS ONE*, vol. 6, no. 7, e22701, 2011.
- [168] M. Otero, N. Schweigmann, and H. G. Solari, "A stochastic spatial dynamical model for *Aedes aegypti*," *Bulletin of mathematical biology*, vol. 70, no. 5, pp. 1297–325, 2008.
- [169] V. Romeo Aznar, M. Otero, M. S. De Majo, S. Fischer, and H. G. Solari, "Modeling the complex hatching and development of *Aedes aegypti* in temperate climates," *Ecological Modelling*, vol. 253, pp. 44–55, 2013.
- [170] A. M. Lutambi, M. A. Penny, T. Smith, and N. Chitnis, "Mathematical modelling of mosquito dispersal in a heterogeneous environment," *Mathematical Biosciences*, vol. 241, no. 2, pp. 198–216, 2013.
- [171] S. J. de Almeida, R. P. Martins Ferreira, Á. E. Eiras, R. P. Obermayr, and M. Geier, "Multi-agent modeling and simulation of an *Aedes aegypti* mosquito population," *Environmental Modelling and Software*, vol. 25, no. 12, pp. 1490–1507, 2010.

- [172] S. Maneerat and E. Daudé, “A spatial agent-based simulation model of the dengue vector *Aedes aegypti* to explore its population dynamics in urban areas,” *Ecological Modelling*, vol. 333, pp. 66–78, 2016.
- [173] H. Barclay and M. Mackauer, “The sterile insect release method for pest control: A density-dependent model,” *Environmental Entomology*, vol. 9, no. 6, pp. 810–817, 1980.
- [174] S. M. White, P. Rohani, and S. M. Sait, “Modelling pulsed releases for sterile insect techniques: Fitness costs of sterile and transgenic males and the effects on mosquito dynamics,” *Journal of Applied Ecology*, vol. 47, no. 6, pp. 1329–1339, 2010.
- [175] L. Esteva and H. Mo Yang, “Mathematical model to assess the control of *Aedes aegypti* mosquitoes by the sterile insect technique,” *Mathematical Biosciences*, vol. 198, no. 2, pp. 132–147, 2005.
- [176] N. Alphey, L. Alphey, and M. B. Bonsall, “A Model Framework to Estimate Impact and Cost of Genetics-Based Sterile Insect Methods for Dengue Vector Control,” *PLoS ONE*, vol. 6, no. 10, e25384, 2011.
- [177] L. Yakob and M. B. Bonsall, “Importance of space and competition in optimizing genetic control strategies,” *Journal of Economic Entomology*, vol. 102, no. 1, pp. 50–57, 2009.
- [178] C. P. Ferreira, H. M. Yang, and L. Esteva, “Assessing the suitability of sterile insect technique applied to *Aedes Aegypti*,” *Journal of Biological Systems*, vol. 16, no. 04, pp. 565–577, 2008.
- [179] C. Dufourd and Y. Dumont, “Impact of environmental factors on mosquito dispersal in the prospect of sterile insect technique control,” in *Computers and Mathematics with Applications*, vol. 66, 2013, pp. 1695–1715.
- [180] P. R. Crain, J. W. Mains, E. Suh, Y. Huang, P. H. Crowley, and S. L. Dobson, “Wolbachia infections that reduce immature insect survival: Predicted impacts on population replacement,” *BMC Evolutionary Biology*, vol. 11, no. 1, p. 290, 2011.
- [181] P. A. Hancock, S. P. Sinkins, H. C. J. Godfray, P. A. Hancock, S. P. Sinkins, and H. C. J. Godfray, “Population Dynamic Models of the Spread of *Wolbachia*,” *American Naturalist*, vol. 177, no. 3, pp. 323–333, 2011.
- [182] P. A. Hancock, S. P. Sinkins, and H. C. J. Godfray, “Strategies for introducing *Wolbachia* to reduce transmission of mosquito-borne diseases,” *PLoS Neglected Tropical Diseases*, vol. 5, no. 4, e1024, 2011.

- [183] P. A. Hancock, V. L. White, S. A. Ritchie, A. A. Hoffmann, and H. C. J. Godfray, "Predicting *Wolbachia* invasion dynamics in *Aedes aegypti* populations using models of density-dependent demographic traits," *BMC Biology*, vol. 14, no. 1, p. 96, 2016.
- [184] P. Schofield, "Spatially Explicit Models of Turelli-Hoffmann *Wolbachia* Invasive Wave Fronts," *Journal of Theoretical Biology*, vol. 215, pp. 121–131, 2002.
- [185] N. H. Barton and M. Turelli, "Spatial Waves of Advance with Bistable Dynamics: Cytoplasmic and Genetic Analogues of Allee Effects," *The American Naturalist*, vol. 178, no. 3, E48–75, 2011.
- [186] M. Turelli and A. A. Hoffmann, "Rapid spread of an inherited incompatibility factor in California *Drosophila*," *Nature*, vol. 353, no. 6343, pp. 440–442, 1991.
- [187] E. Caspari and G. S. Watson, "On the evolutionary importance of cytoplasmic sterility in mosquitoes," *Evolution*, vol. 13, no. 4, pp. 568–570, 1959.
- [188] V. A. A. Jansen, M. Turelli, H. Charles, and J. Godfray, "Stochastic spread of *Wolbachia*," *Proceedings of the Royal Society B: Biological Sciences*, vol. 275, 2008.
- [189] M. Turelli, A. A. Hoffmann, M. Turelli, and A. A. Hoffmann, "Microbe-induced cytoplasmic incompatibility as a mechanism for introducing transgenes into arthropod populations," *Insect Molecular Biology*, vol. 8, no. 2, pp. 243–255, 1999.
- [190] M. Turelli, "Cytoplasmic incompatibility in populations with overlapping generations," *Evolution*, vol. 64, no. 1, pp. 232–241, 2010.
- [191] J. G. Schraiber, A. N. Kaczmarczyk, R. Kwok, M. Park, R. Silverstein, F. U. Rutaganira, T. Aggarwal, M. A. Schwemmer, C. L. Hom, R. K. Grosberg, *et al.*, "Constraints on the use of lifespan-shortening *Wolbachia* to control dengue fever," *Journal of Theoretical Biology*, vol. 297, pp. 26–32, 2012.
- [192] M. Turelli and N. H. Barton, "Deploying dengue-suppressing *Wolbachia* : Robust models predict slow but effective spatial spread in *Aedes aegypti*," *Theoretical Population Biology*, vol. 115, pp. 45–60, 2017.
- [193] T. P. Oléron Evans and S. R. Bishop, "A spatial model with pulsed releases to compare strategies for the sterile insect technique applied to the mosquito *Aedes aegypti*," *Mathematical Biosciences*, vol. 254, no. 1, pp. 6–27, 2014.

- [194] M. Legros, C. Xu, A. Morrison, T. W. Scott, A. L. Lloyd, and F. Gould, "Modeling the dynamics of a non-limited and a self-limited gene drive system in structured *Aedes aegypti* populations," *PLoS ONE*, vol. 8, no. 12, 2013.
- [195] P. A. Hancock, V. Linley-White, A. G. Callahan, H. C. J. Godfray, A. A. Hoffmann, and S. A. Ritchie, "Density-dependent population dynamics in *Aedes aegypti* slow the spread of *wMel Wolbachia*," *Journal of Applied Ecology*, 2016.
- [196] P. A. Hancock and H. C. J. Godfray, "Modelling the spread of *Wolbachia* in spatially heterogeneous environments.," *Journal of the Royal Society, Interface*, vol. 9, no. 76, pp. 3045–54, 2012.
- [197] T. L. Schmidt, N. H. Barton, G. Rašić, A. P. Turley, B. L. Montgomery, I. Iturbe-Ormaetxe, P. E. Cook, P. A. Ryan, S. A. Ritchie, A. A. Hoffmann, *et al.*, "Local introduction and heterogeneous spatial spread of dengue-suppressing *Wolbachia* through an urban population of *Aedes aegypti*," *PLoS Biology*, vol. 15, no. 5, e2001894, 2017.
- [198] M. P. Atkinson, Z. Su, N. Alpey, L. S. Alpey, P. G. Coleman, and L. M. Wein, "Analyzing the control of mosquito-borne diseases by a dominant lethal genetic system," *Proceedings of the National Academy of Sciences*, vol. 104, no. 22, pp. 9540–9545, 2007.
- [199] H. Hughes and N. F. Britton, "Modelling the Use of *Wolbachia* to Control Dengue Fever Transmission," *Bulletin of Mathematical Biology*, vol. 75, no. 5, pp. 796–818, 2013.
- [200] M. Z. Ndi, R. I. Hickson, D. Allingham, and G. N. Mercer, "Modelling the transmission dynamics of dengue in the presence of *Wolbachia*," *Mathematical Biosciences*, vol. 262, pp. 157–166, 2015.
- [201] M. Z. Ndi, D. Allingham, R. I. Hickson, and K. Glass, "The effect of *Wolbachia* on dengue outbreaks when dengue is repeatedly introduced," *Theoretical Population Biology*, vol. 111, no. 13, pp. 9–15, 2016.
- [202] M. Z. Ndi, D. Allingham, R. I. Hickson, and K. GLASS, "The effect of *Wolbachia* on dengue dynamics in the presence of two serotypes of dengue: symmetric and asymmetric epidemiological characteristics," *Epidemiology and Infection*, vol. 144, no. 13, pp. 1–9, 2016.
- [203] N. M. Ferguson, D. T. Hue Kien, H. Clapham, R. Aguas, V. T. V. T. Trung, T. N. Bich Chau, J. Popovici, P. A. Ryan, S. L. O'Neill, E. A. McGraw, *et al.*, "Modeling the impact on virus

- transmission of *Wolbachia*-mediated blocking of dengue virus infection of *Aedes aegypti*,” *Science Translational Medicine*, vol. 7, no. 279, 279ra37–279ra37, 2015.
- [204] R. A. Erickson, S. M. Presley, L. J. Allen, K. R. Long, and S. B. Cox, “A dengue model with a dynamic *Aedes albopictus* vector population,” *Ecological Modelling*, vol. 221, no. 24, pp. 2899–2908, 2010.
- [205] P. M. Luz, T. Vanni, J. Medlock, A. D. Paltiel, and A. P. Galvani, “Dengue vector control strategies in an urban setting: an economic modelling assessment,” *The Lancet*, vol. 377, no. 9778, pp. 1673–1680, 2011.
- [206] P. Reiter, “Oviposition, Dispersal, and Survival in *Aedes aegypti*: Implications for the Efficacy of Control Strategies,” *Vector-Borne and Zoonotic Diseases*, vol. 7, no. 2, pp. 261–273, 2007.
- [207] J. Wong, S. T. Stoddard, H. Astete, A. C. Morrison, and T. W. Scott, “Oviposition Site Selection by the Dengue Vector *Aedes aegypti* and Its Implications for Dengue Control,” *PLoS Neglected Tropical Diseases*, vol. 5, no. 4, e1015, 2011.
- [208] I. Hanski, T. Pakkala, M. Kuussaari, and G. Lei, “Metapopulation persistence of an endangered butterfly in a fragmented landscape,” *Oikos*, pp. 21–28, 1995.
- [209] I. Hanski, T. Schulz, S. C. Wong, V. Ahola, A. Ruokolainen, and S. P. Ojanen, “Ecological and genetic basis of metapopulation persistence of the Glanville fritillary butterfly in fragmented landscapes,” *Nature Communications*, vol. 8, p. 14504, 2017.
- [210] Z. G. Davies, R. J. Wilson, T. M. Brereton, and C. D. Thomas, “The re-expansion and improving status of the silver-spotted skipper butterfly (*Hesperia comma*) in Britain: A metapopulation success story,” *Biological Conservation*, vol. 124, no. 2, pp. 189–198, 2005.
- [211] D. R. Cox, “Regression models and life-tables,” *Journal of the Royal Statistical Society: Series B (Methodological)*, vol. 34, no. 2, pp. 187–202, 1972.
- [212] J. Clobert, M. Baguette, T. G. Benton, and J. M. Bullock, *Dispersal Ecology and Evolution*, Oxford University Press. 2012.
- [213] C. C. Lord, “Density dependence in larval *Aedes albopictus* (Diptera: Culicidae),” *Journal of Medical Entomology*, vol. 35, no. 5, pp. 825–829, 1998.
- [214] H. Briegel, “Metabolic relationship between female body size, reserves, and fecundity of *Aedes aegypti*,” *Journal of Insect Physiology*, vol. 36, no. 3, pp. 165–172, 1990.

- [215] R. S. Nasci, "The size of emerging and host-seeking *Aedes aegypti* and the relation of size to blood-feeding success in the field," *J Am Mosq Control Assoc*, vol. 2, no. 1, pp. 61–62, 1986.
- [216] M. T. White, J. T. Griffin, T. S. Churcher, N. M. Ferguson, M.-G. Basáñez, and A. C. Ghani, "Modelling the impact of vector control interventions on *Anopheles gambiae* population dynamics.," *Parasites & vectors*, vol. 4, no. 1, p. 153, 2011.
- [217] M. B. Hoshen and A. P. Morse, "A weather-driven model of malaria transmission.," *Malaria Journal*, vol. 3, no. 1, p. 32, 2004.
- [218] L. Harrington, A. Ponlawat, J. Edman, T. Scott, and F. Vermeulen, "Influence of Container Size, Location, and Time of Day on Oviposition Patterns of the Dengue Vector, *Aedes aegypti*, in Thailand," *Vector-Borne and Zoonotic Diseases*, vol. 8, no. 3, pp. 415–424, 2008.
- [219] N. Zahiri and M. E. Rau, "Oviposition attraction and repellency of *Aedes aegypti* (Diptera: Culicidae) to waters from conspecific larvae subjected to crowding, confinement, starvation, or infection," *Journal of Medical Entomology*, vol. 35, no. 5, pp. 782–787, 1998.
- [220] I.-K. Yoon, A. Getis, J. Aldstadt, A. L. Rothman, D. Tannitisupawong, C. J. M. Koenraadt, T. Fansiri, J. W. Jones, A. C. Morrison, R. G. Jarman, *et al.*, "Fine Scale Spatiotemporal Clustering of Dengue Virus Transmission in Children and *Aedes aegypti* in Rural Thai Villages," *PLoS Neglected Tropical Diseases*, vol. 6, no. 7, e1730, 2012.
- [221] T. W. Scott, A. C. Morrison, L. H. Lorenz, G. G. Clark, D. Strickman, P. Kittayapong, H. Zhou, and J. D. Edman, "Longitudinal Studies of *Aedes aegypti* (Diptera: Culicidae) in Thailand and Puerto Rico: Population Dynamics," *Journal of Medical Entomology*, vol. 37, no. 371, pp. 77–88, 2000.
- [222] M. Otero, H. G. Solari, and N. Schweigmann, "A stochastic population dynamics model for *Aedes aegypti*: Formulation and application to a city with temperate climate," *Bulletin of Mathematical Biology*, vol. 68, no. 8, pp. 1945–1974, 2006.
- [223] P. Sheppard, W. Macdonald, R. Tonn, and B. Grab, "The dynamics of an adult population of *Aedes aegypti* in relation to dengue haemorrhagic fever in bangkok," *The Journal of Animal Ecology*, pp. 661–702, 1969.

- [224] R. L. Iman and W. J. Conover, "A distribution-free approach to inducing rank correlation among input variables," *Communications in Statistics - Simulation and Computation*, vol. 11, no. 3, pp. 311–334, 1982.
- [225] G. LaCon, A. C. Morrison, H. Astete, S. T. Stoddard, V. A. Paz-Soldan, J. P. Elder, E. S. Halsey, T. W. Scott, U. Kitron, and G. M. Vazquez-Prokopec, "Shifting Patterns of *Aedes aegypti* Fine Scale Spatial Clustering in Iquitos, Peru," *PLoS Neglected Tropical Diseases*, vol. 8, no. 8, e3038, 2014.
- [226] J. R. Schneider, A. C. Morrison, H. Astete, T. W. Scott, and M. L. Wilson, "Adult size and distribution of *Aedes aegypti* (Diptera: Culicidae) associated with larval habitats in Iquitos, Peru," *Journal of Medical Entomology*, vol. 41, no. 4, pp. 634–642, 2004.
- [227] C. Costantini, S.-G. Li, A. Della Torre, N. Sagnon, M. Coluzzi, C. E. Taylor, A. della Torre, N. Sagnon, M. Coluzzi, and C. E. Taylor, "Density, survival and dispersal of *Anopheles gambiae* complex mosquitoes in a West African Sudan savanna village.," *Medical and Veterinary Entomology*, vol. 10, no. 3, pp. 203–219, 1996.
- [228] J. T. Midega, C. M. Mbogo, H. Mwambi, M. D. Wilson, G. Ojwang, J. M. Mwangangi, J. G. Nzovu, J. I. Githure, G. Yan, J. C. Beier, *et al.*, "Estimating dispersal and survival of *Anopheles gambiae* and *Anopheles funestus* along the Kenyan coast by using mark-release-recapture methods.," *Journal of Medical Entomology*, vol. 44, no. 6, pp. 923–9, 2007.
- [229] W. Mamai, F. Simard, D. Couret, G. A. Ouédraogo, D. Renault, K. R. Dabiré, and K. Mouline, "Monitoring dry season persistence of *Anopheles gambiae s.l.* populations in a contained semi-field system in southwestern Burkina Faso, West Africa," *Journal of medical entomology*, vol. 53, no. 1, pp. 130–138, 2015.
- [230] J. Charlwood, R. Vij, and P. Billingsley, "Dry season refugia of malaria-transmitting mosquitoes in a dry savannah zone of East Africa.," *American Journal of Tropical Medicine and Hygiene*, vol. 62, no. 6, pp. 726–732, 2000.
- [231] L. C. Harrington, J. J. Jones, S. Kitthawee, R. Sithiprasasna, J. D. Edman, and T. W. Scott, "Age-dependent survival of the dengue vector *Aedes aegypti* (Diptera: Culicidae) demonstrated by simultaneous release-recapture of different age cohorts.," *Journal of Medical Entomology*, vol. 45, no. 2, pp. 307–313, 2008.

- [232] A. Clements and G. Paterson, "The analysis of mortality and survival rates in wild populations of mosquitoes," *Journal of Applied Ecology*, pp. 373–399, 1981.
- [233] A. Wilder-Smith, S. Yoksan, A. Earnest, R. Subramaniam, and N. I. Paton, "Serological evidence for the co-circulation of multiple dengue virus serotypes in Singapore," *Epidemiology and Infection*, vol. 133, no. 4, pp. 667–671, 2005.
- [234] K. S. Lee, S. Lo, S. S. Y. Tan, R. Chua, L. K. Tan, H. Xu, and L. C. Ng, "Dengue virus surveillance in Singapore reveals high viral diversity through multiple introductions and in situ evolution," *Infection, Genetics and Evolution*, vol. 12, no. 1, pp. 77–85, 2012.
- [235] M. L'Azou, J. Assoukpa, K. Fanouillere, E. Plennevaux, M. Bonaparte, A. Bouckenoghe, C. Frago, F. Noriega, B. Zambrano, R. L. Ochiai, *et al.*, "Dengue seroprevalence: Data from the clinical development of a tetravalent dengue vaccine in 14 countries (2005-2014)," *Transactions of the Royal Society of Tropical Medicine and Hygiene*, vol. 112, no. 4, pp. 158–168, 2018.
- [236] H. C. Hapuarachchi, C. Koo, J. Rajarethinam, C. S. Chong, C. Lin, G. Yap, L. Liu, Y. L. Lai, P. L. Ooi, J. Cutter, *et al.*, "Epidemic resurgence of dengue fever in Singapore in 2013-2014: A virological and entomological perspective," *BMC Infectious Diseases*, vol. 16, no. 1, p. 300, 2016.
- [237] E. E. Ooi, "Changing pattern of dengue transmission in singapore.," *Dengue Bulletin* 25:41, 2001.
- [238] T. S. Ler, L. W. Ang, G. S. L. Yap, L. C. Ng, J. C. Tai, L. James, and K. T. Goh, "Epidemiological characteristics of the 2005 and 2007 dengue epidemics in Singapore - similarities and differences," *Western Pacific Surveillance and Response*, vol. 2, no. 2, e1–e1, 2011.
- [239] J. Rajarethinam, L. W. Ang, J. Ong, J. Ycasas, H. C. Hapuarachchi, G. Yap, C. S. Chong, Y. L. Lai, J. Cutter, D. Ho, *et al.*, "Dengue in Singapore from 2004 to 2016: Cyclical epidemic patterns dominated by serotypes 1 and 2," *American Journal of Tropical Medicine and Hygiene*, vol. 99, no. 1, pp. 204–210, 2018.
- [240] G. Yap, C. Li, A. Mutalib, Y. L. Lai, and L. C. Ng, "High rates of inapparent dengue in older adults in Singapore," *American Journal of Tropical Medicine and Hygiene*, vol. 88, no. 6, pp. 1065–1069, 2013.

- [241] K. Goh, "Changing epidemiology of dengue in Singapore," *The Lancet*, vol. 346, no. 8982, p. 1098, 1995.
- [242] S. L. Low, S. Lam, W. Y. Wong, D. Teo, L. C. Ng, and L. K. Tan, "Dengue seroprevalence of healthy adults in Singapore: Serosurvey among blood donors, 2009," *American Journal of Tropical Medicine and Hygiene*, vol. 93, no. 1, pp. 40–45, 2015.
- [243] E. E. Ooi, T. J. Hart, H. C. Tan, and S. H. Chan, "Dengue seroepidemiology in Singapore," *The Lancet*, vol. 357, no. 9257, pp. 685–686, 2001.
- [244] C. Lee, I. Vythilingam, C. S. Chong, M. A. A. Razak, C. H. Tan, C. Liew, K. Y. Pok, and L. C. Ng, "Gravitraps for management of dengue clusters in Singapore," *American Journal of Tropical Medicine and Hygiene*, vol. 88, no. 5, pp. 888–892, 2013.
- [245] C. Andrieu, A. Doucet, and R. Holenstein, "Particle Markov chain Monte Carlo methods," *Journal of the Royal Statistical Society Series B-Statistical Methodology*, vol. 72, no. 3, pp. 269–342, 2010.
- [246] D. J. Wilkinson, "Stochastic modelling for systems biology," *Chapman and Hall*, 2006.
- [247] A. Gelman, H. S. Stern, J. B. Carlin, D. B. Dunson, A. Vehtari, and D. B. Rubin, "Bayesian data analysis," *Chapman and Hall*, 2013.
- [248] W. K. Hastings, "Monte carlo sampling methods using markov chains and their applications," *Oxford University Press*, 1970.
- [249] P. H. Garthwaite, Y. Fan, and S. A. Sisson, "Adaptive optimal scaling of Metropolis-Hastings algorithms using the Robbins-Monro process," *Communications in Statistics - Theory and Methods*, vol. 45, no. 17, pp. 5098–5111, 2016.
- [250] R. Maciel-de Freitas, C. T. Codeço, and R. Lourenço-de Oliveira, "Daily survival rates and dispersal of *Aedes aegypti* females in Rio de Janeiro, Brazil.," *American Journal of Tropical Medicine and Hygiene*, vol. 76, no. 4, pp. 659–665, 2007.
- [251] J. Wong, H. Astete, A. C. Morrison, and T. W. Scott, "Sampling Considerations for Designing *Aedes aegypti* (Diptera: Culicidae) Oviposition Studies in Iquitos, Peru: Substrate Preference, Diurnal Periodicity, and Gonotrophic Cycle Length," *Journal of Medical Entomology*, vol. 48, no. 1, pp. 45–52, 2011.
- [252] D. L. Kline, "Traps and Trapping Techniques for Adult Mosquito Control," *Journal of the American Mosquito Control Association*, vol. 22, no. 3, pp. 490–496, 2007.

- [253] C. B. Ocampo, C. González, C. A. Morales, M. Pérez, D. Wesson, and C. S. Apperson, "Evaluation of community-based strategies for *Aedes aegypti* control inside houses," *Biomedica*, vol. 29, no. 2, pp. 282–297, 2009.
- [254] L. Rapley, P. Johnson, C. Williams, R. Silcock, M Larkman, S. Long, R. Russell, and S. Ritchie, "A lethal ovitrap-based mass trapping scheme for dengue control in Australia: II Impact on populations of the mosquito *Aedes aegypti*," *Medical and Veterinary Entomology*, vol. 23, no. 4, pp. 303–316, 2009.
- [255] R. E. Coleman, P. Mahapibul, B. Burge, C. Noigamol, R. Sithiprasasna, B. C. Zeichner, M. J. Perich, S. S. Schleich, S. L. W. Norris, and J. W. Jones, "Field Evaluation of a Lethal Ovitrap for the Control of *Aedes aegypti* (Diptera: Culicidae) in Thailand," *Journal of Medical Entomology*, vol. 40, no. 4, pp. 455–462, 2009.
- [256] M. Perich, A Kardec, I. Braga, I. Portal, R Burge, B. Zeichner, W. Brogdon, and R. Wirtz, "Field evaluation of a lethal ovitrap against dengue vectors in Brazil," *Medical and Veterinary Entomology*, vol. 17, no. 2, pp. 205–210, 2003.
- [257] O. T. Lewis, C. D. Thomas, J. K. Hill, M. I. Brookes, T. P. Crane, Y. A. Graneau, J. L. Mallet, and O. C. Rose, "Three ways of assessing metapopulation structure in the butterfly *Plebejus argus*," *Ecological Entomology*, vol. 22, no. 3, pp. 283–293, 1997.
- [258] E. Fleishman, C. Ray, P. Sjögren-Gulve, C. L. Boggs, and D. D. Murphy, "Assessing the roles of patch quality, area, and isolation in predicting metapopulation dynamics," *Conservation Biology*, vol. 16, no. 3, pp. 706–716, 2002.
- [259] I. Hanski and O. Ovaskainen, "The metapopulation capacity of a fragmented landscape," *Nature*, vol. 404, no. 6779, pp. 755–758, 2000.
- [260] O. Ovaskainen, K. Sato, J. Bascompte, and I. Hanski, "Metapopulation Models for Extinction Threshold in Spatially Correlated Landscapes," *Journal of Theoretical Biology*, vol. 215, no. 1, pp. 95–108, 2002.
- [261] A. Deredec, A. Burt, and H. C. J. Godfray, "The population genetics of using homing endonuclease genes in vector and pest management," *Genetics*, vol. 179, no. 4, pp. 2013–2026, 2008.
- [262] P. A. Eckhoff, E. A. Wenger, H. C. J. Godfray, and A. Burt, "Impact of mosquito gene drive on malaria elimination in a computational model with explicit spatial and temporal

- dynamics,” *Proceedings of the National Academy of Sciences*, vol. 114, no. 2, E255–E264, 2017.
- [263] H. Salje, J. Lessler, I. M. Berry, M. C. Melendrez, T. Endy, S. Kalayanarooj, A. A-Nuegoonpipat, S. Chanama, S. Sangkijporn, C. Klungthong, *et al.*, “Dengue diversity across spatial and temporal scales: Local structure and the effect of host population size,” *Science*, vol. 355, no. 6331, pp. 1302–1306, 2017.
- [264] P. Bhoomiboonchoo, R. V. Gibbons, A. Huang, I. K. Yoon, D. Buddhari, A. Nisalak, N. Chansatiporn, M. Thipayamongkolgul, S. Kalanarooj, T. Endy, *et al.*, “The Spatial Dynamics of Dengue Virus in Kamphaeng Phet, Thailand,” *PLoS Neglected Tropical Diseases*, vol. 8, no. 9, e3138, 2014.

Appendix A

Figure Permissions

Figure 1.1 : Reprinted with permission from Elsevier (S. B. Halstead, "Dengue," The Lancet, vol. 370, no. 9599, pp. 1644–1652, 2007)

07/03/2019

RightsLink Printable License

**ELSEVIER LICENSE
TERMS AND CONDITIONS**

Mar 07, 2019

This Agreement between Clare McCormack ("You") and Elsevier ("Elsevier") consists of your license details and the terms and conditions provided by Elsevier and Copyright Clearance Center.

License Number	4543560196382
License date	Mar 07, 2019
Licensed Content Publisher	Elsevier
Licensed Content Publication	The Lancet
Licensed Content Title	Dengue
Licensed Content Author	Scott B Halstead
Licensed Content Date	10–16 November 2007
Licensed Content Volume	370
Licensed Content Issue	9599
Licensed Content Pages	9
Start Page	1644
End Page	1652
Type of Use	reuse in a thesis/dissertation
Portion	figures/tables/illustrations
Number of figures/tables/illustrations	1
Format	electronic
Are you the author of this Elsevier article?	No
Will you be translating?	No
Original figure numbers	Figure 3
Title of your thesis/dissertation	Modelling the dynamics and control of Aedes aegypti populations at fine spatial scales
Expected completion date	Mar 2019
Estimated size (number of pages)	200
Requestor Location	Clare McCormack Imperial College London St Mary's Campus London, other W2 1PG United Kingdom Attn:
Publisher Tax ID	GB 494 6272 12
Total	0.00 GBP

Figure 1.2 : Reprinted with permission from eLife under the Creative Commons Attribution license (M. U. Kraemer, M. E. Sinka, K. A. Duda, A. Q. Mylne, F. M. Shearer, C. M. Barker, C. G. Moore, R. G. Carvalho, G. E. Coelho, W. Van Bortel, et al., “The global distribution of the arbovirus vectors *Aedes aegypti* and *Ae. albopictus*,” eLife, vol. 4, e08347, 2015.)

<https://creativecommons.org/licenses/by/2.0/uk/>

Figure 1.3 : Reprinted with permission from PLoS Neglected Tropical Diseases under the Creative Commons Attribution license (N. L. Achee, F. Gould, T. A. Perkins, R. C. Reiner, A. C. Morrison, S. A. Ritchie, D. J. Gubler, R. Teysou, and T. W. Scott, “A Critical Assessment of Vector Control for Dengue Prevention,” PLoS Neglected Tropical Diseases, vol. 9, no. 5, e0003655, 2015)

<https://www.plos.org/license>

Figures 1.4 and 1.5: No permission required as author of article (I. Dorigatti, C. McCormack, G. Nedjati-Gilani, and N. M. Ferguson, “Using Wolbachia for Dengue Control: Insights from Modelling,” Trends in Parasitology, vol. 34, no. 2, pp. 102–113, 2018.)

07/03/2019

Rightslink® by Copyright Clearance Center

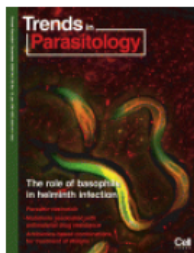


RightsLink®

Home

Account Info

Help



Title: Using Wolbachia for Dengue Control: Insights from Modelling
Author: Iliara Dorigatti, Clare McCormack, Gemma Nedjati-Gilani, Neil M. Ferguson
Publication: Trends in Parasitology
Publisher: Elsevier
Date: February 2018

Logged in as:
Clare McCormack
Account #:
3001416829

LOGOUT

© 2017 Elsevier Ltd. All rights reserved.

Please note that, as the author of this Elsevier article, you retain the right to include it in a thesis or dissertation, provided it is not published commercially. Permission is not required, but please ensure that you reference the journal as the original source. For more information on this and on your other retained rights, please visit: <https://www.elsevier.com/about/our-business/policies/copyright#Author-rights>

BACK

CLOSE WINDOW

Copyright © 2019 Copyright Clearance Center, Inc. All Rights Reserved. [Privacy statement](#). [Terms and Conditions](#).
Comments? We would like to hear from you. E-mail us at customercare@copyright.com

Table 1.1 : Reproduced with permission from Oxford University Press (A. C. Morrison, K. Gray, A. Getis, H. Astete, M. Sihuincha, D. Focks, D. Watts, J. D. Stancil, J. G. Olson, P. Blair, et al., "Temporal and Geographic Patterns of *Aedes aegypti* (Diptera: Culicidae) Production in Iquitos, Peru," *Journal of Medical Entomology*, vol. 41, no. 6, pp. 1123–1142, 2004)

07/03/2019

RightsLink Printable License

**OXFORD UNIVERSITY PRESS LICENSE
TERMS AND CONDITIONS**

Mar 07, 2019

This Agreement between Clare McCormack ("You") and Oxford University Press ("Oxford University Press") consists of your license details and the terms and conditions provided by Oxford University Press and Copyright Clearance Center.

License Number	4543591331542
License date	Mar 07, 2019
Licensed content publisher	Oxford University Press
Licensed content publication	Journal of Medical Entomology
Licensed content title	Temporal and Geographic Patterns of <i>Aedes aegypti</i> (Diptera: Culicidae) Production in Iquitos, Peru
Licensed content author	Morrison, Amy C.; Gray, Kenneth
Licensed content date	Nov 1, 2004
Type of Use	Thesis/Dissertation
Institution name	
Title of your work	Modelling the dynamics and control of <i>Aedes aegypti</i> populations at fine spatial scales
Publisher of your work	n/a
Expected publication date	Mar 2019
Permissions cost	0.00 GBP
Value added tax	0.00 GBP
Total	0.00 GBP
Title	Modelling the dynamics and control of <i>Aedes aegypti</i> populations at fine spatial scales
Institution name	n/a
Expected presentation date	Mar 2019
Portions	Table 2
Requestor Location	Clare McCormack Imperial College London St Mary's Campus London, other W2 1PG United Kingdom Attn:
Publisher Tax ID	GB125506730
Billing Type	Invoice
Billing Address	Clare McCormack Imperial College London St Mary's Campus London, United Kingdom W2 1PG Attn: Clare McCormack
Total	0.00 GBP

Appendix B

Sample Code

Example 1: Particle Filtering (condensed version)

Condensed version of function I wrote implementing the PMMH algorithm for a give study site

```
void Particle_Filter_Parallel(long k, double* result,.....) {
int t1, start, thread_no;
double log_lik, mean_w, sum;
int thread_count = omp_get_max_threads();
omp_set_num_threads(thread_count);
/*Step 1 - read in proposed parameter values*/
/*Step 2 - obtain value for mu_I from equation for R_M (Equation XXX)*/
/*Step 3 - generate carrying capacities and initial values for state variables based on proposed parameter value*/
/*Step 4 - populate release matrix*/
/*Step 5 - calculate log-likelihood across time series*/
int t_end = Site.Adult_Data[0][0].no_weeks;
int days = int(7 * (t_end + RUN_IN)*(1 / DT));
/*run model forward to get new particle values, calculate likelihood at these values and normalise weights*/
for (int t = 0; t < t_end; t++) {
    sum=0;
    if (t == 0) {
        start = 0;
        t1 = int(7 * RUN_IN*(1 / DT));/*run-in model for RUN_IN weeks*/
    }
    else {
        start = t1;
        t1 = int(start + 7 * (1 / DT));/*time step of one week*/;
    }
    /*run particles in parallel*/
    #pragma omp parallel for private(thread_no) schedule(static,1)
    for (int thread_no = 0; thread_no < thread_count; thread_no++) {
        for (int m = thread_no; m < M; m += thread_count) {
            /*run model forward to time t1*/
            Stochastic_Model(thread_no, m, start, t1, 1, Site, params, model_type);
            /*calculate log-likelihood*/
            double l = 0;
            l += Log_Likelihood(Site.Adult_Data.F_WT, Site.Patches[m].F_WT[t1],
                Site.Loc_Params.p_f, Site.Loc_Params.psi, t); (see Example 2 below)
            l += Log_Likelihood(Site.Adult_Data.M_WT, Site.Patches[m].M_WT[t1],
                Site.Loc_Params.p_m*Site.Loc_Params.p_f, Site.Loc_Params.psi, t);
            l += Log_Likelihood(Site.Adult_Data.M_WB, Site.Patches[m].M_WB[t1],
                Site.Loc_Params.p_wb*Site.Loc_Params.p_f, Site.Loc_Params.psi, t);}
        }
    }
}
```

```

    /*check if there is egg data*/
    int week = Site.Adult_Data.Week[t];
    int year = Site.Adult_Data.Yr[t];
    int no_weeks = Site.Egg_Data.no_weeks;
    for (int s = 0; s < no_weeks; s++) {
        if (Site.Egg_Data.Week[s] == week && Site.Egg_Data.Yr[s] == year) {
            l += Log_Likelihood(Site.Egg_Data.E_v, Site.Patches[m].E_v[t1],
                Site.Loc_Params.p_e, Site.Loc_Params.psi_e, s);
            l += Log_Likelihood(Site.Egg_Data.E_nv, Site.Patches[m].E_nv[t1],
                Site.Loc_Params.p_e, Site.Loc_Params.psi_e, s);
            break;
        }
    }
    /*store log-likelihood value for each particle*/
    Site.P[m][t + 1] = l;
}

/* weight each particle values based on likelihood value*/
for (int m = 0; m < M; m++) { W[m][t + 1] = Site.P[m][i][j][t + 1]; }
for (int m = 0; m < M; m++) { W[m][t + 1] = exp(W[m][t + 1]); sum += W[m][t + 1]; }

/*normalise weights*/
for (int m = 0; m < M; m++) { W[m][t + 1] = W[m][t + 1] / sum; }

/* resample particle values based on weights*/
Resample_Values(Site, W, Z, M, t + 1, t1); (see Example 3 below)
}

/*Step 6– calculate log-likelihood across whole time series using sample trajectory*/
log_lik = 0;
log_lik += Sample_Trajectory(Site, W, Z, M, t_end);

result[0] = log_lik;
}}

```

Example 2: Log-Likelihood Function

Function I wrote to calculate the log-likelihood of observing data $Y[t]$ at week t given total predicted population size N , mean trapping proportion p and overdispersion parameter ψ (Equation 5.71)

```
double Log_Likelihood(int*Y, double N, double p, double psi, int t) {
double log_lik;
/*check if  $\psi$  is non-zero, else set log-likelihood to a very low value*/
if (psi > 0) {
    double z = 1 / psi;
    /*if observed data point  $Y[t]$  is larger than total predicted population size  $N$ , set log-likelihood to a very low value*/
    if (Y[t] > N) {log_lik = -20000; }
    else {
        log_lik = l_Binomial_Coeff(N, Y[t]) +
        lBeta_Function(Y[t] + p*(z - 1), N - Y[t] + (1 - p)*(z - 1)) -
        lBeta_Function(p*(z - 1), (1 - p)*(z - 1));}
    }
else log_lik = -20000;
return log_lik;
}
```

Example 3: Resampling Particle Values

Function I wrote to resample particle values at a given timestep for a given study site with weights W

```
void Resample_Values(site Site, double**W, double*Z, int M, int t, int t1) {
int k; patch*S; S = new patch[M];
/*store weights at time t in array Z*/
    for (int m = 0; m < M; m++) { Z[m] = W[m][t];
/*store current population values for each particle in structure S*/
    for (int m = 0; m < M; m++) {
        S[m].V[t] = Site.Patches[m].V[t1];
        S[m].M_WT[t] = Site.Patches[m].M_WT[t1];
        S[m].F_WT[t] = Site.Patches[m].F_WT[t1];
        S[m].M_WB[t] = Site.Patches[m].M_WB[t1];
        S[m].E_v[t] = Site.Patches[m].E_v[t1];
        S[m].E_nv[t] = Site.Patches[m].E_nv[t1];
        S[m].L[t] = Site.Patches[m].L[t1];
    }
/* using the GNU Scientific Library (GSL) for C++, get discrete distribution F with weights of particles*/
    F = gsl_ran_discrete_preproc(M, Z);
/*resample particle values with replacement*/
    for (int m = 0; m < M; m++) {
        k = int(gsl_ran_discrete(g1, F)); /*randomly pick index from distribution F*/
        Site.Path[m][t] = k; /*keep track of resampled indices*/
        Site.P[m][t] = Site.P[k][t]; /*store resampled log-likelihood value*/
/*store resampled values*/
        Site.Patches[m].V[t1] = S[k].V[t];
        Site.Patches[m].M_WT[t1] = S[k].M_WT[t];
        Site.Patches[m].F_WT[t1] = S[k].F_WT[t];
        Site.Patches[m].M_WB[t1] = S[k].M_WB[t];
        Site.Patches[m].E_v[t1] = S[k].E_v[t];
        Site.Patches[m].E_nv[t1] = S[k].E_nv[t];
        Site.Patches[m].L[t1] = S[k].L[t];
    }
/*delete memory stored*/
    delete[] S;
    gsl_ran_discrete_free(F);
}
```